VILNIUS GEDIMINAS TECHNICAL UNIVERSITY

Viktor GRIBNIAK

SHRINKAGE INFLUENCE ON TENSION-STIFFENING OF CONCRETE STRUCTURES

DOCTORAL DISSERTATION

TECHNOLOGICAL SCIENCES,
CIVIL ENGINEERING (02T)

VGTU
LEIDYKLA
TECHNIKA
Vilnius 2009

Doctoral dissertation was prepared at Vilnius Gediminas Technical University in 2003–2009.
The dissertation is defended as an external work.

Scientific Consultant

Prof Dr Habil Gintaris KAKLAUSKAS (Vilnius Gediminas Technical University, Technological Sciences, Civil Engineering – 02T).

http://leidykla.vgtu.lt
VGTU leidyklos TECHNIKA 1652-M mokslo literatūros knyga

ISBN 978-9955-28-470-3

Viktor.Gribniak@st.vgtu.lt

VILNIAUS GEDIMINO TECHNIKOS UNIVERSITETAS

Viktor GRIBNIAK

SUSITRAUKIMO ĮTAKA GELŽBETONINIŲ ELEMENTŲ TEMPIAMOSIOS ZONOS ELGSENAI

DAKTARO DISERTACIJA

TECHNOLOGIJOS MOKSLAI,
STATYBOS INŽINERIJA (02T)

VGTU
LEIDYKLA
TECHNIKA
Vilnius 2009

Disertacija rengta 2003–2009 metais Vilniaus Gedimino technikos universitete.
Disertacija ginama eksternu.

Mokslinis konsultantas

prof. habil. dr. Gintaris KAKLAUSKAS (Vilniaus Gedimino technikos universitetas, technologijos mokslai, statybos inžinerija – 02T).

Dedicated to my wife Sigita

Abstract

Due to the use of refined ultimate state theories as well as high strength concrete and reinforcement, resulting in longer spans and smaller depths, the serviceability criteria often limits application of modern reinforced concrete (RC) superstructures. In structural analysis, civil engineers can choose between traditional design code methods and numerical techniques. In order to choose a particular calculation method, engineers should be aware of accuracy of different techniques. Adequate modelling of RC cracking and, particularly, post-cracking behaviour, as one of the major sources of nonlinearity, is the most important and difficult task of deformational analysis. In smeared crack approach dealing with average cracking and strains, post-cracking effects can be modelled by a stress-strain tension-stiffening relationship. Most known tension-stiffening relationships have been derived from test data of shrunk tension or shear members. Subsequently, these constitutive laws were applied for modelling of bending elements which behaviour differs from test members. Furthermore, such relationships were coupled with shrinkage effect. Therefore, present research aims at developing a technique for deriving a *free-of-shrinkage* tension-stiffening relationship using test data of shrunk bending RC members. The main objective of this PhD dissertation is to investigate shrinkage influence on deformations and tension-stiffening of RC members subjected to short-term loading.

Present study reviews empirical and numerical techniques of deformation analysis of RC members as well as material models with the emphasis on shrinkage and tension-stiffening effects. Experimental investigation results on concrete shrinkage effect on cracking resistance, tension-stiffening and short-term deformations of lightly reinforced beams have been reported.

An *innovative* numerical procedure has been proposed for deriving *free-of-shrinkage* tension-stiffening relationships using moment-curvature relationships of RC flexural members. The proposed procedure has been applied to the test data reported by the author. For beams of same reinforcement ratio, it was shown that tension-stiffening was more pronounced in those with a larger number of tensile reinforcing bars.

A statistical procedure for checking adequacy of theoretical predictions to the test data taking into account inconsistency of the data has been developed. Using this procedure, comparative statistical analyses of various free shrinkage and deflection/curvature prediction models have been performed.

It was concluded that accuracy of deflection/curvature predictions by design codes and numerical techniques varied for different ranges of reinforcement ratio and load intensity. Numerical techniques gave more accurate predictions of short-term deflections when shrinkage effect was taken into account.

Reziumė

Pastaraisiais metais vis plačiau taikant stiprųjį betoną bei armatūrą, konstrukcijų perdengiamos angos didėja, o skerspjūviai mažėja. Todėl projektuojant standumo (įlinkių) sąlyga vis dažniau tampa lemiamu veiksniu. Inžinieriai gelžbetoninių konstrukcijų apskaičiavimams gali taikyti empirinius normų arba skaitinius metodus. Vieno ar kito skaičiavimo metodo parinkimas turi būti pagrįstas statistiniais tikslumo analizės rezultatais.

Yra žinoma, kad adekvatus gelžbetoninio elemento pleišėjimo (ypač plyšių vystymosi stadijos) modeliavimas yra vienas sudėtingiausių netiesinės mechanikos uždavinių. Toks uždavinys gali būti išspręstas taikant vidutinių plyšių koncepciją, kai pleišėjimo proceso modeliavimui naudojama tempiamojo betono vidutinių įtempių ir deformacijų diagrama. Dauguma tokių diagramų gautos, naudojant tempimo arba šlyties bandymo rezultatus. Pabrėžtina, kad šių diagramų taikymas lenkiamųjų gelžbetoninių elementų modeliavime duoda nemažas paklaidas. Kitas svarbus aspektas yra tai, kad gelžbetoniniuose bandiniuose, iki juos apkraunant trumpalaike apkrova, vyksta betono susitraukimas. Šiame darbe buvo siekiama sukurti metodą, leidžiantį pagal eksperimentinius lenkiamųjų gelžbetoninių elementų duomenis gauti tempiamojo betono vidutinių įtempių ir deformacijų diagramas, įvertinant betono susitraukimo įtaką. Pagrindinis disertacijos tikslas yra įvertinti ikieksploatacinių betono susitraukimo ir valkšnumo poveikį gelžbetoninių elementų, apkrautų trumpalaike apkrova, įtempių ir deformacijų būviui.

Disertacijoje apžvelgti skaitiniai ir analiziniai gelžbetoninių elementų deformacijų skaičiavimo metodai bei aptarti medžiagų modeliai, akcentuojant betono susitraukimo ir betono bei armatūros sąveikos reiškinius. Pasiūlyta nauja skaitinė procedūra, leidžianti pagal gelžbetoninių lenkiamųjų elementų momentų ir kreivių priklausomybes gauti tempiamojo betono vidutinių įtempių ir deformacijų diagramas, eliminuojant susitraukimo įtaką. Atlikti silpnai armuotų gelžbetoninių sijų, apkrautų trumpalaike apkrova, eksperimentiniai tyrimai. Iki apkrovimo buvo matuotos betono laisvojo susitraukimo bei valkšnumo deformacijos. Taikant šiuos eksperimentinius duomenis bei pasiūlytąją procedūrą, gautos tempiamojo betono įtempių ir deformacijų diagramos.

Buvo sukurta skaičiavimo metodų tikslumo analizės statistinė procedūra, kuri įvertina eksperimentinių duomenų nehomogeniškumą. Taikant šią procedūrą, atlikta skirtingais skaičiavimo metodais apskaičiuotų betono laisvojo susitraukimo bei gelžbetoninių elementų įlinkių/kreivių tikslumo analizė. Analizė parodė, kad didžiausią įtaką visų metodų įlinkių apskaičiavimo tikslumui turi armavimo koeficientas bei apkrovimo intensyvumas. Skaitinių metodų tikslumas padidėjo, įvertinus betono susitraukimą.

Notations

Symbols

A_c	is the area of plain concrete net section;
A_s	is the area of reinforcement;
A_{s1}	is the area of tensile reinforcement;
A_{s2}	is the area of compressive reinforcement;
A/C	is the aggregate-to-cement ratio;
B	is the class of concrete (see page 18) or the beta function (see page 96);
C	is the creep parameter (see page 155) or the cement content (see page 157);
C_c	is the centroid of plain concrete net section;
C_{RC}	is the centroid of reinforced concrete section;
dD	is the energy corresponding to the area between the loading and unloading curves, has been dissipated (see page 21);
E_c	is the initial (tangent) modulus of concrete (see page 18);
$E_{c,sec}$	is the secant (deformation) modulus of concrete;
E_{ca}	is the age-adjusted modulus of concrete (see page 52);
E_{cm}	is the secant modulus of concrete (see page 18);
$E_{i,sec}$	is the secant (deformation) modulus of the i-th layer;
$E_{i,k}$	is the secant (deformation) modulus derived at the i-th loading increment and the k-th iteration (see page 68);
E_s	is the elastic modulus of steel;

E_s' , $E_{s,sec}$ is the secant (deformation) modulus of steel;
EI is the flexural stiffness;
F is the *Fisher*'s statistics;
G_F is the specific tensile fracture energy per unit volume;
$G_{F,c}$ is the specific compressive fracture energy per unit volume;
I_{cr} is the moment of inertia for the fully cracked section at the yielding of reinforcement;
I_e is the moment of inertia of the cracked section (see page 47);
I_{el} is the moment of inertia of the uncracked section (see page 48);
I_g is the moment of inertia for uncracked concrete section ignoring reinforcement;
I_{red} is the reduced moment of inertia of fully cracked section;
I_α is the incomplete beta function (see page 96);
J is the compliance function;
M is the bending moment;
M' is the level of load intensity (see page 103);
M_{cr} is the cracking bending moment;
M_{cs} is the fictitious (shrinkage-induced) bending moment (see page 59);
M_{ext} is the external bending moment;
N_{cs} is the fictitious (shrinkage-induced) axial force (see page 54);
$\overline{N}_{cs}$ is the effective fictitious (shrinkage-induced) axial force (see page 55);
P is the short-term external axial load;
RH is the relative humidity;
T is the time level (see page 93);
dU is the energy stored in an elastic body (see page 21);
W is the water content;
W/C is the water-to-cement ratio;
$X_{\Delta,1/2}$ is the sample median of the relative error Δ (see page 96);
a_2 is the cover depth of the compressive reinforcement;
b is the width of a section;
b_i is the width of the i-th layer;
d is the effective depth of a section;
f_c' is the specified cylinder compressive strength of concrete at test (see page 18);
f_{cm} is the 28-day mean compressive cylinder strength of concrete (see page 18);
$f_{cm,cube}$ is the 28-day mean compressive cube strength of concrete (see page 18);
f_{ck} is the characteristic concrete compressive strength;
f_{cp} is the compressive prism strength of concrete (see page 48);
f_{ct} is the tensile strength of concrete;
$f_{ct,cs}$ is the modified tensile strength of concrete (see page 57);
$f_{ct,n}$ is the characteristic tensile strength of concrete (see page 48);
f_{cu} is the compressive cube strength of concrete at test;
f_r is the modulus of rupture (see page 47);

f_{su} is the ultimate strength of steel;
f_{sy} is the yield strength of steel;
f_y is the yield strength;
h is the height of a section;
h_0 is the average thickness of a member (see page 149);
l_0 is the span of a flexural member;
l_D is the measurement length of surface strain;
m_Δ is the sample mean of the relative error Δ (see page 95);
n is the number of test points in the statistical analysis;
n' is the number of test points in the statistical analysis after sliced data transformation;
p is the reinforcement ratio;
s is the transfer length (see page 30) or the factor depending on a loading case covering the shape of moment distribution (see page 46);
s_Δ is the sample standard deviation of the relative error Δ;
s_Δ^2 is the sample variance of the relative error Δ (see page 95);
t is the age of specimen or t-statistics (*Student's*);
Δt is the time interval measured from start of loading or drying (see pages 151, 153);
t_i is the thickness of the i-th layer;
t_s is the age of specimen at beginning shrinkage;
u_α is the point of a standard normal inverse cumulative distribution function;
w is the crack width;
w_c is the critical crack width;
y_c is the coordinate of centroid of plain concrete net section;
y_i is the distance of the i-th layer from the top edge of the section;
y_{RC} is the coordinate of centroid of reinforced concrete section;
Δ is the relative error of prediction (see pages 94, 103);
α is the confidence (significance) level;
β is the bond factor (see page 38) or strain parameter (see page 44);
δ is the mid-span deflection;
δ_k is the prediction error obtained at the k-th iteration (see page 68);
δ_k' is the first derivation of the prediction error obtained at the k-th iteration (see page 69);
ε is the strain;
ε_c , ε_{cc} is the strain of compressive concrete;
$\varepsilon_{c,cs}$ is the shrinkage-induced strain of concrete in a reinforced concrete member (see page 41);
$\varepsilon_{c,ult}$ is the ultimate strain of compressive concrete;
$\varepsilon_{c,\sigma}$ is the strain in compressive due to acting stress (see page 55);
ε_{cr} is the tensile strain capacity;
ε_{creep} is the shrinkage-induced creep strain;
ε_{cs} is the shrinkage strain of concrete;

$\overline{\varepsilon}_{cs}$ is the effective shrinkage strain of concrete (see pages 55, 61);
ε_{el} is the elastic strain;
ε_{pl} is the plastic strain;
ε_s is the strain of steel;
ε_{sm} is the mean strain of tensile reinforcement;
$\varepsilon_{s,cr}$ is the tensile reinforcement strain in the cracked section (see page 48);
$\varepsilon_{s,cs}$ is the shrinkage-induced strain of a reinforced concrete member (see pages 41, 54);
ε_t , ε_{ct} is the strain of tensile concrete;
$\varepsilon_{t,ult}$ is the ultimate strain of tensile concrete;
ε_y is the yielding strain;
κ is the curvature;
μ_Δ is the expectation of the relative error Δ ;
$\xi_{\Delta,1/2}$ is the median of the relative error Δ ;
ρ_c is the density of concrete (see page 19);
σ is the stress;
σ_Δ^2 is the variance of the relative error Δ ;
σ_c , σ_{cc} is the stress of compressive concrete;
$\sigma_{c,cs}$ is the shrinkage-induced stress in concrete;
σ_s is the stress of steel;
σ_t , σ_{ct} is the stress of tensile concrete;
σ_{ult} is the ultimate stress;
τ , t_0 is the age of specimen at loading;
φ is the creep factor;
φ_{nl} is the non-linear notional creep coefficient (see page 149);
χ is the ageing coefficient;
χ^2 is the χ -*square* statistics;
ψ_s is the tension-stiffening factor (see page 48);

Abbreviations

ANOVA procedure of analysis of variance;
GFRP glass fibre reinforced polymer;
FE finite element;
FPZ fracture process zone;
HPC high-performance concrete;
HSC high-strength concrete;
LEFM linear elastic fracture mechanics;
MRA modified running-average;
RC reinforced concrete.

Contents

[1]The annexes are supplied in the enclosed compact disc

List of Figures

[*]The reference is given in the list of publications by the author on the topic of the dissertation

List of Tables

Introduction

Concrete is by far (and for a long time still to come) the material most widely used in the world: the range of performance (physical and mechanical) it can provide continues to grow. Because of the extensive research work carried out in different countries, the ultimate load behaviour of flexural members is now quite well understood. Due to the use of the refined ultimate state theories as well as high strength concrete and reinforcement, resulting in longer spans of and smaller depths, the serviceability criteria often limits the use of modern RC superstructures. Cracking and deformations must be controlled to secure serviceability of such structures. Shrinkage deformations are one of major causes of defects in bridge structures in all over the world. Often the failure mechanism starts with the formation of transverse cracks from shrinkage and overloads. Various factors that influence the behaviour of the shrunk members (such as concrete mixture proportions and material properties, method of curing, ambient temperature and humidity conditions, and geometry of the concrete element) need to be taken into account during the construction of concrete structures.

In structural analysis, civil engineers can choose between traditional design code methods and numerical techniques. Although design code methods ensure safe design, they do not reveal the actual stress-strain behaviour of cracked structures and often lack physical interpretation. Numerical methods are based on universal principles and can include material nonlinearities.

Cracking and tension-stiffening parameters probably have the most significant effect on results of numerical modelling of flexural concrete elements subjected to short-term loading. Tension-stiffening effects usually need to be included in such analysis. In order to choose a particular calculation method, engineers should be aware of accuracy of different techniques.

Reasons for Investigation

Concrete structural components exist in buildings and bridges in different forms. Understanding the response of these components during loading is crucial to the development of an overall efficient and safe structure. Numerical methods, which were rapidly progressing within last four decades, can include all possible effects such as material nonlinearities, concrete cracking, creep and shrinkage, reinforcement slip, etc, being responsible for complexity of this material. However, the progress is mostly related to the development of mathematical apparatus, but not material models, or in other words, the development was rather qualitative than quantitative. Constitutive relationships often are too simplified and do not reflect complex nature of the material.

Composite action of tensile and compressive steel, compressive concrete and tensile concrete is responsible for deformational behaviour of RC members. Modelling stress-strain relationship for steel is simple. A large number of stress-strain relationships have been proposed for compressive concrete, however these relationships result in similar deformation predictions for flexural members providing a constant concrete modulus of elasticity was assumed. Adequate modelling of RC cracking and, particularly, post-cracking behaviour, as one of the major sources of nonlinearity, is the most important and difficult task of deformational analysis. In smeared crack approach dealing with average cracking and strains, post-cracking effects can be modelled by a stress-strain tension-stiffening relationship attributed to tensile concrete. Two main deficiencies can be noted concerning most known tension-stiffening relationships:

- Tension-stiffening relationships were derived using test data of tension or shear RC members. Subsequently, these constitutive laws were applied for modelling of bending elements which behaviour differs from tension or shear members.
- The RC members employed for deriving the constitutive laws had been exposed to shrinkage. Therefore, tension-stiffening was coupled with shrinkage effect.

While being confident about sufficient accuracy of deflection analysis of structures with moderate or large amounts of reinforcement, investigators often

raise concerns about the validity of chosen tension-stiffening parameters for lightly reinforced members. Complexity of the issue is indicated by the widespread use of different code techniques and disparity of their prediction results. To check accuracy of the predictive models, very few reports on accurately performed tests of lightly reinforced flexural members are available.

Present research is dedicated to developing a technique for deriving a *free-of-shrinkage* tension-stiffening relationship using test data of shrunk bending RC members.

Research Object

The *object* of present study is deformation behaviour of shrunk RC members subjected to short-term loading.

Main Objective and Tasks

The main *objective* is to investigate shrinkage influence on deformations and tension-stiffening of RC members subjected to short-term loading. In order to achieve the objective, the following problems had to be solved:

1. To review empirical and numerical techniques of deformation analysis of RC members as well as material models with the emphasis on shrinkage and tension-stiffening effects.
2. To develop a *Layer* section model for deformation analysis of cracked RC members subjected to short-term loading taking into account shrinkage and accompanying creep effect.
3. To propose a numerical procedure for deriving a *free-of-shrinkage* tension-stiffening relationship using test data of shrunk flexural members.
4. To investigate experimentally concrete shrinkage effect on cracking resistance, tension-stiffening and short-term deformations of lightly reinforced beams.
5. To derive *free-of-shrinkage* tension-stiffening relationships using the proposed procedure and the test data.
6. To collect test data on free shrinkage strain of plain concrete specimens and deflections of RC bending members.
7. To develop a statistical procedure for checking adequacy of theoretical predictions to the test data taking into account inconsistency of the data.

8. To perform comparative statistical analysis of various free shrinkage and deflection/curvature prediction models using the proposed statistical procedure and the collected test data.

Research Methods

To investigate the *object*, the following *research methods* are chosen:

- *Action*: theoretical (analysis and synthesis) study should be performed to improve strategies in order to find the solution of the problem.
- *Classification*: summarising strength, weaknesses and gaps of literature, the dissertation research object should be recognized and understood.
- *Experience*: the solution of the problem should be found being guided using intuition and experience.
- *Experimental*: the hypothesis should be tested by taking a practical test.
- *Statistical*: conclusions should be drawn collecting, analysing and explaining the statistical data.

Scientific Novelty and Originality

The aspects of scientific novelty on theoretical and experimental investigation of shrinkage influence on deformations of RC members and tension-stiffening effect are as follows:

1. As a very limited number of tests on deformation behaviour of lightly reinforced concrete beams have been reported so far, new experimental data has been obtained on cracking resistance, tension-stiffening and short-term deformations of such members. Tests on eight beams (four couples of twin specimens) having constant reinforcement ratio 0,4%, but different bar diameter have been carried out. Prior to the tests of the beams, measurements on concrete shrinkage and creep were performed.
2. An *innovative* numerical procedure has been proposed for deriving *free-of-shrinkage* tension-stiffening relationships using test data (moment-curvature relationships) of flexural RC members. The proposed procedure based on *Layer* approach combines *direct* and *inverse* techniques. In the *direct* technique, moment-curvature diagrams are calculated for assumed material stress-strain relationships. The *inverse* technique proposed by the supervisor of present dissertation is aimed at determining tension-stiffening relationships from flexural tests of RC members. Shrinkage is eliminated by assuming reverse (expanding) shrinkage strain. A simple

transformation formula has been proposed for symmetrically reinforced tension and bending members for deriving a *free-of-shrinkage* tension-stiffening relationship.

3. The proposed numerical procedure has been applied to the test data for deriving *free-of-shrinkage* tension-stiffening relationships. For beams of same reinforcement ratio, it was shown that tension-stiffening was more pronounced in those with a larger number of tensile reinforcing bars.
4. A statistical procedure has been proposed for checking adequacy of theoretical predictions to the test data taking into account inconsistency of the data. The proposed procedure based on grouping of statistical data allows obtaining results that are more reliable. Using the proposed procedure, a comparative analysis has been carried out to assess accuracy of predictions of free shrinkage strains occurring at relatively early age of concrete (up to 150 days). Similar analysis has been performed for deflection/curvature predictions by different code and numerical methods.

Basic Statements to be Defended

The following statements based on the results of present investigation may serve as the official hypotheses to be defended:

1. The numerical technique proposed allows eliminating shrinkage and associated creep effects from moment-curvature and tension-stiffening relationships.
2. The developed statistical procedure for assessing accuracy of predictions takes into account inconsistency of the test data.
3. Accuracy of deflection/curvature predictions by design codes and numerical techniques vary for different ranges of reinforcement ratio and load intensity.
4. To obtain more accurate predictions of short-term deflections, shrinkage should be taken into account. Tension-stiffening has to be modelled by a *free-of-shrinkage* relationship.
5. *Layer* section model secures reasonable accuracy of deflection predictions of RC members applying a simplified linear tension-stiffening relationship and taking into account shrinkage effect. Tensile strength of concrete and the ultimate strain are considered as the most important parameters of this relationship.

Participation in Research Projects

The author has participated in five research projects:

International Projects

- 2006–2010: *Urban Habitat Constructions under Catastrophic Events*, funded by the EU under the *COST action C26*. Participation as a member of the Managing Committee.
- 2002–2006: *UPTUN – Cost-Effective, Sustainable and Innovative Upgrading Methods for Fire Safety in Existing Tunnels*, funded by the EU under the programme *FRAMEWORK 5*. Participation as a researcher.

National Projects

- 2009: *Constitutive Model for Stress-Strain Analysis of Fibre Reinforced Concrete Members* (*Dispersiškai armuotų gelžbetoninių elementų įtempių ir deformacijų modelis*), funded by the *Lithuanian State Fund of Research and Studies*. Participation as a researcher.
- 2008: *Constitutive Model for Reinforced Concrete Members Taking into Account Concrete Creep and Shrinkage at Pre-Loading Stage* (*Gelžbetoninių elementų deformacijų modelis, įvertinantis betono susitraukimą ir valkšnumą ikieksplotacinėje stadijoje*), funded by the *Lithuanian State Fund of Research and Studies*. Participation as a researcher.
- 2005: *New Method for Deformation Analysis of Reinforced Concrete Structures* (*Naujo inžinerinio gelžbetoninių elementų deformacijų skaičiavimo metodo kūrimas*), funded by the *Lithuanian State Fund of Research and Studies*. Participation as a researcher.

Reporting Results at Scientific Conferences

The author has made 29 presentations at 18 scientific conferences:

2008

- The Eighth International Conference *Creep, Shrinkage and Durability of Concrete and Concrete Structures* (*ConCreep 8*), Ise-Shima, Japan.
- The Sixth International Conference *Analytical Models and New Concepts in Concrete and Masonry Structures* (*AMCM'2008*), Lodz, Poland.

- The International Symposium *Urban Habitat Constructions under Catastrophic Events*, Valetta, Malta.

2007

- The International ***fib*** Conference *Fire Design of Concrete Structures*. Coimbra, Portugal.
- The Ninth International Conference *Modern Building Materials, Structures and Techniques*, Vilnius, Lithuania.
- The International COST-C26 Workshop *Urban Habitat Constructions under Catastrophic Events*, Prague, Czech Republic.

2006

- The Ninth International *Fatigue Congress*, Atlanta, USA.
- The Lithuanian Conference *Building Constructions – Design of Civil Engineering Constructions using Eurocode*, Vilnius, Lithuania.
- The Ninth Lithuanian Conference of Young Scientists *Science – Future of Lithuania*, Vilnius, Lithuania.

2005

- The ***fib*** Symposium *Structural Concrete and Time*, La Plata, Portugal.
- The Eleventh International Scientific and Practical Conference of Students, Post-Graduates and Young Scientists *Modern Techniques and Technologies* (*MTT 2005*), Novosibirsk, Russia.
- The Sixth International Conference *Computational Modelling 2005*, St. Petersburg, Russia.
- The Eighth Lithuanian Conference of Young Scientists *Science – Future of Lithuania*, Vilnius, Lithuania.

2004

- The Tenth International Conference *Computing in Civil and Building Engineering* (*ICCCBE-X*). Weimar, Germany.
- The Eighth International Conference *Modern Building Materials, Structures and Techniques*. Vilnius, Lithuania.
- The Forty Third International Conference *Actual Problems of Strength*, Vitebsk, Byelorussia.

- The International Conference *MSC.Software: Complex Technologies of Virtual Products Development*, Moscow, Russia.
- The Seventh Lithuanian Conference of Young Scientists *Science – Future of Lithuania*, Vilnius, Lithuania.

Structure of the Dissertation

Structure of the dissertation is sketched in Fig. 1. The dissertation is structured around four main chapters.

Chapter 1 reviews material models in regard to deformation behaviour of RC members. Although the study deals with deformations of members subjected to short-term loading, shrinkage and associated creep effects are taken into account. Various models of free shrinkage and creep have been presented. Shrinkage influence on crack resistance and deformations of RC members has been discussed. Experimental investigations of tension-stiffening and deformations of RC members have been reviewed. Different approaches in tension-stiffening and methods of deflection analysis of RC members have been observed. Chapter 1 concludes in formulating of main objective and tasks of present investigation.

Chapter 2 investigates shrinkage influence on tension-stiffening and stress-strain state of RC members subjected to short-term loading. An *innovative* numerical procedure has been proposed for deriving *free-of-shrinkage* tension-stiffening relationships using test data of bending RC members. The procedure combines *direct* and *inverse* techniques of analysis of RC members. Annex B presents computer codes of above techniques using *MATLAB*. Chapter 2 also discusses the computational aspects of convergence of the *inverse* procedure.

Chapter 3 presents experimental investigation results on cracking, tension-stiffening and deformations of 8 lightly reinforced concrete beams subjected to short-term loading. Prior to the beam tests, measurements on concrete shrinkage and creep were performed. Based on the numerical procedure discussed in Chapter 2, *free-of-shrinkage* tension-stiffening relationships were derived from the moment-curvature diagrams of the beam specimens. Annex C gives experimental measurements of curvature and deflections of the beam specimens.

Chapter 4 presents a statistical procedure for assessing accuracy of predictions taking into account inconsistency of test data. Results of statistical analyses on predictions by various techniques (reviewed in Chapter 1 and Annex A) of free shrinkage strain and deflections/curvatures of RC members have been discussed.

General conclusions as well as recommendations for further research summarises the present study. It is followed by an extensive list of references and a list of 34 publications by the author on the topic of the dissertation.

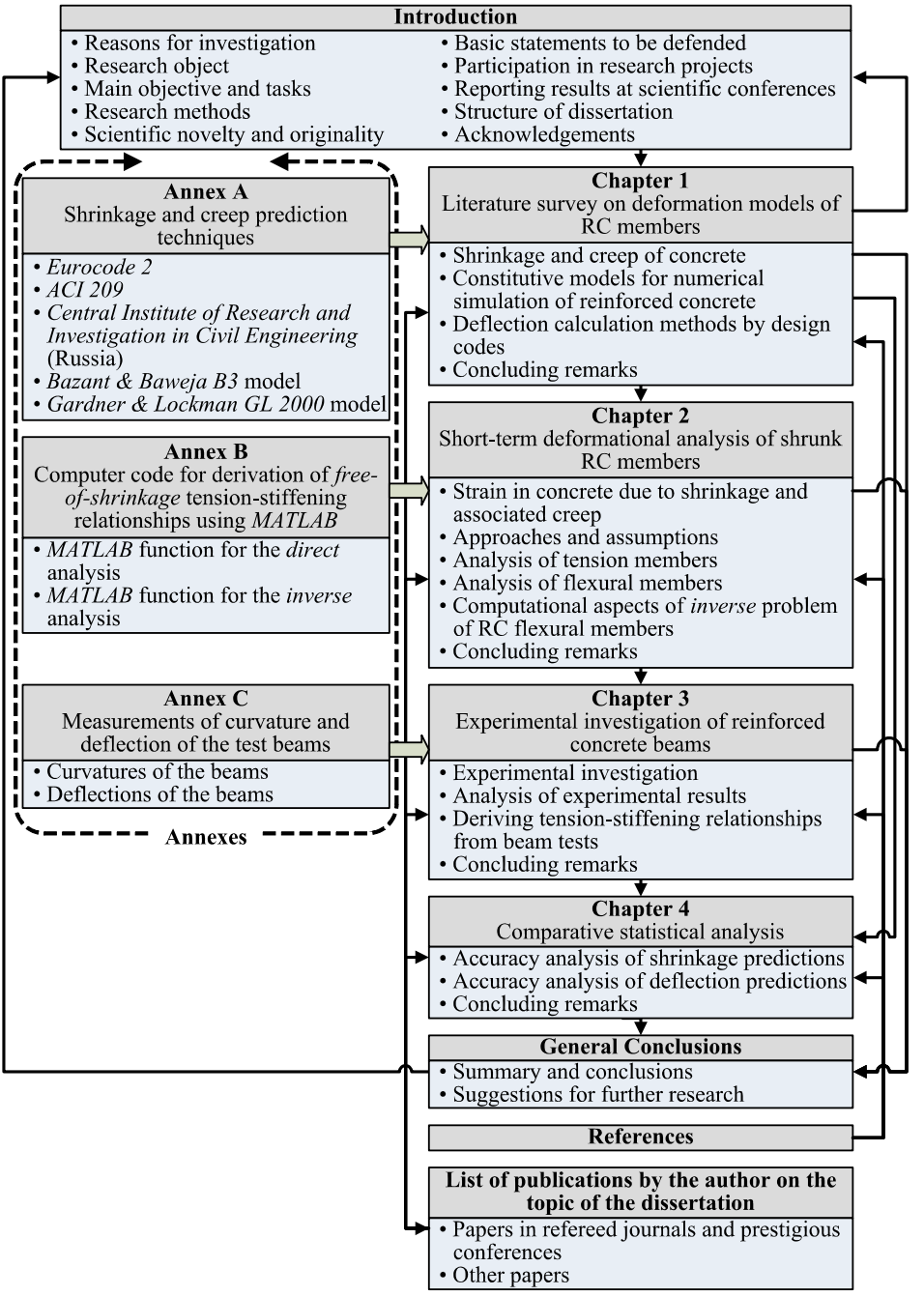

Fig. 1. Structure of the dissertation

Dissertation without annexes consists of 146 pages. Count of equations, figures and tables in all Chapters is given in Table 1.

Table 1. Content of the dissertation (excluding Annexes)

Chapters	**Numbered equations**	**Figures**	**Tables**
Introduction	0	1	1
Chapter 1	13	17	4
Chapter 2	25	18	1
Chapter 3	2	13	6
Chapter 4	21	7	9
General conclusions	0	0	0
Total count	**61**	**56**	**21**

Acknowledgements

The author expresses his deepest gratitude and acknowledgement to his supervisor, Professor *Gintaris Kaklauskas*, Head of the *Department of Bridges and Special Structures* of *Vilnius Gediminas Technical University*, for providing a great deal of guidance and assistance along the way.

Special gratitude and thanks are due to Dr. *Darius Bacinskas*, Associate Professor at *Vilnius Gediminas Technical University*, for his help and friendship throughout this research.

The financial support provided by the *Lithuanian State Fund of Research and Studies*, and by the complementary financial support provided by the *Agency of International Programs of Scientific and Technology Development in Lithuania* is gratefully acknowledged.

1

Literature Survey on Deformation Models of RC Members

This Chapter reviews material models in regard to deformation behaviour of RC members. Although present investigation deals with deformations of members subjected to short-term loading, shrinkage and associated creep effects are taken into account. Various models of free shrinkage and creep are presented. Shrinkage influence on crack resistance and deformations are discussed. Experimental investigations of cracking, tension-stiffening and deformations of RC members are reviewed. Different approaches in tension-stiffening and methods of deflection analysis of RC members are observed. This Chapter concludes in formulating of main objective and tasks of present investigation.

1.1. Shrinkage and Creep of Concrete

1.1.1. Physical Phenomena

1.1.1.1. Shrinkage of Concrete

The four main types of shrinkage associated with concrete are plastic shrinkage, autogenous shrinkage, carbonation shrinkage, and drying shrinkage. *Plastic*

shrinkage is associated with moisture loss from freshly poured concrete into the surrounding environment. *Autogenous shrinkage* is the early shrinkage of concrete caused by loss of water from capillary pores due to the hydration of cementitious materials, without loss of water into the surrounding environment. This type of shrinkage tends to increase at lower water to cementitious materials ratio and at a higher cement content of a concrete mixture. *Carbonation shrinkage* caused by the chemical reactions of various cement hydration products with carbon dioxide present in the air. *Drying shrinkage* is a volumetric change caused by the movement and the loss of water squeezing out from the capillary pores since the internal humidity attempts to make uniform with a lower environmental humidity. *Gribniak et al*. (2007a, 2008)* carried out a comprehensive investigation on various aspects of shrinkage.

The magnitude of shrinkage deformations depends on concrete mixture proportions and material properties, method of curing, ambient temperature and humidity conditions, and geometry of the concrete element. *Tremper* (1961) has pointed out these factors affecting the overall shrinkage of concrete:

- Characteristics of the cement. The proportion of gypsum added to the clinker during grinding has a large effect on shrinkage.
- Clay-like particles and coating on aggregates increase drying shrinkage.
- Aggregates, even though clean, vary in their contribution to drying shrinkage. Aggregates of high absorption tend to produce greater shrinkage.
- There is a general relationship between drying shrinkage and unit water content. This statement is compatible with that restraint to shrinkage is proportional to the absolute volume of aggregate. Aggregates of smaller maximum size require more mixing water and produce more shrinkage.
- Higher slump require more water and produce greater shrinkage.
- The higher the temperature of concrete at the time of mixing, the greater the quantity of water required to produce a given slump.
- Concrete that held in a transit mixer with the drum rotating beyond 70 revolutions, the minimum required to produce thorough mixing, requires more mixing water because of the formation of dust of abrasion and the absorption of heat of work.
- Admixtures have effects on shrinkage. Water-reducing retarders that have been compounded to destroy the retarding effect, as a class, appear to produce the greatest increase in drying shrinkage.

Generally only two shrinkage components (drying and autogenous) taken into account into structural analysis of concrete members. Figure 1.1 schematically illustrated the ratio of autogenous and drying components in total shrinkage of concrete (Gribniak *et al*. 2007a)*. In the case of normal-strength concrete,

*The reference is given in the list of publications by the author on the topic of the dissertation

shrinkage may be treated without distinguishing between autogenous and drying shrinkage because for such concrete autogenous shrinkage strain varies between 20 and 110 micro-strains. This is only 10 to 20% of the long-term shrinkage (Silliman & Newtson 2006).

Consequently, autogenous shrinkage was neglected for many years. On the other hand, in the case of high-strength concrete (HSC), autogenous and drying shrinkage should be distinguished because the ratio of these shrinkages to total shrinkage varies with respect to age when concrete is exposed to drying conditions (Sakata & Shimomura 2004). *Persson* (2001) and *Miller et al*. (2006) reported results of more recent investigations on various aspects of shrinkage.

The term *free shrinkage* commonly used for the contraction of hardened concrete exposed to air, with relative humidity less than 100%. Free shrinkage develops gradually with time; the word *free* refers to the case of a member that can shorten without any restraint, thus producing no stresses. Typically, for ordinary concrete about 40 and 90% of the ultimate shrinkage will have occurred after 1 and 12 months, respectively (Gribniak *et al*. 2007a)*.

One of major properties of concrete elements that concrete shrink as it dries under ambient conditions. Tensile stresses in concrete occur when free shrinkage is restrained. The combination of high tensile stresses with low fracture resistance of concrete often results in cracking. This cracking reduces the durability of a concrete structure (El-Babry & Ghali 2001). Several factors are known to affect element's cracking including structural design, concrete mixture design and mixture materials, placing, finishing and curing practices. It has been shown that the primary source of the bridge's deck cracking is attributed to a combination of shrinkage and thermal stresses, which are influenced by above factors (Gribniak *et al*. 2007a)*. The cracking phenomena will be observed in Section 1.2.3.

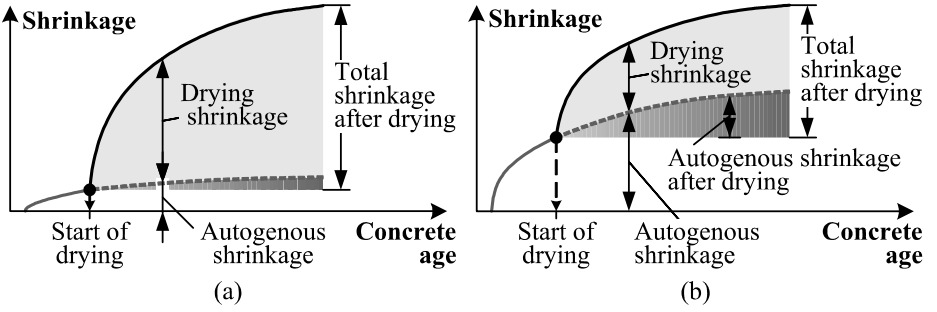

Fig. 1.1. Shrinkage strain components in normal (a) and high-strength (b) concrete (Gribniak *et al.* 2007a)*

*The reference is given in the list of publications by the author on the topic of the dissertation

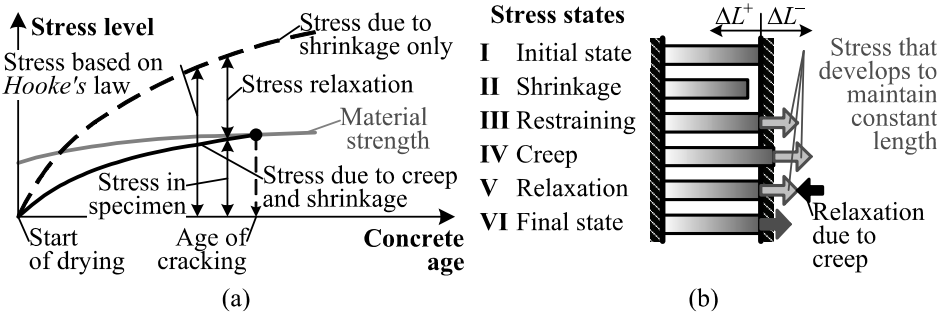

Fig. 1.2. Shrinkage-induced stresses in a restrained concrete member (Weiss 1999): stress development (a) and creep relaxation (b)

Figure 1.2a compares development of the time dependent strength (cracking resistance) and shrinkage-induced stresses. If strength and residual stress development is as shown in Fig. 1.2a, it is likely that the specimen will crack when these two lines intersect. Similarly, if strength of the concrete is always greater than the developed stresses, no cracking will occur.

The residual shrinkage-induced stress that develops in concrete because of restraint may sometimes be difficult to quantify. This residual stress cannot be calculated directly by multiplying the free shrinkage strain by the elastic modulus (i.e., *Hooke's* law) since stress relaxation occurs. Stress relaxation is similar to creep, however while creep can be thought of as the time dependent deformation due to sustained load, stress relaxation is a term used to describe the reduction in stress under constant deformation. This reduction of stress is illustrated in Fig. 1.2b in which a specimen of original length (I) is exposed to drying and a uniform shrinkage strain develops across the section. For unrestrained specimen, the applied shrinkage would cause the specimen to undergo a change in length of ΔL^+ (II). To maintain the condition of perfect restraint (i.e., no length change), a *fictitious* load can envision to be applied (III). However, it should be noted that if the specimen was free to displace under this fictitious loading the length of the specimen would increase (due to creep) by an amount ΔL^- (IV). Again, to maintain perfect restraint (i.e., no length change) an opposing fictitious stress is applied (V) resulting in an overall reduction in shrinkage stress (VI). This illustrates that creep can play a very significant role in determining the magnitude of stresses that develop at early ages and has been estimated to relax the stresses by 30% to 70% (Weiss 1999).

1.1.1.2. Creep of Concrete

Creep of concrete may be separated into two components: *basic creep* and *drying creep*. *Basic creep* occurs in a sealed condition, without any exchange of

water between the concrete and its surroundings. *Drying creep* involves water movement to the surrounding environment. The creep experienced by the innermost region of a large concrete member is predominantly basic creep, since very little water is lost to the outside environment.

Totally, the water contents of concrete plays an essential role in creep: concrete, which has dried to the state where evaporable water has been eliminated, is not subject to creep. Completely two mechanisms are apparent from kinetic analysis of *basic creep* for pure cement pastes (Guénot-Delahaie 1997) and concretes (Acker & Ulm 2001). Both mechanisms are compatible with the mobility of water. The short characteristic time of the first mechanism about 10 days suggests a stress-induced water movement towards the largest diameter pores (characteristic distance of the order of 0,1–1 mm). This short-term creep mechanism was first suggested by *Ruetz* (1966), and pursued by *Wittmann* (1982). The second mechanism corresponds to an irreversible viscous behaviour. This long-term creep occurs under almost constant volume, which is consistent with a viscous slippage mechanism (Ulm *et al*. 1999).

Drying creep, also called the *Pickett effect*, is the increase in creep observed in specimens undergoing drying (Pickett 1942). The interpretation of the excess deformation and its mechanisms has been a matter of controversy among researchers, and several hypotheses have been presented over the last 70 years to explain this effect (Altoubat & Lange 2002). Two major views exist in the literature regarding the *Pickett effect*. One explains the excess deformation by apparent mechanisms related to shrinkage-induced stresses and associated cracking (Wittmann & Roelfstra 1980), and the second considers real mechanisms by which creep interact with drying (Bažant & Chern 1985 and Bažant & Xi 1994). However, neither of the views alone fully explains the phenomenon, and a combination of the two views has prevailed in the literature. Drying creep is now widely understood to be the sum of at least two components, an intrinsic drying creep with its own mechanisms and a structural drying creep resulting from micro-cracking effect due to the non-uniformity of drying in the concrete specimen. There was no experimental data in the literature that clearly differentiated the different mechanisms of drying creep until the study of *Bažant & Xi* (1994). The authors found that drying creep has two sources: micro-cracking and stress-induced shrinkage. The latter was found to increase continuously, whereas the former first increases and then decreases. The basic design of their experiment limited its applicability to compressive creep, and was not adapted for tension. Thus, there are no available test data on the different mechanisms of tensile drying creep, and the contribution of each mechanism is still a matter of research.

At the initial stage of drying, the surface layer of the specimen shrinks more than the inner layers. As a result, the surface layer undergoes tension that causes micro cracking. Due to the nonlinear inelastic behaviour and irrecoverable creep of concrete caused by the tensile stress, the micro cracks cannot fully close when

the moisture distribution finally approaches a uniform state. Consequently, the measured shrinkage of the drying specimen is always less than the true shrinkage. However, if the concrete specimen is under compression, the micro cracking effect is counteracted. Therefore, larger shrinkage will occur in the loaded specimen than in a free shrinkage specimen, which may falsely appear as creep by the traditional definition of creep. *Wittmann & Roelfstra* (1980) showed higher shrinkage in specimens loaded in compression than in unloaded specimens. This led *Wittmann* to suggest that tensile cracking might perhaps explain all of the excess deformation at drying. In contrast to the compression case, when the concrete specimen is under tension, the tensile load promotes the surface micro cracking and reduces the shrinkage below that of the free specimen. The increase in micro cracking by the tensile load led *Kovler* (1995) to question the effect of micro cracking as a mechanism of tensile drying creep. However, since tensile creep and shrinkage are opposite to each other in direction, we believe that the reduction in shrinkage of the tension specimen will falsely appear as an additional tensile drying creep. Thus, the effect of micro cracking remains explainable (Altoubat & Lange 2002).

Experimental results highlight that even thin cement paste specimen's exhibit drying creep strains (Thelandersson *et al.* 1988), although they not submitted to a prominent drying-induced cracking. Moreover, numerical simulations show that the micro cracking effect fails to retrieve alone the whole part of drying creep (Thelandersson *et al.* 1988). Therefore, many authors proposed an intrinsic mechanism to explain the additional part that could not be reproduced by micro cracking. Among them, one can find the seepage theory (Ruetz 1968 and Tamtsia & Beaudoin 2000), the stress-induced shrinkage (Bažant & Chern 1985 and Bažant & Xi 1994), the drying-induced creep (Kovler 1995), and the pore stress effect (Brooks 2001), or thermo pre-stress relaxation (Bažant *et al*. 1997). None of these theories has been universally accepted in the scientific community yet. The most used theory is probably the stress-induced shrinkage one, proposed by *Bažant & Chern* (1985). These authors suggested that simultaneous drying and loading cause micro-diffusion of water molecules between micropores and macro-pores. This enhances bond breakage in cement gel, which results in intrinsic drying creep strain.

Altoubat & Lange showed that the *Pickett effect* as in tension (2002) as in case of restrained concrete specimens (2001) has two sources: stress-induced shrinkage and micro cracking. The components of the *Pickett effect* are shown in Fig. 1.3a. In other words, tensile loads in a restrained concrete specimen subjected to drying reduce the shrinkage of the concrete with respect to the unloaded free shrinkage specimen. This reduction in shrinkage *Altoubat & Lange* (2001, 2002) called stress-induced shrinkage. The avoidance of shrinkage (reduction) reflects as a positive creep strain, i.e. the net difference between the

stress-induced shrinkage (no softening) and the micro cracking (softening) viewed as increase in tensile creep, and it explains the avoidance of shrinkage. *Altoubat & Lange* (2002) stated that in the external drying case, softening due to micro cracking is inevitable, and this softening reduces the contribution of the stress-induced shrinkage term. This suggests that micro cracking must have a different sign than stress-induced shrinkage (see Fig. 1.3a).

Another important aspect revealed by the analysis is the shrinkage behaviour under tensile stress. The total shrinkage under the tensile stress is equal to the free shrinkage plus the stress-induced shrinkage; typical results for the concrete shown in Fig. 1.3b. The results indicated that the tensile stress substantially reduced the shrinkage of concrete, and the assumption of equal shrinkage for restrained and unrestrained concrete is responsible in part for the observed extra creep deformation (*Pickett effect*). However, recent investigation on tensile creep by *Reinhardt & Rinder* (2006) indicates that shrinkage of loaded specimens is larger than of non-loaded ones. Latter phenomenon seems to be in agreement with *Powers'* creep theory (Powers 1965, 1968).

Wittmann (1993) has stated that the influence of stress on shrinkage of concrete is most likely sufficient to explain quantitatively the difference between shrinkage and creep when taking place separately, and shrinkage and creep when taking place simultaneously. The analytical results of this research indicated that the stress-induced shrinkage is a major mechanism of the *Pickett effect*, but not the only mechanism. On the other hand, the surface micro cracking formed a significant portion of this effect. The surface micro cracking profoundly influenced the time of first cracking and mechanical behaviour of restrained concrete.

Apparent creep induced by micro cracking forms a significant part of the tensile creep of plain concrete (Altoubat & Lange 2001, 2002). Thus, shrinkage does not depend only on the moisture diffusion and state of stress, but also on the strain softening (Bažant & Raftshol 1982, Alvaredo & Wittmann 1993).

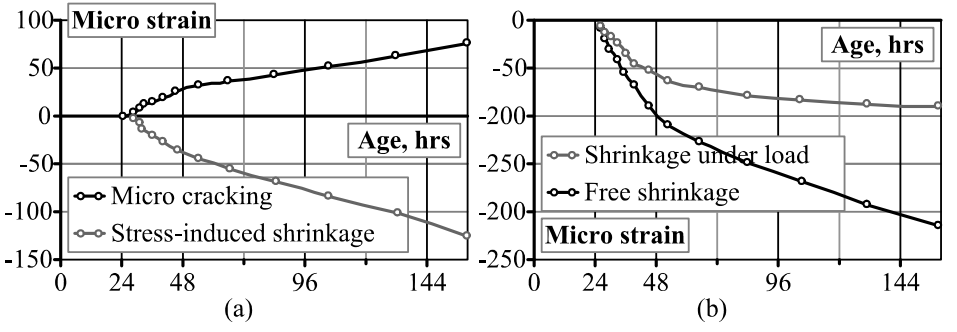

Fig. 1.3. Components of the *Pickett* effect (drying creep) (a) and effect of tensile stress on shrinkage (b) (Altoubat & Lange 2002)

1.1.2. Shrinkage and Creep Prediction Techniques

Since 1990, there have been numerous shrinkage and creep prediction models put forward, generally by three main contributors; the *Comité Euro International du Béton* (CEB), the *American Concrete Institute* (ACI), and *Réunion Internationale des Laboratoires d'Essais et de recherche sur les Matériaux et les Constructions* (RILEM). Present study discusses accuracy of five predictions models, namely the *Eurocode 2*, *ACI 209*, *Central Institute of Research and Investigation in Civil Engineering* (*CNIIS*, Russia), *Bažant & Baweia* (*B3*) and *Gardner & Lockman* (*GL 2000*). These calculation techniques are listed in Annex A.

Modulus of elasticity (*Young*'s modulus) of concrete is one of major input parameter of material models (Howells *et al*. 2005, Pintea *et al*. 2008*). It is defined as the tangent modulus of elasticity at the origin of the stress-strain diagram. The tangent modulus E_c is approximately equal to the secant modulus E_{cm} of unloading which is usually measured in tests ($E_c \approx 1,05 \cdot E_{cm}$). Table 1.1 presents formulas for deriving of modulus of elasticity according to some design codes. In this table E_{cm} is the secant modulus defined as the slope of the line drawn from zero stress to a stress $0,4 \cdot f_{cm}$ or $0,45 \cdot f_c'$ for the *Eurocode 2* and the *ACI* approaches, respectively; E_0 is the asymptotic modulus introduced in the *B3* model; f_{cm} and $f_{cm,cube}$ are the 28-day mean compressive cylinder and cube strength (class of concrete $B \approx 0,778 \cdot f_{cm,cube}$, $f_{cm,cube} \approx 1,25 \cdot f_{cm}$), respectively; f_c' is the specified cylinder compressive strength at test. *ACI Committee 209* (2008) recommended taking into consideration influence of concrete density ρ_c on secant modulus E_{cm} (see Table 1.1).

The *Young*'s modulus evolves substantially with the hardening of the material and it increases from zero to a value near its service value. Similarly as the compressive strength, it can be regarded as a monotonically increasing continuous function of the maturity of the concrete (Acker & Ulm 2001). Elastic modulus at time *t*, $E_{cm}(t)$, can be determined by the equation (CEN 2004):

$$E_{cm}(t) = (\beta_{cc})^{0,3} E_{cm}, \quad \beta_{cc} = \exp\left\{s\left[1 - \sqrt{28/t}\right]\right\}. \tag{1.1}$$

Here *t* is the age of the concrete (days); *s* is a coefficient which depends on the type of cement (for normal cement is equal to 0,25).

The *Young*'s modulus of concrete depends on the type of the aggregate, the curing conditions and the test method. The influences of these factors are largely responsible for the significant scatter that can be observed when experimental values of the modulus of elasticity are plotted against the concrete strength (Takács 2002: 14). Applying the measured elastic modulus into analysis may improve the deformation prediction or may corrupt it (Takács 2002: 30).

*The reference is given in the list of publications by the author on the topic of the dissertation

Table 1.1. Formulas for modulus of elasticity of concrete

Design method	***Young*'s modulus [MPa]**
Eurocode 2 (CEN 2004)	$E_{\mathrm{cm}} = 22000\left(0{,}1\cdot f_{\mathrm{cm}}\right)^{0{,}3}$
CEB-FIP Model Code 1990 (CEB-FIP 1991)	$E_{\mathrm{cm}} = 9980\sqrt[3]{f_{\mathrm{cm}}}$
ACI 318 (2008)	$E_{\mathrm{cm}} = 4734\sqrt{f_{\mathrm{c}}'}$
ACI 209 (2008)	$E_{\mathrm{cm}} = 0{,}043\sqrt{\rho_{\mathrm{c}}^{3} f_{\mathrm{c}}'}$
SP 52-101 (Russian code) (NIIZhB 2006)	$E_{\mathrm{c}} = 54300\cdot B/\left(21+B\right)$
B3 (Bažant & Baweja 1995a, 1995b)	$E_0 = 7890\sqrt{f_{\mathrm{cm}}}$
GL 2000 (Gardner 2004)	$E_{\mathrm{cm}}\left(t\right) = 3500 + 4300\sqrt{f_{\mathrm{cm}}\left(t\right)}$

1.1.3. Shrinkage and Creep Models in Comparison

Test results on shrinkage and creep are marked with large scatter, at least from the perspective of existing approach in modelling. The prediction model parameters and corresponding limitations are presented in Table 1.2. In this table A/C is the aggregate-to-cement ratio; W/C is the water-to-cement ratio; τ or t_{s} are the age of concrete at loading and beginning shrinkage, respectively.

The shrinkage strain and the creep compliance given by the theoretical models are seen as the expected average value of the responses and the prediction is characterised by the corresponding measure of variation. Consequently, the structural response should be considered as a statistical variable rather than a deterministic value (Kudzys *et al*. 2004). The expected statistical variation has to be taken into account in the structural design. The reported coefficient of variation is 35% for the shrinkage strain and 20% for the creep compliance for the *MC 90* (CEB-FIP 1991). The same values are 34% and 23% for the *B3* model (Bažant & Baweja 1995a, 1995b).

Al-Manaseer & Lakshmikantan (1999) performed a comparison of creep prediction models. The analysis showed that the *Eurocode 2*, *ACI 209* and *B3* models overestimated the creep for 39%, 23% and 42% of the total number of data points, respectively. The mean coefficient of variation for the residuals for the *Eurocode 2*, *ACI 209* and *B3* models were 31%, 39% and 32%, respectively.

Meyerson et al. (2002) carried out a comprehensive investigation on accuracy of shrinkage and creep prediction models. It has been shown that the *Eurocode 2* predicts the creep and shrinkage strain of concrete with the best accuracy. *Al-Manaseer & Lam* (2005) performed comparative analysis of shrinkage and creep models using experimental data from *RILEM Data Bank*. It has been

found that *B3* is the best model to predict shrinkage and creep effects, *Eurocode 2* predictions of creep were also considered accurate.

Schellenberg et al. (2005) compared the creep and shrinkage predictions made by *Eurocode 2* and *ACI 209*. It has been stated that the differences between codes can be significant in the early stages of construction. For longer periods there was found no essential difference between predictions. It has been pointed out that the moist importance is taking the shrinkage and creep effects into consideration, while it is only secondary importance which code is applied.

Table 1.2. Limits of variables in creep and shrinkage prediction models

Variable	***Eurocode 2***	***ACI 209***	***CNIIS***	***B3***	***GL 2000***
f_{cm} [MPa]	20–90(120)	–	13–67	17–69	20–82
A/C	–	–	–	2,5–13,5	–
Cement [kg/m^3]	–	–	–	160–720	–
W/C	–	–	–	0,35–0,85	–
RH [%]	40–100	40–100	≤ 90	40–100	40–100
Cement type	N, S or R	N or R	–	N, S or R	N, S or R
τ or t_s (moist cured)	–	≥ 7 days	–	$t_s \leq t_0$	–
τ or t_s (steam cured)	–	≥ 1 day	–	$t_s \leq t_0$	–

1.2. Constitutive Models for Numerical Simulation of Reinforced Concrete

Deformational behaviour of cracked RC members is a complex process including a wide range of effects, such as, different strength and deformation properties of steel and concrete, concrete cracking, tension-softening and tension-stiffening, bond slip between reinforcement and concrete, etc. Even under low load, the behaviour can be non-linear, which presents a challenge for calculation of deformations of RC members.

1.2.1. Idealisation of Constitutive Laws

Rather than attempting to provide a complete mechanical description of the behaviour of concrete, reinforcement and their interaction, physical models are aimed at which are as simple as possible and reflect the main influences governing the response of structural concrete. This Section presents some principles for idealisation of material models (Sigrist 1995).

The diagrams shown in Figs. 1.4a–1.4c illustrate some basic aspects of idealisations of stress-strain characteristics. Non-linearly elastic response is shown in Fig. 1.4a: there is a unique relationship between strains and applied stresses, the deformations are completely reversible, and no energy is dissipated.

The strain energy per unit volume (shown in Fig. 1.4a by the shaded area below the stress-strain curve), corresponding to the energy stored in an elastic body, can be given as following:

$$dU = \int_0^{\varepsilon_1} \sigma(\varepsilon)\, d\varepsilon \,. \tag{1.2}$$

Figure 1.4b shows an elastic-plastic stress-strain relationship (the deformations are not fully reversible). Upon unloading, only the portion of the strain energy below the unloading curve is released. The remaining energy *dD*, corresponding to the area between the loading and unloading curves, has been dissipated. Strain-hardening branches of stress-strain curves are characterised by irreversible deformation and energy dissipation under increasing loads and deformation. Strain-softening branches of stress-strain curves, exhibiting decreasing loads with increasing deformation is presented in Fig. 1.4c. Such curves can be recorded by means of strict deformation control.

Figures 1.4d–1.4g illustrate some commonly used idealisations of stress-strain relationships. In the bilinear idealisation shown in Fig. 1.4d, the response is linear elastic for stresses below the yield stress f_y. For higher stresses a linear strain-hardening takes place. Unloading is assumed to occur parallel to the initial elastic loading. If only ultimate loads and initial stiffness are of interest, a linear elastic-perfect plastic idealisation (see Fig. 1.4e) may be employed.

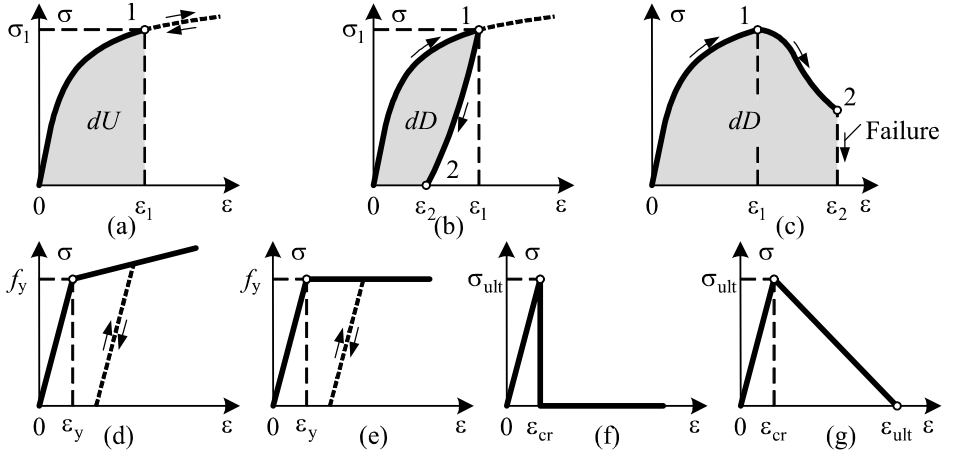

Fig. 1.4. Stress-strain idealisations: elastic (a); elastic-plastic (b); strain-softening behaviour (c); bilinear strain hardening (d); linear elastic-perfectly plastic (e); brittle fracture (f) and bilinear strain softening (g)

A simple brittle cracking idealisation is presented in Fig. 1.4f. Brittle behaviour is characterised by the full reduction of the strength after the strength criterion ($\sigma > \sigma_{ult}$) has been violated. Figure 1.4g illustrate bilinear stress-strain relationship with linear strain softening branch. The latter two stress-strain relationships are often used for idealisation of plain and reinforced tensile concrete behaviour, respectively. Material properties determined from tests depend on the particular testing method used. Therefore, to allow for a direct comparison of test results, standardised testing methods (including specimen geometry, loading ratio and testing device) should be applied (Kaufmann 1998).

1.2.2. Plain Concrete and Steel

1.2.2.1. Concrete in Compression

The uniaxial compressive strength is often the only concrete property specified and measured. The response of concrete in uniaxial compression is usually obtained from cylinders with a height to diameter ratio of two as shown in Fig. 1.5a. The standard in Europe cylinder is 300 mm high by 150 mm in diameter. Compressive strength can be also determined from 150 mm cube test (Fig. 1.5b). Smaller size cylinders and cubes are standard in some countries (for instance in Japan and Canada compressive strength is determined using cylinder 200 mm high by 100 mm in diameter). It is well known that strengths measured on smaller specimens are typically higher than those determined from bigger ones since the end zones of the specimens are laterally constrained by the stiffer loading plates. This effect is more pronounced in small cubes. The difference between the cube strength and the cylinder strength decreases with increasing concrete strength. Table 1.3 presents compressive strength conversion factors taking ∅150×300 mm cylinder as reference specimen (CEB-FIP 1990, CEN 2004).

In early numerical simulation (Hand *et al.* 1973, Lin & Scordelis 1975), an ideally elastic-plastic diagram (Fig. 1.4e) has been assumed for modelling of compressive concrete. It has been considered that plastic structural deformations were mainly due to cracking of tensile concrete and plastic steel strains but not due to plastic deformation of compressive concrete. However, soon importance of plastic strains of compressive concrete on total behaviour of structure has been recognised and numerical analyses have employed a great number of stress-strain relationships developed from uniaxial tests. Such relationships were proposed by *Ros* (1950), *Hognestad* (1951), *Hognestad et al*. (1955), *Smith & Young* (1956), *Young* (1960), *Szulczynski & Sozen* (1961), *Liebenberg* (1962), *Roy & Sozen* (1963), *Barnard* (1964), *Saenz* (1964), *Popovics* (1970, 1973), *Kent & Park* (1971), *Park & Paulay* (1975), *Wang et al*. (1978), *Dilger et al*. (1984), *Shah & Ahmad* (1985), *CEB-FIP* (1991), *Mansur et al*. (1997), *Debernardi & Taliano* (2001) etc.

The relationship of compressive concrete recommended by *CEN* (2004) is used in present study (see Section 2.5.2.2 and Fig 2.12b). As shown in Fig 1.5c, the compressive stress-strain response of concrete in the pre-peak range can be approximated by a parabola. *Hognestad* (1951: 45) proposed one of the most widely used expressions:

$$\sigma_c = f_c\left[2\overline{\varepsilon} - \overline{\varepsilon}^2\right]; \quad \overline{\varepsilon} = \varepsilon_c/\varepsilon_0; \quad \varepsilon_0 = 2f_c/E_c\,. \tag{1.3}$$

Here σ_c and ε_c are the stress and strain of the compressive concrete, respectively; and E_c is the initial (tangent) modulus of elasticity.

The response of concrete in compression in the post-peak range is characterised by decreasing carrying capacity with increasing deformation, i.e. *strain-softening* in compression (see Fig. 1.5c). The strain-softening behaviour of concrete in compression is more complicated than that in tension, and no generally accepted model such as the *fictitious crack* model for the behaviour in tension (Hillerborg *et al*. 1976) has yet been established. One reason for this is that the specific fracture energy per unit volume $G_{F,c}$ (see Fig. 1.5c) can be evaluated from tests only if the *fracture process zone* (FPZ) is known (Kaufmann 1998).

The size and shape of the FPZ, which in cylinder test may be assumed to extend over a length of double cylinder diameter (Sigrist 1995), cannot be trivially determined for more complicated geometries. The softening branch of long specimens is steeper than that of short ones (Fig. 1.5c). This fact may be attributed to the localisation of deformation in FPZ, while the other parts of the specimen remain undamaged.

The strain-softening behaviour of concrete in compression depends not only on the specimen size, but also on the rate of loading and on the concrete strength (Fig 1.5d). High-strength concrete fails in a much more brittle manner than normal-strength concrete, while the specific fracture energy increases only slightly with the concrete strength (Markeset 1993).

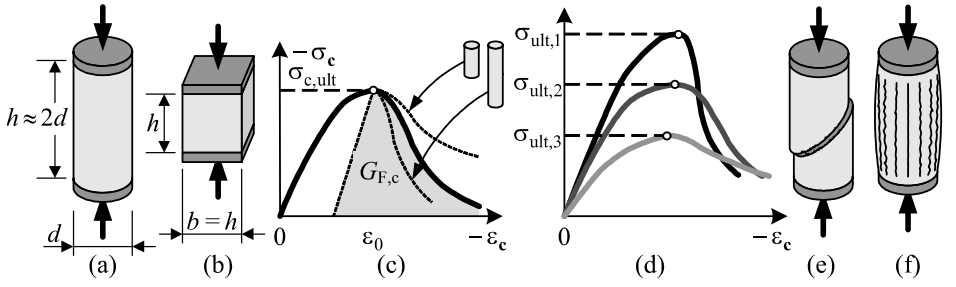

Fig. 1.5. Compression test specimens (a) and (b); influence of specimen length (c) and concrete strength (d) on stress-strain response and strain-softening; influence of concrete strength on type of failure (e) and (f)

High-strength concrete cylinders often fail by laminar splitting (see Fig. 1.5f). If there was no friction between the specimen and the loading plates, specimens of normal strength concrete would have failed in a similar way. In practical applications with constrained specimen ends, sliding failure, as shown in Fig. 1.5e, is generally observed for normal-strength concrete. For more details and comprehensive survey on other models of compressive failure, see study performed by *Wang & Shrive* (1995).

Table 1.3. Conversion factors for compressive strength of concrete

Strength, MPa	∅150×300	∅100×200	100×100	150×150	200×200
< 50	1,0	0,93	0,75	0,80	0,84
50	1,0	0,93	0,75	0,83	0,87
75	1,0	0,93	0,77	0,83	0,87
100	1,0	0,93	0,83	0,83	0,87

1.2.2.2. Concrete in Tension

The *tensile strength* f_{ct} and *tensile strain capacity* ε_{cr} of concrete are widely used for evaluating the occurrence of cracks in concrete members. The *tensile strain capacity* defined as the maximum tensile strain that concrete can withstand without crack forming (Wee *et al.* 2000). Based on the tensile strain capacity rather than the tensile strength, it is more convenient and simpler to evaluate cracking (Swaddiwudhipong *et al.* 2003).

The tensile strength of concrete is relatively low: the ratio between uniaxial tensile and compressive strength may vary considerably but usually ranges between 0,05 and 0,1. Furthermore, tensile capacity of the member may be affected by additional factors such as restrained shrinkage stresses. Therefore, it is common practice to neglect the concrete tensile strength in strength calculations of structural concrete members. However, the tensile behaviour of concrete is a key factor in serviceability considerations such as the assessment of crack width and spacing, concrete and reinforcement stresses and deformations.

Compared to compression tests on concrete, tensile tests are much more problematic to perform because of difficulties in applying the concentric load. Strongly stochastic nature of test data also complicates interpretation of experimental results (Lemnitzer *et al*. 2008). Generally, the tensile strength of concrete may be determined from direct tension tests as shown in Fig. 1.6a. Over the years, for instance, special grips and special shapes (like the dog-bone type specimens) have been designed in order to prevent stress consolidations. However, direct tensile tests are rarely used. Usually, the concrete tensile strength is evaluated indirectly using different techniques (see Figs. 1.6b–1.6d): the bending test (determination of the modulus of rupture), the double punch test or the split-

ting test. Determining the tensile strength by indirect methods requires assumptions about the stress state within the specimen in order to calculate the strength from measured failure load. It should be noted that the tensile strength measured from flexural test or splitting test are evaluated on the assumption that the concrete is linearly elastic until failure, while in reality, the stress-strain curve becomes nonlinear when the concrete is close to failure (Zeng *et al.* 2001). Therefore, calculation of the tensile strength using empirical relationships based on uniaxial compressive strength is a common practice. In present study (see Chapter 3), tensile strength at age t was calculated using compressive cylinder strength f_{cm} measured at t = 28 days (CEN 2004):

$$f_{\mathrm{ct}}(t) = \begin{cases} \beta \cdot f_{\mathrm{ct}}, & t < 28 \text{ days} \\ \beta^{2/3} f_{\mathrm{ct}}, & t \geq 28 \text{ days} \end{cases}; \quad \beta = \exp\left[0{,}25\left(1 - \sqrt{28/t}\right)\right];$$
$$f_{\mathrm{ct}} = \begin{cases} 0{,}30\left(f_{\mathrm{cm}} - 8\right)^{2/3}, & f_{\mathrm{cm}} \leq 58 \text{ MPa}; \\ 2{,}12 \ln\left(1 + f_{\mathrm{cm}}/10\right), & f_{\mathrm{cm}} > 58 \text{ MPa}. \end{cases} \tag{1.4}$$

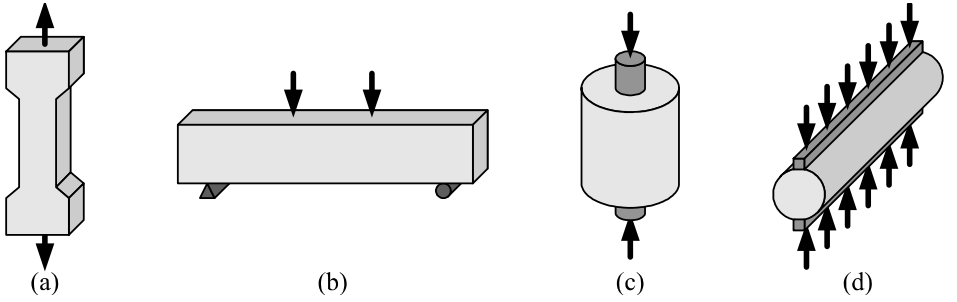

Fig. 1.6. Tension tests: direct tension test (a); bending or modulus of rupture test (b); double punch test (c) and split cylinder test (d)

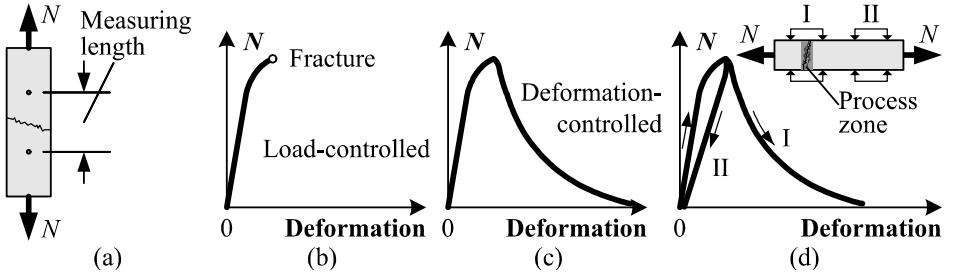

Fig. 1.7. Tension test (a); sketched behaviour of concrete in a load controlled (b) and deformation controlled (c) tension tests; and influence of a crack localisation on test measurements (d)

In early experimental investigations (load-controlled), the tensile load was increased until the specimen fractured (see Fig. 1.7b). *Gonnerman & Shuman* (1928) performed a comprehensive investigation in which the load was applied by special grips. In 1960th, in analogy to that was observed in compression, it was investigated whether a post-peak behaviour also exists for tensile loading, as shown in Fig. 1.7c (Rüsch & Hilsdorf 1963, Hughes & Chapman 1966 and Evans & Marathe 1968). In these investigations, the results were presented in stress-strain relationships. However, in the tests it is not a strain was measured, but a deformation over a certain *measuring* length l_{meas}. By assuming a uniform stress distribution over the measuring length (see Fig. 1.7a), given deformation results a strain. In the pre-peak region, this transformation is acceptable, but in the post-peak region, this has no meaning because the total deformation is the sum of elastic deformation and crack opening. Such behaviour implies that fracture of concrete in tension is a local phenomenon.

Figure 1.7d presents a concrete specimen strained in uniaxial tension when deformation-controlled test is performed. A linear load-deformation relation almost to the peak load will be obtained. At peak load, the strains start to localise within a *process* zone (*softening* zone) of micro-cracking, leading to a continuous macro-crack development. The process zone will occur at the weakest section of the tension specimen. If this zone develops within the measuring length which deformation is used as control parameter, then a load-deformation relation, as shown by line I in Fig. 1.7d, will be obtained. The load should be reduced with an increasing deformation of the process zone and as a result, the concrete outside process zone unloads (line II in Fig. 1.7d).

As was mentioned, the deformation measurements always consist of two parts: the crack opening within process zone and elastic deformation over total measuring length. When varying the measuring length, the first contribution remains constant, while the latter one changes. Figure 1.8a illustrates this influence. It can be observed that the decreasing branch becomes steeper for an increasing measuring length. In this example, a *relative* length $l_{\text{meas}}/l = 1$ yields a stress-strain relationship with a so-called *snap-back*. If this length is used as control parameter for the deformation, then a sudden jump will occur, as indicated by the dashed line. In most experimental set-ups, the equipment will not be fast enough to overcome such a jump and the result will be unstable fracture, and the obtained stress-deformation relationships no longer represents the actual material behaviour. It should be pointed out that the same phenomenon is also of great importance in numerical analyses (Bosco *et al*. 1990a, Hordijk 1991).

Tests show that as in compression, the softening branch of stress-average strain relationship of longer specimens is steeper than that of shorter ones (Fig. 1.8b). For specimens longer than a certain *critical length*, the softening branch cannot be recorded at all (Hordijk 1991). Continuum mechanics models (using stress-strain relationship) cannot explain the fact that long specimens fail in a more brittle manner than the short ones (Ozbolt & Reinhardt 2002).

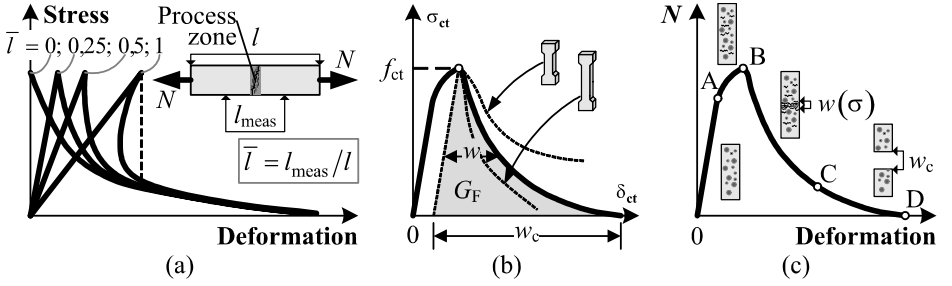

Fig. 1.8. Stress-deformation relationship as influenced by measuring length (Hordijk 1991) (a); influence of specimen length on the tensile behaviour (b) and typical load-deformation response of a quasi-brittle material in tension (Karihaloo 1995) (c)

Figure 1.8c sketches behaviour of tensile concrete in the FPZ. *Karihaloo* (1995) stated that the pre-peak nonlinearity (AB) and region of tension-softening diagram after the attainment of peak load (BC) are primarily a result of micro-cracking. The tail region of tension-softening diagram (CD) results from aggregate interlock and other frictional effects. Fracture of the tensile specimen has been completed when critical crack width w_c is reached. Due to the quasi-brittle nature of concrete, linear elastic fracture mechanics (LEFM) cannot be applied either, with exception of infinitely large specimens (Liu *et al*. 2008).

Hillerborg et al. (1976) and *Hillerborg* (1983, 1985a, and 1985b) have proposed *fictitious crack* model (*cohesive crack* model). According to this model, the behaviour of concrete under tensile loading can be split into a stress-strain relation for the concrete outside a crack *process zone*, and a stress-crack opening w relation for the crack itself (see Fig. 1.8b). The area under the *softening* curve (shaded in Fig. 1.8b) is defined as the *fracture energy*. The *fracture energy*, G_F, is defined, as the energy required forming a complete crack. According to *Wittmann* (2002), *fracture energy* and *softening* curve depend on the composite structure of the material: due to the mechanical interaction between aggregates and matrix, fracture energy of the composite material becomes considerably larger than G_F of both the aggregates and the matrix. The value of G_F can be estimated by the method proposed in the *MC 90* (CEB-FIP 1991), in which G_F is a function of the compressive strength of the concrete and the maximum aggregate size. However, recent research by *Darwin et al.* (2001) indicates that it is relatively independent of the concrete strength or aggregate size.

Generally, the most direct way to measure the *softening* curve is by means of stable tensile tests (Petersson 1981). This kind of tests seem to provide the whole stress-crack width relationships as a direct output from the experiment. However, the test results have shown that such an approach is extremely difficult (if not impossible) because of two major drawbacks (Elices *et al*. 2002):

- The localisation of the crack is not known a priori, and in most occasions multiple cracking may occurs (Planas & Elices 1986, Guo & Zhang 1987, Philips & Binsheng 1993).
- When a small crack is introduced to initiate fracture, the specimen tends to asymmetric models of fracture, and the crack opening is not uniform across the specimen (Rots 1988, Hordijk 1991, Mier van & Vervuut 1995). Moreover, when the rotations are avoided using very short specimens and a very stiff test machine, or by means of special servo-controlled system, the single cracks formed at two opposite sides of the specimen tend to get away from each other and overlap never creating one transverse crack (Carpinteri & Ferro 1994, Mier van & Vervuut 1995).

The above difficulties led investigators to apply indirect methods, known as inverse analysis, to determine the softening curve based on parametric fitting of the test results. These methods usually do not yield identical results for the same concrete due to different weight assigned to various test data (Elices *et al.* 2002). Stable tests on notched beams or compact specimens are commonly used to fit the softening curve (Yamamoto & Vecchio 2001).

1.2.2.3. Reinforcing Steel

The use of iron to reinforce concrete structures date is the mid of the 19th century, marks the birth of reinforced concrete construction. In 1848, *Joseph-Louis Lambot* first found that adding thin steel bars or steel fibres to concrete greatly increases concrete strength, making it better for use in a variety of applications. In the beginning, there were several reinforced system, using different shapes and types of iron or steel. Today, common reinforcement types are deformed steel bars of circular cross-section for passive reinforcement and steel bars, wires or seven-wire strands for pre-stressed reinforcement.

Structural concrete elements are generally designed such that failure will be governed by yielding of the reinforcement. The yield stresses typically amount to 400…600 MPa. The deformation capacity of structural concrete elements, an important aspect in the design of such structures, mainly depends on the ductility of the reinforcement (Sigrist 1995). Therefore, ductility of the reinforcement is as essential to structural concrete as its strength.

The reinforcing bars exhibit a uniaxial response, having strength and stiffness characteristics in the bar direction only. Two different types of stress-strain characteristics of reinforcing steel can be distinguished. Figure 1.9a illustrate the response of hot-rolled, low carbon or micro-alloyed steel bar in tension exhibits an initial linear elastic portion, $\sigma_s = E_s\varepsilon_s$, a yield plateau $\sigma_s = f_{sy}$ (stress level beyond which the strain increases under constant loading), and strain-hardening range until rupture occurs at the tensile strength, $\sigma_s = f_{su}$. The extension of the yield plateau depends on the steel grade: its length generally decreases with increasing strength.

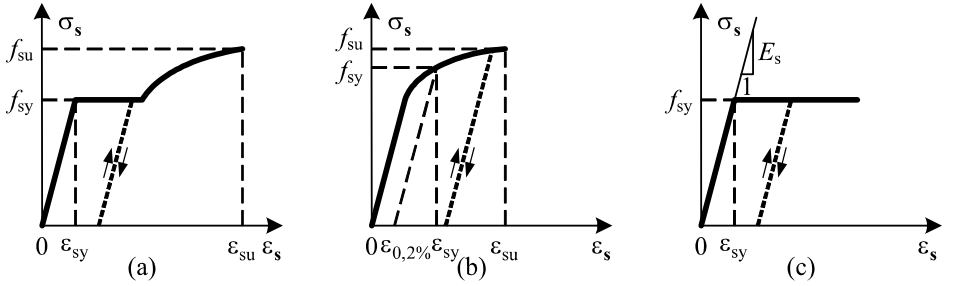

Fig. 1.9. Stress-strain characteristic of reinforcement in uniaxial tension: hot-rolled, heat-treated, low-carbon or micro-alloyed steel (a); cold-worked or high-carbon steel (b) and linear-elastic ideally-plastic material model (c)

Cold-worked and high-carbon steels exhibit a smooth transition from the initial elastic phase to the strain-hardening branch, without a distinct yield point (see Fig. 1.9b). The yield stress is often defined as the stress at which a permanent strain of 0,2% remains after unloading or, alternatively, the yield strain ε_{sy} can be specified directly. Unloading at any point of the stress-strain diagram occurs with approximately the same stiffness as initial loading. In the present study, aimed at the serviceability issues, an ideal elastic-plastic stress-strain response of reinforcement is applied. Figure 1.9c presents such an idealisation.

1.2.3. Cracking Behaviour of Reinforced Concrete Members

Cracking is a complete or incomplete separation into two or more parts produced by breaking or fracturing (ACI 201 2001). Cracks formed in RC members can be classified into two main categories: cracks caused by externally applied load and cracks that occur independently of the loads (Leonhardt 1977). The latter cracks cause problems in concrete structures for construction, resulting from thermal stress due to heat of hydration and dry shrinkage strain after wet curing. External loading induced cracks may be not orthogonal to the reinforcement (shear or torsion cracks) and orthogonal (tensile or flexural cracks). As present study concentrates on the latter cracks, inclined shear cracks are not discussed here.

Figure 1.10a presents a typical load-strain curve of RC members subjected to tension. This curve can be divided into three regions (Somayaji & Shah 1981). First region represents the elastic behaviour of the member up to start of cracking. Second region covers deformation behaviour from first *primary* crack to the *final cracking* point. Third region aims at the behaviour from the final cracking point to the yielding of the reinforcement. Before cracking the concrete tensile stress (represented by grey-filled area in Fig. 1.10a) increases with load. When the stress in concrete first reaches the tensile strength at a weakest section, cracking occurs. After cracking, the stress in the concrete at the crack drops to

zero. The concrete stress increases with distance from the crack due to the bond action, until at distance s, called the *transfer length*, from the crack the concrete stress is not affected by the crack, as shown in Fig. 1.10b. Slip at the concrete-steel interface in the region of significant bond stress (s on either side of the crack) causes the crack to open. A relatively small increase in load will cause a second crack to develop at a cross-section at some distance from the first crack. Under load increasing, the primary cracks form at somewhat regular intervals ($s < l \le 2 \cdot s$, see Fig. 1.10b) along the member and primary crack pattern is established. The concrete tensile stress at each crack is zero, rising to a value σ_{ct}, which never reach the tensile strength of the concrete (see Fig. 1.10b).

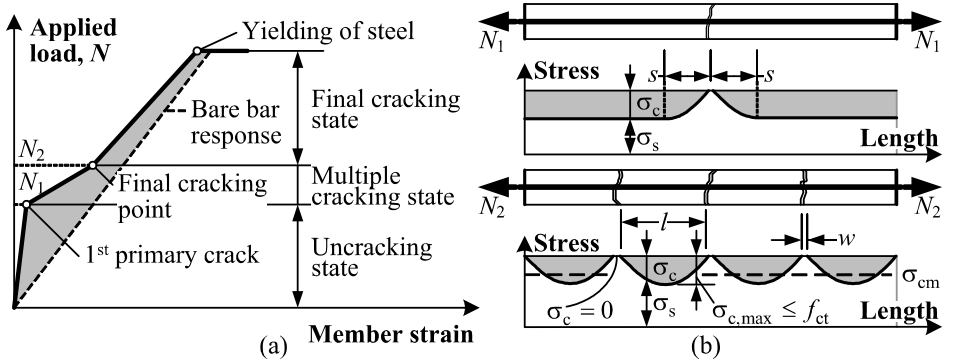

Fig. 1.10. Tension member: cracking stages (Somayaji & Shah 1981) (a) and distribution of axial stresses and strains (Fields & Bischoff 2004) (b)

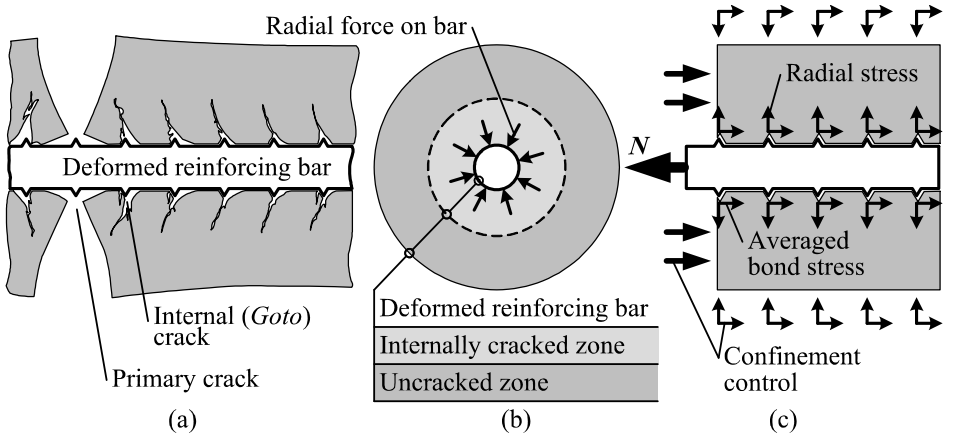

Fig. 1.11. Formation of secondary cracks (Goto 1971) (a) and (b), and idealized bond behaviour (Wu & Gilbert 2008) (c)

After the formation of the *first primary crack* up to the *final crack*, concrete contribution steadily decreases (Gupta & Maestrini 1990). At the *final cracking* point, the stable crack pattern has been reached. Increase in load will result in further decrease of concrete contribution due to bond-slip causing *cover-controlled* cracks to develop between the primary cracks and a gradual breaking down of the bond (Wu & Gilbert 2008). *Goto* (1971) described this process as the formation of internal *secondary* cracks along the deformed bar due to bond stress transfer to the sound concrete in between primary cracks (see Fig. 1.11a).

Similarly as for tensile members (see Fig 1.10a), cracking behaviour of flexural members can be also divided into three phases: the *uncracked*, the *crack formation* and the *stabilised cracking* (Borosnyói & Balázs 2005). During uncracked phase, concrete and steel behave elastically. At the start of crack formation phase, first *primary* crack is formed in a locally weak section. Flexural cracks are formed in the tensile zone of the member. After formation of a crack, some elastic recovery takes place in concrete on the member surface, contributing to the crack width. However, some stress and strain is maintained in concrete surrounding the reinforcement due to *bond-action*. As it is in tensile members, this contributes to a reduction in the crack width near the bar compared to that at the concrete surface (Base *et al.* 1966, Husain & Ferguson 1968, and Goto 1971). The compatibility of strains between concrete and reinforcement is no longer maintained in *the tension chord*, as concrete stress drops to zero at the crack. At some distance from the crack, the compatibility of strains is recovered. As shown in Fig. 1.12a, with increasing load, new primary cracks can be formed decreasing average crack spacing.

The stabilised cracking phase is supposed to be reached when practically no more new cracks can be formed. An increase of load causes an increase of the crack width only. The *bond-action* effect dissipates completely, though if there is transverse steel or stirrups, some residual ring or hoop, tension will be carried (Clark & Speirs 1978). Radial thrusts develop of the bar deformations and must be resisted by the ring tension as shown in Figs. 1.11b and 1.12b. In flexural members, the reinforcing bars are usually located close to the surface of the member, and the contribution of concrete in tension is different at various locations within a member. Thus, conception of *effective concrete area* in tension (which is not identical with the concrete area under neutral axis, i.e. concrete in tension), was introduced for cracking analysis (CEB-FIP 1991).

Flexural cracks in a varying moment region of a beam develop at a regular interval; however, in a constant moment region, these cracks develop at discrete intervals (as in tensile member). Their locations depend partly on the occurrence and distribution of zone of local weakness in concrete and therefore cracking is somewhat a random process (Warner *et al*. 1998, Fantilli *et al*. 1998b). As a result, the exact locations of cracks in a constant moment region may not be predicted accurately. However, maximum and minimum spacing of adjacent cracks

(see Fig. 1.12a) may be predicted with sufficient accuracy by investigating concrete stresses developed in the tensile zone of a member.

After cracking, stiffness of the member along its length varies, which makes the calculation of deformations complicated. In a cracked member, the stiffness is largest at section within the uncracked region, while it is smallest at cracked section. This is because at cracked section, the tensile concrete does not contribute to the load carrying mechanism. However, at intermediate sections between adjacent cracks, the concrete around reinforcement retains some tensile force due to the *bond-action*, which effectively stiffens the member response and reduces deflections (see Fig. 1.12b). This effect is known as *tension-stiffening*.

A number of researchers (Clark & Speirs 1978, Bosco *et al*. 1990b, Polak & Blackwell 1998, Sule & Breugel 2004, Fantilli *et al.* 2005, Beeby & Scott 2006, Kaklauskas *et al*. 2008b*, Gribniak *et al.* 2009*) have investigated the reinforcement bar size and spacing dependence on cracking and tension-stiffening. *Clark & Speirs* (1978) reported that tension-stiffening effect decreases with increasing of bar spacing when the latter exceeds a critical value. *Sule & Breugel* (2004) stated that reinforcement configuration has more influence on cracking resistance of bending members than reinforcement ratio. For given reinforcement ratios, tension-stiffening is more pronounced in the members reinforced with bars of smaller diameters (Fantilli *et al*. 2005 and Gribniak *et al*. 2009*). In the investigation of minimum amount of reinforcement for high strength members in flexure, *Bosco et al*. (1990b) reported new experimental results on reinforcement ratio and beam depth influence on cracking resistance.

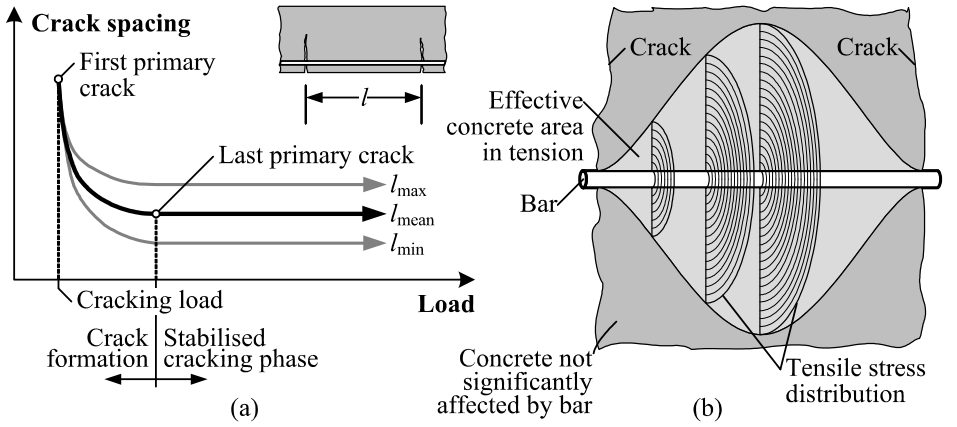

Fig. 1.12. Flexural cracking (Borosnyói & Balázs 2005): crack formation and crack spacing (a); conception of effective concrete area in tension (b)

*The reference is given in the list of publications by the author on the topic of the dissertation

Many investigators have noted that at the *stabilised cracking* stage tension-stiffening decreases with increase of load due to deterioration of bond (Collins & Mitchell 1991, Belarbi & Hsu 1994 and Bischoff 2001). If tension-stiffening not taken into account, the calculated deflection can become larger dramatically than the actual value (Gilbert & Warner 1978, Kaklauskas 2001, Robert-Nicoud *et al*. 2005). For accurate assessment of deflection, tension-stiffening needs to be incorporated in the calculation.

1.2.4. Approaches in Tension-Stiffening

The first studies to define the behaviour of concrete under tensile stress began towards the end of 19th century when, though the intense activity of skilful builders, the technique of RC reached certain stages that were fundamental for its subsequent success. *Joly* (1898a, 1898b) and *Considère* (1899a, 1899b) who made a decisive contribution to explaining the behaviour of RC flexural and tensile members performed first intuitions on the *tension-stiffening*. After the response of the elements to the applied actions had been explained, its behaviour was defined though mathematical models, necessary for the calculation theories which, according to *Albenga* (1945), were many and contradictory.

In the early development of the theory of RC, deformation problems were simply ignored. First attempts to assess deflections of flexural RC members were based on classical principles of strength of materials. However, elastic calculations may significantly underestimate deflections of cracked members. On the other hand, disregard of the tensile concrete may lead to a significant overestimation of deflections, particularly for lightly reinforced members. The intact concrete between cracks carries tensile force due to the bond between the steel and concrete. The average tensile stress in the concrete can be a significant fraction of the tensile strength of concrete. This effect is called by *tension-stiffening* and is often accounted for in design by an empirical adjustment to the stiffness of the fully cracked cross-section.

Many theoretical models of RC in tension have been proposed to predict cracking and deformations of RC members. Generally, these models may be separated into four main approaches:

- *Semi-empirical*: the earliest approaches were developed based on the analysis of test data. Such simplified calculation techniques are broadly presented in the design codes.
- *Stress transfer*: these approaches aim at modelling bond between concrete and reinforcement steel.
- *Fracture mechanics*: such approaches use the fracture mechanics principles to predict cracking behaviour of RC elements.
- *Average stress-average strain*: simple approaches, extensively used in numerical analyses, based on *smeared crack* model.

1.2.4.1. Semi-Empirical

This type of research covers perhaps the largest portion of work done on the cracking modelling up to around 1970 (Sjoberg 1999). That it forms the largest portion of research, is largely a result of the amount of time in which research has been performed. French papers published in 1899 are the pioneer records of research found relating to the cracking behaviour of RC members (Siviero & Simoncelli 1997). It should be noted that many of the early studies were carried out using plain reinforcing bars.

Murashev (1950) and *Gvozdev et al*. (1962) quite independently carried out the research in the East, and by *Branson* (1963) and *Ghali & Favre* (1986), in the West. In Russia, based on a large amount of test data, *Murashev* (1950) has developed a qualitatively new method for the calculation of deformations and deflections of cracked flexural members. This theory was based on the beam theory (plane section assumption) and accounted for nonlinear strains of the compressive concrete and tension-stiffening. The latter effect was assessed by a factor ψ_s taken as the ratio of the average steel strain between two adjacent cracks and the steel strain in the cracked section. The method, further developed by *Gvozdev* and his co-workers (1962), was adopted in the Russian design code. In 2006th a new issue of the code (*SP 52-101*) has been proposed by *Concrete and Reinforced Concrete Research and Technological institute* (NIIZhB 2006). It is relevant to note that the *SP 52-101* method employs a lesser number of empirical parameters than the previous one. Furthermore, this code has adopted a numerical approach based on plane section hypothesis and use of stress-strain relationships for steel and concrete, both in tension and compression. In the USA, *Branson* (1963) proposed perhaps the best known method in the West (based on *effective* moment of inertia) which was adopted in the codes of the USA (ACI 318 2008), Canada, Australia, New Zealand and a number of countries in South America. The *Eurocode 2* method (CEN 2004) gives an alternative approaches. These simple design models describe the global behaviour and serve everyday engineering design well. However, it can be observed that different formulas are used in different codes, which raises a question of their objectivity.

1.2.4.2. Stress Transfer

This approach is based on bond-slip relationship, which models the *bond-action* between concrete and reinforcement. *Saliger* (1936) has first published the basis for all theories using this approach. As discussed in Section 1.2.3, the *bond-action* at the interface of steel bars and surrounding concrete has great influence on the initiation and propagation of cracks in RC members. The bond-action is the main contributing factor to the tension-stiffening effect in concrete structures. In a cracked RC member, an increase in loading will result in an increase in steel strain, causing an extension of the reinforcing bar. Consequently, ribs in the bar will tend to move towards the nearest crack relative to the surrounding

concrete, i.e. *bond-slip* is initialised (see Fig. 1.11a). This will increase the rib bearing stress on concrete, contributing to the bond-slip.

In a tensile specimen, before any cracks are formed, the slip at the mid point between the two ends due to symmetry will be equal to zero. The bond stress at the two ends of the specimen will also be equal to zero, although the slip is the largest at these points. The same behaviour is valid for concrete section between two adjacent cracks. Usually, variation of the bond stress between these three points is established experimentally and represented by analytical relationships. *Lackner & Mang* (2003) distinguished two main categories of such models:

- The first one is characterised by adding extra-stiffness and force terms to the stiffness matrix. These terms may be related to the strain in the steel bar (Feenstra & Borst de 1995). *Ngo & Scordelis* (1967) modelled bond behaviour by linear springs to compute the additional stiffness force terms. This approach was improved by introducing non-linearity of springs (Kwak & Filippou 1995, Monti & Spacone 2000).
- The second one uses so-called tension-stiffening factor, which reflects a specific bond-stress distribution along the reinforcement bars. *Floegl & Mang* (1982) have determined this factor assuming a constant distribution of the bond-stress. *Choi & Cheung* (1996) have extended this approach.

In analytical investigations of RC members, the bond stress-slip relationship is of fundamental importance. Such relationships are analogous to the average stress-strain laws for concrete or steel (Nilson 1972, Edwards & Yannopoulos 1979). Unlike the constitutive laws for steel or concrete, a unique relationship for the bond stress-slip is not yet available despite the large number of investigations carried out. *Nilson* (1972), *Mirza & Houde* (1979), *Ciampi et al*. (1981), *Jiang et al*. (1984), *Giuriani et al*. (1991), *Kankam* (1997), *Wu & Gilbert* (2008) and many other researchers who have developed such relationships. Various aspects of *stress transfer* approaches has been investigated by *Floegl & Mang* (1986), *Fantilli et al*. (1998b), *Manfredi & Pecce* (1998); *Polak & Blackwell* (1998), Kwak & Song (2002), *Lackner & Mang* (2003), *Foster & Marti* (2003), *Borosnyói & Balázs* (2005), *Eckfeldt* (2005) , *Ruiz et al*. (2007), *Vollum et al*. (2008) and etc. *Piyasena* (2002) and *Leutbecher & Fehlng* (2009) have performed a comprehensive survey on the bond stress-slip relationships.

Stress transfer approach realistically models cracking, crack widths and deformations. However, accuracy of numerical results depends on the assumed bond stress-slip relationship. Besides, as compared to *smeared approach*, it is more complex and relatively rarely used in practice.

1.2.4.3. Fracture Mechanics

Initiated in 1960th by *Kaplan* (1961), the study of *fracture mechanics* has progressed by the turn of the century. *Kesler et al*. (1972) showed that the LEFM of

sharp cracks was inadequate for normal concrete structures. It was also supported by the results of *Walsh* (1972, 1976). Inspired by the softening and plastic models of FPZ initiated in the works of *Barenblatt* (1959, 1962), *Dugdale* (1960), *Hillerborg et al*. (1976) have proposed the first nonlinear theory of *fracture mechanics* for concrete.

In the early 1980s, it was recognised that plain concrete is not a perfectly brittle material in the *Griffith*'s sense, but it has some residual load-carrying capacity after reaching the tensile strength. This has led to the replacement of brittle crack model by *tension-softening* approach, in which a descending branch was introduced to model the gradually diminishing tensile strength of concrete upon further crack is opening. Such a descending branch also emerges in most *tension-stiffening* models and much confusion has existed ever since about modelling *tension-softening* and *tension-stiffening* in RC (Borst de 2002).

The introduction of *tension-softening* in crack models was also motivated on theoretical grounds. It was observed that use of strength models (Cedolin & Bažant 1980) or the straightforward use of strain-softening models led to an unacceptable and unphysical mesh sensitivity (Bažant 1976, Crisfield 1982). Recent developments in the application of *fracture mechanics* to concrete have made it possible to analyse effectively the post-cracking behaviour of plain concrete using the finite element (FE) method. These applications have incorporated *tension-softening* models to describe the gradual decay of stress/strain *softening* in plain concrete in tension as cracking propagates. Several researchers adopting a *tension-softening* model have obtained consistent results (Bažant & Oh 1983, Cornelissen *et al.* 1986, Hordijk 1991, Mier van 1991 and Carpinteri 1994).

Numerical modelling of plain and reinforced concrete started in the late 1960s with the landmark papers of *Ngo & Scordelis* (1967) and *Rashid* (1968) in which the *discrete* and *smeared* crack models were introduced. In the *discrete crack* model, cracking is assumed to occur as soon as the nodal force normal to FE boundaries exceeds the maximum tensile force that can be sustained and continuous re-meshing is required. In the *smeared crack* model, a cracked solid is imagined to be a continuum, describing the behaviour of cracked concrete by stress-strain relationships. This implies that the topology of the original FE mesh remains preserved. The latter approach leads to a straightforward computer implementation, and widespread using in practice (Li & Zimmerman 1998). With nonlinear fracture mechanics, the range of validity of both approaches was extended, leading to the *fictitious crack* model (Hillerborg *et al*. 1976) and to the *crack band* model (Bažant & Oh 1983). These methods have been well evaluated by *Cope et al*. (1979), *Zimmerman* (1986) and *Elices & Planas* (1989).

The *fictitious crack* model (Hillerborg *et al*. 1976) is a suitable and simple model for FPZ, which may be viewed as a specialisation of other more general approaches (Elices *et al*. 2002). For example, *Broberg* (1999) for materials that

fail by crack growth and coalescence depicts the appearance of FPZ in a cross-section normal to the crack edge. He proposes to describe FPZ, in general, by decomposing it into cells. The behaviour of the single sell is defined by relationships between its boundary forces and displacements. This is very similar to the definition of FE in computations, and when these cells are assumed to be cubic (or prismatic) and to lie along the crack path, the resulting model is very similar to the *smeared crack* approach used for concrete, and, more specifically to the *Bažant*'s *crack band* approach (Bažant & Planas 1998). The latter model was found to be in good agreement with the basic fracture data (Bažant & Oh 1983), and has been recognised convenient for programming. Based on the *crack band* model, two crack models were distinguished: the *fixed crack* and the *rotating crack*. In both models, a crack is initiated when the maximum principal stress violates the tensile strength of concrete and the initial orientation of the crack is normal to the maximum principal strain. In the *fixed crack* model, the crack plane is fixed during the total analysis process, whereas *rotating crack* model allows the crack plane to rotate (Cope *et al*. 1979). It is nowadays the main concrete fracture model used in industry and commercial FE codes: *DIANA* (Rots 1988), *SBETA* (Cervenka & Pukl 1994, Cervenka *et al*. 1998) and *ATENA* (Cervenka *et al*. 2002).

It is commonly accepted that the consideration of *tension-softening* is indispensable in analysing the behaviour of concrete structures with relatively large un-reinforced areas (see Fig. 1.13a). The *fracture mechanics* model is often used for modelling behaviour of RC structures in combination with other approaches. *Feenstra & Borst de* (1995) proposed a numerical model, which combines fracture mechanics concepts with tension-stiffening. It is assumed that the behaviour of cracked RC member, sketched in Fig. 1.13b, can be obtained by superposition of the stiffness of plain concrete, a stiffness of reinforcement and additional stiffness due to interaction between concrete and reinforcement. The latter effect was simulated using model proposed by *Cervenka et al.* (1990). *Fantilli et al*. (1998a) modelled behaviour of tensile RC members combining the *fracture mechanics* and the *stress transfer* approaches.

1.2.4.4. Average Stress-Average Strain

This simple approach, extensively applied in numerical analyses, is based on use of average stress-strain tension-stiffening relationship. The approach introduced by *Rashid* (1968) is based on *smeared crack* model, i.e. the cracks are smeared out in the continuous fashion and the cracked concrete is assumed to remain a continuum. The concrete becomes orthotropic with one of the material axes being oriented along the direction of cracking.

Differently from the *discrete crack* model tracing individual cracks, *smeared crack* model deals with average strains and stresses. This model can handle single, multiple and distributed cracks in a unified manner. Thus, it can be used

for both, plain and RC structures (Cervenka 1995). In FE analysis, *smeared crack* model has proven to be more flexible and more computationally effective concerning the *discrete crack* model since no topological constraints exist.

Tension-stiffening can be attributed either to tensile reinforcement (*steel-related* model) or to concrete (*concrete-related* model). In the latter approach, it may be assumed that tension-stiffening is effective either in the whole tension area or in the specified zone (close to reinforcement), called the *effective area*.

Gilbert & Warner (1978), *Cervenka et al.* (1990), *Hofstetter & Mang* (1995), *Feenstra & Borst de* (1995), *Salys et al*. (2009)* have used the steel-related approach. It should be noted that this approach is relatively rarely applied.

In the *effective area* approach, the influence of tension-stiffening is limited to a volume of concrete in relatively close proximity to the bar (*tension-stiffening* zone in Fig. 1.13a). In *Model Code 90* (CEB-FIP 1991) tension-stiffening zone was limited to concrete area within 7,5 bar diameters from the reinforcement (Fig. 1.13a). Outside this zone, the second mechanism of post-cracking prevails, that of tension-softening (Vecchio & Collins 1986, Stramandinoli & Rovere 2008).

Most of the continuum-based FE methods incorporate tension-stiffening by the constitutive law of tensile concrete (Suidan & Schnobrich 1973, Lin & Scordelis 1975, Prakhya & Morley 1990, Barros *et al*. 2001, Ebead & Marzouk 2005, Gribniak & Kondratenko 2005*, Gribniak & Girdžius 2005*, Gribniak *et al*. 2005*, 2006*, 2007b*, 2007d*, Kaklauskas *et al*. 2007a* and Bacinskas *et al*. 2007*). In present research, behaviour of RC member is modelled assuming a uniform tension-stiffening relationship over the whole tension area of concrete. Stress in the concrete is taken as the combined stress due to tension-stiffening and tension-softening, collectively called the *tension-stiffening*. Based on the above approach, a number of stress-strain constitutive relationships for cracked tensile concrete have been proposed. *Kaklauskas* (2001) and *Bischoff* (2001) have carried out a comprehensive review of the relationships. In the analysis of tension members, *Bischoff* (2001) has introduced bond factor β representing the ratio of average tensile stress in concrete and the cracking stress. Figure 1.14a shows a number of tension-stiffening relationships expressed in terms of β.

Figure 1.14b illustrates how the axial load in a cracked tension member is shared between the reinforcement and the concrete. At the cracked section of the member, all tension is carried by reinforcement. However, the concrete continues to carry tensile stresses between the cracks because of bond action. Tension-stiffening represents the tensile forces carried by concrete between cracks. Although crack spacing and crack widths depend on the bond quality, *Bischoff* (2001) stated that tension-stiffening is independent from bond parameters.

*The reference is given in the list of publications by the author on the topic of the dissertation

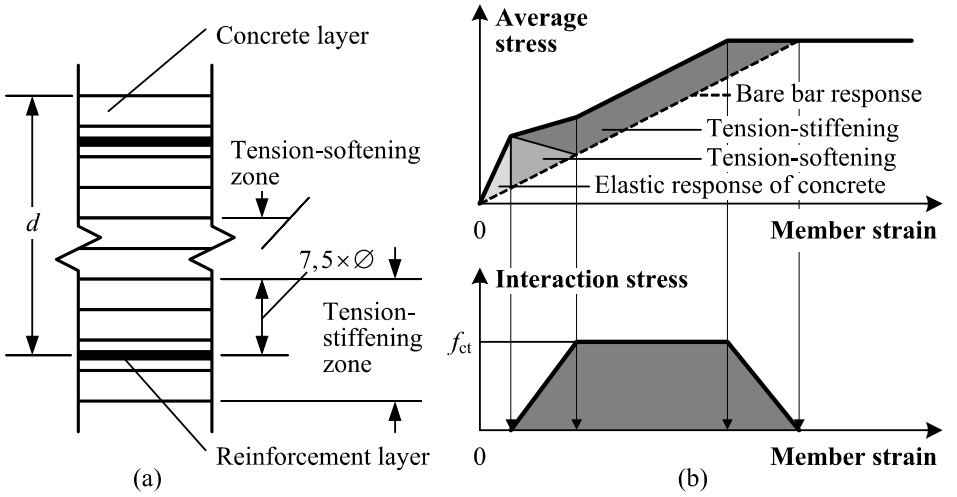

Fig. 1.13. Layered RC element with tension-stiffening zone (CEB-FIP 1991) (a); model of tensile RC element (Feenstra & Borst de 1995) (b)

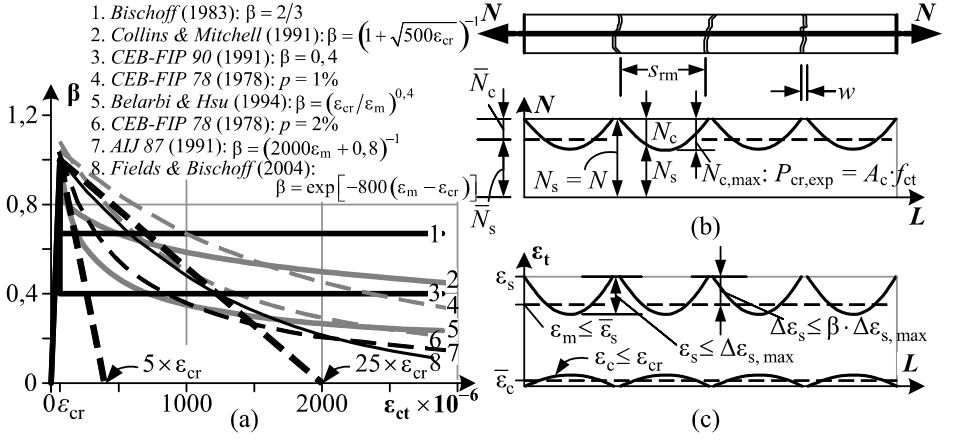

Fig. 1.14. Tension member (Fields & Bischoff 2004): expressions for the tension-stiffening bond factor (a); distribution of axial forces (b) and strains (c)

Most tension-stiffening relationships were derived using experimental data of tension (Bischoff 2001, Fields & Bischoff 2004) or shear (Vecchio & Collins 1986, Sato *et al*. 2004, Bentz 2005, Debernardi & Taliano 2006) RC members. These constitutive laws were applied for modelling flexural members, although their behaviour differs from tension or shear members.

The supervisor of the dissertation in co-authorship (Kaklauskas & Ghaboussi 2001) has proposed an alternative approach for deriving tension-stiffening relationships from test moment-curvature diagrams of RC members. Based on *inverse* technique, tension-stiffening relationships were computed from the equilibrium equations for incrementally increasing bending moment assuming portions of the relationships obtained from the previous increments. Due to stochastic distribution of test data, a probabilistic approach, based on *Monte Carlo* technique (Mosegaard & Tarantola 1995, Tarantola 2005, Kaklauskas *et al.* 2007b*), can be assumed in the *inverse* problem.

In most cases, tension-stiffening relationships were derived using test data of RC members exposed to shrinkage. Therefore, the derived constitutive relationships in an integrated manner have included the effects of tension-softening, tension-stiffening and shrinkage.

1.2.5. Shrinkage Influence on Stress-Strain Behaviour of RC Members

The crack classification proposed by *Leonhardt* (1977) and presented in Section 1.2.3, cover an ideal case when RC member subjected to external loading or some internal processes separately. However, a real structure always has been under complex action of above factors (Vítek *et al*. 2004, Lopes *et al*. 2008*).

The necessity to assess shrinkage influence on deformation behaviour of cracked RC members has been recognised in the beginning of the 2nd half of XX century by *Lash* (1953), *L'Hermite* (1955), *Figarovskij* (1962), *Nemirovski & Kochetkov* (1969) and by *Gilbert & Warner* (1978). Recently *Gilbert* (1999, 2001), *Bischoff* (2001), *Fields & Bischoff* (2004), *Kaklauskas & Gribniak* (2005b)*, *Tanimura et al*. (2005), *Sato et al*. (2007), *Bischoff & Johnson* (2007), *Scanlon & Bischoff* (2008) and *Kaklauskas et al*. (2009) who have reported experimental and theoretical results of shrinkage influence on tension-stiffening. It has been shown that the local bond stress is not only dependent of the local slip, but also on the stress-strain behaviour of the reinforcing steel, the duration of the applied load and the level of shrinkage. Early shrinkage causes a reduction in the cracking load and, under sustained service loads; shrinkage initiates the formation of additional primary cracks with time and causes a time-dependent degradation of the steel-concrete bond (Wu & Gilbert 2008). Different investigators reported that shrinkage might significantly affect cracking resistance and deformations of RC members' subjected to short-term loading (Bischoff 1983, Foster *et al*. 1996, Gilbert 1999, 2001, Bischoff 2001, Fields & Bischoff 2004, Kaklauskas & Gribniak 2005b*, Girdžius & Gribniak 2005*, Bischoff & Johnson

*The reference is given in the list of publications by the author on the topic of the dissertation

2007, Scanlon & Bischoff 2008, Kaklauskas *et al*. 2006a*, 2006b*, 2008a*, 2008c*, Gribniak *et al*. 2008* and 2009*).

Present research aims at shrinkage influence on deformational behaviour of RC members subjected to short-term loading. Figure 1.15 presents deformational behaviour of plain and RC members, assuming the uniform distribution of shrinkage strain across the section. As shown in Figs. 1.15a and 1.15c, shrinkage of an isolated plain concrete member would merely shorten it without causing camber. Reinforcement embedded in a concrete member provides restraint to shrinkage leading to compressive stresses in reinforcement and tensile stresses in concrete (see Figs. 1.15b and 1.15d). If the reinforcement asymmetrically placed in a section, shrinkage causes non-uniform stress-strain distribution within the height of the section (see Figs. 1.15e–1.15g). The maximal tensile stresses appear on the extreme concrete fibre, close to larger concentration of reinforcement. These effects will be comprehensively discussed in Chapter 2.

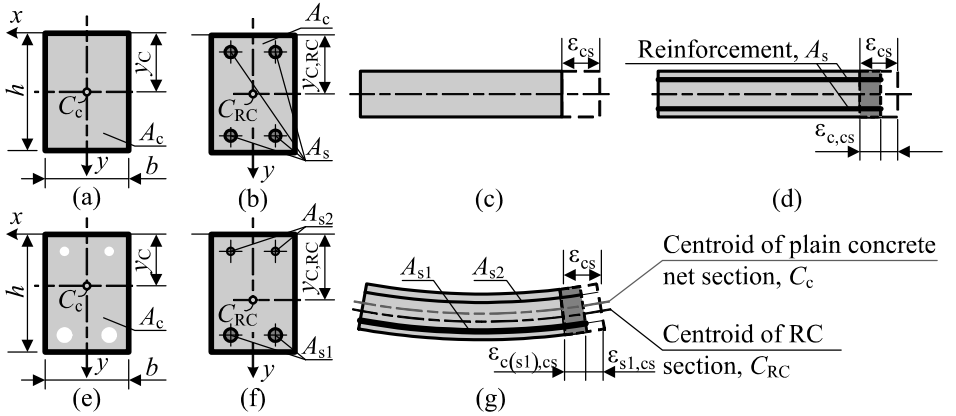

Fig. 1.15. Deformations of concrete and RC members due to shrinkage: plain concrete section (a); symmetrical RC section (b); free shrinkage deformation (c); shrinkage-induced deformations in a symmetrically reinforced element (d); asymmetrical RC net section (e); asymmetrical RC section (f) and deformations in an asymmetrically reinforced element (g)

1.2.6. Review on Experimental Investigations

Lightly reinforced members are a particular case of deformation analysis as the stress-strain state of such elements is significantly affected by cracked tensile concrete. Due to this, deformation prediction for lightly reinforced members is far less accurate in comparison to the beams with moderate and large reinforce-

*The reference is given in the list of publications by the author on the topic of the dissertation

ment ratios. Therefore, experimental investigation of RC members with small amounts of reinforcement is to be of higher preference in present study.

Lash (1953) in his investigations of ultimate strength and cracking resistance of lightly reinforced beams has tested twelve beams with reinforcement ratio ranging from $0{,}18\%$ to $1{,}15\%$. *Figarovski* (1962) has carried out a broad experimental programme on investigation of deformations of lightly reinforced members. In these tests, 24 beams (out of the total number of 34) had reinforcement ratio p below $0{,}70\%$. *Gushcha* (1967) has performed tests on four ($p = 0{,}28\ldots0{,}80\%$) and *Nemirovski & Kochetkov* (1969) on thirteen ($p = 0{,}20\ldots1{,}50\%$) beams. Experimental programme of *Clark & Speirs* (1978) was devoted to investigation of the tension-stiffening effect in flexural members. Fourteen beams and nine slabs with various depths, bar diameter and reinforcement ratios ($0{,}44 - 1{,}99\%$) were tested. *Fantilli et al*. (2005) have performed experimental investigations on five beams having different bar diameter ($p = 0{,}20\%$). *Gilbert* (2006, 2007) has reported test data of eleven one-way reinforced slabs with reinforcement ratio ranging from $0{,}18\%$ to $0{,}84\%$. It should be noted that in most of the above tests measurements on concrete shrinkage were not performed, with the exception of *Figarovski* (1962) who has simultaneously performed tests on concrete shrinkage and creep.

Japanese researchers (Hashida & Yamazaki 2002, Tanimura *et al*. 2002, 2005, 2007, and Sato *et al.* 2007) have carried out a comprehensive experimental and theoretical investigation on shrinkage effect on different types of RC members. Recently *Bischoff* (2001), *Fields & Bischoff* (2004), *Bischoff & Mac Laggan* (2006) and *Bischoff & Johnson* (2007) have reported on experimental and theoretical investigations of shrinkage influence on tension-stiffening. They have performed tests on tensile RC members being imposed to different levels of shrinkage strain. By means of a numerical procedure, the effect of shrinkage has been excluded from the tension-stiffening relationships. A similar analysis for flexural members has been carried out in (Bischoff & Johnson 2007).

Bischoff & Paixao (2004) has performed investigations on tensile concrete members reinforced with non-metallic reinforcement, i.e. GFRP bars. They have shown that due to low modulus of elasticity of GFRP bars, tension-stiffening has a more pronounced effect on deformations of such members in respect to ordinary RC elements. Besides, as the serviceability requirements in most cases of design of GFRP members is the critical condition, adequate assessment of tension-stiffening effect is of prime significance (Bischoff & Paixao 2004).

Scott & Beeby (2005) were among the first who performed investigations on decay of tension-stiffening in the case of long-term loading. On a basis of these tests, they have shown that tension-stiffening was decreasing in time at a higher rate than it was previously thought. According to their results, the concrete force representing the tension-stiffening effect has lost half of its value within 20 days.

Persson (2001) carried out a comprehensive test programme on factors affecting shrinkage of normal and HPC. *Branch et al*. (2002) conducted research on the factors affecting plastic shrinkage for HPC. *Lee et al.* (2003) studied the stresses created due to autogenous shrinkage of high-performance concrete (HPC). It was found that the shrinkage of concrete developed at a much higher rate than the tensile strength of concrete. *Dias* (2003) studied the effect of mix constituents, retarding and air entraining admixtures, additives, and environmental factors on plastic shrinkage of concrete. *Dulinskas et al*. (2007*, 2008*) investigated influence of curing condition on creep of compressive concrete. *Sakata et al*. (2009) have collected comprehensive database of creep and shrinkage tests performed in Japan.

Bosnjak & Kanstad (1997) demonstrated the use of advanced numerical techniques for the deformation problem. They calculated the deflections in *Mjøsund Bridge* in Norway, which has a main span length of 185 m. Deflections in the early part of the construction were observed within ±10% of the computed values when the *MC 90* creep and shrinkage model was used. *Griffin et al*. (2004) tested at deck contraction induced deflection in a HPC bridge. The purpose of the study was to calculate HPC highway bridge deflections due to shrinkage and temperature changes in the deck and to compare with the analytical results obtained from the finite element model of the bridge.

1.2.7. Numerical Techniques Employed in the Analysis

1.2.7.1. *Layer* Section Model

Layer section model (Kaklauskas 2001) employed in present research is based on plane section hypothesis and use of material laws. The non-linear stress-strain relationship recommended by *Eurocode 2* is adopted for idealisation of behaviour of compressive concrete. It should be noted that no significant difference is observed when different relationships are used in numerical procedures for deformational analysis of cracked RC beams (Stramandinoli & Rovere 2008).

Concrete cracking, tension-softening and tension-stiffening in an integrated manner was modelled by a linear tension-stiffening relationship shown in Fig. 2.3a. Recent investigations (Kaklauskas & Gribniak 2005b*, Gribniak *et al*. 2008*, Bacinskas *et al*. 2008*, Kaklauskas *et al*. 2008a*, 2008c* and 2009*) have shown that application of such a simple law, simultaneously taking into account shrinkage effect, secures reasonable accuracy of deflection predictions of RC members. Tensile strength of concrete f_{ct} and the ultimate strain $\beta \cdot \varepsilon_{cr}$ are considered as the most important parameters of the relationship. The supervisor of this dissertation, based on the result of *inverse* analysis, has derived an equation for calculation of factor β (Kaklauskas & Ghaboussi 2001):

*The reference is given in the list of publications by the author on the topic of the dissertation

$$\beta = \frac{\varepsilon_{ct}}{\varepsilon_{cr}} = \begin{cases} 32{,}8 - 27{,}6p + 7{,}12p^2; & p < 2\%, \\ 5; & p \geq 2\%. \end{cases} \tag{1.5}$$

Here p is the tensile reinforcement ratio. For members reinforced with plain bars, factor β is reduced by 20% (Kaklauskas 2001).

To avoid excessive stiffness of RC members due to assumption of the simplified tension-stiffening law, tensile strength f_{ct}, calculated by *Eurocode 2*, is reduced by 20% (Kaklauskas *et al*. 2008a*, 2008c* and 2009*). A more sophisticated tension-stiffening law is under development in a parallel PhD project carried out in the research group. The numerical implementation of the *Layer* procedure is comprehensively discussed in Section 2.5.

1.2.7.2. Finite Element Code *ATENA*

In recent years, the use of finite element (FE) analysis has increased due to progressing knowledge and capabilities of computer software and hardware. Numerical techniques have been rapidly progressing for decades and commercial FE packages (*ABAQUS*, *DIANA*, *ATENA*, etc) now offer very powerful and general analytical tool for analysis of RC structures (Peiretti *et al*. 1991, Argyris & Kacianauskas 1996, Kaklauskas *et al*. 2004*). In FE approach, tension-stiffening effect and consequently deflection can be predicted rationally (Gribniak *et al.* 2004*, 2007d*). Present research employed FE code *ATENA* considered to be as one of the most successful software dedicated to analysis of RC structures.

Concrete models in *ATENA* software (Cervenka 1985, Cervenka *et al*. 2002) are based on smeared crack concept and damage approach. Concrete without cracks is considered as an isotropic material and concrete with cracks as an orthotropic material. In present study the *fixed crack* model was used, see Fig. 1.16a.

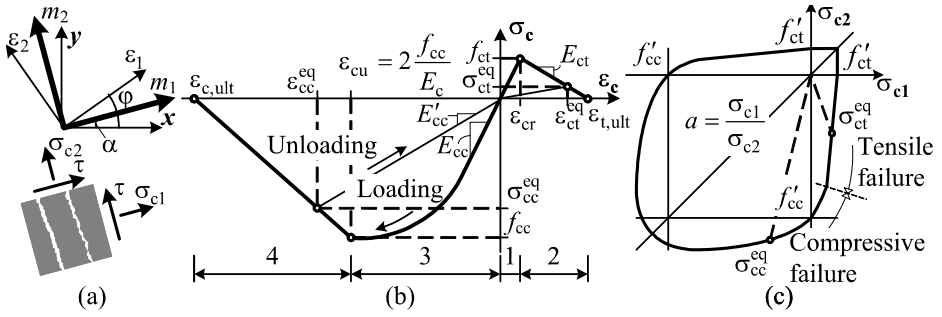

Fig. 1.16. The fixed crack model (a); uniaxial stress-strain law for concrete (b) and biaxial failure function for concrete (c)

*The reference is given in the list of publications by the author on the topic of the dissertation

In the *fixed crack* model crack direction and material axes are defined by the principal stress direction at the onset of cracking when the principal stress exceeds the tensile strength. In further analysis, this direction is fixed and cannot be changed though direction of principal strains may vary. A rotation of principal strain axes generates a shear stress on the crack plane. Consequently, the model of shear in cracked concrete becomes important. In the model a variable shear retention factor according to *Kolmar* (1986) is used, in which the shear modulus on the crack plane reduces with the crack opening.

The stress response is defined by means of the *equivalent* uniaxial stress-strain law as shown in Fig. 1.16b. This law illustrated by Fig. 1.16c describes the development of material state variables σ_{c1} and σ_{c2}, and covers the complete material behaviour under monotonically increasing load including pre- and post-peak softening in compression and tension. In case of a uniaxial stress state, it reflects experimentally observed behaviour. In a bi-axial state, the *equivalent* strain is defined as

$$\varepsilon_c^{eq} = \sigma_c^{eq} / E_c' \,. \tag{1.6}$$

Here E_c' is the secant modulus of concrete; σ_c^{eq} is the principal stress in concrete. This operation eliminates the *Poisson*'s effect. In uncracked concrete, the material is considered as isotropic and the secant modulus describes its damage. In cracked concrete, two elastic modules are defined for tensile and compressive material axes, respectively. The effect of a stress state on strength is considered by modifying σ_c^{eq} using the failure functions shown in Fig. 1.16c. As can be expected, an increase of strength due to confinement in compression (based on *Kupfer*'s experiments) is relatively small in plane stress state.

The above-described relation is applicable for the pre-peak response and, unfortunately, cannot be simply extended into the post-peak range. It is known from material research that post-peak softening is structure-dependent and a strain-based model may not objective. This concerns the material states 2 and 4 in Fig. 1.16b. Therefore, a fracture mechanics approach is employed in *ATENA* for softening behaviour and is based on the *crack band* model (Bažant & Oh 1983). Such a model substantially reduces mesh sensitivity (Cervenka & Pukl 1995). In this model, discrete cracks and compression failure zones representing discontinuities are modelled by means of strain localization within bands in FE displacement fields. The model is based on the assumption of equal energy dissipation. A unified approach is used for tensile and compressive softening.

It should be noted that the tension-stiffening effect is not explicitly included as a constitutive law in the above model. However, the fracture mechanics-based model reaches almost the same effect, where distinct cracks formed and a contribution of concrete between cracks generates a tension-stiffening effect, as was

shown by *Cervenka* (2002). Of course, this model has its limits bound to numerical discretization and is objective only for sufficiently fine mesh sizes.

1.3. Deflection Calculation Methods by Design Codes

This Section presents deflection calculation techniques from most widely used design codes: *Eurocode 2*, *ACI 318* and the *Russian Code* (*SP 52-101*). In these techniques, the beam theory (with plane section) is assumed and the stiffness of cracked cross section is based on tension-stiffening models derived from experiments. It is understood that, in open cracks, the action of concrete is reduced and the action of reinforcement is dominant, while concrete between cracks contributes to the stiffness significantly. The simple design models describe the global behaviour and serve everyday engineering design well. However, it can be observed that different formulas are used in different codes, which raises a question of their objectivity. Based on large amount of data, complex material effects are taken into account by means of empirical factors and expressions, which often lack physical interpretation. They are not able to account for an actual stress state and reinforcement detailing and are limited to simple cases of structural form and loading. It is common for all approximate methods based on the *beam* model to calculate the mid-span deflection from the formula representing an approximate integration of curvature:

$$\delta = s\kappa l_0^2 . \tag{1.7}$$

Here s is the factor depending on a loading case covering the shape of moment distribution; κ is the curvature corresponding to the maximum moment; and l_0 is the beam span. Curvature is determined by the well-known expression $\kappa = M/EI$ where M is the bending moment and EI is the flexural stiffness.

1.3.1. *Eurocode 2*

In the *Eurocode 2* model (CEN 2004), a reinforced concrete member is divided into two regions: *region I*, uncracked, and *region II*, fully cracked. In *region I*, both the concrete and steel behave elastically, while in *region II* the reinforcing steel carries all the tensile force on the member after cracking. The average curvature is expressed as

$$\kappa = (1-\zeta)\kappa_1 + \zeta\kappa_2 . \tag{1.8}$$

Here κ_1 and κ_2 correspond to the curvatures in *regions I*, and *II*, respectively. A coefficient ζ indicates how close the stress-strain state is to the condition

causing cracking. It takes a value of zero at the cracking moment and approaches unity as the loading increases above the cracking moment:

$$\zeta = 1 - \beta\left(M_{\mathrm{cr}}/M\right)^2 . \tag{1.9}$$

Here β is a factor taken as 1,0 for the case of short-term loading; M_{cr} and M are the cracking and the applied bending moments, respectively.

1.3.2. *ACI 318*: *Branson*'s Effective Moment of Inertia

Branson (1963, 1977) has proposed to calculate the *effective* moment of inertia I_{e} of the cracked section as follows:

$$I_{\mathrm{e}} = \left(M_{\mathrm{cr}}/M\right)^{\mathrm{m}} I_{\mathrm{g}} + \left[1 - \left(M_{\mathrm{cr}}/M\right)^{\mathrm{m}}\right] I_{\mathrm{cr}} . \tag{1.10}$$

In this I_{g} represents the moment of inertia for uncracked concrete section ignoring reinforcement and I_{cr} is calculated for the fully cracked section at the yielding of reinforcement; M is the applied moment; $M_{\mathrm{cr}} = f_{\mathrm{r}} I_{\mathrm{g}}/y_{\mathrm{t}}$ is the cracking moment; $f_{\mathrm{r}} = 0,623\lambda\sqrt{f_{\mathrm{c}}'}$ [MPa] is the modulus of rupture; y_{t} is the distance from the centre to the extreme tension fibre; f'_{c} is the specified compressive concrete cylinder strength (see Section 1.1.2); factor λ for normal-weight concrete assumed equal to 1.

Above equation was derived empirically by applying a *Newmark* numerical procedure to the test of 58 laboratory beams (Branson 1963). *Branson* initially expected a squared term in the expression, but found that the power *m* needed to be increased from 2 up to 3 for average member behaviour or 4 for section behaviour. The value of 3 was originally applied to a simply supported beam subjected to a uniformly distributed load and the value of 4 applied to a beam with central point load (Gohnert & Xue 2000). This equation represents a weighted average of uncracked ($E_{\mathrm{c}} I_{\mathrm{g}}$) and cracked ($E_{\mathrm{c}} I_{\mathrm{cr}}$) member stiffness, and a higher power was required because the computed response tends to be pulled toward the stiffer uncracked rigidity (especially for lightly reinforced members). However, the computed member response is much too stiff for members with an $I_{\mathrm{g}}/I_{\mathrm{cr}} \approx 15$ (Bischoff 2008).

The *ACI* adopted $m = 3$ in Equation (1.10) without specifying any application restrictions concerning the type of loading or boundary conditions. Such equation has been recommended by *ACI Committee 435* since 1966 and has been used in *ACI 318* since 1971. Accuracy of deflection prediction using both approaches (i.e. the power $m = 3$ and 4) has been investigated in Section 4.2.

1.3.3. Russian Code (*SP 52-101*)

1.3.3.1. Analytical Approach

Curvature of uncracked and cracked member is expressed as following:

$$\kappa = \begin{cases} \dfrac{M}{0{,}85E_{\mathrm{c}}I_{\mathrm{el}}}, & M \le M_{\mathrm{cr}}; \\ \dfrac{M}{E_{\mathrm{cr}}I_{\mathrm{red}}}, & M > M_{\mathrm{cr}}, \end{cases} \quad \text{where} \quad \begin{aligned} E_{\mathrm{cr}} &= \frac{2000}{3} f_{\mathrm{cp}}; \\ M_{\mathrm{cr}} &= \frac{f_{\mathrm{ct,n}} I_{\mathrm{el}}}{y_{\mathrm{t}}}. \end{aligned} \tag{1.11}$$

In this equation, I_{el} represents the moment of inertia for the uncracked section; I_{red} is the reduced moment of inertia of fully cracked section; E_{c} is the tangent modulus of elasticity (see Table 1.1); f_{cp} and $f_{\mathrm{ct,n}}$ are the compressive prism and characteristic tensile strength of concrete, respectively. The latter strengths are listed in Table 1.4.

The reduced moment of inertia takes into consideration tension-stiffening effect attributed to the tensile reinforcement using factor ψ_{s}, which modified deformation modulus of tensile reinforcement E_{s1}:

$$E_{\mathrm{s1,cr}} = E_{\mathrm{s1}} / \psi_{\mathrm{s}}; \quad \psi_{\mathrm{s}} = \varepsilon_{\mathrm{sm}} / \varepsilon_{\mathrm{s,cr}} = 1 - 0{,}8 \cdot M_{\mathrm{cr}} / M \,. \tag{1.12}$$

Here $\varepsilon_{\mathrm{sm}}$ is the mean strain in tensile reinforcement; $\varepsilon_{\mathrm{s,cr}}$ is the steel strain in the cracked section.

1.3.3.2. Numerical Approach

A simple iterative numerical procedure proposed in the *Russian Code* employs a concept of *secant* deformation modulus (analogous to the technique discussed in Section 1.2.7.1). An elastic-plastic diagram has been adopted for idealisation of reinforcement behaviour. Tension-stiffening is modelled in a similar way as in the analytical technique [see Equation (1.12)] using factor $\psi_{\mathrm{s,i}}$ that modifies deformation modulus of the *i*-th layer of tensile reinforcement $E'_{\mathrm{s,i}}$:

$$\sigma_{\mathrm{s,i}} = \frac{E'_{\mathrm{s,i}} \varepsilon_{\mathrm{s,i}}}{\psi_{\mathrm{s,i}}}; \quad \psi_{\mathrm{s,i}} = \left(1 + 0{,}8 \frac{\varepsilon^{\mathrm{cr}}_{\mathrm{s,i}}}{\varepsilon_{\mathrm{s,i}}} \right)^{-1} . \tag{1.13}$$

Here $\varepsilon_{\mathrm{s,i}}$ and $\varepsilon^{\mathrm{cr}}_{\mathrm{s,i}}$ are the strains of the *i*-th layer of steel at loading and just after cracking, respectively.

Three-linear stress-strain diagram shown in Fig. 1.17 has been introduced for idealisation of concrete behaviour, both in compression and tension. In this figure E_{c} is the tangent modulus of elasticity (see Table 1.1); f_{cp} and f_{ct} are the compressive prism and tensile strength of concrete, respectively. These parameters are given in Table 1.4.

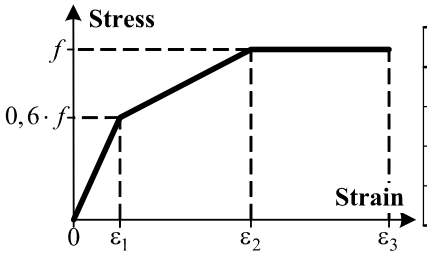

Parameter	Tension	Compression
f	f_{ct}	f_{cp}
ε_1	$0{,}6 \cdot f_{ct}/E_c$	$0{,}6 \cdot f_{cp}/E_c$
ε_2	0,0001	0,002
ε_3	0,00015	0,0035

Fig. 1.17. The stress-strain diagram of concrete (NIIZhB 2006)

Table 1.4. Strength of concrete (NIIZhB 2006)

Strength	Normative strength (Class) of concrete *B*, MPa										
	10	**15**	**20**	**25**	**30**	**35**	**40**	**45**	**50**	**55**	**60**
f_{cp}	6,0	8,5	11,5	14,5	17,0	19,5	22,0	25,0	27,5	30,0	33,0
f_{ct}	0,56	0,75	0,9	1,05	1,15	1,3	1,4	1,5	1,6	1,7	1,8
$f_{ct,n}$	0,85	1,1	1,35	1,55	1,75	1,95	2,1	2,25	2,45	2,6	2,75

1.4. Concluding Remarks of Chapter 1

While being confident about sufficient accuracy of deflection analysis of structures with moderate or large amounts of reinforcement, investigators often raise concerns about the validity of chosen tension-stiffening parameters for lightly reinforced members. Complexity of the issue is indicated by the wide-spread use of different code techniques and disparity of their prediction results. To check the accuracy of the predictive models, very few reports on accurately performed tests of lightly reinforced flexural members are available.

Cracking and tension-stiffening parameters probably have the most significant effect on numerical results of concrete members subjected to short-term loading. Tension-stiffening effects usually need to be included in an analysis that uses averaged stresses and strains to predict member behaviour. Such analysis can be performed using smeared FE, *Layer* section approach or truss modelling which incorporates compatibility of overall averaged strains. These techniques require a suitable material model for cracked concrete, and tension-stiffening results can be used to obtain the post-cracking stress-strain response of concrete. Two main deficiencies can be noted concerning most known tension-stiffening relationships:

- Tension-stiffening relationships were derived using test data of tension or shear RC members. Subsequently, these constitutive laws were applied

for modelling bending elements which behaviour differs from tension or shear members.

- The RC members employed for deriving the constitutive laws were exposed to shrinkage. Therefore, tension-stiffening was coupled with shrinkage effect.

Effects of shrinkage and accompanying creep of concrete along with cracking provide the major concern to the structural designer because of the inaccuracies and unknowns that surround them. In general, these effects are taken into account of long-term deformation and pre-stress loss analysis of reinforced concrete structures. Though considered as long-term effects, shrinkage and creep also have influence on crack resistance and deformations of RC members subjected to short-term loading. Future tests should carry out shrinkage recordings for subsequent elimination of this effect.

Present research is dedicated to developing a technique for deriving *free-of-shrinkage* tension stiffening relationships using test data of shrunk bending RC members. It is intended to develop an *inverse* technique that uses moment-curvature diagrams of shrunk RC members.

Test results on shrinkage and in some cases on deformations of RC members are marked with large scatter. Due to stochastic distribution of test the data, a probabilistic point of view, based on *Monte Carlo* technique, can be assumed in the *inverse* problem. Accuracy of the predictions often varies within ranges of various parameters. Therefore, the author is aiming to develop a statistical procedure for assessing accuracy of the predictions in regard to test data taking into account inconsistency of the data.

Based on the literature survey performed, following basic issues should be raised:

1. Developing a *Layer* section model for short-term deformation analysis of cracked reinforced concrete members subjected to short-term loading taking into account shrinkage and accompanying creep effects.
2. Investigating experimentally Concrete shrinkage effect on short-term deformations of lightly reinforced beams.
3. Developing a numerical procedure for deriving *free-of-shrinkage* tension-stiffening relationships using test data of shrunk flexural members.
4. Developing a statistical procedure for assessing accuracy of deflection predictions of reinforced concrete members, taking into account inconsistency of the test data.
5. Test data on free shrinkage of plain concrete specimens and deflections/curvatures of reinforced concrete bending members should be collected to perform comparative statistical analysis of various calculation methods.

2

Short-Term Deformational Analysis of Shrunk RC Members

This Chapter investigates shrinkage influence on tension-stiffening and stress-strain state of RC members subjected to short-term loading. A simple transformation formula has been proposed for eliminating shrinkage from tension-stiffening relationships of symmetrically reinforced members. An *innovative* numerical procedure has been developed for deriving *free-of-shrinkage* tension-stiffening relationships using test data of bending RC members. The procedure combines *direct* and *inverse* techniques of analysis of RC members. To eliminate shrinkage effect, a reverse shrinkage (expansion) strain was taken in the *direct* technique. This Chapter also deals with the computational aspects of convergence of the *inverse* procedure in order to provide a reliable and simple technique.

2.1. Strain in Concrete due to Shrinkage and Associated Creep

Most known tension-stiffening relationships have been derived using test data of shrunk RC members. Therefore, tension-stiffening was coupled with shrinkage effect. As shown in Section 1.2.5 shrinkage of an isolated plain concrete member would merely shorten. Reinforcement embedded in a concrete member pro-

vides restraint to shrinkage leading to compressive stresses in reinforcement and tensile stresses in concrete (see Figs. 1.15b and 1.15d). If the reinforcement asymmetrically placed on a section, shrinkage causes a non-uniform stress-strain distribution within the height of the section. The maximal tensile stresses appear on the extreme concrete fibre, close to larger concentration of reinforcement. As shrinkage is a long-term effect, creep always relieves shrinkage-induced stresses. Since concrete is an ageing material, its strength and modulus of elasticity increase with time as well as does shrinkage strain. Analysis is also complicated by interdependence between stress history and creep strain. *Trost-Bažant* method, called *the age adjusted modulus* method (Bažant 1972), gives a simple procedure for computing a strain under a varying stress. The method introduces the ageing coefficient $\chi(t,\tau)$ that assesses that the stress $\Delta\sigma_c(t,\tau)$ gradually applied from time τ to t will cause smaller strain than the stress $\Delta\sigma_c(t,\tau)$ instantly applied at time τ and kept constant until time t. For the shrinkage analysis of a non-cracked member assuming zero initial stress at time τ, strain in concrete can be expressed as follows (Gilbert 1988):

$$\begin{aligned}\varepsilon_c(t,\tau) &= \frac{\Delta\sigma_c(t,\tau)}{E_c(\tau)} + \frac{\Delta\sigma_c(t,\tau)}{E_c(\tau)}\varphi(t,\tau)\chi(t,\tau) + \varepsilon_{cs}(t,\tau) \\ &= \frac{\Delta\sigma_c(t,\tau)}{E_{ca}(t,\tau)} + \varepsilon_{cs}(t,\tau); \quad E_{ca}(t,\tau) = \frac{E_c(\tau)}{1+\varphi(t,\tau)\chi(t,\tau)}.\end{aligned} \tag{2.1}$$

Here $E_{ca}(t,\tau)$ is the age-adjusted effective modulus of concrete; $E_c(\tau)$ is the modulus of elasticity of concrete at time τ; $\varphi(t,\tau)$ is the creep factor and $\varepsilon_{cs}(t,\tau)$ is the mean free shrinkage strain of concrete taken negative. If creep factor is related to elastic deformation of concrete at 28 days, the age-adjusted effective modulus has the following form (CEB-FIP 1997):

$$E_{ca}(t,\tau) = E_c(\tau)\left[1+\chi(t,\tau)\frac{E_c(\tau)}{E_c(28)}\varphi(t,\tau)\right]^{-1}. \tag{2.2}$$

The above formulas were derived for compressive concrete assuming the linear creep law. The non-linear creep effect arising at advanced stress levels may also be taken into account (CEB-FIP 1991). Few investigations have been carried out concerning tensile creep (Gilbert 1988). In most practical cases, Equations (2.1) and (2.2) are used to assess creep in tension members.

Stresses due to shrinkage in a RC member can be derived based on equilibrium and compatibility of strains under the condition of perfect bond. For *n* layers of steel, a set of *n* equations with *n* unknowns has to be solved. In an alternative approach, shrinkage effect is modelled by equivalent *fictitious* actions (axial force and bending moment) (Gilbert 1988).

2.2. Approaches and Assumptions

Present investigation is aimed at developing non-linear stress-strain calculation techniques of shrunk RC members subjected to short-term external load. The techniques are based on the following approaches and assumptions: 1) smeared crack approach; 2) linear strain distribution within the depth of the section implying perfect bond between concrete and reinforcement; 3) uniform shrinkage within the section; 4) shrinkage-induced stresses do not exceed tensile strength of concrete f_{ct}; 5) all concrete fibres in the tension zone follow a uniform stress-strain tension-stiffening law.

It has been assumed that members at time τ started shrinking and at time t were exposed to external loading. Two stages of stress-strain behaviour have been considered: 1) pre-loading stage assessing long-term effects of shrinkage and accompanying creep, and 2) loading stage dealing with short-term action of the external load. Figure 2.1 illustrates stress-strain behaviour of tensile concrete assumed for these two stages. At the pre-loading stage (see Fig. 2.1a), stresses are modelled using the age-adjusted effective modulus of elasticity $E_{ca}(t,\tau)$. At the loading stage (see Fig. 2.1b), stresses prior to cracking are governed by the modulus of elasticity $E_c(t) > E_{ca}(t,\tau)$. Behaviour of cracked tensile concrete was modelled using linear tension stiffening relationship shown in Fig. 2.1b.

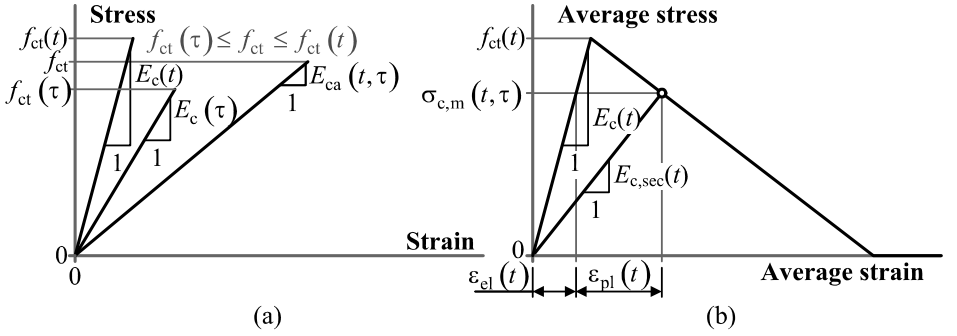

Fig. 2.1. Models of non-cracked (a) and cracked (b) tensile concrete

2.3. Analysis of Tension Members

2.3.1. Shrinkage-Induced Stresses at Pre-Loading Stage

Although there are known analytical solutions for shrunk tensile members (Bischoff 2001), it was intended on the example of this simple element to illustrate the proposed technique. As shown in Fig. 2.2c, shrinkage is modelled by *ficti-*

tious axial force $N_{cs}(t,\tau)$ having adequate effect on the stress-strain state of the member. To derive $N_{cs}(t,\tau)$, consider a plain concrete member (see Figs. 2.2a and 2.2c) having section area A_c and deformation modulus $E_{ca}(t,\tau)$ [see Equation (2.1)]. To impose axial strain $\varepsilon_{cs}(t,\tau)$, the member has to be subjected to such compressive force (see Figs. 2.2c and 2.2d):

$$N_{cs}(t,\tau)=\varepsilon_{cs}(t,\tau)E_{ca}(t,\tau)A_c\,. \tag{2.3}$$

Here A_c is the area of concrete net section. *F*orce $N_{cs}(t,\tau)$ is applied at the centroid of RC section. For a symmetrical section, member strain is calculated by

$$\varepsilon_{s,cs}(t,\tau)=\frac{N_{cs}(t,\tau)}{E_{ca}(t,\tau)A_c+E_sA_s}=\frac{\varepsilon_{cs}(t,\tau)E_{ca}(t,\tau)A_c}{E_{ca}(t,\tau)A_c+E_sA_s}\,. \tag{2.4}$$

Here A_s and E_s are the area and the elastic modulus of reinforcement, respectively. Shrinkage-induced internal forces acting in the steel and concrete are equal, but have opposite signs. Based on this equilibrium condition, stress in concrete can be expressed as

$$\sigma_{c,cs}(t,\tau)=-\frac{\varepsilon_{cs}(t,\tau)E_sp}{1+E_sp/E_{ca}(t,\tau)}\,. \tag{2.5}$$

Here $p=A_s/A_c$ is the reinforcement ratio.

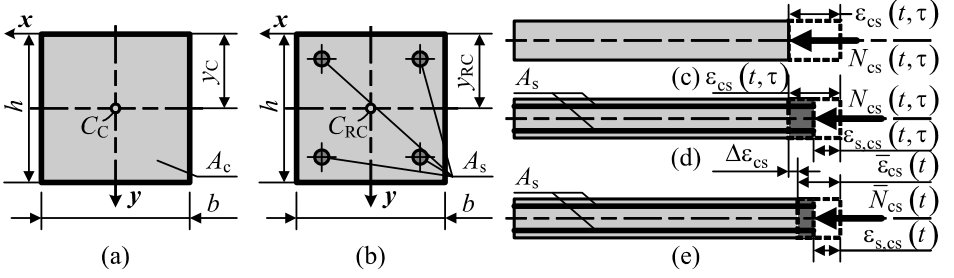

Fig. 2.2. Deformations of symmetrically reinforced concrete member due to shrinkage: plain concrete section (a); reinforced section (b); modelling of free shrinkage deformation (c); deformations due to restrained shrinkage neglecting and taking into consideration creep effect (d) and (e), respectively

2.3.2. Stress-Strain Analysis of Shrunk Members Subjected to Short-Term Loading

Consider a case when a shrunk member is subjected to a short-term axial load *P*. For a non-cracked member, strain in reinforcement at time *t* can be calculated using the principle of superposition:

$$\varepsilon_{\mathrm{s}}(t)=\varepsilon_{\mathrm{s,cs}}(t,\tau)+P\Big/\left[E_{\mathrm{c}}(t)A_{\mathrm{c}}+E_{\mathrm{s}}A_{\mathrm{s}}\right] =\frac{\varepsilon_{\mathrm{cs}}(t,\tau)E_{\mathrm{ca}}(t,\tau)A_{\mathrm{c}}}{E_{\mathrm{ca}}(t,\tau)A_{\mathrm{c}}+E_{\mathrm{s}}A_{\mathrm{s}}}+\frac{P}{E_{\mathrm{c}}(t)A_{\mathrm{c}}+E_{\mathrm{s}}A_{\mathrm{s}}}. \tag{2.6}$$

If the member cracks, the non-linear analysis is performed using a tension stiffening relationship (see, for instance, one shown in Fig. 2.1b). It should be noted that Equation (2.6) needed for the calculation has two different moduli of elasticity of concrete, i.e. $E_{\mathrm{c}}(t)$ and $E_{\mathrm{ca}}(t,\tau)$ or alternatively, $E_{\mathrm{c}}(\tau)$, see Equation (2.1) and Fig. 2.1a. Therefore, in a given form Equation (2.6) cannot be used for the non-linear analysis. Taking $E_{\mathrm{c}}(t)$ as a reference modulus of elasticity, the first member of Equation (2.6) is rearranged in the following way:

$$\varepsilon_{\mathrm{s,cs}}(t,\tau)=\varepsilon_{\mathrm{s,cs}}(t)=\bar{\varepsilon}_{\mathrm{cs}}(t)E_{\mathrm{c}}(t)A_{\mathrm{c}}\Big/\left[E_{\mathrm{c}}(t)A_{\mathrm{c}}+E_{\mathrm{s}}A_{\mathrm{s}}\right]. \tag{2.7}$$

Here $\varepsilon_{\mathrm{s,cs}}(t)$ is the steel strain due to shrinkage assumed a short-term action. In the Equation (2.7), *effective* shrinkage strain $\bar{\varepsilon}_{\mathrm{cs}}(t)$ has been introduced. *Effective* shrinkage strain is calculated from the condition of equality of the steel strains defined by Equations (2.4) and (2.7):

$$\bar{\varepsilon}_{\mathrm{cs}}(t)=\varepsilon_{\mathrm{cs}}(t,\tau)\frac{1+pE_{\mathrm{s}}/E_{\mathrm{c}}(t)}{1+pE_{\mathrm{s}}/E_{\mathrm{ca}}(t,\tau)}. \tag{2.8}$$

The non-linear analysis based on the *secant deformation modulus* conception takes into account varying material properties. It is performed using the following equation (see Fig. 2.2e):

$$\varepsilon_{\mathrm{s}}(t)=\varepsilon_{\mathrm{c}}(t)=\frac{\bar{N}_{\mathrm{cs}}(t)+P}{E_{\mathrm{c,sec}}(t)A_{\mathrm{c}}+E_{\mathrm{s,sec}}A_{\mathrm{s}}};\quad \bar{N}_{\mathrm{cs}}(t)=\bar{\varepsilon}_{\mathrm{cs}}(t)E_{\mathrm{c,sec}}(t)A_{\mathrm{c}}\,. \tag{2.9}$$

Here $E_{\mathrm{c,sec}}(t)$ and $E_{\mathrm{s,sec}}$ are the secant deformation moduli of concrete (see Fig. 2.1b) and steel, respectively. Strain in concrete due to acting stress

$$\varepsilon_{\mathrm{c},\sigma}(t)=\varepsilon_{\mathrm{c}}(t)-\bar{\varepsilon}_{\mathrm{cs}}(t). \tag{2.10}$$

The non-linear analysis is performed iteratively through the following steps:
Effective shrinkage strain $\bar{\varepsilon}_{\mathrm{cs}}(t)$ is calculated by the Equation (2.8).

1. Elastic properties of concrete and steel are assumed in the first iteration.
2. Strain in reinforcement $\varepsilon_{\mathrm{s}}(t)$ and strain in concrete $\varepsilon_{\mathrm{c},\sigma}(t)$ are calculated by Equations (2.9) and (2.10), respectively.
3. For the assumed constitutive laws, mean stresses and corresponding secant deformation moduli, $E_{\mathrm{c,sec}}(t)=\sigma_{\mathrm{c,m}}(t)\big/\varepsilon_{\mathrm{c},\sigma}(t)$ and $E_{\mathrm{s,sec}}=\sigma_{\mathrm{s,m}}/\varepsilon_{\mathrm{s}}$, are calculated for concrete and steel, respectively.

4. The above secant deformation moduli are compared with the ones initially assumed or computed in the previous iteration. If the agreement is not within the assumed precision, a new iteration is started from step 3 using new values of secant deformation modulus.

The above analysis based on *effective* shrinkage strain $\overline{\varepsilon}_{cs}(t)$, gives adequate stress and strain in steel as well as stress and total strain in concrete. Total strain in concrete, being equal to steel strain [see Equation (2.9)], can be split into these components:

$$\varepsilon_c(t,\tau) = \varepsilon_{cs}(t,\tau) + \varepsilon_{creep}(t,\tau) + \varepsilon_{el}(t) + \varepsilon_{pl}(t). \tag{2.11}$$

Here $\varepsilon_{el}(t)$ and $\varepsilon_{pl}(t)$ are the mean elastic and plastic strains, respectively, due to the contemporary effect of shrinkage and external loading; $\varepsilon_{creep}(t,\tau)$ is the shrinkage-induced creep strain which occurred at the pre-loading stage. Elastic and plastic strains due to stress $\sigma_{c,m}(t)$ can be assessed from Fig. 2.1b. Creep strain is calculated at stress $\sigma_{c,cs}(t,\tau)$ using the Equations (2.1) and (2.5).

2.3.3. Numerical Investigation of Tension-Stiffening

Shrinkage effect on tension-stiffening has been investigated numerically. The investigation procedure is described as follows.

1. Consider a fully defined symmetrically reinforced member subjected to axial tension. The linear constitutive relationship shown in Fig. 2.3a was used to model tension stiffening whereas behaviour of reinforcement was assumed linear elastic. Basic geometrical and material parameters used in this numerical investigation are presented in Table 2.1 (*Member-1*) and Fig. 2.3b.
2. Three analyses assuming different values of free concrete shrinkage strain, ε_{cs}, i.e. 0, –200 and –400 micro-strain, have been carried out using the technique described above. The calculated load-deformation diagrams are shown in Figs. 2.3c and 2.3d. The initial shortenings of the member due to shrinkage are shown in Fig. 2.3c. As in general testing practice these initial deformations are ignored, the load-deformation diagrams were moved to zero point (see Fig. 2.3d). Based on this figure, it can be concluded that tensile stresses in concrete induced by shrinkage significantly reduced cracking resistance and stiffness of the member.
3. Based on the load-sharing concept (Bischoff 2001), tension-stiffening relationships were derived from the load-deformation diagrams shown in Fig. 2.3d. The calculated relationships for different values of shrinkage are presented in Fig. 2.3e. As expected, the relationship derived for the non-shrunk member ($\varepsilon_{cs} = 0$) was the same as the originally assumed (see Fig. 2.3b). Although the maximal stresses in the remaining two curves were well below the tension strength, their descending branches were identical to the original relationship. As shown in Fig. 2.3e, negative stress portions were present in the curves resulting in reduction of factor β (see Fig. 2.3a).

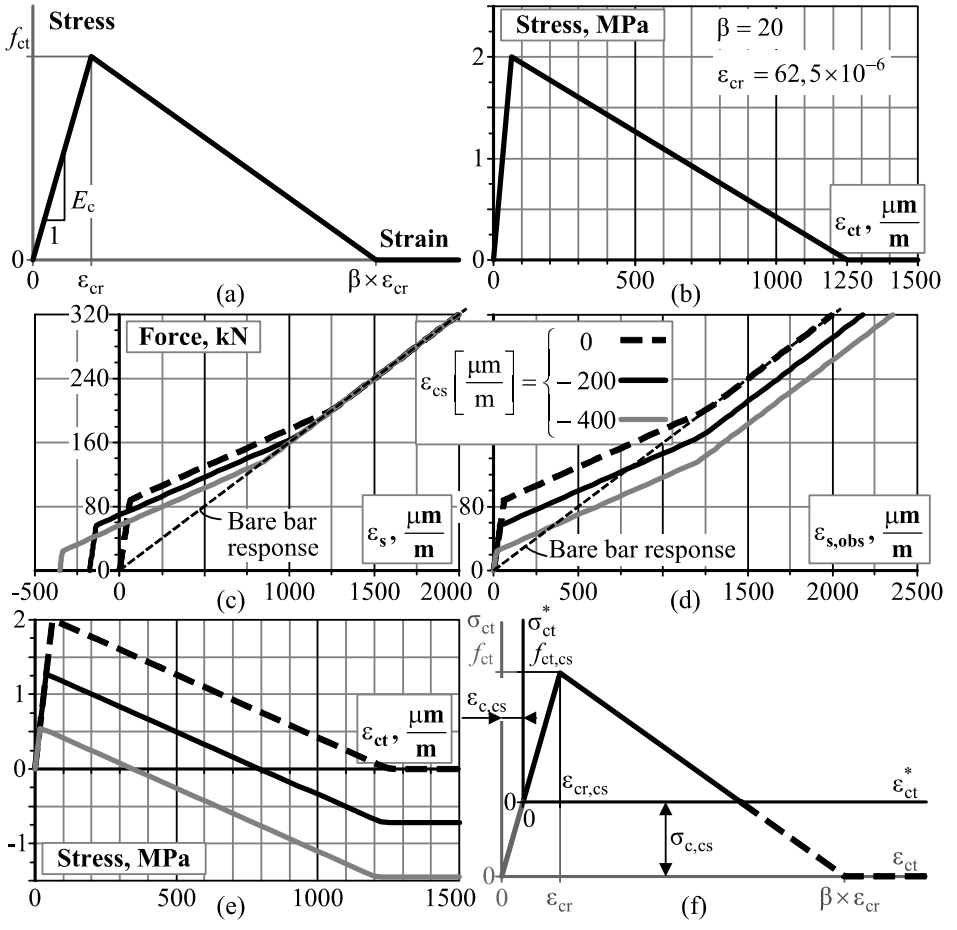

Fig. 2.3. Numerical modelling of tension RC member: linear tension-stiffening relationship (a); the relationship used in numerical analysis (b); shrinkage effect on load-deformation behaviour of modelled member (c); load-deformation diagram neglecting pre-loading displacements due to shrinkage (d); tension-stiffening relationships derived from the load-deformation diagrams (e) and transformation of tension-stiffening relationship (f)

Based on the above numerical results, it has been perceived that summation of the maximal stress of the curves shown in Fig. 2.3e and the stress induced by shrinkage [see Equation (2.5)] results in tension strength of concrete. Then the *modified* tension strength of concrete of a shrunk member can be expressed as

$$f_{ct,cs} = f_{ct} - \sigma_{c,cs}\,. \tag{2.12}$$

Graphically it is shown in Fig. 2.3f. With the introduction of a new coordinate system, it can be written in the following way:

$$\left\{\varepsilon_{ct}^{*} = \varepsilon_{ct} - \varepsilon_{c,cs};\quad \sigma_{ct}^{*} = \sigma_{ct} - \sigma_{c,cs}\right\}. \tag{2.13}$$

The above transformation formulae can be used for deriving a *free-of-shrinkage* tension-stiffening relationship from tests of shrunk members. Equations (2.13) imply that the stress-strain analysis of shrunk tension members can be performed by two approaches. In the first approach, shrinkage is assessed in the analysis (see Section 1.2.7.1) employing a *free-of-shrinkage* tension-stiffening relationship. In the second approach, shrinkage effect is taken into account by modifying the tension-stiffening relationship using Equations (2.13).

Table 2.1. Basic parameters of RC members

No.	Element	h	d	b	A_{s1}	A_{s2}	f'_c	E_s	p	$\varepsilon_{cs,obs}$
		mm			mm^2		MPa	GPa	%	μm/m
1.	*Member-1*	200	–	200	800	–	–	200	2,0	–
2.	*NS:15M* (Fields & Bischoff 2004)	250	–	250	400	400	41,2[1]	190	1,3	–232
3.	*HS:15M* (Fields & Bischoff 2004)	250	–	250	400	400	81,0	190	1,3	–337
4.	*NS:20M* (Fields & Bischoff 2004)	250	–	250	600	600	54,9[1]	198	1,9	–261
5.	*HS:20M* (Fields & Bischoff 2004)	250	–	250	600	600	81,0[1]	200	1,9	–337
6.	*Member-2*	250	225	180	284	284	25,4	200	0,7[2]	–
7.	*V-01-13WB* (Sato *et al.* 2007)	200	160	150	253	–	30,6[1]	193	1,1[2]	–263
8.	*V-01-13DB* (Sato *et al.* 2007)	200	160	150	253	–	32,5[1]	193	1,1[2]	–5,6
9.	*Z1* (Gilbert 2007)	100	82	850	141	–	38,4	200	0,2[2]	–
10.	*Z2* (Gilbert 2007)	100	81	850	227	–	38,4	200	0,3[2]	–
11.	*Z3* (Gilbert 2007)	100	80	850	354	–	38,4	200	0,5[2]	–
12.	*Z4* (Gilbert 2007)	100	79	850	565	–	48,4	200	0,8[2]	–

2.3.4. Application to Test Data

Transformation Equations (2.13) were applied to test data reported by *Fields & Bischoff* (2004). Four 3,5 m long symmetrically reinforced members of square section were tested under axial tension. Main geometrical and material properties of the members are listed in Table 2.1 (elements No. 2–5).

First, tension-stiffening relationships were calculated from experimental load-strain diagrams using the load-sharing concept (Bischoff 2001). The obtained

[1]Cylinder strength from $\varnothing 100 \times 200$ mm specimens.
[2]Reinforcement ratio $p = A_{s1}/(b \cdot d) \times 100\%$.

relationships are shown in Fig. 2.4a. The stresses were normalised based on tension strength $f_{\mathrm{ct,EC2}}$ calculated by *Eurocode 2*. Based on Fig. 2.4a, two points can be noted: 1) maximal stresses were well below (40 to 57%) the tension strength of concrete; 2) as shrinkage was not assessed in the analysis, significant portions of negative stresses were present.

Second, Equations (2.13) were applied to eliminate shrinkage effect from the tension-stiffening relationships. The resulting curves are shown in Fig. 2.4b. The maximal stresses have increased, both having reached about 80% of the tension strength. This has resulted in reduction of negative stress intervals.

2.4. Analysis of Flexural Members

2.4.1. Stress-Strain Analysis of Shrunk Loaded Beams

As shown in Fig. 2.5, *fictitious* shrinkage force $N_{\mathrm{cs}}(t,\tau)$ in a non-symmetrical section acts with eccentricity exerting bending upon the member:

$$M_{\mathrm{cs}}(t,\tau) = N_{\mathrm{cs}}(t,\tau)\left[y_{\mathrm{c}} - y_{\mathrm{RC}}(t,\tau)\right]. \tag{2.14}$$

Curvature and strain at any fibre *i* of a non-cracked member (see Fig. 2.5e) due to shrinkage can be calculated by the formulae:

$$\begin{aligned} \kappa_{\mathrm{cs}}(t,\tau) &= M_{\mathrm{cs}}(t,\tau)\Big/\left[E_{\mathrm{ca}}(t,\tau)\,I_{\mathrm{tr}}(t,\tau)\right]; \\ \varepsilon_{\mathrm{i,cs}}(t,\tau) &= \kappa_{\mathrm{cs}}(t,\tau)\left[y_{\mathrm{i}} - y_{\mathrm{RC}}(t,\tau)\right] + N_{\mathrm{cs}}(t,\tau)\Big/\left[E_{\mathrm{ca}}(t,\tau)\,A_{\mathrm{tr}}(t,\tau)\right]. \end{aligned} \tag{2.15}$$

Here $A_{\mathrm{tr}}(t,\tau)$ and $I_{\mathrm{tr}}(t,\tau)$ are the area and the second moment of area of the transformed section, respectively.

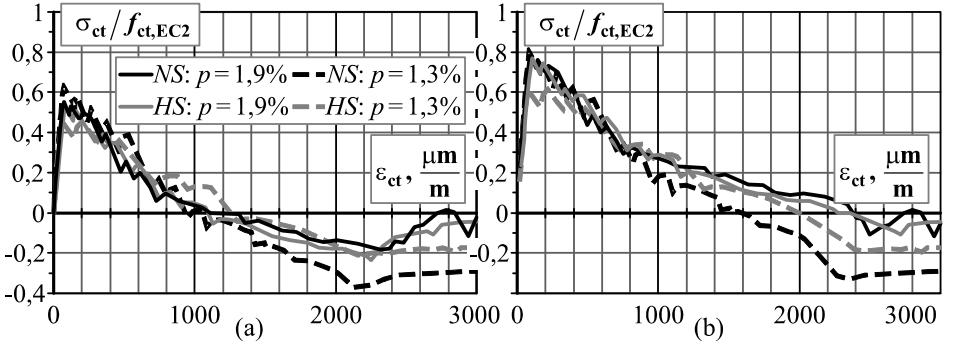

Fig. 2.4. Tension-stiffening diagrams derived from *Fields & Bischoff* (2004) test data: ignoring (a) and taking into consideration (b) shrinkage effect

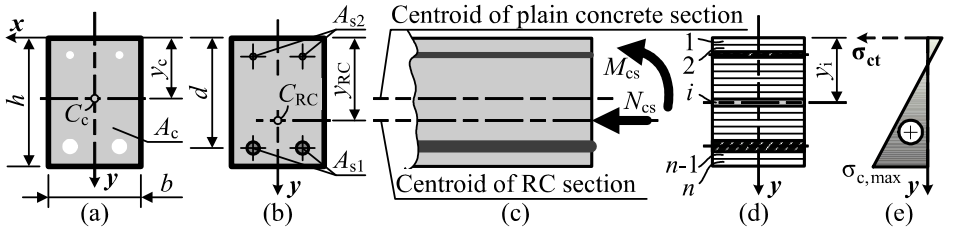

Fig. 2.5. Shrinkage effect in asymmetrically reinforced section: plain concrete net section (a); RC section (b); equivalent system of *fictitious* shrinkage force and bending moment (c); *Layer* section model (d) and distribution of stresses in concrete across the section (e)

Consider a case when a shrunk member is exposed to external short-term bending. If the member is not cracked, components of strains (curvatures) and shrinkage-induced stresses and external bending moment M can be calculated based on superposition principle. For the analysis of cracked members, the non-linear procedure described in (Kaklauskas 2004) can be used. It is based on the *Layer* section model and varying material properties assessed in terms of secant deformation modulus. Using the above approach, curvature and strain at any layer i (see Fig. 2.5e) can be calculated by the formulae:

$$\kappa(t)=\frac{\bar{M}_{cs}(t)+M}{IE(t)};\quad \varepsilon_i(t)=\frac{\bar{M}_{cs}(t)+M}{IE(t)}\left[y_i-y_{RC}(t)\right]+\frac{\bar{N}_{cs}(t)}{AE(t)};$$

$$\bar{M}_{cs}(t)=\bar{N}_{cs}(t)\left[y_c(t)-y_{RC}(t)\right];\quad AE(t)=\sum_{i=1}^{n}b_i t_i E_{i,sec}(t); \qquad (2.16)$$

$$IE(t)=\sum_{i=1}^{n}\left\{b_i t_i^3/12+b_i t_i\left[y_i-y_{RC}(t)\right]^2\right\}E_{i,sec}(t).$$

Here n is the total number of layers; b_i and t_i are the width and thickness of the i-th layer; y_i is the distance of the i-th layer from the top edge of the section; $E_{i,sec}(t)$ is the secant deformation modulus of i-th layer. $y_{RC}(t)$ and $y_c(t)$ are the coordinates of centroids of RC and plain concrete section, respectively, (see Fig. 2.5d) calculated as follows:

$$y_{RC}(t)=\frac{\sum_{i=1}^{n}b_i t_i y_i E_{i,sec}(t)}{\sum_{i=1}^{n}b_i t_i E_{i,sec}(t)};\quad y_c(t)=\frac{\sum_{i=1}^{n}b_i t_i y_i E_{i,sec}(t) l_i}{\sum_{i=1}^{n}b_i t_i E_{i,sec}(t) l_i}. \qquad (2.17)$$

Here l_i is the factor taken 1 for concrete and 0 for reinforcement layers. Due to changing material properties of different layers, coordinates of centroids $y_{RC}(t)$ and $y_c(t)$, vary with increasing load, and are different from those used in Equation (2.14).

In analogy with tension members, the concept of *effective* shrinkage strain, $\overline{\varepsilon}_{cs}(t)$ has been applied. Due to complex $\overline{\varepsilon}_{cs}(t)$ analytical expression for asymmetrical sections, it is recommended to be defined numerically:

$$\overline{\varepsilon}_{cs}(t) = \varepsilon_{cs}(t,\tau)\varepsilon'_{s,cs}(t,\tau)/\varepsilon'_{s,cs}(t). \tag{2.18}$$

Here $\varepsilon'_{s,cs}(t,\tau)$ and $\varepsilon'_{s,cs}(t)$ are the strains in the reinforcement layer with the largest area, including and excluding creep effect, respectively.

2.4.2. *Free-of-shrinkage* Tension-Stiffening Relationships

The proposed method for eliminating shrinkage from tension-stiffening relationships based on *Layer* approach combines *direct* and *inverse* techniques of analysis of RC members. In the *direct* technique, moment-curvature diagrams are calculated for assumed material stress-strain relationships. The *inverse* technique aims at determining tension-stiffening relationships for cracked tensile concrete from flexural tests of RC members. For given moment-curvature curves, the material stress-strain relation (including the descending branch) is computed from the equilibrium equations for incrementally increasing moment assuming portions of the relations obtained from the previous increments (see Section 2.5).

This Section presents an improved technique for deriving *free-of-shrinkage* tension-stiffening relations from test data of shrunk flexural members. The analysis is performed in the following steps sketched in Fig. 2.6.

Step 1. Using the test moment-curvature diagram shown in Fig. 2.6a, a tension-stiffening relationship is derived (see Fig. 2.6b) by the *inverse* technique.

Step 2. The tension-stiffening relationship obtained in Step 1 (shown also in Fig. 2.6c) is applied in the *direct* analysis assuming reverse (expanding) shrinkage strain $\varepsilon_{expn} = -\overline{\varepsilon}_{cs}$ [see Equation (2.18)]. The calculated *free-of-shrinkage* moment-curvature diagram is shown in Fig. 2.6d along with the experimental curve. It should be noted that due to the expansion of concrete, initial negative curvature was obtained. In absolute value, it is equal to the initial curvature (the positive one) due to shrinkage.

Step 3. As unloaded non-shrunk beam has no curvature, the *free-of-shrinkage* moment-curvature diagram obtained in Step 2, is shifted to zero point as shown in Fig. 2.6e. Using this diagram, a *free-of-shrinkage* tension-stiffening relation is obtained by the *inverse* analysis. This relationship is shown in Fig. 2.6f along with the one obtained from the test of shrunk member (see Fig. 2.6b).

2.4.3. Numerical Investigation of Tension-Stiffening

This Section numerically investigates shrinkage influence on cracking resistance, deformations and tension-stiffening of bending members. To begin with,

analysis was performed to investigate whether the stress-strain transformation technique described in Section 2.3.3 is applicable to bending members. Transformation Equations (2.13) require knowledge of shrinkage-induced stress $\sigma_{c,cs}$. However, shrinkage in asymmetrically reinforced sections induces a non-uniform stress state (see Fig. 2.5e). Therefore, a symmetrically reinforced section was used in the analysis assuming stress $\sigma_{c,cs}$ from the Equation (2.5). Basic geometrical and material characteristics are given in Table 2.1 (see *Member-2*). Stress-strain relationship recommended by *Eurocode 2* (CEN 2004) was assumed for the compressive concrete, whereas the behaviour of cracked tensile concrete was modelled by the diagram shown in Fig. 2.3b.

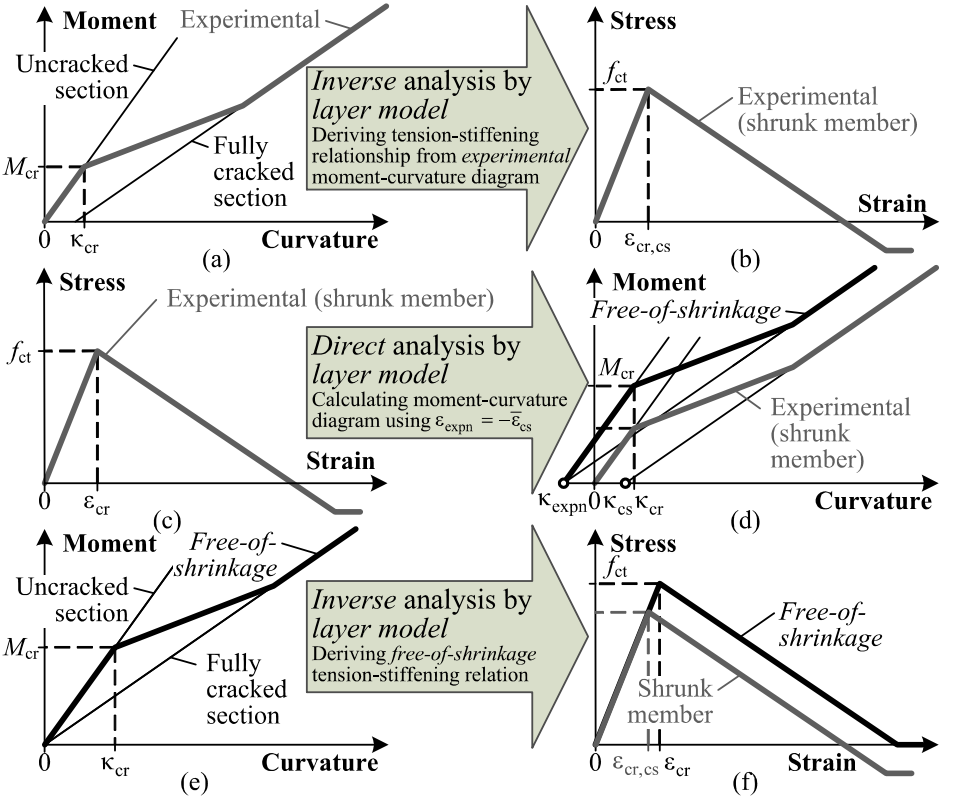

Fig. 2.6. Technique for deriving *free-of-shrinkage* tension-stiffening relationships from RC beam tests: deriving tension-stiffening relationship from test results (a) and (b); calculating *free-of-shrinkage* moment-curvature diagrams (c) and (d); deriving *free-of-shrinkage* tension-stiffening relationships (e) and (f)

Based on the numerical procedure, described in Section 2.4.1, the analysis was performed using three ε_{cs} values: 0; –200 and –400 micro-strain. Figure 2.7a presents the calculated moment-curvature diagrams. Although shrinkage had relatively little effect on initial curvatures (no external bending), it has significantly reduced cracking resistance and stiffness of cracked members.

Next analysis has assumed *modified* tension-stiffening relationships [see Equations (2.13)] and $\varepsilon_{cs} = 0$. Figure 2.7b shows the resulting moment-curvature diagrams by dotted lines. As the diagrams calculated by the two approaches coincided, it can be concluded that the stress-strain transformation technique is applicable to symmetrically reinforced bending members.

For asymmetrical sections, a more sophisticated procedure described in Section 2.4.2 was applied for deriving *free-of-shrinkage* tension-stiffening relationships. Based on this technique, the relationships were derived from test data of bending RC members reported by *Sato et al*. (2007) and *Gilbert* (2007).

Sato et al. have performed four point bending tests on singly reinforced beams. The tests have included shrinkage and creep recordings. Basic parameters of two beams (*V-01-13WB* and *V-01-13DB*) employed in the analysis are given in Table 2.1. Most of the characteristics, excepting curing conditions, were very similar for both beams. Beam *V-01-13WB* was prevented from shrinking (wet curing), whereas beam *V-01-13DB* was exposed to drying condition. This resulted in different shrinkage strains (see Table 2.1).

A bilinear stress-strain relationship has been adopted for reinforcement material idealization. The *Eurocode 2* stress-strain relationship was assumed for the compressive concrete. Figure 2.8 illustrates the steps of the proposed technique for deriving *free-of-shrinkage* tension-stiffening relationship for the beams.

First, tension-stiffening relationships were obtained from moment-curvature diagrams of two experimental beams (see Fig. 2.8a). The relationship derived from data of the beam *V-01-13DB* contains a portion of negative stress. Second, using the obtained tension-stiffening relationships, *free-of-shrinkage* moment-curvature diagrams were calculated (see Fig. 2.8b). It should be pointed out that due to similar beam parameters, the calculated diagrams were very close to each other. Third, *free-of-shrinkage* tension-stiffening relationships were derived using the *inverse* technique (see Fig. 2.8c). The calculated relationships were also similar and the portions of negative stresses practically disappeared.

Similar analysis has been carried out for the test data of singly reinforced slabs reported by *Gilbert* (2007). Basic parameters of the slabs *Z1-Z4* with reinforcement ratio $0{,}20\ldots0{,}84\%$ are given in Table 2.1. Due to missing data in the original paper, a typical free shrinkage strain $-200\,\mu m/m$ for concrete at 28 days (see Chapter 4), has been assumed in this analysis. The calculated tension-stiffening relationships with normalised stresses (concerning tension strength $f_{ct.EC2}$ assessed by *Eurocode 2*) are shown in Fig. 2.9. Tension-stiffening relationships calculated neglecting shrinkage effect are shown in Fig. 2.9a.

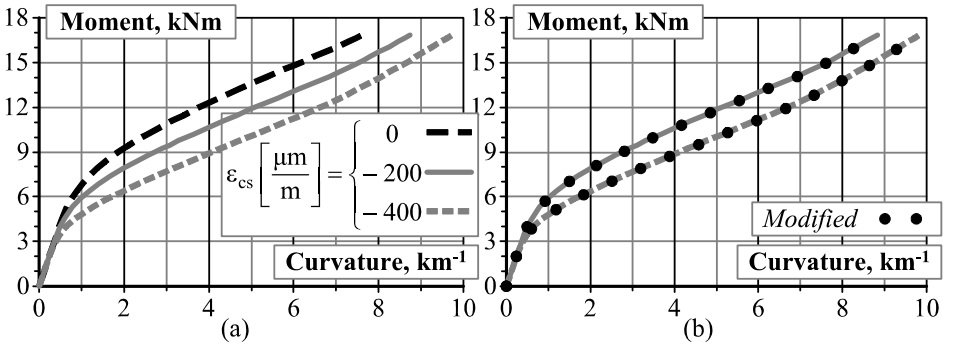

Fig. 2.7. Calculated moment-curvature diagrams taking into consideration shrinkage effect

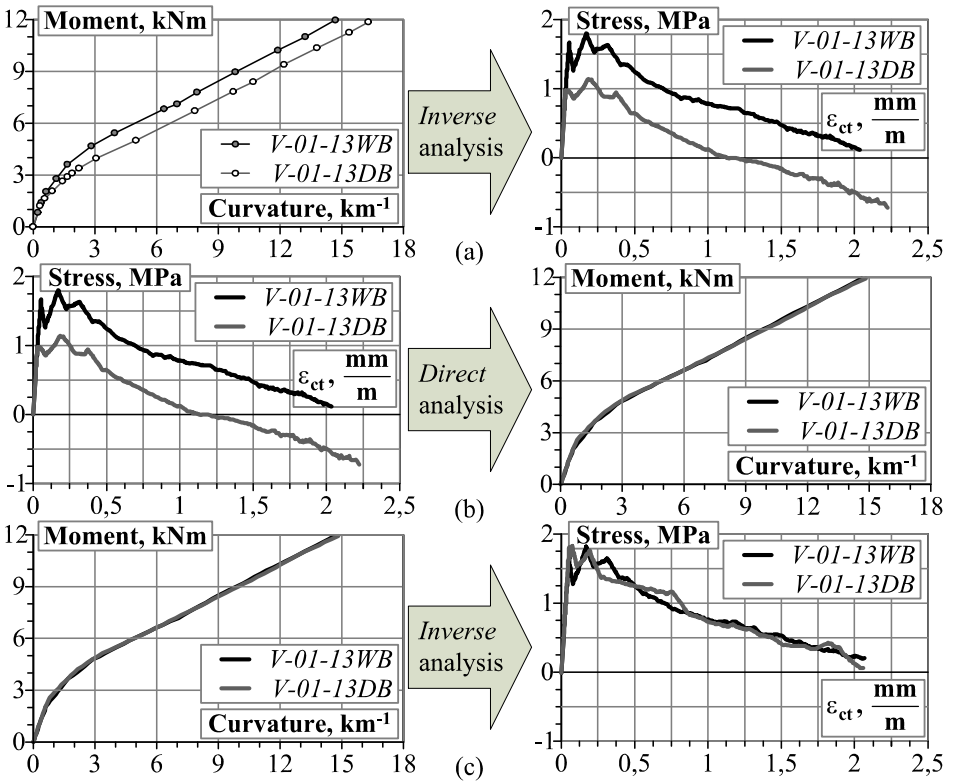

Fig. 2.8. Deriving tension-stiffening relationships *free-of-shrinkage* from data reported by *Sato et al*. (2007)

For slabs with higher reinforcement ratios (*Z3* and *Z4*), the relationships had smaller maximal stresses and less expressed tension-stiffening effect. In the analysis when shrinkage was eliminated, the calculated tension-stiffening relationships have approached each other (see Fig. 2.9b). The change in stresses due to elimination of shrinkage was more evident for the members with higher reinforcement ratios. It should be noted that the oscillations in the stress-strain curves shown in Figs. 2.8 and 2.9 were due to numerical peculiarities of *inverse* procedure (discussed in Section 2.5) reflecting the phenomenon of discrete cracking.

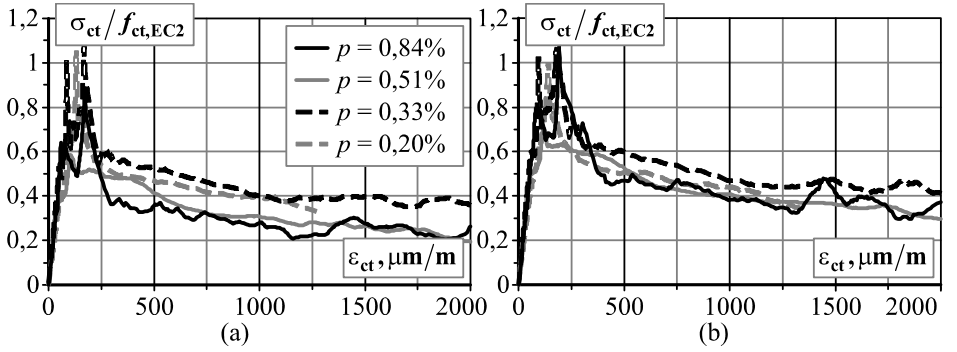

Fig. 2.9. Tension-stiffening relationships derived from *Gilbert* test data (2007) ignoring (a) and taking into consideration (b) shrinkage effect

2.5. Computational Aspects of *Inverse* Problem of RC Flexural Members

In usual structural analysis problems, called the *simulation* or the *forward* ones, strength and strains (curvature) have to be defined when material properties are given. Unfortunately, assumed material stress-strain relationships often are too simplified, do not reflect a complex multi-factor nature of the material and therefore are inaccurate. Due to bond with steel, tensile concrete in cracked RC structures has different properties from those that are obtained from tests of plain concrete specimens. It must be noted that concrete stress-strain curves obtained from tension tests of RC members do not necessarily assure accurate results for calculation of bending elements. Therefore, quite naturally a researcher is challenged by the idea to solve an *inverse* problem of bending analysis: to derive concrete material stress-strain relationships for given test moment-strain (curvature) diagrams.

The supervisor of this dissertation in co-authorship has proposed a method for deriving constitutive relationships from test data of flexural composite elements (Kaklauskas & Ghaboussi 2001). The proposed technique has been exten-

sively used in solving *inverse* problems of RC beams (Gribniak *et al*. 2007c* and Kaklauskas *et al*. 2007b*, 2008b*, 2008c*, 2009*). For numerical purposes, the test moment-curvature diagram has to be smoothed. This results in derivations from the original and consequently inaccurate constitutive law shape. In some cases, the constitutive relationships cannot to be obtained at all. This Section deals with computational improvement of the above method with the objective of providing a reliable and simple technique for reduction of prediction errors.

2.5.1. *Direct* Analysis Using *Layer* Section Model

As noted, the *inverse* procedure uses a simple iterative technique of deformational analysis of composite members based on *Layer* section model (Kaklauskas 2004). The calculation is based on formulae of strength of materials extended to application of *Layer* section model and material diagrams. The following assumptions have been adopted: 1) average strain, also called as smeared crack, concept; 2) linear strain distribution within the depth of the section; 3) perfect bond between layers. This Section describes *direct* technique.

Consider a doubly reinforced concrete member subjected to pure bending. A cross-section for such member is presented in Fig. 2.10a. The member's cross-section is divided into horizontal layers corresponding to either concrete or reinforcement (see Fig. 2.10b). Thickness of the reinforcement layer is taken from the condition of the equivalent area. The analysis needs to assume material laws for reinforcement and compressive and tensile concrete schematically shown in Figs. 2.10f and 2.10g.

Curvature and strain at any layer *i* [see Fig. 2.10d and Equation (2.16)] can be calculated by the formulae:

$$\kappa = \frac{M_{\text{ext}}}{IE};\quad \varepsilon_{\text{i}} = \frac{M_{\text{ext}}}{IE}\left[y_{\text{i}} - y_{\text{RC}}\right];\quad y_{\text{RC}} = \frac{SE}{AE};\quad AE = \sum\nolimits_{\text{i=1}}^{\text{n}} b_{\text{i}} t_{\text{i}} E_{\text{i,sec}};$$
$$SE = \sum\nolimits_{\text{i=1}}^{\text{n}} b_{\text{i}} t_{\text{i}} y_{\text{i}} E_{\text{i,sec}};\quad IE = \sum\nolimits_{\text{i=1}}^{\text{n}} \left\{ b_{\text{i}} t_{\text{i}}^3 / 12 + b_{\text{i}} t_{\text{i}} \left[y_{\text{i}} - y_{\text{RC}}\right]^2 \right\} E_{\text{i,sec}}. \tag{2.19}$$

Here M_{ext} is the external bending moment; *AE*, *SE* and *IE* are the area, the first and the second moments of the area multiplied by *secant* modulus.

For the given strains and constitutive laws (see Figs. 2.10d and 2.10c), stresses and corresponding secant modulus are calculated. The analysis is performed iteratively until convergence of secant modulus at each layer is reached. Figures 2.10d and 2.10e illustrate strain and stress distributions within the *Layer* section model. Annex B.1 presents implementation of the *direct* procedure using *MATLAB* software.

*The reference is given in the list of publications by the author on the topic of the dissertation

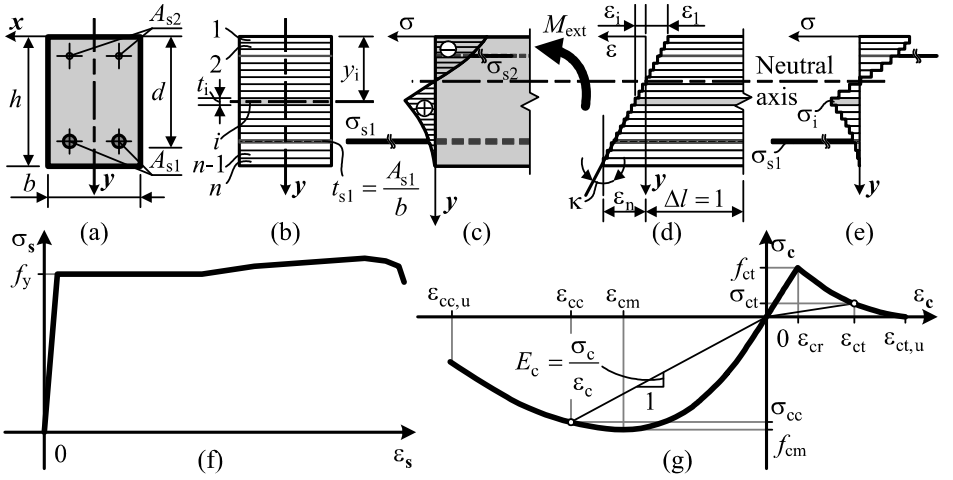

Fig. 2.10. *Layer* section model of RC section (a)–(e) and a constitutive relationships for reinforcement steel (f) and concrete (g)

2.5.2. Numerical Procedure for Solving *Inverse* Problem

2.5.2.1. Formulation

The proposed method aims at deriving average stress-average strain relationships of cracked tensile concrete using test data of flexural RC members. The experimental data can be as follows: a) moment-average strain at any layer or b) moment-curvature relationship. Using material test data, constitutive relationships for steel and compressive concrete should be defined. The *inverse* method also employs constitutive laws for steel and compressive concrete assumed either from tests or analytically. The technique is based on the *direct* method discussed in Section 2.5.1 and uses one additional assumption: 4) all fibres in the tensile concrete zone follow the same stress-strain law. Figure 2.11 presents a flow-chart of the *inverse* procedure. Based on geometrical parameters of the cross-section, *Layer* section model has to be composed.

Present analysis is based on use of a moment-curvature relationship. Computations are performed iteratively for incrementally increasing bending moment. For given load increment, initial value of secant deformation modulus of tensile concrete is assumed. Based on *direct* analysis, curvature is calculated. If it differs from the experimental value more than the assumed tolerance Δ, the analysis is proceeded using the hybrid *Newton-Raphson & Bisection* procedure (Verzhbitsky 2005). A secant deformation modulus of tensile concrete calculated for the extreme tensile fibre of the section is defined at each of iterations. The root locating procedure is started using the *Newton-Raphson* method. For moment increment *i*, secant deformation modulus $E_{i,k}$ at iteration *k* is defined:

$$E_{i,k} = E_{i,k-1} - \frac{\delta_{k-1}}{\delta'_{k-1}} = E_{i,k-1} - \frac{\delta\left(E_{i,k-1}\right)}{\delta'\left(E_{i,k-1}\right)}, \quad \delta(E) = \frac{\kappa_{th,i}}{\kappa_{obs,i}} - 1 . \qquad (2.20)$$

Here $E_{i,k-1}$ and $\delta\left(E_{i,k-1}\right)$ are, respectively, the secant deformation modulus and the prediction error obtained in the previous iteration; $\kappa_{th,i}$ and $\kappa_{obs,i}$ are, respectively, the calculated and experimental curvatures at load increment i; $\delta'\left(E_{i,k-1}\right)$ is the first derivation of the error obtained numerically by this central-difference equation:

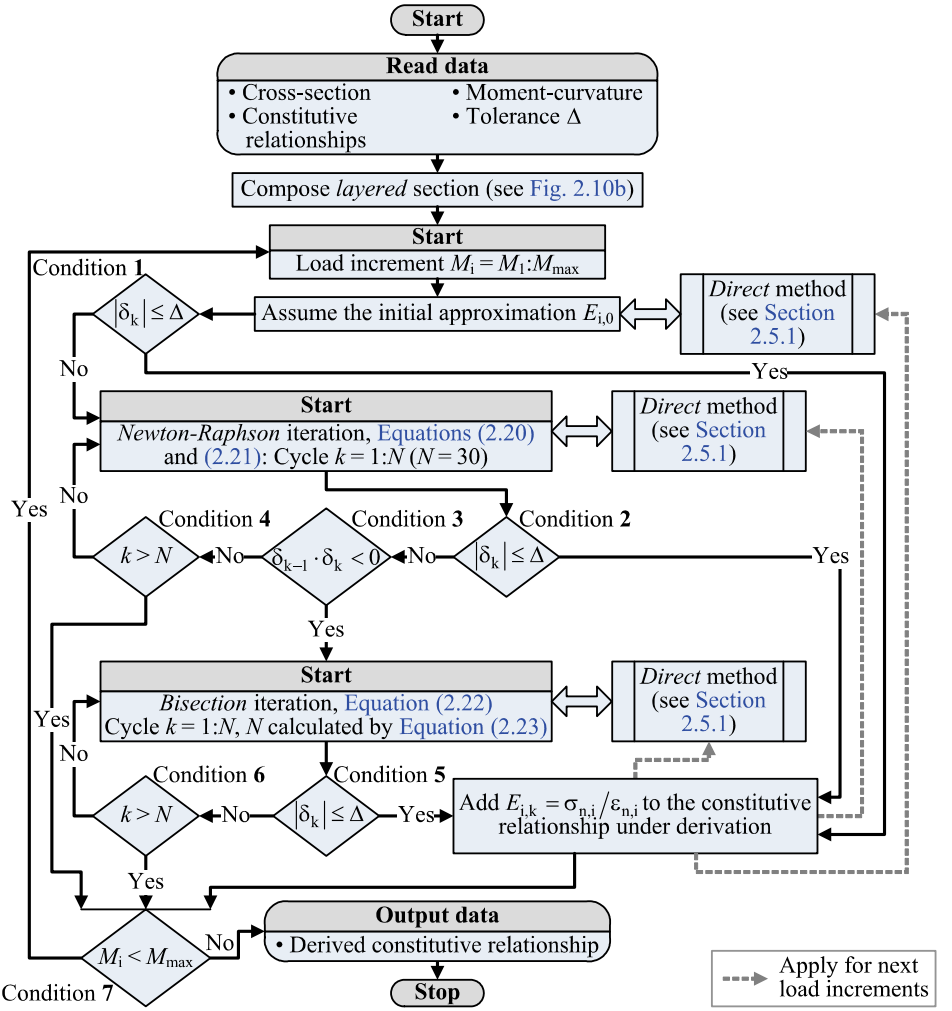

Fig. 2.11. Flow chart of the procedure for solving *inverse* problem

$$\delta'(E) = \frac{-\delta_2 + 8\cdot\delta_1 - 8\cdot\delta_{-1} + \delta_{-2}}{12\cdot h}, \qquad \delta_p = \delta(E + p\cdot h),\ \ p = -2; -1; 1; 2. \tag{2.21}$$

Here h is the difference grid size in this analysis assumed to be 0,1. For simplicity, indexes of deformation modulus E in the above equation are missing.

Using the above method, only one initial approximation (E_i) is required for solving the *inverse* problem. However, it requires five evaluations of the function $\delta(E)$ per iteration [see Equations (2.20) and (2.21)], i.e. the *direct* algorithm should be run five times. The *Newton-Raphson* procedure is applied until the solution is found, root interval is determined or the limit iteration number N is reached (see Fig. 2.11). If the solution is found, i.e. Condition (2) is satisfied, the obtained value of $E_{i,k}$ is fixed (used for further analysis steps) and the analysis is moved to the next load increment. When the limit iteration number is exceeded, the defined $E_{i,k}$ is rejected and the analysis moves to the next load step.

Although the *Newton-Raphson* method is fast, in some cases it may not found a solution. Therefore, in case when the root is localised (Condition (3) is satisfied), the analysis is proceeded using the *Bisection* method. The latter technique, though slower, always gives the solution, if it exists. Using the *bisection* method, the ends of the interval in a systematic way are moved closer and closer to each other until the localisation interval is small enough. The number N of repeated bisections needed to guarantee that the N^{th} iteration is an approximation to a root has an error less than the pre-assigned value Δ is estimated as following (Verzhbitsky 2005):

$$N \le \left\lceil \log_2\left(\frac{E_k^{(2)} - E_k^{(1)}}{\Delta} \right) \right\rceil. \tag{2.22}$$

Here the brackets $\lceil x \rceil$ mean the ceiling (rounding toward infinity) of argument x; $\left[E_k^{(1)}; E_k^{(2)} \right]$ is the root localisation interval at iteration k.

This method will require only one evaluation of the function δ_E per iteration. Secant modulus is defined by the equation:

$$E_{i,k} = \frac{E_{k-1}^{(2)} - E_{k-1}^{(1)}}{2}; \qquad \left\{ E_k^{(1)},\ E_k^{(2)} \right\} = \begin{cases} \left\{ E_{k-1}^{(1)},\ E_{i,k} \right\}, & \delta\left(E_{k-1}^{(1)}\right)\cdot\delta\left(E_{i,k}\right) \le 0; \\ \left\{ E_{i,k},\ E_{k-1}^{(2)} \right\}, & \delta\left(E_{k-1}^{(1)}\right)\cdot\delta\left(E_{i,k}\right) > 0. \end{cases} \tag{2.23}$$

2.5.2.2. Numerical Implementation Using Test Data

Numerical implementation of the proposed method has been illustrated using data of two RC beams (*S-1* and *S-4*) tested by the author (see Chapter 3). The constitutive laws assumed in this analysis are shown in Fig. 2.12. Experimentally obtained and the idealised stress-strain relationships for steel are shown in Fig. 2.12a. The constitutive law presented in *Eurocode 2* has been accepted for compressive concrete (Fig. 2.12b).

Present analysis was based on use of test moment-curvature relationships as shown in Fig. 2.12c. As noted, the *inverse* analysis is performed incrementally, using the constitutive law for tensile concrete obtained at previous loading stages. This means that errors made at a given moment increment will have influence on the shape of the constitutive law under derivation. Therefore, a particular care of avoiding errors should be taken at the early stages of the analysis associated to small curvatures. Though similar in absolute terms at all loading stages, errors of curvature measurements at early stages have much higher relative effect on the derived constitutive law. Therefore, as concrete in tension prior to cracking essentially behaves elastically, a limitation on curvature value used in the analysis has been introduced. The curvature should not be less than the calculated one by Equation (2.19) using elastic material parameters. If this limitation is not satisfied, it is recommended to replace the test curvature by the calculated one.

To illustrate the proposed technique, a detailed step-by-step numerical analysis has been performed for beam *S-1*. Consider load increment No. 20 marked in the moment-curvature diagram (see Fig. 2.12c). The constitutive stress-strain relationship under construction is shown in Fig. 2.12d. Stress-strain points and corresponding secant modulus derived at load stages No. 1–19 are also presented in the figure. The analysis was performed according to the flow-chart described in Section 2.5.2.1. At this load increment, convergence was reached after eight iterations (3 + 5 iterations of *Newton-Raphson* and *Bisection* procedures, respectively). Initial value of secant deformational modulus was assumed equal to zero. Intermediate solution points along with the initial point corresponding to $E_{20,0} = 0$ and the derived portion of stress-strain diagram at load increment No. 20 are also shown in Fig. 2.12d.

Convergence rate, an important aspect of the proposed procedure, has been also investigated. Analysis has shown that for this particular case, such factors as a number of layers, initial value of secant modulus $E_{\mathrm{i},0}$ and assumed tolerance Δ had significant influence on convergence rate. Results of convergence investigation for beam *S-1* are presented in Fig. 2.13. The analysis included all 39 experimental points shown in Fig. 2.13a. Convergence rates for varying number of layers, initial value of secant modulus and assumed tolerance are given in Fig. 2.13b. The convergence rate is presented in relative terms, as a reference assuming the minimal computation time.

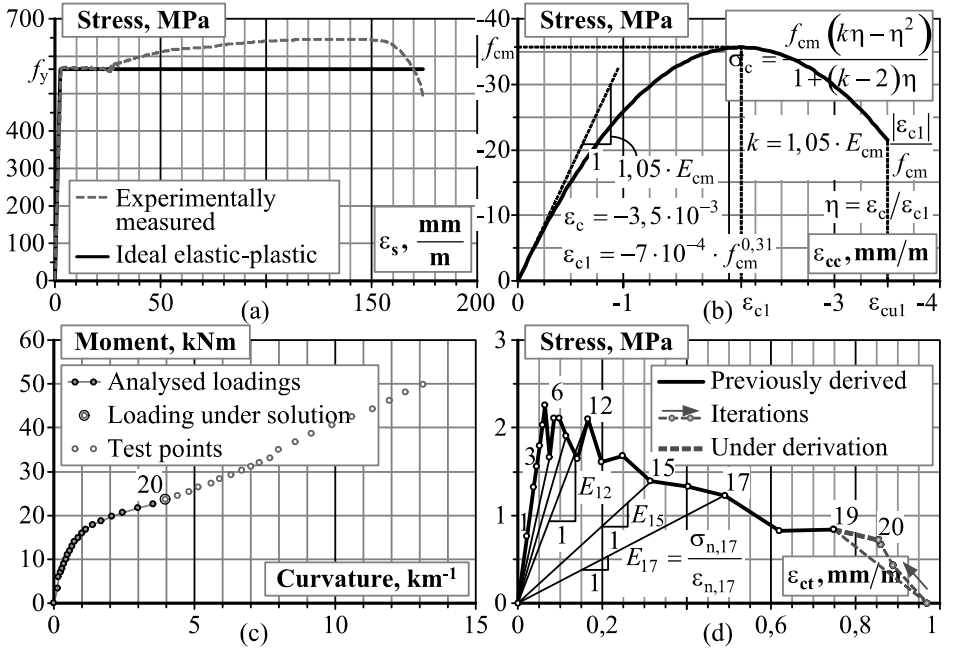

Fig. 2.12. Constitutive relationships assumed in the analysis for reinforcement steel (a) and compressive concrete (b); solution of inverse problem at fixed load increment (c) and (d)

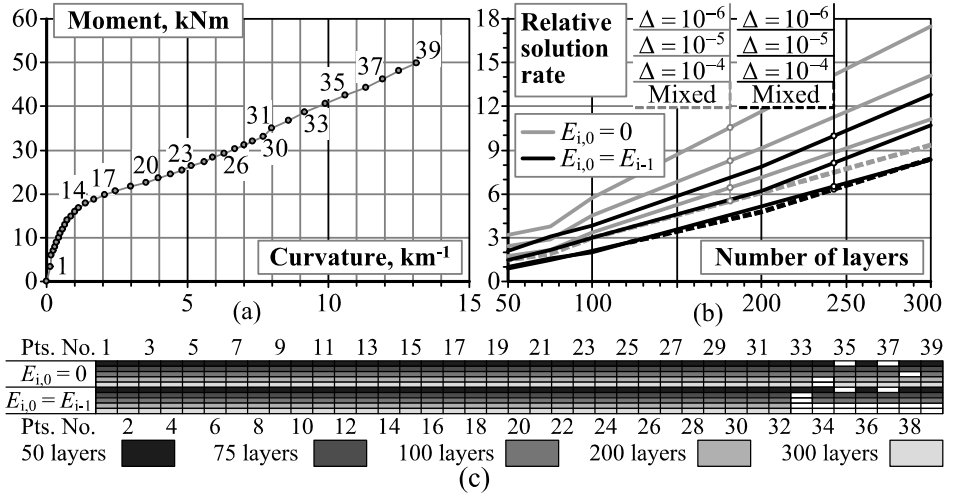

Fig. 2.13. Analysis of convergence speed in respect to number of layers and the tolerance

Number of layers and the tolerance were ranging from 50 to 300 and from 10^{-4} to 10^{-6}, respectively. The latter values were assumed for convergence of both curvatures and deformation modulus. *Mixed* tolerance concept was also investigated assuming 10^{-4} and 10^{-5} for curvatures and deformation modulus $E_{\mathrm{i.k}}$, respectively.

Two cases of initial value of deformation modulus were investigated: $E_{\mathrm{i},0} = 0$ and $E_{\mathrm{i},0} = E_{\mathrm{i}-1}$ (assuming the converged value from the previous load increment). The corresponding resulting lines are shown in Fig. 2.13b in grey and black, respectively. Analysis has shown that a number of layers has the most significant influence on computation time. For instance, with increase of number of layers from 100 to 300, the computation time approximately trebles. The tolerance has lesser effect: if it is reduced from 10^{-4} to 10^{-6}, the computation time increases less than twice. *Mixed* technique has proved to be among the most effective.

Initial value of deformation modulus has also quite significant influence on computation rate. It should be noted that the assumption $E_{\mathrm{i},0} = 0$ always leads to longer computation. However, it has advantages regarding the convergence process itself. The convergence process is illustrated graphically in Fig. 2.13c were different grey colour intensities represent varying layer numbers. Non-converged load increments are indicated by void areas. As clearly seen from Fig. 2.13c, the computation procedure under assumption $E_{\mathrm{i},0} = 0$ has reached convergence at almost all load increments. The computation assuming $E_{\mathrm{i},0} = E_{\mathrm{i}-1}$ was not as stable as the previous one and in some cases, a single non-converged point triggered convergence failure in the remaining load steps.

For cases when lager numbers of layers were assumed (200 and 300), such a point was load increment No. 33. This could be explained by unstable processes due to sudden changes in curvature increment rates at loads preceding the critical point. Such critical load points for beams *S-1* and *S-4* are indicated in Fig. 2.14a with corresponding curvature increment rates shown in Fig. 2.14b. Sensitivity analysis has shown that such input parameters as layer number $n = 100$, $E_{\mathrm{i},0} = 0$ and *mixed* tolerance conception allowed reaching optimal convergence. The above set of parameters was used in further analysis. Computer code implementation using *MATLAB* software is given in Annex B.2.

Tension-stiffening relationships derived using the proposed technique are shown in Figs. 2.15a and 2.15b. Fragments of the relationships in more details are shown in Figs. 2.15c and 2.15d. The figures also illustrate convergence process with indicated intermediate solution points. The derived relationships have significant oscillations. This was due to changes in curvature increment rate caused by discrete cracking nature of reinforced concrete. The oscillations were more clearly expressed in beam *S-4* designed for given tensile reinforcement area to have smaller number of bars of larger diameter (see Section 3.1.1). It is well established that reduction in diameter leads to smaller crack width and spacing in the ideal case approaching to smeared cracking.

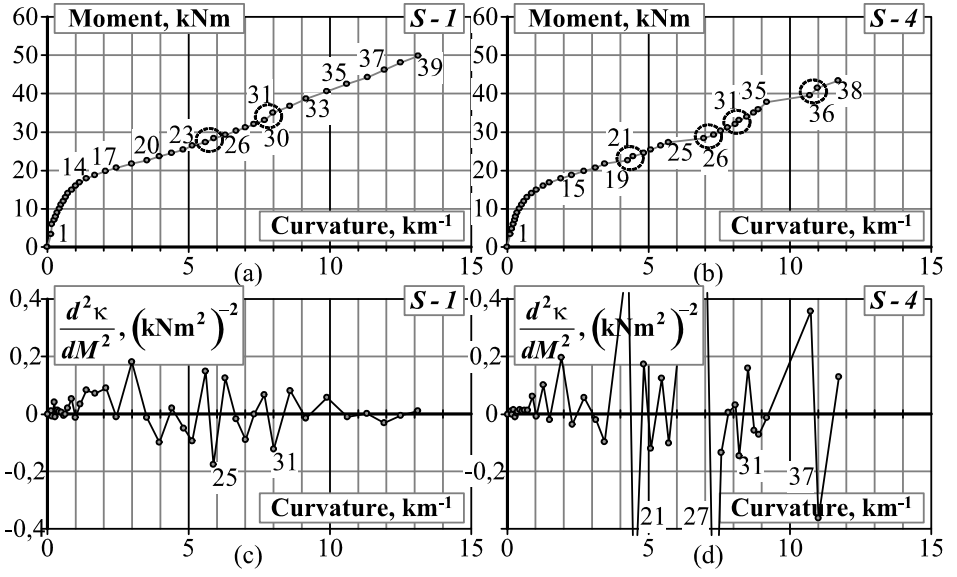

Fig. 2.14. Analysis of convergence speed in respect to number of layers and the tolerance

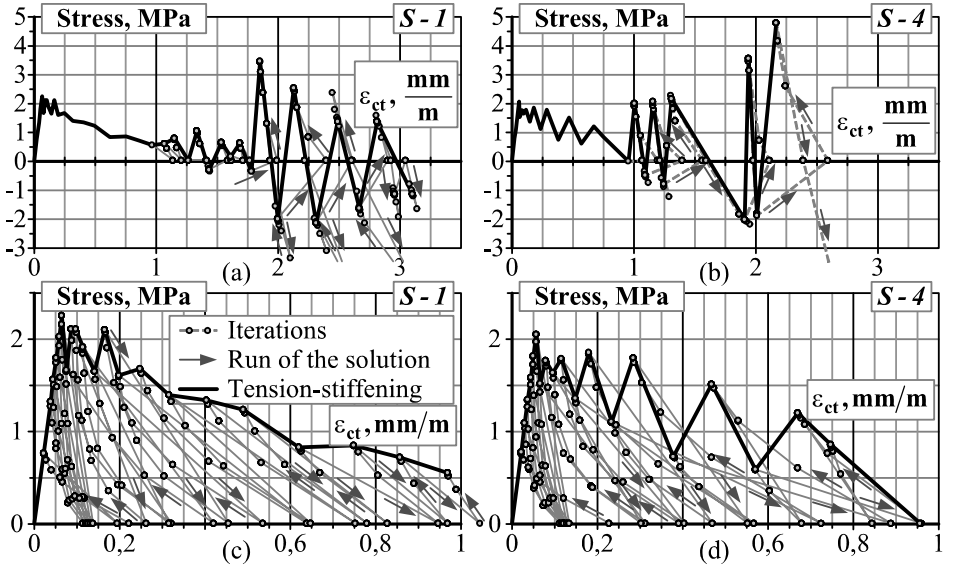

Fig. 2.15. Derived tension-stiffening relationships with iterations

It should be noted that the initial oscillations, mainly caused by discrete cracking, further on might become dramatic due to accumulative nature of the *inverse* procedure (Kondratenko & Gribniak 2004*, Kaklauskas *et al*. 2007b* and 2008c*). Following the assumption of uniform constitutive law for all tensile layers, each inadequate stress increment should be compensated by respective stress change of opposite sign. In such a way, as shown in Figs. 2.15a and 2.15b, the oscillations may obtain dramatic character. Naturally, such relationships cannot be straightforwardly assumed as constitutive laws. To eliminate the oscillations, a smoothing procedure has been proposed and is described in the next Section.

2.5.3. Technique for Smoothing Oscillations of the Solution

The procedure proposed for solving the *inverse* problem is strongly affected by the composition of initial data set (i.e. the points of moment-curvature diagram). To reduce sudden changes in curvature increment rates at load increments, two data sets were constructed from the experimental data. Figure 2.16 shows tension-stiffening relationships derived using even and odd test points (1st and 2nd sets, respectively) of moment-curvature diagram. Only the first and the last points were used in both sets. The differences in the derived tension-stiffening relationships are obvious (see Figs. 2.15a and 2.15b) referring to stochastic nature of given test data. It should be noted that dividing initial data into sub-sets is strongly recommended, if the number of data points exceeds 80. In general, such division may be considered as an additional tool for smoothing.

As noted, the oscillations are triggered by sudden changes in curvature increment rate. In previous investigations (Kaklauskas 2001, 2004, Kaklauskas & Gribniak 2005a*, 2005b*), to avoid the oscillations, moment-curvature diagrams were numerically smoothed, most often simply rejecting some test points. The smoothing technique was based on trial-and-error approach and involved some subjective judgement having influence on the resulting stress-strain relationship. In other words, the result (deformation modulus of the extreme tensile fibre) derived at each step is dependent on the results obtained at all previous steps.

In order to avoid subjective judgement in the smoothing procedure, in present research smoothing was performed on the resulting (tension-stiffening) relationship. For this, the *modified running-average* (MRA) method based on *Hardy*'s formula (Pollard 1979) has been applied. Potential of MRA method can be exploited more extensively, if large amount of input points is used. In general, moment-curvature diagram possesses about 20–30 test points only, which would restrict application of MRA method. To increase the amount of input data, extra pseudo-experimental data sets were generated. Assuming that the initial data set

*The reference is given in the list of publications by the author on the topic of the dissertation

generally has a stochastic nature, the *Monte Carlo* method could be applied for construction of pseudo-experimental data sets (Mikūta & Gribniak 2006)*.

Multiple analyses were performed for several sets of moment-curvature diagrams with randomly selected test points. Thus, no modifications were made in the moment-curvature diagrams and, in fact, practically all test points were used in the analysis. The proposed smoothing procedure is based on the following hints: 1) adjacent test points were moved into separate sets, thus reducing sudden changes in curvature increment rate; 2) to suppress oscillations of numerical origin, extra pseudo-experimental data points were randomly introduced by means of linear interpolation; 3) the resulting stress-strain relationships obtained from different simulations were averaged.

In general, the effectiveness of the smoothing procedure will favour of the larger number of sets. Various cases of composition of test data were analysed. For illustration, one of such cases is discussed below.

As shown in Fig. 2.17a, three data sets of moment-curvature diagrams were generated. Sets No. 1 and 2 were made using odd and even experimental points, respectively, with random introduction of extra-points. Set No. 3 differs from set No. 2 by a number of extra-points. Stress-strain relationships derived from the above test data are shown in Fig. 2.17b. As noted, averaging the resulting curves is based on the *modified running-average* method (Pollard 1979):

$$f_{\mathrm{i,aver}} = \left(w_0 - \left[n^2 - 1 \right] \Delta^2 w_{-1} \Big/ \left[24n^2 \right] \right) \Big/ n; \quad \Delta^2 w_{-1} = w_1 - 2w_0 + w_{-1}; \\ w_{-1} = \sum_{\mathrm{i}-(3\mathrm{n}-1)/2}^{\mathrm{i}-(\mathrm{n}+1)/2} f_{\mathrm{k}}; \quad w_0 = \sum_{\mathrm{i}-(\mathrm{n}-1)/2}^{\mathrm{i}+(\mathrm{n}-1)/2} f_{\mathrm{k}}; \quad w_1 = \sum_{\mathrm{i}+(\mathrm{n}+1)/2}^{\mathrm{i}+(3\mathrm{n}-1)/2} f_{\mathrm{k}}. \tag{2.24}$$

Here $f_{\mathrm{i,aver}}$ is the average value of *i*-th point; w_{-1}, w_0 and w_1 are the sum of preceding, central and succeeding *n* ordinates; f_{k} is the value of *k*-th point.

The tension-stiffening relationships were derived using the procedures described in Sections 2.5.1 and 2.5.2. The resulting *free-of-shrinkage* tension-stiffening relationships obtained for test beams *S-1* and *S-2* are presented in Fig. 2.18. The specific strain energy *dD* (see Figs. 1.4b and 1.4c) may serve as a characteristics of tension-stiffening. This energy corresponds to the area under the *free-of-shrinkage* tension-stiffening curve and can be calculated using the *trapezoidal* rule:

$$dD = \int_0^{\varepsilon_{\max}} \sigma \mathrm{d}\varepsilon = 0{,}5 \cdot \sum_{\mathrm{i}=1}^{\mathrm{m}-1} \left(\sigma_{\mathrm{i}+1} + \sigma_{\mathrm{i}} \right) \left(\varepsilon_{\mathrm{i}+1} - \varepsilon_{\mathrm{i}} \right), \quad \varepsilon_{\mathrm{m}} = \varepsilon_{\max}. \tag{2.25}$$

Here $\varepsilon_{\max}$ is the maximal strain; σ_{i} and ε_{i} are the averaged stress and corresponding strain, respectively. By this, energy *dD* was found to be equal to 2,249 and 1,632 kJ/m^3 for beams *S-1* and *S-4*, respectively.

*The reference is given in the list of publications by the author on the topic of the dissertation

Along with the derived relationships, a simple linear tension-stiffening relation is shown in Fig. 2.18 by grey line. In present study, the latter was introduced in the *Layer* section model (see Section 1.2.7.1) further applied in the numerical analysis (see Section 4.2). The strain energy (area of the triangle limited by the grey lines) is equal to 1,630 and 2,158 kJ/m^3 for beams *S-1* and *S-4*, respectively. Comparison of the strain energy obtained for the numerically derived and the simplified relationships has shown satisfactory agreement. It allows concluding that application of linear tension-stiffening relationships is objective enough.

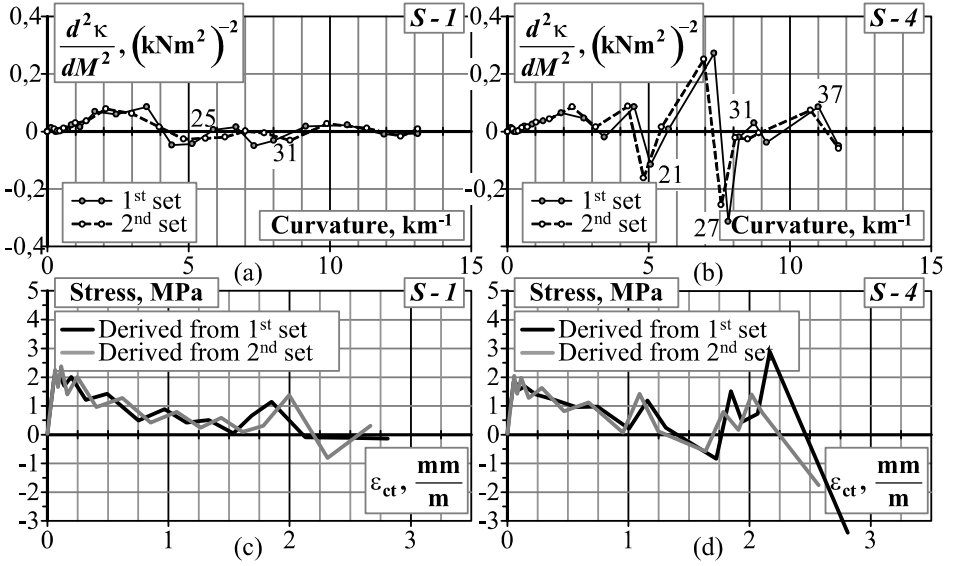

Fig. 2.16. Tension-stiffening relationships derived using different data sets

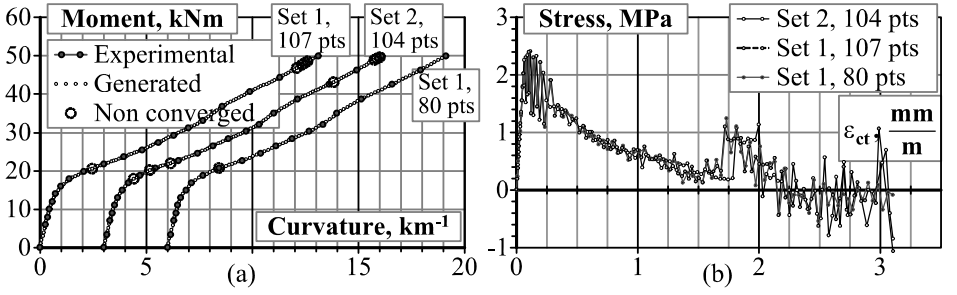

Fig. 2.17. Generation of extra-points using *Monte-Carlo* technique and derived constitutive relationships from extended data sets

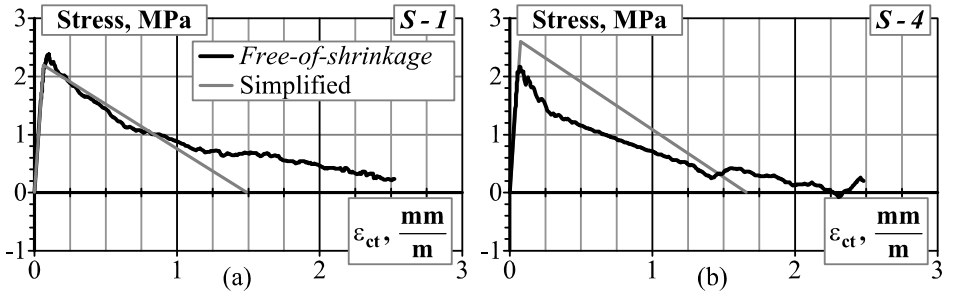

Fig. 2.18. Comparison of the linear and *free-of-shrinkage* tension-stiffening relationships derived from experimental data

2.6. Concluding Remarks of Chapter 2

This Chapter presents investigation results of shrinkage influence on deformations and tension-stiffening effect in tension and bending concrete members subjected to short-term loading. Two numerical techniques, the *direct* and the *inverse*, have been proposed. In the *direct* technique, moment-curvature diagrams are calculated for the assumed material stress-strain relationships. The *inverse* technique aims at determining tension-stiffening relationships for cracked tensile concrete from flexural tests of RC members. The techniques are based on the following approaches and assumptions:

- smeared crack approach;
- *Layer* section model;
- linear strain distribution within the depth of the section implying perfect bond between reinforcement and concrete;
- all concrete fibres in the tension zone follow a uniform stress-strain tension-stiffening law.

Based on numerical experiments of tension members, a simple transformation formula has been proposed for eliminating shrinkage from tension-stiffening relationships. The formula has appeared to be applicable to symmetrically reinforced bending members. These transformation formulae can be used for deriving a *free-of-shrinkage* tension-stiffening relationship from tests of shrunk members.

An *innovative* numerical procedure has been proposed for deriving *free-of-shrinkage* tension-stiffening relationships using test data (moment-curvature relationships) of bending reinforced concrete members. The procedure combines the *direct* and the *inverse* techniques. To eliminate shrinkage effect, a reverse shrinkage (expansion) strain was assumed in the *direct* technique.

Numerical implementation of the *inverse* procedure was discussed and the issue of convergence was investigated. Optimal convergence was achieved in the *inverse* problems when such input parameters were assumed:

- layer number $n = 100$;
- initial value of deformation modulus $E_{i,0} = 0$;
- *mixed* tolerance conception (assuming tolerance 10^{-4} for curvatures and 10^{-5} for deformation modulus).

Mainly due to discrete cracking phenomenon, experimental moment-curvature relationships usually have some oscillations. After the *inverse* technique is applied, the resulting tension-stiffening relationships also have oscillations that may become dramatic due to accumulative nature of the proposed procedure. Naturally, such relationships cannot be assumed as constitutive laws. In order to assess the stochastic nature of test data and to reduce influence of extreme measurement points on the results, a smoothing procedure based on the *Monte-Carlo* simulation and the *modified running-average* method has been proposed. Division of the initial data set into sub-sets has been incorporated as an additional tool into the smoothing procedure proposed.

Shrinkage influence on stress-strain state of reinforced concrete members has been investigated using the test data reported by the author and other researchers. It was shown that shrinkage might significantly reduce cracking resistance and stiffness of the members. Based on the proposed techniques, *free-of-shrinkage* tension-stiffening relationships were derived for the experimental reinforced concrete members.

To compare quantitatively the derived tension-stiffening relationships, a concept of specific strain energy (energy dissipated per unit of volume) has been introduced. The energy corresponds to the area under a *free-of-shrinkage* tension-stiffening curve. It has been shown that application of linear tension-stiffening relationship (used in the *Layer* section model) is objective enough.

3

Experimental Investigation of Reinforced Concrete Beams

This Chapter presents an experimental investigation of shrinkage effect on cracking, tension-stiffening and short-term deformations of lightly reinforced members. Experimental results on tests of eight RC beams (four couples of twin specimens) having constant reinforcement ratio about 0,40%, but different bar diameter are reported. Prior to the tests, measurements on concrete shrinkage and creep were performed (Gribniak *et al*. 2007c)*. Based on numerical procedure discussed in Chapter 2, *free-of-shrinkage* tension-stiffening relationships were derived from the moment-curvature diagrams of the beam specimens.

3.1. Experimental Investigation

The tests were performed in the laboratory of *Civil Engineering Faculty* of *Vilnius Gediminas Technical University* in 2005. The following objectives of the experimental program have been pursued: 1) investigating concrete shrinkage effect on cracking, tension stiffening and deformations of lightly reinforced members; 2) exploring whether bar diameter has influence on deformations of flexural members.

*The reference is given in the list of publications by the author on the topic of the dissertation

3.1.1. Description of Beam Specimens

The beams were tested under a four-point loading scheme. All the specimens were of rectangular section, with nominal length 3280 mm (span 3000 mm), depth 300 mm and width 280 mm. Longitudinal and cross sectional reinforcement of beam specimens is shown in Figs. 3.1a and 3.1b. The experimental programme has comprised of two series of beams. In the beams of the first series (*S-1* and *S-2*), the tensile reinforcement consisted of four ∅10 mm bars, whereas the beams of the second series (*S-3* and *S-4*) had two ∅14 mm bars. Reinforcement ratio for the beams of both series was practically the same, i.e. about 0,40%. Main other parameters of the experimental beams are listed in Table 3.1. For each beam, a twin specimen designated with extra '*R*' was produced from the same batch. As it is seen in Fig. 3.1, the specimens '*R*' had heavy top reinforcement of three ∅18 mm bars (instead of two ∅6 mm bars). This was done in order to eliminate shrinkage effects on cracking resistance. Figure 3.2 illustrates that the stresses in the extreme bottom fibre of specimens '*R*' induced by shrinkage are expected to be around zero.

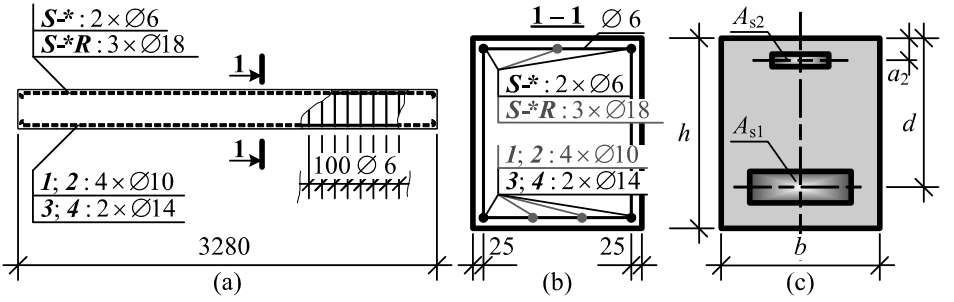

Fig. 3.1. Longitudinal (a) and cross-sectional (b) reinforcement of the beam specimens; notation of cross-section (c)

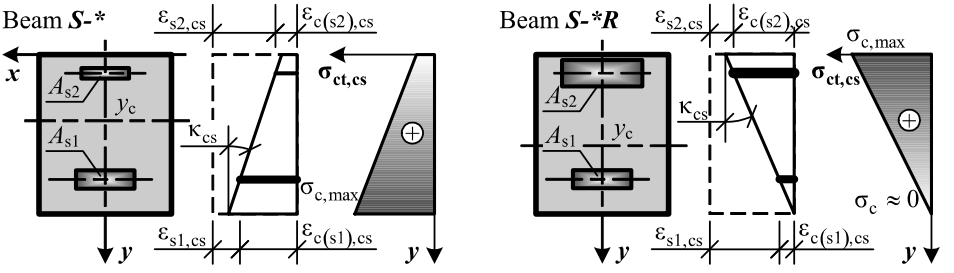

Fig. 3.2. The distribution of shrinkage strains and stresses across the section of the beam specimens

Table 3.1. Main characteristics of the beam specimens (see notations in Fig. 3.1c)

Series	Beam	h	b	d	a_2	A_{s1}	A_{s2}	Date of casting	Age	f_{cu}
		mm				mm^2		yyyy.mm.dd	days	GPa
I	*S-1*	300	280	276	23	309	56,6	2005.09.30	48	47,3
	S-1R	299	281	276	28	309	749	2005.09.30	47	47,3
	S-2	300	280	282	25	309	56,6	2005.10.24	28	48,7
	S-2R	300	282	279	31	309	749	2005.10.24	29	48,2
II	*S-3*	300	277	277	26	303	56,6	2005.10.14	31	41,1
	S-3R	299	281	278	28	303	749	2005.10.14	32	41,2
	S-4	300	277	274	26	303	56,6	2005.10.07	32	54,2
	S-4R	301	283	281	29	303	749	2005.10.07	34	54,2

3.1.2. Production of the Beams and Material Properties

Each couple of twin beams were cast from one batch into steel formwork (see Fig. 3.3). The concrete was placed in the forms in three lifts. Between each lift the concrete was tamped. The specimens were vibrated for approximately 20 s and struck off using a steel trowel. Concrete test specimens such as 100 and 150 mm concrete cubes and 100×100×400 mm and 280×300×350 mm prisms were produced. The latter specimens were cast in the moulds of the beam specimens and were used for shrinkage measurements. The beams were demoulded in about 3–4 days after casting.

The experimental beams and concrete specimens were cured under the laboratory conditions at average relative humidity (RH_m) 64,7% and average temperature 13,1 °C. Variation of humidity and temperature within curing period is shown in Fig. 3.4. The dates of casting and age of the beams at testing (ranging from 28 and 48 days) is given in Table 3.1.

Fig. 3.3. Casting the beams and test specimens

Concrete. Concrete mix proportion taken to be uniform for all experimental specimens is given in Table 3.2. The ordinary Portland cement and crushed granite aggregate (16 mm maximum nominal size) were used. Water/cement and aggregate/cement ratio by weight were taken as 0,42 and 2,97, respectively.

In order to determine material properties of concrete, twelve 100 mm and three 150 mm cubes and fifteen 100×100×400 mm prisms were cast with each couple of twin beam specimens. The latter specimens were cast in the moulds of the beam specimens and were used for shrinkage measurements. Compressive strength and deformation tests were performed at test day and at three time points prior to the tests, approximately in 1, 2 and 4 weeks after casting. Three 100 mm cubes and three 100×100×400 mm prisms were tested at each age for each mixture. The latter specimens were also used for deriving the stress and strain relationship. At test day, three 150 mm cubes were tested; variation of cube compressive strength in time is given in Table 3.3.

Reinforcement. ∅10 and ∅14 mm deformed bars of mild steel were used for the main reinforcement. Three samples of each diameter were tested and several lengths were weighed to check the nominal size. The stresses and modulus of elasticity are based on nominal diameters. Yield strength of ∅10 mm and ∅14 bars was 566 and 542 MPa, respectively. Elastic modules of reinforcing bars were obtained to be 212 GPa.

Table 3.2. Mix proportion of the experimental specimens [kg/m^3]

Material	**Amount**
Sand 0/4 mm	905 ± 2%
Crushed aggregate 5/8 mm	388 ± 1%
Crushed aggregate 11/16 mm	548 ± 1%
Cement *CEM I 42,5 N*	400 ± 0,5%
Water	123,8 ± 5%
Concrete plasticizer *Muraplast FK 63.30*	2 ± 2%

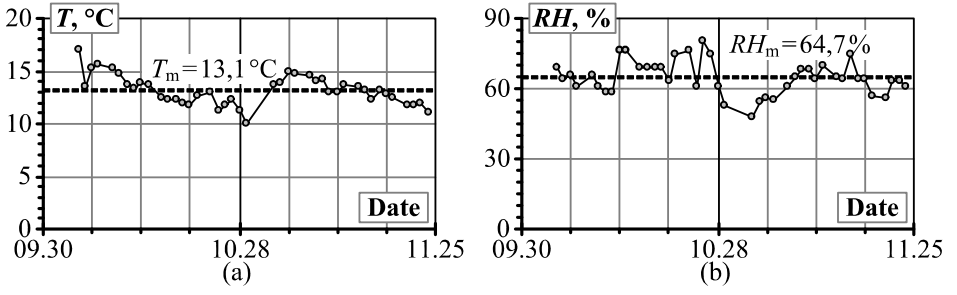

Fig. 3.4. Variation of the temperature (a) and relative humidity (b)

Table 3.3. 150 mm cube strengths [MPa]

Beam	Parameter	1	2	3	4
S-1, *S-1R*	f_{cu}	36,9	40,9	–	47,3
	Age	7	14	–	47
S-2, *S-2R*	f_{cu}	45,4	47,7	55,5	52,9
	Age	7	13	31	35
S-3, *S-3R*	f_{cu}	32,4	37,7	41,2	41,6
	Age	6	15	31	32
S-4, *S-4R*	f_{cu}	34,4	39,9	48,7	48,2
	Age	5	11	28	29

3.1.3. Investigations of Concrete Shrinkage and Creep

Free shrinkage measurements were performed on prisms of 100×100×400 mm and 280×300×350 mm in size. As noted, the latter specimens were the fragments of the beams. After demolding, their ends were isolated with polyester film. The specimens and instrumentation for measurement of shrinkage deformations are shown in Fig. 3.5. Steel gauge studs, with the base 200 mm, were either glued on the concrete surface (see Figs. 3.5a and 3.5b) or embedded in fresh concrete (see Fig. 3.5c). In the latter case, free shrinkage measurements were initiated in 24 h after casting whereas measurements on other prisms were started in 3–4 days.

Shrinkage deformation variation in time is shown in Fig. 3.6a. It is clearly seen the difference between the deformations measured on 280×300×350 mm and 100×100×400 mm prisms. The latter effect is caused by the only factor, i.e. the difference in cross section.

The size conversion factors obtained from the tests and predicted by the *ACI 209* (2008) and *Eurocode 2* (CEN 2004) design code formulas are given in Table 3.4. It is seen that the *Eurocode 2* predictions were adequate whereas the *ACI 209* technique has significantly overestimated the factor.

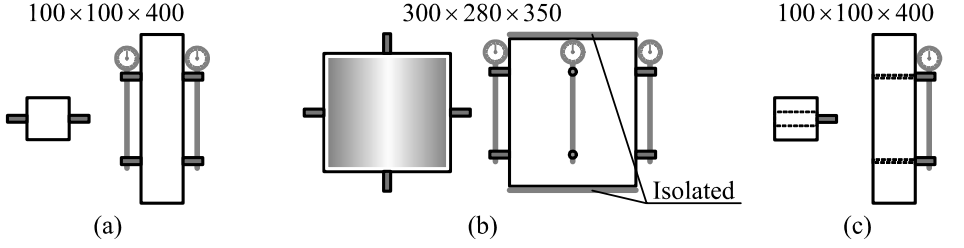

Fig. 3.5. Specimens for measurement of shrinkage deformations

Figure 3.6b plots experimental points obtained for both types of prisms using experimental size correction factor (see Table 3.4). Predicted shrinkage variation curves using the *ACI 209* and *Eurocode 2* methods for 280×300×350 mm prisms, based on averaged parameters of test specimens are also shown in Fig. 3.6b. The experimental free shrinkage strains against the predicted ones by the *ACI 209* and *Eurocode 2* methods are compared in Table 3.5. It can be noted that the latter method has predicted the experimental shrinkage strains more accurately.

Table 3.4. Size factor (converting shrinkage strain from 100×100×400 mm prisms to 280×300×350 mm prisms)

Beams	***ACI 209***	***Eurocode 2***	**Derived experimentally**
S-1, S-1R	0,679	0,491	0,45
S-2, S-2R	0,649	0,465	0,45
S-3, S-3R	0,657	0,453	0,50
S-4, S-4R	0,657	0,490	0,45

Table 3.5. Shrinkage deformations of 280×300×350 mm prisms at test

Beam	t_0	**Predicted by**		**Experimental**
		ACI 209	***Eurocode 2***	
S-1	4 days	$-2{,}265\times10^{-4}$	$-1{,}970\times10^{-4}$	$-1{,}946\times10^{-4}$
S-1R	4 days	$-2{,}240\times10^{-4}$	$-2{,}196\times10^{-4}$	$-1{,}882\times10^{-4}$
S-2	3 days	$-1{,}806\times10^{-4}$	$-1{,}587\times10^{-4}$	$-1{,}526\times10^{-4}$
S-2R	3 days	$-1{,}856\times10^{-4}$	$-1{,}620\times10^{-4}$	$-1{,}557\times10^{-4}$
S-3	4 days	$-1{,}705\times10^{-4}$	$-1{,}629\times10^{-4}$	$-1{,}370\times10^{-4}$
S-3R	4 days	$-1{,}736\times10^{-4}$	$-1{,}657\times10^{-4}$	$-1{,}396\times10^{-4}$
S-4	4 days	$-1{,}752\times10^{-4}$	$-1{,}727\times10^{-4}$	$-1{,}720\times10^{-4}$
S-4R	4 days	$-1{,}789\times10^{-4}$	$-1{,}778\times10^{-4}$	$-1{,}770\times10^{-4}$

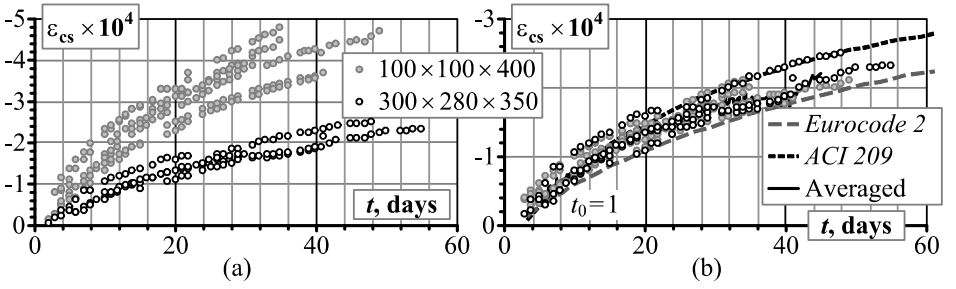

Fig. 3.6. Free shrinkage deformations measured on different size prisms (a) and reduced to size of beam specimens (b)

Creep strains were measured by compressive tests on 100×100×400 mm prisms at the stress level corresponding to 40% of the measured prism strength. Creep strain was deduced from the total strain of a loaded specimen reduced by the shrinkage strain measured on unloaded prisms. Test set-up and results on variation of creep factor in time are given in Fig. 3.7.

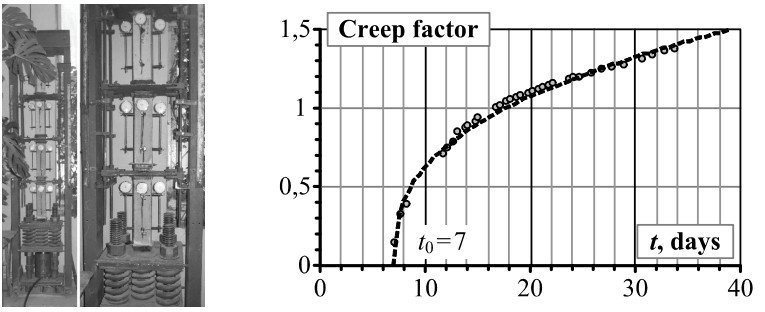

Fig. 3.7. Set-up of creep test and variation of creep factor with time

3.1.4. Instrumentation of the Beams

The loading scheme and the gauge positioning are shown in Fig. 3.8. The beams were loaded with a 100 kN hydraulic jack in a stiff testing frame. The test was performed with small increments (2 kN) and paused for short periods (about 2 minutes) to take readings of gauges and to measure crack development. On average, it took 80 load increments with total test duration of 3 hours. The testing equipment acting on the beam weighed 232 kg. The latter summed up with the beam's own weight has in the mid-span induced a 3,5 kNm bending moment.

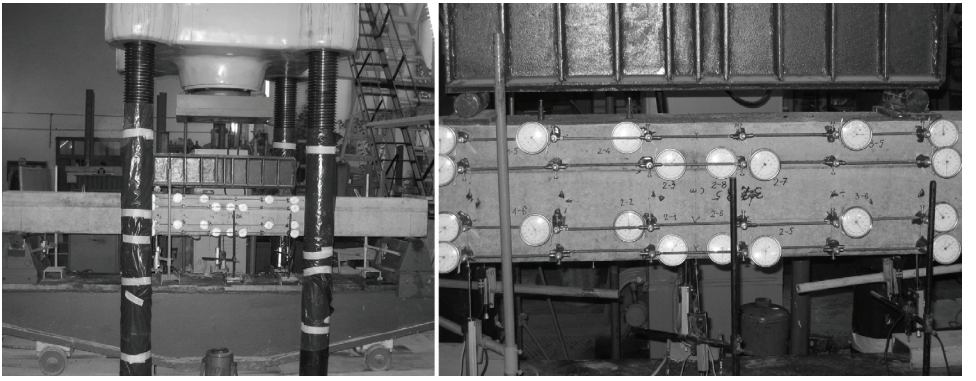

Fig. 3.8. Experimental set-up of the beam

3.2. Analysis of Experimental Results

Concrete surface strains were measured throughout the length of the pure bending zone on a 200 mm gauge length, using 0,001 mm mechanical gauges. As shown in Fig. 3.9 (view 'A'), four continuous gauge lines were located at different depths. The two extreme gauge lines were placed along the top and the bottom reinforcement. Measured strains were averaged along each gauge line. The averaged strains were employed for the assessment of curvature increment:

$$\Delta\kappa = \sum\nolimits_{k<m} \left(\Delta D_k - \Delta D_m\right) \Big/ \left(6 \cdot h_{k,m}\right), \quad k = 1; 2; 3 . \tag{3.1}$$

Here ΔD_k and ΔD_m are the increments of the averaged strains along k and m lines, respectively; $h_{k,m}$ is the distance between these lines.

Deflections of each of the beam were also measured using linear variable differential transducers (L 1–L 8, see Fig. 3.9) placed beneath the soffit of the beam at the load position. Increment in average curvature over the constant moment zone was defined from the deflection gauge readings by the formula:

$$\Delta\kappa = 2\left(\Delta\delta\right) \Big/ \left[\left(0,5 \cdot a\right)^2 + \left(\Delta\delta\right)^2\right], \quad a = 1,0 \text{ m} . \tag{3.2}$$

Here $\Delta\delta$ is the increment of the deflection over the pure bending zone; a is the length of constant bending zone.

Measured surface strains and deflections are presented in Annex C. Moment-curvature diagrams are shown in Fig. 3.10 for each of the beams. This figure includes curvatures obtained both from average surface strains and from deflections over the pure bending zone. Good agreement of these diagrams can be stated. Further analysis will be based on data derived from the average strains. Diagrams of surface strains of concrete at different levels within the pure bending zone of the beams (see Fig. 3.9) are shown in Fig. 3.11. Cracking moments estimated on a basis of these diagrams are indicated in Figs. 3.10 and 3.11 with the numerical values given in Table 3.6. In this table, Δ indicates the difference between cracking moments (either calculated or measured) of twin specimens.

As seen in Figs. 3.10 and 3.11, the beams of *Series I* had higher cracking resistance than the beams of *Series II*. As diameter of tensile reinforcement was the only different parameter between the series, it is to be responsible for the difference. The ratio of reinforcement perimeter and area, characterising bond between reinforcement and concrete, was quite different, i.e. 403 and 288 mm^{-1} for the beams of the first and second series, respectively.

Beams *S*-**R* with heavy top reinforcement possessed higher cracking resistance in regard to beams *S*-*. This could be due to: 1) difference in tensile stress in the extreme bottom fibre induced by shrinkage; 2) increase in section modulus due to heavy top reinforcement.

Table 3.6. Theoretical and experimental values of cracking moment M_{cr}

Beam	Calculated				Measured	
	Ignoring shrinkage		Including shrinkage			
	M_{cr}, kNm	Δ , kNm	M_{cr}, kNm	Δ , kNm	M_{cr}, kNm	Δ , kNm
S-1	13,3	0,6	11,5	2,0	16,8	3,0
S-1R	13,9		13,5		19,8	
S-2	13,7	0,5	12,2	1,6	15,9	2,0
S-2R	14,2		13,8		17,9	
S-3	12,0	0,8	10,7	1,8	15,8	–
S-3R	12,8		12,5		–	
S-4	14,6	0,8	13,0	2,1	13,9	2,1
S-4R	15,4		15,1		16,0	

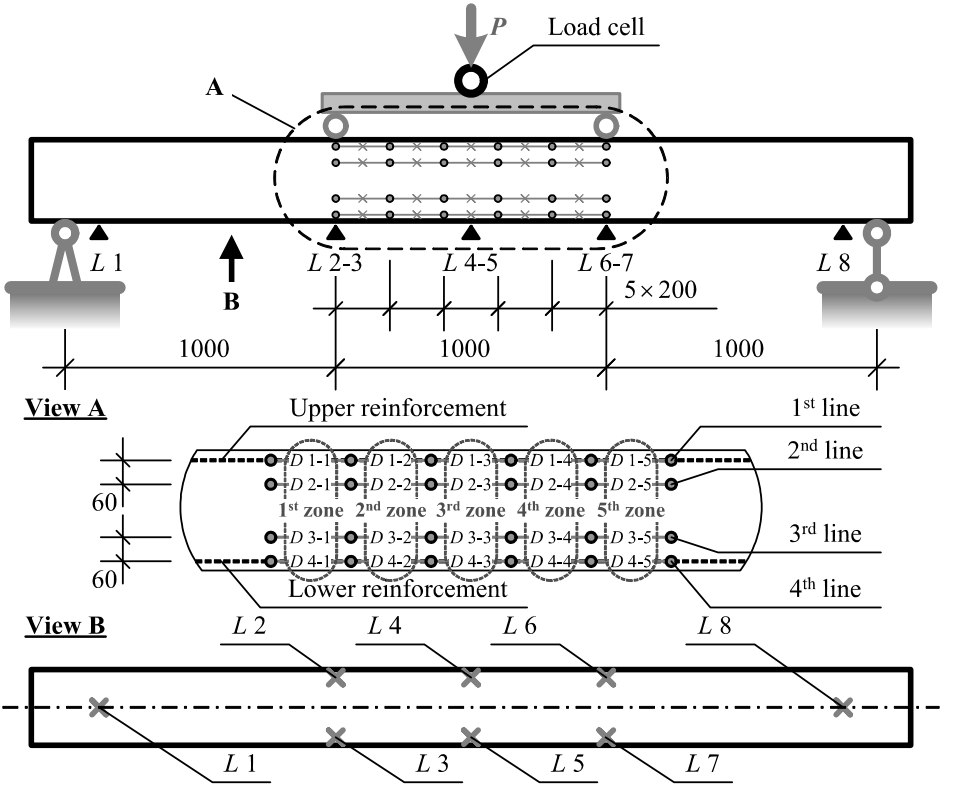

Fig. 3.9. Structural system and arrangement of the measurements

The estimated concrete stress distribution within section depth at cracking load is shown for beams *S-1* and *S-1R* in Fig. 3.12a. The figure includes three stress diagrams due to: 1) restrained shrinkage, 2) external load, and 3) collective action of the shrinkage and external load.

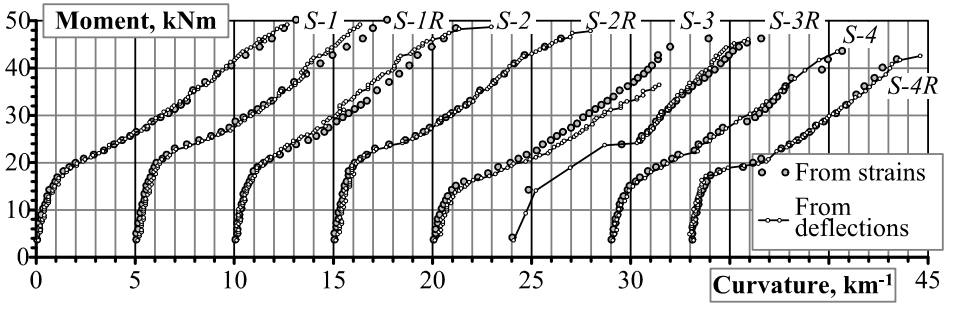

Fig. 3.10. Curvatures of the beams given from surface strains and deflections

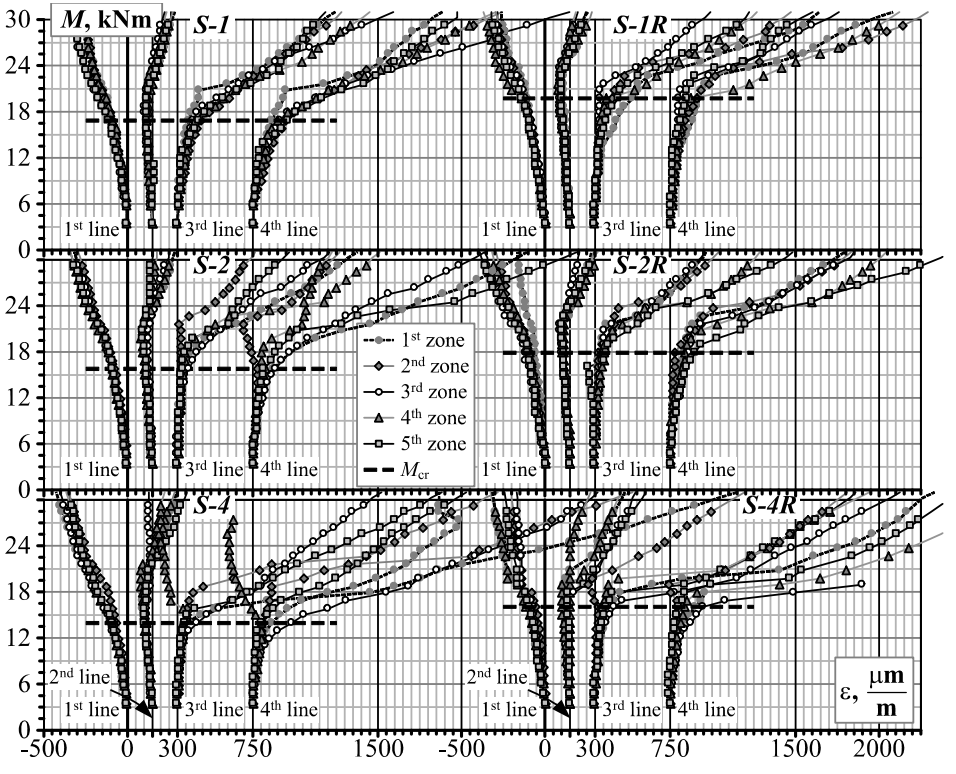

Fig. 3.11. Measured surface strains of the beams

Moment-curvature diagrams often are depicted in terms of effective moment of inertia versus bending moment (*I-M*). Such diagrams for the beam specimens are shown in Fig. 3.12b in relative terms, i.e. $I/I_{\mathrm{el,EC2}}$ and $M/M_{\mathrm{cr,EC2}}$ were $M_{\mathrm{cr,EC2}}$ is the theoretical cracking moment and $I_{\mathrm{el,EC2}}$ is moment of inertia, both based on elastic material properties. Tensile strength and elastic modulus of concrete were calculated by *Eurocode 2* using experimental cube strength (see Table 3.3). Although being equal at the stages of non-cracked and fully cracked behaviour, the stiffness was different at the stage when the *tension-stiffening* effect was present. Figure 3.12b shows that tension-stiffening was far more pronounced for the beams of *Series I* in respect to the beams of *Series II*.

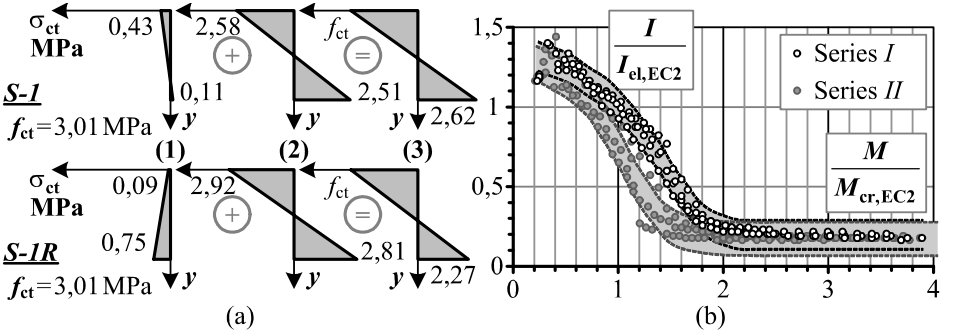

Fig. 3.12. Distribution of stress in concrete across section of the beam specimens (a), and relative diagram of effective moment of inertia of the beams versus bending moment with 90% prediction intervals (b)

3.3. Deriving Tension-Stiffening Relationships from Beam Tests

In this Section, tension-stiffening relationships were derived from the above test data using inverse procedure discussed in Chapter 2. The proposed method has been applied to present test data and *free-of-shrinkage* tension-stiffening relationships were derived for each beam. The relative stress ($\sigma_{\mathrm{ct}}/f_{\mathrm{ctm,EC2}}$) and strain (in term of coefficient $\beta = \varepsilon_{\mathrm{ct}}/\varepsilon_{\mathrm{cr,EC2}}$) diagrams are shown in Fig. 3.13 where $f_{\mathrm{ctm,EC2}}$ and $\varepsilon_{\mathrm{cr,EC2}}$ are the tension strength and cracking strain, respectively, calculated according to *Eurocode 2*. It can be concluded that the relationships obtained for each series were in good agreement. However, the differences between the series were quite significant. The average curves representing each series have indicated that the beams of *Series I* have possessed higher tension stiffening than the beams of *Series II*. As noted earlier, that this was due to different reinforcement diameter used in the series.

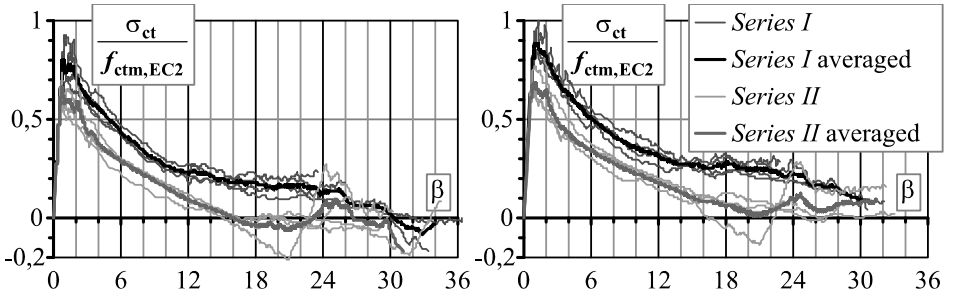

Fig. 3.13. Normalised tension-stiffening diagrams derived from the test data directly (left) and eliminating shrinkage effect (right)

3.4. Concluding Remarks of Chapter 3

Present experimental research has been pursuing the following objectives: 1) investigating concrete shrinkage effect on cracking, tension stiffening and short-term deformations of lightly reinforced members; 2) exploring whether bar diameter has influence on deformations of flexural members.

Conclusions are based on experimental study conducted on eight lightly reinforced concrete beams (four couples of twin specimens) having constant reinforcement ratio ($\approx 0,40\%$), but different bar diameter. In the beams of the first series, the tensile reinforcement consisted of four ∅10 mm bars, whereas the beams of the second series had two ∅14 mm bars. Prior to the tests of the beams, measurements on concrete shrinkage and creep were performed. In order to exclude shrinkage influence on cracking resistance of the beams, large amounts of top reinforcement were assumed in half of the specimens.

The proposed numerical procedure has been applied to the test data for deriving *free-of-shrinkage* tension-stiffening relationships. The relationships obtained for each series were in good agreement. However, the relationships were different for the both series. The following conclusions can be drawn:

1. The beams having heavy top reinforcement possessed slightly higher cracking resistance. This was mainly due to difference in tensile stress in the extreme bottom fibre induced by shrinkage.
2. Tension-stiffening was far more pronounced for the beams of *Series I* having a larger number of bars of tensile reinforcement. These beams at the load corresponding to 50% of the ultimate bending moment o had n average 33% smaller curvatures than the beams of *Series II*.
3. The average stresses in the derived tension stiffening relationships for the beams of *Series I* were about 1,35 times higher than the stresses of the beams of *Series II*.

4

Comparative Statistical Analysis

This Chapter consists of two parts. The first part discusses accuracy of free shrinkage predictions made by various methods reviewed in Section 1.1.2. Present study was aiming at free shrinkage strains occurring at relatively early age of concrete (up to 150 days). The comparative statistical analysis was carried out for experimental data reported by the author and other researchers.

The second part presents investigation on short-term deflections of RC bending members. The analysis has employed data of seven experimental programs, one of which was reported by the author. The comparative study was based on the predictions made by design codes (*Eurocode 2*, *ACI 318* and *SP 52-101*) and numerical techniques (FE package *ATENA* and *Layer* section model).

4.1. Accuracy Analysis of Shrinkage Predictions

Effect of shrinkage of concrete along with cracking provides the major concern to the structural designer because of the inaccuracies and unknowns that surround it. In general, shrinkage effect is taken into account of long-term deformation of reinforced and pre-stressed concrete structures (Ghali & El-Badry 1987, Peiretti *et al*. 1991, El-Badry & Ghali 2001, Vítek *et al*. 2004, Robert-Nicoud *et al*. 2005, etc). Though considered as a long-term effect, shrinkage also has influ-

ence on crack resistance and deformations of RC members subjected to short-term loading. In the code methods based on experimental data, shrinkage effect on deformations of such members is assessed indirectly. In the numerical approaches, shrinkage should be taken into account as a separate factor (Kaklauskas & Gribniak 2005b*, Kaklauskas *et al*. 2006b*, 2008b*, 2008c*, and 2009*). As in the proposed strain/deflection calculation technique, shrinkage is taken into account, it seems appropriate to perform comparison of free shrinkage strain predictions by different methods. The analysis is limited to relatively short duration (up to 150 days), characteristic to the age of a structure first loaded.

4.1.1. Experimental Data for the Analysis

Present analysis was based on experimental data of free shrinkage strain reported by the author and other researchers. The data set consists of 23 experimental programs, 351 specimens and 7391 measurements. Only specimens with consistently distributed test points were included in the data set. The test specimens had different geometry, curing durations, and strength of concrete. Main characteristics of the specimens are given in Table 4.1 where k is the number of test specimens in each program; n' and n are the number of test measurements in the program before and after *sliced* data transformation (see Section 4.1.3), respectively; C is the class of concrete [see comment for Equation (A.3)]; t_{cs} is the period when shrinkage deformations were measured; S is the shape of cross-section (1, 2 and 3 represent slab, cylinder and square prism, respectively) and h_0 is the average thickness [see Equation (A.8)].

4.1.2. Calculation Techniques Employed for the Analysis

The comparative analysis of free shrinkage predictions was based on these techniques: *Eurocode 2* (CEN 2004) (see Annex A.1.1); *ACI 209* (ACI Committee 209 2008) (see Annex A.2.1); *Russian Institute of Civil Engineering* (CNIIS 1983) (see Annex A.3.1); *Bažant & Baweja* (1995a, 1995b) *B3* model (see Annex A.4.1); *Gardner & Lockman* (2001) *GL 2000* model (see Annex A.5.1).

4.1.3. *Sliced* Data Transformation

The experimental programs employed in the analysis were pursuing different objectives and were covering different time intervals with different measurement intensities. To assure even contribution of each experimental specimen and consistency of the statistical analysis, a procedure called the *sliced* data transformation has been developed. It based on following steps:

*The reference is given in the list of publications by the author on the topic of the dissertation

Step 1. Free shrinkage strains were calculated at all time points of each test specimen using all the techniques.
Step 2. Ten fixed time levels T were introduced:

$$T = \{7; 14; 21; 28; 35; 42; 60; 90; 120; 150\} \quad [\text{days}]. \tag{4.1}$$

Step 3. As shown in Fig. 4.1, the experimental and calculated shrinkage strain versus time diagrams were *sliced* at the above time levels. The target points were derived by means of linear interpolation.

Table 4.1. Main characteristics of shrinkage test data

Author	k	n'	n	$f_{cm,28}$	RH	C	t_s	t_{cs}	S	h_0
	Number			MPa	%		Days			mm
1. *Tritsch et al.* (2005)	35	2593	342	26–59	51	N	3–14	4–356	3	38
2. *Kaklauskas et al.* (2008)	29	1418	196	43–50	76	N	1–4	2–89	2/3	50–145
3. *Mokarem* (2002)	140	934	1400	36–51	50	S/N	1	7–180	3	38
4. *Persson* (2001)	52	813	514	18–107	60	N	1	2–2631	2	28–50
5. *Townsend* (2003)	20	392	148	86–92	50	N	1–7	2–105	2/3	25–38
6. *Gribniak et al.* (2009)*	11	336	54	33–43	65	N	1–4	2–55	3	50–145
7. *Takemura et al.* (1987)	8	130	48	32–69	60	N/R	28	29–178	3	50
8. *Furushima et al.* (1993)	3	121	30	29–34	82	N	5	6–189	3	50
9. *Kawasumi et al.* (1973)	6	112	56	44	50	N	2	5–592	2	75
10. *Kawahara et al.* (1964)	12	102	120	15–27	50	N	2–6	9–736	3	38
11. *Ulickij et al.* (1960)	6	72	48	16	88	N	7	10–127	3	36–51
12. *Tongaroonsri & Tangtermsirikul* (2009)	6	69	17	20–55	75	N	7–14	8–28	3	38
13. *Umezu et al.* (2003)	2	52	18	34–49	60	N	7	12–175	2	50
14. *Tomita* (1994)	3	38	24	26–31	60	N	7	8–135	3	50
15. *Persson* (1998)	3	37	30	55–68	55	N	6	7–1230	2	28
16. *Umezu et al.* (2001)	3	36	27	33–36	60	N	7	14–189	2	80
17. *Asanuma et al.* (1995)	2	36	18	30	66	N	7	17–187	3	80
18. *Ozaki et al.* (2001)	3	27	30	69–72	60	N	1	2–366	2	100
19. *Takafumi et al.* (2003)	1	18	7	31	60	N	7	12–97	3	50
20. *Kim & Lee* (1998)	2	16	8	28–44	68	N	7	8–37	1	300
21. *Nakato et al.* (2000)	2	16	14	14–32	60	N	7	10–98	3	50
22. *Liu et al.* (2001)	1	14	5	28	60	N	7	10–49	3	50
23. *Murao* (1997)	1	9	9	44	60	N	7	8–189	3	50

*The reference is given in the list of publications by the author on the topic of the dissertation

Step 4. Accuracy of the predictions has been estimated by means of a relative error taken as

$$\Delta_{i,k} = \varepsilon_{cs,calc} / \varepsilon_{cs,obs}, \quad i = 1; 2; 3; \ldots 9; 10, \quad k = 351. \tag{4.2}$$

Here $\varepsilon_{cs,calc}$ and $\varepsilon_{cs,obs}$ are the shrinkage strains linearly interpolated at the level T using calculated and original test data, respectively (see zoomed selection in Fig. 4.1 with *target* points shown by void circles); k is the total number of specimens. In the ideal case, the relative error Δ should be equal to unity.

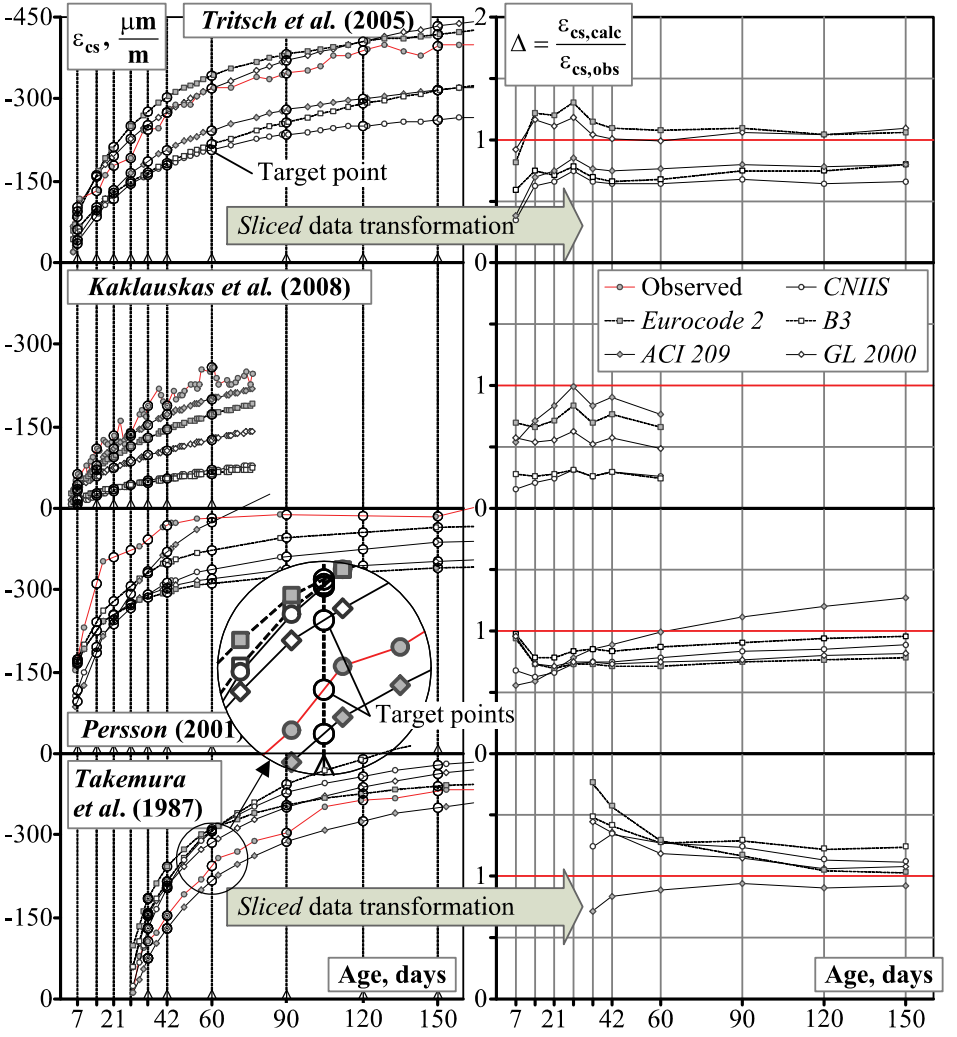

Fig. 4.1. Illustration of *sliced* transformation of shrinkage-time diagrams

Application of the proposed technique has resulted in reduction of experimental measurements from 7391 input points n' to 3163 output points n (see Table 4.1). It should be noted that not every test specimen after *sliced* transformation contained output points at all time levels indicated in Equation (4.1). If a specimen was missing consistent experimental points needed for interpolation, it had a lesser number of output points (see Fig. 4.1).

4.1.4. Statistical Background

In present research, the error Δ is considered as a random variable; therefore, errors of prediction techniques can be assessed using statistical methods. Statistics estimating the *central tendency* and *variability* serve to measure precision of the predictions. The central tendency can be regarded as a consistency parameter of a calculation method. The postulate of minimum variance was used to evaluate accuracy of a model (Soong 2004). It should be noted that the type of distribution of the random variable plays a very important role making conclusions of the statistical analysis (Gribniak & Kaklauskas 2004*, Bacinskas *et al*. 2009*).

If the distribution is symmetrical, the mean and the median will coincide. If not, the median as a measure of central tendency is preferred to the mean, particularly for the distribution characterised by a small number of extreme values (Soong 2004). If the distribution of probability of the variable under investigation (i.e. the relative error Δ) is *normal*, the central tendency and the variability are reflected by the expectation μ_Δ and the variance σ_Δ^2, which measures the dispersion or spread of random variable about μ_Δ. These parameters can be estimated by the statistics:

$$m_\Delta = \frac{1}{n}\sum\nolimits_{i=1}^{n}\Delta_i;\quad s_\Delta^2 = \frac{1}{n-1}\sum\nolimits_{i=1}^{n}\left(\Delta_i - m_\Delta\right)^2,\quad n = 3163. \tag{4.3}$$

Here m_Δ is the mean of a sample (data set); s_Δ^2 is the variance of a sample and n is the size of a data set.

The confidence intervals for the expectation μ_Δ and the variance σ_Δ^2 can be also constructed using the sample mean m_Δ and the standard deviation s_Δ. The latter is the square root of the variance of a sample. The $1-\alpha$ confidence interval for the expectation can be determined by

$$\mu_\Delta \in \left[m_\Delta - t_{1-\alpha/2}\left(n-1\right)\times\frac{s_\Delta}{\sqrt{n}};\quad m_\Delta + t_{1-\alpha/2}\left(n-1\right)\times\frac{s_\Delta}{\sqrt{n}} \right]. \tag{4.4}$$

Here $t\left(n-1\right)$ is the t-statistics (*Student*'s) having $(n-1)$ degrees of freedom and significance level $\alpha/2$; $1-\alpha$ is the confidence coefficient.

*The reference is given in the list of publications by the author on the topic of the dissertation

If the distribution of probability of Δ is *not normal*, the central tendency and the variability can be measured using the median $\xi_{\Delta,1/2}$ and the inter-quartile distance $\xi_{\Delta,3/4} - \xi_{\Delta,1/4}$, respectively (David & Nagaraja 2003). The latter parameter can be estimated by $1-\alpha$ confidence interval:

$$\left[\xi_{\Delta,1/4}; \xi_{\Delta,3/4}\right] \in \left[x_{(r)}; x_{(s)}\right]. \tag{4.5}$$

Here $x_{(r)}$ and $x_{(s)}$ are the *r*-th and *s*-th elements of the data set sorted out in the ascending order. The problem of construction of above interval can be solved numerically. For symmetrical interval ($s = n - r + 1$), the number *r* can be selected using the trial-and-error procedure from the condition (David & Nagaraja 2003):

$$\begin{gathered} 1-\alpha/2 \le I_{0,25}\left(r; n-r+1\right) = \left[B\left(r; n-r+1\right)\right]^{-1} \int_0^{0,25} t^{r-1}\left(1-t\right)^{n-r}\, dt, \\ B\left(r; n-r+1\right) = \int_0^1 t^{r-1}\left(1-t\right)^{n-r}\, dt. \end{gathered} \tag{4.6}$$

Here $I_{0,25}\left(r; n-r+1\right)$ is the incomplete *beta* function; $B\left(r; n-r+1\right)$ is the *beta* function. The inter-quartile interval contains 50 % of the mass of the distribution (the central part of distribution).

The median $\xi_{\Delta,1/2}$ is the point that divides the mass of the distribution into two equal parts. The median can be estimated by the sample median $X_{\Delta,1/2}$:

$$X_{\Delta,1/2} = \begin{cases} x_{(n/2+1)}, & n \text{ is odd}, \\ 0,5 \cdot \left[x_{(n/2)} + x_{(n/2+1)}\right], & n \text{ is even}. \end{cases} \tag{4.7}$$

Here $x_{(i)}$ is the *i*-th member of the ordered data set. The confidence interval of median can be obtained by counting off $u_{\alpha/2}\sqrt{n}/2$ observations to the left and the right of the sample median and rounding *out* to the next integer (i.e. the lower bound is rounded down and the upper up), where $u_{\alpha/2}$ is the $\alpha/2$ significance point of a standard normal inverse cumulative distribution function (David & Nagaraja 2003).

In order to investigate the normality of the probability distribution, goodness tests of fit statistics to the set of experimental data should be performed. The common approaches to test goodness of fit statistics are the χ-square and *Kolmogorov-Smirnov* criteria. Main disadvantage of these approaches is that the ability to reject a false null hypothesis (termed the *power*) is low (Cohen *et al.* 1974). The power can be increased significantly by using a simple data transformation procedure proposed by *Durbin* (1961). The *Durbin*'s method is described below:

First, a cumulative probability was calculated for each point Δ_j [see Equation (4.2)] assumed to be a part of normally distributed parent population characterised by the parameters $\mu = m_\Delta$ and $\sigma = s_\Delta$:

$$p_{\mathrm{j}} = F\left(\Delta_{\mathrm{j}} \middle| m_{\Delta}, s_{\Delta}\right) = \frac{1}{s_{\Delta}\sqrt{2\cdot\pi}} \int_{-\infty}^{\Delta_{\mathrm{j}}} \exp\left(-\frac{\left[t - m_{\Delta}\right]}{2\cdot s_{\Delta}^{2}}\right) dt, \quad j = 1, 2 \ldots n\,. \tag{4.8}$$

Second, the calculated probabilities p_{j} are sorted in the ascending order $p_{(\mathrm{j})}$ and a new data set is created using the subtraction procedure:

$$C_1 = p_{(1)}; \quad C_{\mathrm{j}} = p_{(\mathrm{j})} - p_{(\mathrm{j}-1)}; \quad C_{\mathrm{n}+1} = 1 - p_{(\mathrm{n})}\,. \tag{4.9}$$

Here n is the size of the initial data set.

Third, in a similar way after sorting in the ascending order the above data, the resulting data set w_{j} is constructed using the formula:

$$\begin{gathered} g_1 = (n+1)C_{(1)}; \quad g_{\mathrm{j}} = (n+2-j)\left[C_{(\mathrm{j})} - C_{(\mathrm{j}-1)}\right], \quad j = 2; 3; \ldots n+1; \\ w_1 = g_1; \quad w_{\mathrm{j}} = g_{\mathrm{j}} + g_{\mathrm{j}-1}, \quad j = 2; 3; \ldots n+1. \end{gathered} \tag{4.10}$$

In conclusion, it is assumed that the random variable Δ is distributed normally, if two conditions are satisfied (Durbin 1961):

$$\begin{gathered} \max_{\mathrm{t}=1\ldots\mathrm{n}+1}\left(t/n - w_{\mathrm{t}}\right) \times \left[\sqrt{n} + 0{,}275 - 0{,}04\cdot(n)^{-0{,}5}\right] \le \tilde{D}_{\mathrm{n}} = 1{,}518\,; \\ -2\cdot\ln\left(\prod_{\mathrm{t}=1}^{\mathrm{n}+1} w_{\mathrm{t}}\right) \le \chi^{2}_{1-\alpha}(2\cdot n). \end{gathered} \tag{4.11}$$

Here $\tilde{D}_{\mathrm{n}}$ is the modified two-sided *Kolmogorov-Smirnov* statistics tabulated in (Stephens 1974); $\chi^2(2\cdot n)$ is the χ-square statistics having $2\cdot n$ degrees of freedom and significance level α (in this study $\alpha = 0{,}05$ was assumed).

4.1.5. Results of the Analysis

Analysis has shown that probability distribution of the error Δ was not normal in neither of time levels of each method. Therefore, accuracy of shrinkage prediction methods was assessed using these two statistical parameters: the *median* characterising the consistency and the *inter-quartile distance* reflecting variation of the predictions. The ideal model is characterised by the median approaching unity and minimal variation. Figure 4.2 presents 95% confidence intervals of above parameters for all shrinkage prediction methods. The results are also listed in Tables 4.2 and 4.3 and are discussed below:

Variation. It is hardly can be considered as a quantitative characteristic and could be used for qualitative comparison of different techniques. As can be seen in Fig. 4.2 and Table 4.2, the smallest and the largest variation was characteristic to the *ACI 209* and *GL 2000* techniques, respectively, whereas other three methods have demonstrated quite similar variation. It can be pointed out that the variation was quite constant throughout the time, excepting the initial intervals.

***Median* (*the central tendency*).** This statistical parameter is discussed separately for each of the method.

Eurocode 2. The median was very close to unity for all time levels. In fact, the deviation was not reaching 2% within $T = 14$–90 days. Above this interval, the predicted shrinkage strains were slightly underestimated.

ACI 209. The predictions were time dependent: at the early age, the calculated shrinkage strains were significantly underestimated (up to 50%) With increasing time, the predictions were constantly improving being accurate at $T = 90$ days.

CNIIS. Excepting the initial stage ($T < 28$ days), very consistent results were achieved with median close to unity. The median was asymmetrically positioned within the inter-quartile interval at all time levels.

***Bažant & Baweja* (*B3*)**. The median, which is slightly underestimated at the early age (8%), is gradually increasing with 11% overestimation at $T = 150$ days. The asymmetry of probability distribution of predictions is very similar to that obtained by the *CNIIS* technique.

***Gardner & Lockman* (*GL 2000*)**. Although time independent, the prediction are overestimated by 11–15%.

Further investigation aimed at comparative predictions analysis of short-term deflection calculation methods uses free shrinkage strain occurring at pre-loading stage. In this study, age of the specimens employed in the deflection analysis was varying from 21 to 63 days. In the author's view, the *B3* and *Eurocode 2* methods gave the most accurate predictions for this time interval. The latter method, as the normative document accepted in the EU, was chosen for further analysis.

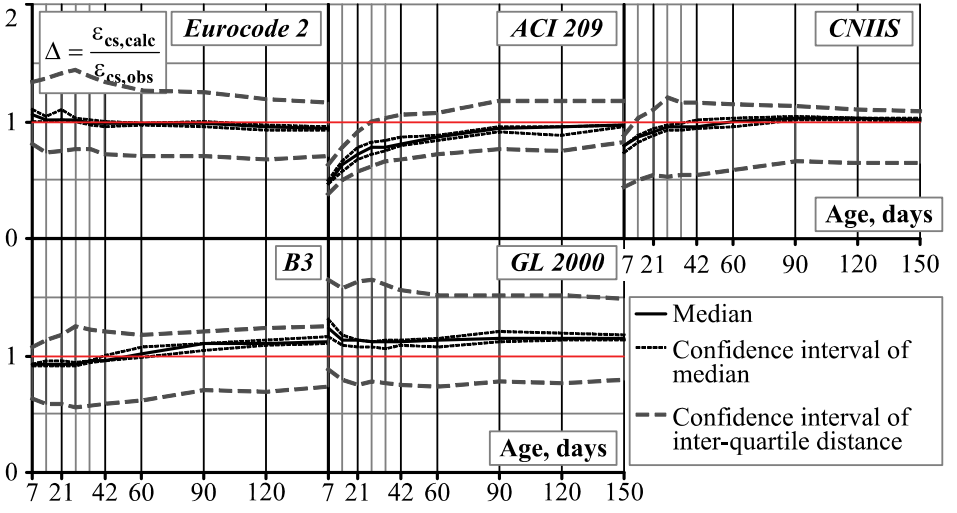

Fig. 4.2. Variation of the sample median of relative error Δ with time and 95% confidence intervals of the median and inter-quartile distance

Table 4.2. Variation of the sample median $X_{\Delta,1/2}$ with time

Age, days	*n*	*Eurocode 2*	*ACI 209*	*CNIIS*	*B3*	*GL 2000*
7	287	1,064	0,478	0,791	0,920	1,232
14	336	1,021	0,637	0,870	0,920	1,131
21	344	1,014	0,719	0,915	0,928	1,127
28	349	1,017	0,775	0,957	0,924	1,111
35	346	0,992	0,777	0,958	0,954	1,117
42	337	0,986	0,809	0,957	0,962	1,123
60	323	0,979	0,866	0,995	1,010	1,131
90	302	0,986	0,937	1,029	1,102	1,149
120	277	0,954	0,956	1,024	1,110	1,147
150	262	0,944	0,967	1,013	1,118	1,147

Table 4.3. 95% confidence intervals of the inter-quartile distance $X^{+}_{3/4} - X^{-}_{1/4}$

Age, days	*Eurocode 2*	*ACI 209*	*CNIIS*	*B3*	*GL 2000*
7	0,527	0,238	0,439	0,450	0,772
14	0,626	0,284	0,529	0,550	0,773
21	0,657	0,342	0,569	0,594	0,878
28	0,683	0,383	0,668	0,680	0,869
35	0,627	0,371	0,625	0,657	0,833
42	0,618	0,382	0,623	0,629	0,812
60	0,553	0,352	0,565	0,568	0,772
90	0,543	0,423	0,476	0,507	0,746
120	0,517	0,418	0,464	0,542	0,748
150	0,454	0,357	0,435	0,519	0,683

4.2. Accuracy Analysis of Deflection Predictions

This Section investigates accuracy of short-term deflection predictions made by the methods described in Sections 1.2.7 and 1.3. Although numerical techniques such as finite element (FE) codes or *Layer* section analysis are extensively used in design, structural engineers are not yet well aware of accuracy of the numerical predictions with respect to design codes. Therefore, in research presented herein, an effort has been made to investigate statistically accuracy predictions made by the FE package *ATENA* and *Layer* section model on one hand, and the *Eurocode 2*, *ACI 318* and *SP 52-101* design code methods on the other.

4.2.1. Experimental Data for the Analysis

Present study was based on experimental data of mid-span deflections/curvatures reported by the author and other researchers. The data set consists of 7 experimental programs, 57 specimens and 1468 measurements. All the specimens were tested under a four-point bending scheme. Main parameters listed in Table 4.4 are span l_0, shear span a, cross-section dimensions (notation see in Fig. 3.1c), tension reinforcement ratio p, compressive 150 mm cube strength f_{cu} and age at testing.

Most of the beams had rectangular cross section, but eight of them had an inverted T-section with flanges in tensile zone (Figarovskij 1962). Three beams were reinforced with plain bars (Figarovskij 1962) whereas the remaining specimens had deformed bars.

Table 4.4. Main characteristic of test members employed in the analysis

Author	l_0	a	b	h	p	f_{cu}	Age
	mm				%	MPa	days
1–8. *Gribniak* (Chapter 3)	3000	1000	277–283	299–301	0,4	41,1–54,2	28–48
9–14. *Ashour* (2000)	3080	1290	200	250	1,2–2,4	60,8–98,1[1]	29
15–31. *Clark & Speirs* (1978)	3200	1000	202–902	201–513	0,4–2,0	23,0–39,6	21–41
32–47. *Figarovskij* (1962)	3000	1000	179–181	249–254	0,2–0,9	22,7–37,1[2]	29
48–50. *Gilbert* (2007)	2000	667	850	100	0,3–0,8	48,0–60,5[1]	28[3]
51–54. *Gushcha* (1967)	3600	1300	152–162	306–312	0,3–0,8	30,9–42,0[2]	27–37
55–57. *Nejadi* (2005)	3500	1167	250–400	161–348	0,5–0,7	45,5–48,6[1]	42–63

4.2.2. Calculation Techniques Employed for the Analysis

The comparative analysis employed these empirical/analytical and numerical deflection calculation techniques: *Eurocode 2* (CEN 2004) (see Section 1.3.1); *ACI 318* (ACI Committee 318 2008) (see Section 1.3.2); *Branson*'s (1963, 1977) method (see Section 1.3.2); Russian code *SP 53-101* (analytical approach, see Section 1.3.3.1, numerical approach, see Section 1.3.3.2); *Layer* section model (Kaklauskas 2001) (see Section 1.2.7.1); FE software *ATENA* (Cervenka *et al*. 2002) (see Section 1.2.7.2).

The characteristics of concrete (modulus of elasticity, tensile strength and fracture energy) needed for the deflection analyses were calculated using measured compressive strength based on the provisions of each technique.

[1]Strength was calculated from $\varnothing 150 \times 300$ mm cylinder test data using factor 1,25
[2]Strength was calculated from 200 mm cube test data using factor 1,05
[3]Age data was missing in the paper

All the calculation methods have been reviewed in Sections 1.2.7 and 2.5.1. Below some details are discussed regarding numerical simulation by *Layer* section model and FE software *ATENA*.

4.2.2.1. *Layer* Section Model

For reinforcement material idealisation, an elastic-plastic stress-strain relationship was adopted. Characteristics of concrete, including the stress-strain relationship for compressive concrete (see Fig. 2.12b), were based on the *Eurocode 2* provisions. For simplicity, the behaviour of cracked tensile concrete was modelled using a linear tension-stiffening relationship shown in Fig. 2.3a. Factor β, controlling tension-stiffening, was defined from Equation (1.5). As a simplified tension-stiffening relationship instead of realistic one (for instance, exponential) was assumed, to avoid excessive stiffness of the model, reduced tensile strength $f_{\mathrm{ct}} = 0{,}8 f_{\mathrm{ctm}}$ was introduced.

4.2.2.2. Finite Element Modelling by Software *ATENA*

FE model of the specimen was considered in a plane stress state with non-linear constitutive laws for concrete and reinforcement. Such approach simplifies the three-dimension action of real structures on one hand, but enables a refinement with respect to the model based on the plane section hypothesis on the other. For concrete, the model *SBETA* offered by *ATENA* was utilized, which is based on the concept of smeared cracks and damage. Concrete without cracks is considered as isotropic and concrete with cracks as orthotropic. In this study, the fixed crack model was used: crack direction and material axes are defined by the principal stress direction at the onset of cracking when the principal stress exceeds the tensile strength. In further analysis, this direction is fixed and cannot be changed. A rotation of principal strain axes generates shear stresses on the crack plane. Consequently, the model of shear in cracked concrete becomes important. For this, a variable shear retention factor is used, in which the shear modulus on the crack plane reduces with the crack opening (Cervenka *et al*. 2002).

As was mentioned, the tension-stiffening effect included into FE model indirectly using principles of fracture mechanics. Investigation of FE mesh dependence on modelling of flexural members showed that such approach is relatively independent from the finite element size in regard to the approach when tension-stiffening relationships (Gribniak *et al*. 2007d*, 2009*). It was also found that models of RC beams having 6–8 finite elements per height demonstrate best accuracy. The finite element model used for the beams is shown in Fig. 4.3. Due to symmetry conditions, only half of the beam has been modelled. Isoparametric quadrilateral finite elements with 8 degrees of freedom and four integration points were used for all the beams. The element size was about 30 mm. Bar reinforcement was modelled by truss elements embedded in concrete elements.

*The reference is given in the list of publications by the author on the topic of the dissertation

Two FE analyses, i.e. excluding and including shrinkage (*ATENA* and $ATENA_{cs}$, respetively) at the pre-loading stage, have been performed. Example of the analysis of beam *S-1* tested by the author (see Section 3.1.1) is shown in Fig. 4.4 and illustrates deformations, cracks and principal stresses in concrete. Moment-curvature response of this beam comparing various methods and experiment is shown in Fig. 4.5. Curvature was calculated by Equation (3.2) where the length of constant moment zone *a* is taken from Table 4.4.

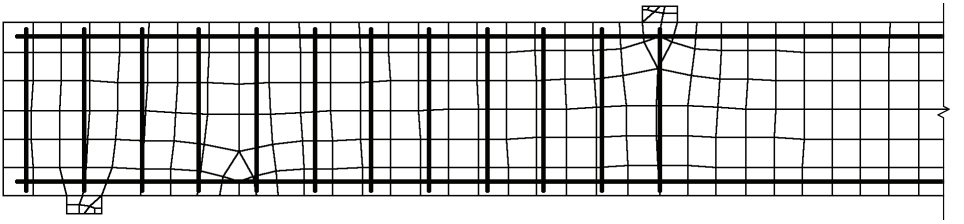

Fig. 4.3. Finite element meshing of a beam using in the analysis

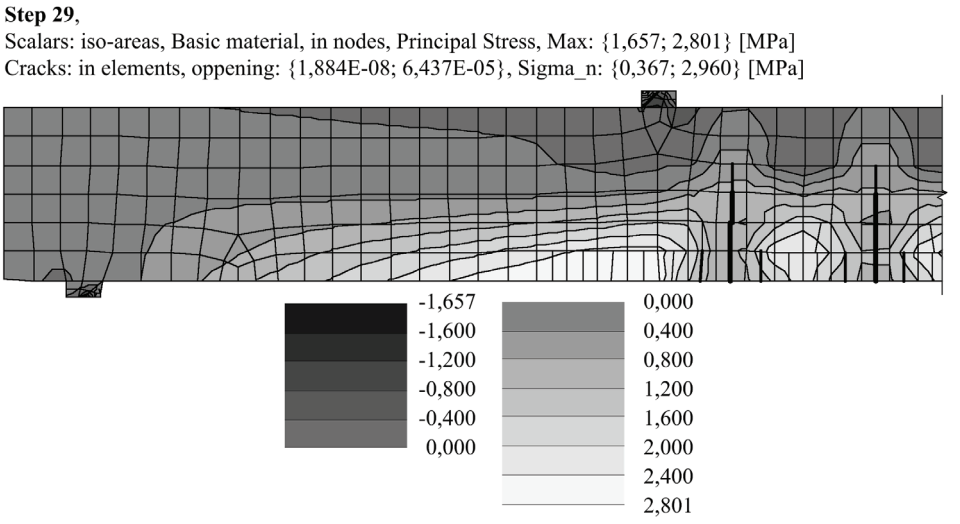

Fig. 4.4. FE simulation of beam *S-1* by *ATENA*: deformations, crack pattern and principal stresses at the level of loading $M' = 0{,}25$ [see Equation (4.12)]

4.2.3. *Sliced* Data Transformation

The experimental mid-span deflections/curvatures were compared with those predicted by the techniques described above. *Sliced* transformation (as described in Section 4.1.3) has been performed with the experimental measurements. The

transformation was based on introducing eleven levels of loading intensity M' taken in relative terms between the cracking and ultimate bending moment:

$$M' = \left(M - M_{\mathrm{cr}}\right) \Big/ \left(M^{*}_{\mathrm{ult}} - M_{\mathrm{cr}}\right); \quad M' = \{0; 0{,}1; 0{,}2; \ldots 0{,}9; 1\}. \tag{4.12}$$

Here M^{*}_{ult} is the pseudo-ultimate bending moment calculated for each member under assumption of yielding strength of tensile reinforcement 400 MPa; M_{cr} is the cracking moment (CEB-FIP 1991):

$$M_{\mathrm{cr}} = I_{\mathrm{el}} f_{\mathrm{ct}} / y_{\mathrm{t}}; \quad f_{\mathrm{ct}} = 0{,}3\sqrt[3]{f'^{2}_{\mathrm{c}}}; \quad f'_{\mathrm{c}} = f_{\mathrm{cu}} / 1{,}25. \tag{4.13}$$

Here f_{cu} is the compressive 150 mm cube strength of concrete (see Table 4.4). Thus, $M' = 0$ and $M' = 1$ corresponds to cracking and pseudo-failure of the RC element, respectively.

Accuracy of the predictions was estimated by means of a relative error $\Delta_{\mathrm{i,k}}$ calculated at each level M' for each of 57 experimental members:

$$\Delta_{\mathrm{i,k}} = x'_{\mathrm{calc}} / x'_{\mathrm{obs}}, \quad i = 1; 2; 3; \ldots 10; 11, \quad k = 57. \tag{4.14}$$

Here x'_{calc} and x'_{obs} are the mid-point deflections/curvatures interpolated at the level M' from calculated and original test data, respectively. It should be noted that not all specimens contained eleven output points as their testing was terminated before reinforcement reached 400 MPa. The transformation resulted in 532 output points covering post-cracking stage (compare to 1468 measured points). Figure 4.5 illustrates such data transformation.

4.2.4. Statistical Analysis of Deflection Predictions

The relative error Δ is considered as a random variable; therefore, the statistical methods described in Section 4.1.4 can be also used for assessing accuracy of deflection prediction techniques. To begin with, testing for normality of probability distribution of Δ at each load level M' has been carried out using the errors $\Delta_{\mathrm{j}}, j = 1 \ldots n$ [see Equation (4.14)]. For this, the *Durbin*'s method, described in Section 4.1.4, was applied. As expected, distribution of the test data was not normal.

The normality condition can be violated when the test data have more than one group of local concentration (David & Nagaraja 2003). Previous investigations by the author and his associates have shown that accuracy of deflection predictions is mainly affected by such a parameter as reinforcement ratio, p (Gribniak *et al*. 2004*, 2007d*, and 2009*). Therefore, it was decided to split the experimental data into a number of groups, each with normal probability distribution. For this purpose, the following procedure has been proposed.

*The reference is given in the list of publications by the author on the topic of the dissertation

Step 1. Based on reinforcement ratio criteria, all the test members are sorted in the ascending order.

Step 2. First three members are taken and normality test is performed for test data at each load level M'. If the normality test is satisfied, test data of next member is added.

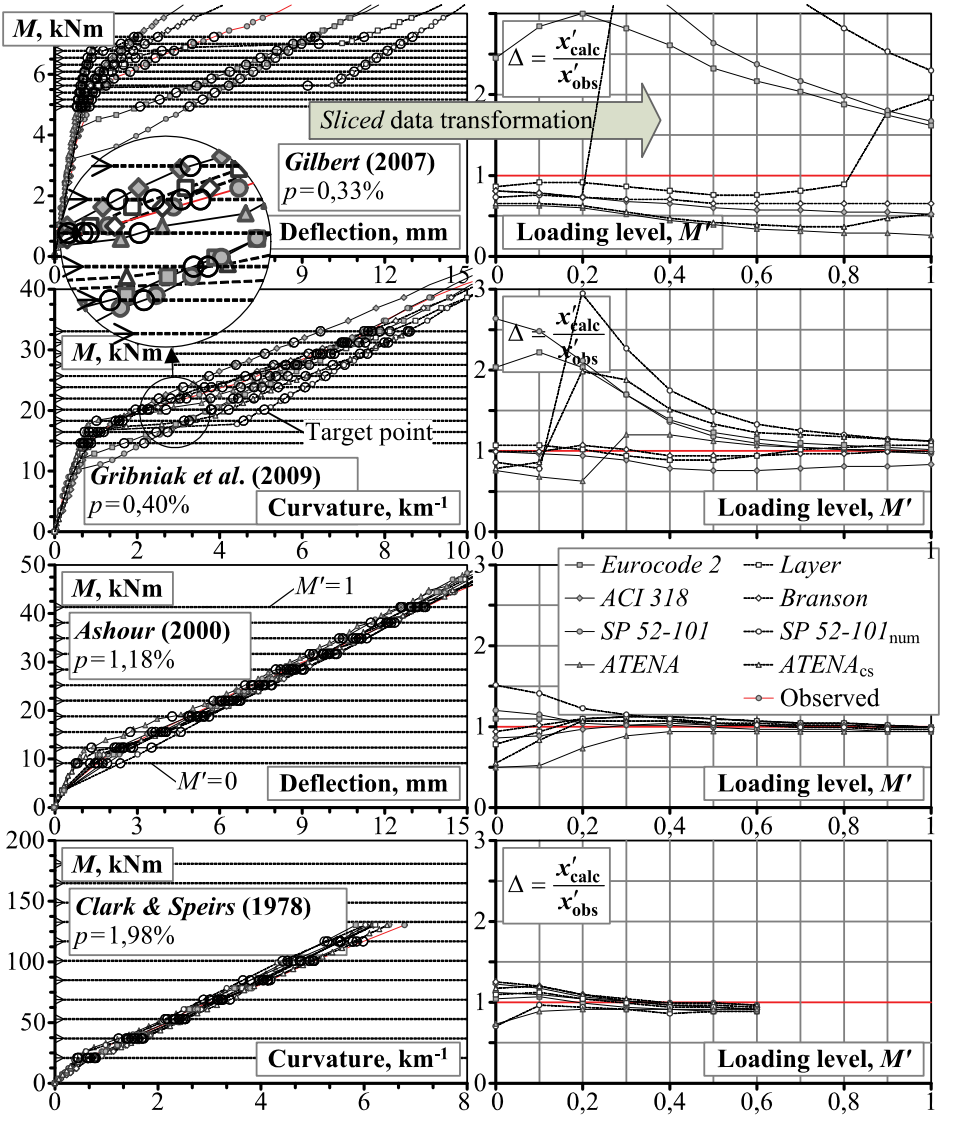

Fig. 4.5. *Sliced* transformation of moment-deflection/curvature diagrams

Step 3. The normality is checked adding the data of each next member until the test is violated. If so, the last member is excluded from the current data set.
Step 4. Next three members including the discarded one, start a new data set. Analysis is proceeded starting from Step 2.

In practical application of the procedure, it was intended at each normalised load level to define reinforcement ratio intervals with normal probability distribution of relative error Δ valid for all the methods under consideration. Analysis performed has resulted in three such intervals:

$$\textbf{\textit{1}}: p \le 0,4\%; \quad \textbf{\textit{2}}: 0,4 < p \le 0,8\%; \quad \textbf{\textit{3}}: p > 0,8\%. \tag{4.15}$$

Under the assumption of the above intervals, m_Δ and s_Δ were calculated at each normalised load level. The statistics for each of the deflection calculation method are presented in Tables 4.5 and 4.6. It can be seen that m_Δ and s_Δ of some adjacent load levels were of similar value. To obtain more reliable results (to increase the number of data points within the intervals and reduce the variation of Δ_j), the adjacent load intervals having homogeneous variances and means can be joined into common intervals. Testing equality of several means can be performed using the technique called the *analysis of variance* (ANOVA). It compares the variance among groups to the variances within groups (Raudys & Young 2004). Two cases are encountered in ANOVA: 1) two independent samples are analysed and 2) more than two samples are analysed. Below these two cases are discussed.

Analysis of two samples allows applying a relatively simple comparison procedure based on *F*-test proposed by *Fisher* (1925) and modified by *Mardia & Zemroch* (1978). Let two samples, $X = \{x_1 \dots x_n\}$ and $Y = \{y_1 \dots y_r\}$, be independent normally distributed random variables with unknown expectations and variances μ_x, μ_y and σ_x^2, σ_y^2, respectively. Let m_x, m_y and s_x^2, s_y^2 be the sample means and empirical variances, respectively. Then the hypothesis on homogeneity of variances σ_x^2 and σ_y^2 is assumed acceptable, if following condition is satisfied (Fisher 1925):

$$F_{\alpha/2}(f_1, f_2) \le s_x^2 / s_y^2 \le F_{1-\alpha/2}(f_1, f_2). \tag{4.16}$$

Here $F(f_1, f_2)$ is the *Fisher*'s statistics having f_1 and f_2 degrees of freedom. The latter can be determined as following (Mardia & Zemroch 1978):

$$\begin{gathered} f_1 = D \cdot (n-1); \quad f_2 = D \cdot (r-1), \quad D = \left[1 + \frac{(n+r-4)(B-3)}{2(n+r-B+3)} \right]^{-1}, \\ B = (n+r) \frac{\sum_{i=1}^{n} (x_i - m_x)^4 + \sum_{i=1}^{r} (y_i - m_y)^4}{\left[\sum_{i=1}^{n} (x_i - m_x)^2 + \sum_{i=1}^{r} (y_i - m_y)^2 \right]^2}. \end{gathered} \tag{4.17}$$

Table 4.5. Basic statistics (mean and standard deviation) for analytical deflection calculation techniques grouped by reinforcement ratio

M'	*n*	*Eurocode 2*		*ACI 318*		*Branson*		*SP 52-101*	
	Pts.	m_Δ	s_Δ	m_Δ	s_Δ	m_Δ	s_Δ	m_Δ	s_Δ
***1*: $p \le 0,4\%$**									
0	23	2,004	0,714	0,945	0,337	0,949	0,336	2,429	0,750
0,1	23	1,963	0,731	0,830	0,309	0,867	0,330	2,143	0,797
0,2	23	1,688	0,741	0,778	0,325	0,863	0,370	1,764	0,806
0,3	23	1,461	0,577	0,750	0,293	0,864	0,346	1,488	0,634
0,4	23	1,298	0,452	0,730	0,254	0,858	0,302	1,301	0,500
0,5	21	1,179	0,339	0,693	0,204	0,824	0,241	1,168	0,387
0,6	20	1,104	0,294	0,690	0,189	0,822	0,215	1,088	0,335
0,7	18	1,059	0,269	0,699	0,187	0,835	0,213	1,037	0,305
0,8	16	1,031	0,250	0,699	0,192	0,832	0,213	1,001	0,277
0,9	16	1,011	0,218	0,714	0,188	0,844	0,204	0,978	0,237
1,0	15	1,012	0,185	0,734	0,190	0,862	0,200	0,973	0,201
***2*: $0,4 < p \le 0,8\%$**									
0	17	1,385	0.421	0.858	0.275	0,863	0,276	1,664	0,441
0,1	17	1,366	0,380	0,856	0,279	0,936	0,310	1,446	0,373
0,2	16	1,213	0,296	0,867	0,254	0,980	0,288	1,242	0,295
0,3	16	1,089	0,156	0,856	0,190	0,967	0,197	1,100	0,151
0,4	16	1,039	0,116	0,869	0,159	0,974	0,148	1,046	0,105
0,5	15	1,029	0,094	0,891	0,140	0,992	0,117	1,034	0,085
0,6	13	1,030	0,080	0,912	0,130	1,010	0,100	1,035	0,070
0,7	13	1,002	0,078	0,911	0,103	1,000	0,075	1,009	0,061
0,8	12	0,986	0,087	0,914	0,085	0,994	0,069	0,999	0,059
0,9	12	0,970	0,092	0,914	0,073	0,987	0,073	0,984	0,061
1,0	9	0,969	0,116	0,901	0,078	0,981	0,099	0,970	0,076
***3*: $p > 0,8\%$**									
0	17	1,022	0,211	0,921	0,172	0,948	0,170	1,139	0,256
0,1	17	1,091	0,177	1,022	0,137	1,109	0,143	1,104	0,202
0,2	17	1,000	0,100	0,990	0,088	1,057	0,094	1,002	0,121
0,3	17	0,958	0,077	0,973	0,072	1,020	0,079	0,966	0,100
0,4	16	0,942	0,078	0,967	0,067	1,000	0,081	0,956	0,094
0,5	15	0,929	0,070	0,959	0,062	0,982	0,075	0,949	0,089
0,6	15	0,907	0,072	0,937	0,065	0,955	0,076	0,932	0,084
0,7	13	0,904	0,079	0,933	0,074	0,948	0,084	0,925	0,094
0,8	12	0,898	0,073	0,926	0,068	0,938	0,077	0,918	0,087
0,9	9	0,896	0,052	0,917	0,046	0,928	0,057	0,894	0,075
1,0	7	0,881	0,066	0,896	0,057	0,906	0,068	0,862	0,066

Table 4.6. Basic statistics (mean and standard deviation) for numerical deflection calculation techniques grouped by reinforcement ratio

M'	n	$SP\ 52\text{-}101_{num}$		*Layer*		*ATENA*		$ATENA_{cs}$	
	Pts.	m_Δ	s_Δ	m_Δ	s_Δ	m_Δ	s_Δ	m_Δ	s_Δ
***1*: $p \le 0,4\%$**									
0	23	0,834	0,304	1,180	0,636	0,680	0,237	0,820	0,441
0,1	23	0,952	0,517	1,157	0,583	0,574	0,210	1,057	0,736
0,2	23	1,943	1,058	1,085	0,536	0,613	0,318	1,261	0,637
0,3	23	1,847	0,880	1,064	0,502	0,910	0,432	1,359	0,666
0,4	23	1,623	0,835	1,015	0,413	0,990	0,394	1,269	0,459
0,5	21	1,446	0,641	0,955	0,340	0,930	0,293	1,164	0,282
0,6	20	1,324	0,552	0,939	0,264	0,945	0,203	1,105	0,237
0,7	18	1,255	0,493	0,933	0,190	0,918	0,200	1,055	0,226
0,8	16	1,219	0,439	0,951	0,155	0,909	0,200	1,025	0,218
0,9	16	1,186	0,371	1,038	0,228	0,915	0,198	1,017	0,187
1,0	15	1,181	0,316	1,089	0,261	0,922	0,192	1,021	0,158
***2*: $0,4 < p \le 0,8\%$**									
0	17	0,669	0,187	0,974	0,324	0,610	0,185	0,773	0,360
0,1	17	1,078	0,383	0,971	0,305	0,611	0,307	1,047	0,462
0,2	16	1,439	0,417	0,975	0,283	0,760	0,281	1,092	0,398
0,3	16	1,233	0,263	0,992	0,183	0,840	0,272	1,021	0,273
0,4	16	1,134	0,208	1,036	0,128	0,856	0,238	1,003	0,200
0,5	15	1,103	0,171	1,069	0,114	0,887	0,206	1,002	0,172
0,6	13	1,093	0,145	1,087	0,105	0,907	0,190	1,020	0,125
0,7	13	1,056	0,131	1,065	0,104	0,911	0,138	1,004	0,096
0,8	12	1,047	0,123	1,062	0,104	0,919	0,119	0,993	0,091
0,9	12	1,046	0,105	1,062	0,097	0,916	0,101	0,983	0,083
1,0	9	1,043	0,112	1,071	0,103	0,908	0,115	0,987	0,099
***3*: $p > 0,8\%$**									
0	17	0,763	0,267	0,995	0,134	0,586	0,108	0,754	0,162
0,1	17	1,144	0,218	1,108	0,158	0,655	0,135	1,060	0,158
0,2	17	1,026	0,145	1,051	0,102	0,813	0,088	1,038	0,082
0,3	17	0,962	0,108	1,010	0,087	0,856	0,069	1,001	0,066
0,4	16	0,936	0,103	0,991	0,090	0,888	0,068	0,992	0,073
0,5	15	0,923	0,070	0,976	0,079	0,902	0,060	0,984	0,063
0,6	15	0,910	0,077	0,953	0,077	0,897	0,061	0,966	0,067
0,7	13	0,917	0,079	0,952	0,083	0,901	0,071	0,963	0,076
0,8	12	0,928	0,071	0,953	0,075	0,902	0,067	0,964	0,071
0,9	9	0,940	0,069	0,960	0,063	0,914	0,042	0,964	0,053
1,0	7	0,929	0,089	0,942	0,073	0,908	0,054	0,955	0,063

Comparative analysis of two expectations μ_x and μ_y can be performed using the *t*-test. Hypothesis about equality of μ_x and μ_y can be accepted, if following condition is satisfied:

$$\frac{\left|m_x - m_y\right|(n+r-2)}{(n-1)s_x^2 + (r-1)s_y^2}\sqrt{\frac{n+r}{n\cdot r}} \le t_{1-\alpha/2}(f), \quad f = n+r-2. \tag{4.18}$$

Here $t(f)$ is the *Student*'s statistics having *f* degree of freedom and significance level $\alpha/2 = 0,025$.

Now consider a case when comparative analysis is performed for more than two data samples. The statistical problem that arises from the use of multiple comparisons tests is that any subsequent test of hypotheses will be performed on the outcome with the same data on which the global test was performed. This can result in an *uncontrolled* type I error rate (the rate of rejecting the null hypothesis when it should not be rejected). Multiple comparison methods have been developed to avoid this problem. In present research, ANOVA is based on the method proposed by *Samiuddin & Atiqullah* (1976) and *Samiuddin et al.* (1978). Let *k* samples of size n_i be independent normally distributed random variables with unknown expectations and variances μ_i and σ_i^2, respectively. Let m_i and s_i^2 be the sample means and empirical variances, respectively. The hypothesis about homogeneity of variances $\sigma_i^2, i = 1\ldots k$ is assumed acceptable, if following condition is satisfied (Samiuddin *et al*. 1978):

$$\max\left(W^*;\ W^{**}\right) \le \chi^2_{1-\alpha}(k-1),$$
$$W^* = \sum_{i=1}^{k}\left[t_i - (1-b_i)T\right]^2 \Big/ \left[t_i T^2\right];\ W^{**} = 4,5\sum_{i=1}^{k} f_i\left[\sqrt[3]{z_i f / f_i} - 1\right]^2. \tag{4.19}$$

Here $\chi^2(k-1)$ is the χ-square statistics having $k-1$ degrees of freedom and significance level $\alpha = 0,05$, other parameters are calculated by the formulas:

$$t_i = \sqrt[3]{s_i^2};\quad b_i = \left(\sqrt{4,5 f_i}\right)^{-1};\quad T = \sqrt[3]{\sum_{i=1}^{k} f_i s_i^2 \Big/ f};$$
$$f_i = n_i - 1;\quad f = \sum_{i=1}^{k} n_i;\quad z_i = f_i s_i^2 \Big/ \sum_{i=1}^{k} f_i s_i^2. \tag{4.20}$$

Chew (1976) has performed investigation on various multi-comparison procedures and came to conclusion that the test developed by *Scheffé* (1959) was most suitable for comparative analysis. Based on this procedure, the sample means m_i are sorted in the ascending order $m_{(i)}$. The hypothesis of equality of $\mu_i, i = 1\ldots k$ can be accepted, if following condition is satisfied:

$$m_{(k)} - m_{(1)} \le \sqrt{d \cdot F_{1-\alpha}(k-1; n-k)},\ n = \sum_{j=1}^{k} n_j;$$
$$d = \left[2(k-1)/n\right]\sum_{j=1}^{k}\sum_{i=1}^{n_j}\left[\left(x_{ij} - \bar{m}\right)^2 \Big/ \left(n_j - 1\right)\right];\ \bar{m} = \left[\sum_{j=1}^{k} m_{(j)}\right]\Big/ k. \tag{4.21}$$

In Equation (4.21), $F(k-1, n-k)$ is the *Fisher*'s statistics having $(k-1)$ and $(n-k)$ degrees of freedom and significance level $\alpha = 0,05$; x_{ij} is the i-th element of j-th sample and n_j is the size of j-th sample.

The above comparison techniques have been used for joining the adjacent load intervals. Each deflection analysis method was treated separately within the designated reinforcement ratio intervals [see Equation (4.15)]. The procedure proposed has similarities to that used for defining reinforcement ratio intervals.

Step 1. Two-sample ANOVA is performed for data points corresponding to the first two normalised load levels. The load levels can be joined, if variances are recognised to be homogeneous [see Equation (4.16)] and the hypothesis of equality of the expectations is valid [see Equation (4.18)]. If any of the conditions is not satisfied, the data of the first load level is rejected. Step 1 is repeated for the data corresponding to the remaining and next load levels.

Step 2. If the analysis performed in Step 1 results in joining two load intervals, data of next load interval is added. Then multiple-comparison ANOVA is performed. The load levels can be joined, if variances are recognised to be homogeneous [see Equation (4.19)] and the hypothesis of equality of the expectations is valid [see Equation (4.21)]. Step 2 is repeated adding data of next load intervals until the above conditions are not satisfied. In that case, the data, which represent the last load interval, is excluded from the current data set.

Step 3. A new data, representing the discarded and next successive load levels, is formed. The analysis is proceeded starting from Step 1.

It should be pointed out that the number of reinforcement ratio intervals was defined from the condition of normal distribution of relative error valid for *all* the methods under consideration. However, this number can be reduced, if individual methods are treated separately. The above procedure with slight modification has been applied to investigate whether the number of reinforcement ratio intervals can be decreased. Analysis has shown that intervals ***1*** and ***2*** can be joined for the deflection analysis results obtained by *ATENA*.

4.2.5. Results of the Analysis

Analysis results are summarised in Tables 4.7 and 4.8 and Figure 4.6. Tables 4.7 and 4.8 present numerical values of means and standard deviations after data grouping was performed. It can be seen from the tables that different number of load intervals was obtained for the methods. For the first two reinforcement ratio intervals, this number was approximately constant varying from four to six. Obviously, this number has reduced for the beams with the largest reinforcement ratio reaching three intervals for all the methods. This number indicates dependence of loading level on accuracy of deflection calculation techniques. The minimal number of intervals shows little dependence. As it was pointed out, joining data intervals contributes to more reliable results due to increase of number

of data points. Such increase results in reduction of variance of data in joined intervals. This can be seen from comparing standard deviations presented in Tables 4.5 and 4.6 on one hand and Tables 4.7 and 4.8 on the other.

Graphical illustration of the analysis results is presented in Figure 4.6 with shown 95% confidence intervals of expectation μ_Δ for the grouped data. Width of the confidence intervals characterises variation of the relative error of predictions [see Equation (4.4)]. It is clearly seen that the variations were different not only for different deflection/curvature prediction methods, but also for different reinforcement ratios and load intensities. Strikingly different results were obtained for the members with minimal reinforcement ratios. Another point of sharp contrast was significantly larger data scatter at early cracking stages. The latter effect is particularly clear for the members with small amounts of reinforcement due to increased share of concrete in resisting tension forces acting in the section. Interpretation of the results presented in Fig. 4.6 will facilitate Fig. 4.7 indicating location of the service load within the normalised load level assumption [see Equation (4.12)]. Thus, for small amounts of reinforcement, service load approaches cracking moment.

Numerical values of mean and standard deviation of Δ calculated at service load are given in Table 4.9. The results, also including confidence intervals of the expectation, are presented for the three intervals of reinforcement ratio. As noted before, consistency of a method is characterised by the *central tendency*. For normally distributed probability of error Δ, the central tendency is characterised by the expectation. A technique will be considered as a consistent, if its confidence interval covers unity. If the confidence intervals do not cover unity, in the author's view, the overestimated deflections/curvatures are more preferable than the underestimated one. The latter results in Table 4.9 are presented in grey filled cells. It should be pointed out that the *ACI 318* method underestimated deflections/curvatures, particularly for the members with relatively low reinforcement ratio ($p \le 0{,}8\%$). For the members with moderate amounts of reinforcement, only *ATENA* (taking into account shrinkage effect) demonstrated consistency, whereas all other methods underestimated deflections/curvatures.

Reasonable results in terms of consistency and variation have been demonstrated using the *Layer* section model. Future investigations are needed to propose a more advanced *free-of-shrinkage* tension-stiffening relationship.

Further, the *t*-tests [see Equation (4.18)] were carried out to check whether the consistency characteristics presented in Table 4.9 were significantly different (5% significance level). Three main conclusions can be made:

- Consistency differences in predictions due to very high variation were not significant for the members with minimal reinforcement ratio ($p \le 0{,}4\%$). Statistically significant differences can be obtained, if the number of test members is increased. Therefore, experimental investigation of lightly reinforced members is of higher priority.

- Consistency of predictions made by the *ACI 318* method for the second reinforcement ratio interval ($0,4 < p \le 0,8\%$) were significantly different concerning other code techniques.
- Difference in consistency of two predictions made by *ATENA* (when shrinkage was ignored and taken into account) was statistically significant. If shrinkage is not assessed, deflections might be underestimated. Therefore, shrinkage effect should be taken into account in the FE analysis of RC structures subjected to short-term load, what is not a common practice.

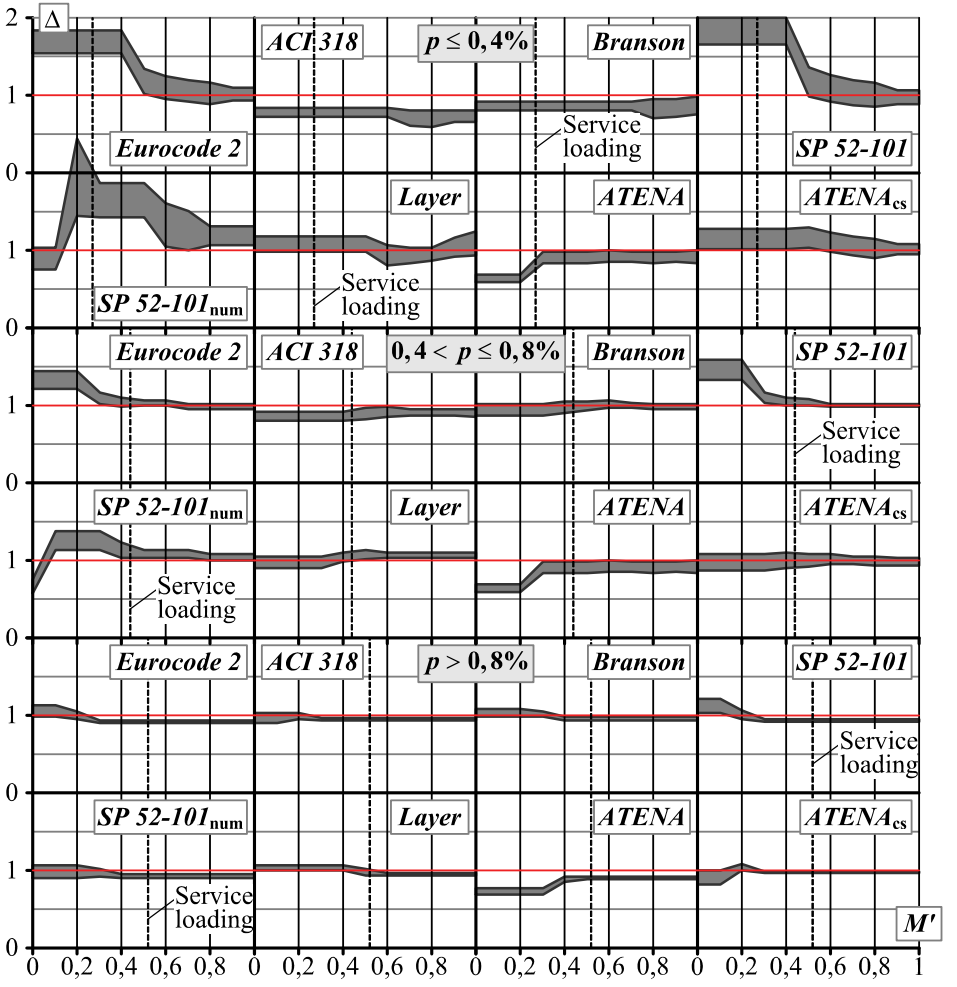

Fig. 4.6. 95% confidence intervals of the expectation for different reinforcement ratio intervals and load levels

Table 4.7. Basic statistics (mean and standard deviation) for analytical deflection calculation techniques after grouping in reinforcement ratio and load level intervals (grouped intervals are shown in grey)

M'	*n*	*Eurocode 2*		*ACI 318*		*Branson*		*SP 52-101*	
	Pts.	m_Δ	s_Δ	m_Δ	s_Δ	m_Δ	s_Δ	m_Δ	s_Δ
***1*: $p \leq$ 0,4%**									
0	23	1,683	0,699	0,776	0,288	0,862	0,300	1,825	0,810
0,1	23								
0,2	23								
0,3	23								
0,4	23								
0,5	21	1,179	0,339					1,168	0,387
0,6	20	1,104	0,294					1,088	0,335
0,7	18	1,059	0,269	0,699	0,187			1,037	0,305
0,8	16	1,031	0,250	0,699	0,192	0,832	0,213	1,001	0,277
0,9	16	1,012	0,200	0,724	0,186	0,844	0,204	0,976	0,217
1,0	15					0,862	0,200		
***2*: 0,4 < $p \leq$ 0,8%**									
0	17	1,323	0,371	0,861	0,232	0,935	0,269	1,454	0,407
0,1	17								
0,2	16								
0,3	16	1,089	0,156					1,100	0,151
0,4	16	1,039	0,116			0,974	0,148	1,046	0,105
0,5	15	1,029	0,086	0,891	0,140	0,992	0,117	1,034	0,085
0,6	13			0,912	0,130	1,010	0,100	1,002	0,066
0,7	13	0,983	0,090	0,912	0,093	1,000	0,075		
0,8	12					0,988	0,077		
0,9	12			0,914	0,073				
1,0	9			0,901	0,078				
***3*: $p >$ 0,8%**									
0	17	1,057	0,195	0,971	0,162	1,038	0,152	1,121	0,228
0,1	17								
0,2	17	1,000	0,100	0,990	0,088			1,002	0,121
0,3	17	0,920	0,074	0,944	0,068	1,020	0,079	0,933	0,091
0,4	16					0,958	0,078		
0,5	15								
0,6	15								
0,7	13								
0,8	12								
0,9	9								
1,0	7								

Table 4.8. Basic statistics (mean and standard deviation) for numerical deflection calculation techniques after grouping in reinforcement ratio and load level intervals (grouped intervals are shown in grey)

M'	n	*SP 52-101*$_{num}$		*Layer*		*ATENA*		*ATENA*$_{cs}$	
	Pts.	m_Δ	s_Δ	m_Δ	s_Δ	m_Δ	s_Δ	m_Δ	s_Δ
***1*: $p \leq$ 0,4%**									
0	23	0,893	0,423	1,076	0,510	0,638	0,262	1,153	0,620
0,1	23								
0,2	23	1,943	1,058						
0,3	23	1,644	0,801			0,909	0,327		
0,4	23								
0,5	21							1,164	0,282
0,6	20	1,324	0,552	0,939	0,264	0,945	0,203	1,105	0,237
0,7	18	1,255	0,493	0,933	0,190	0,918	0,200	1,055	0,226
0,8	16	1,195	0,372	0,951	0,155	0,909	0,200	1,025	0,218
0,9	16			1,038	0,228	0,915	0,198	1,019	0,171
1,0	15			1,089	0,261	0,922	0,192		
***2*: 0,4 < $p \leq$ 0,8%**									
0	17	0,669	0,187	0,978	0,274	**$p \leq$ 0,8%**		0,981	0,393
0,1	17	1,247	0,384						
0,2	16								
0,3	16								
0,4	16	1,134	0,208	1,036	0,128			1,003	0,200
0,5	15	1,085	0,149	1,069	0,114			1,002	0,172
0,6	13			1,069	0,100			1,020	0,125
0,7	13							1,004	0,096
0,8	12	1,045	0,110					0,993	0,091
0,9	12							0,985	0,087
1,0	9								
***3*: $p >$ 0,8%**									
0	17	0,978	0,265	1,031	0,123	0,728	0,150	0,907	0,221
0,1	17								
0,2	17							1,038	0,082
0,3	17	0,962	0,108					0,977	0,067
0,4	16	0,925	0,082			0,888	0,068		
0,5	15			0,976	0,079	0,977	0,067		
0,6	15			0,953	0,073				
0,7	13								
0,8	12								
0,9	9								
1,0	7								

Table 4.9. Basic statistics defined at service loading after grouping data according to reinforcement ratio

Method	Statistics		95 % confidence limits of the expectation	
	m_Δ	s_Δ	m_Δ^-	m_Δ^+
***1*: $p \le 0{,}4\%$, n = 23 pts.**				
Eurocode 2	1,401	0,636	1,252	1,549
ACI 318	0,782	0,316	0,708	0,856
Branson	0,890	0,371	0,803	0,977
SP 52-101	1,547	0,737	1,370	1,719
***SP 52-101*$_{\text{num}}$**	1,710	1,010	1,474	1,946
Layer	1,045	0,514	0,924	1,165
ATENA	0,842	0,309	0,785	0,898
***ATENA*$_{\text{cs}}$**	1,288	0,755	1,112	1,465
***2*: $0{,}4 < p \le 0{,}8\%$, n = 15 pts.**				
Eurocode 2	1,043	0,112	1,010	1,075
ACI 318	0,864	0,177	0,813	0,915
Branson	0,959	0,167	0,911	1,007
SP 52-101	1,058	0,115	1,025	1,091
***SP 52-101*$_{\text{num}}$**	1,159	0,255	1,085	1,233
Layer	1,000	0,156	0,955	1,045
***ATENA*[1]**	–	–	–	–
***ATENA*$_{\text{cs}}$**	0,984	0,222	0,920	1,048
***3*: $p > 0{,}8\%$, n = 15 pts.**				
Eurocode 2	0,922	0,078	0,900	0,945
ACI 318	0,950	0,066	0,931	0,969
Branson	0,973	0,081	0,950	0,997
SP 52-101	0,944	0,089	0,919	0,970
***SP 52-101*$_{\text{num}}$**	0,923	0,095	0,895	0,950
Layer	0,971	0,088	0,945	0,996
ATENA	0,899	0,063	0,881	0,918
***ATENA*$_{\text{cs}}$**	0,979	0,072	0,958	1,000

[1]Reinforcement ratio intervals ***1*** and ***2*** were joined for the prediction results obtained by *ATENA*: the number of data points has increased up to 38 (n = 23 + 15)

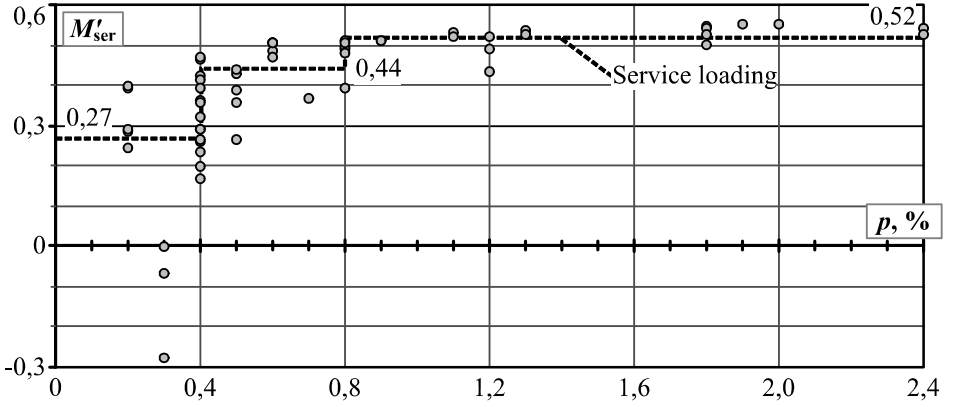

Fig. 4.7. Distribution of service load interval in respect to reinforcement ratio

4.3. Concluding Remarks of Chapter 4

This Chapter presents a transparent statistical procedure developed for analysis of experimental data. It introduces a relative error of predictions $\Delta = x_{calc}/x_{obs}$, were x_{calc} and x_{obs} are, respectively, the values calculated and observed experimentally. The proposed procedure allows checking hypotheses on accuracy of predictions of a calculation technique by analysis of the relative errors. To assure even contribution of each test specimen and consistency of the statistical analysis, a procedure called the *sliced* data transformation has been proposed. The data transformation for each test specimen introduces a fixed number of observation levels further to be used in the analysis.

The statistical investigation consists of two parts: free shrinkage strain and short-term deflection/curvatures prediction accuracy analyses. The first part investigates accuracy of free shrinkage predictions made by various methods reviewed in Section 1.1.2. Though considered as a long-term effect, shrinkage also has influence on crack resistance and deformations of reinforced concrete members subjected to short-term load. In the code methods based on experimental data, shrinkage effect on deformations is assessed indirectly. In the numerical approaches, shrinkage should be taken into account as an independent factor. As shrinkage is taken into account in the proposed strain/deflection calculation technique it seems appropriate to perform comparison of predictions of free shrinkage strain by different methods. The analysis is limited to relatively short duration (up to 150 days), characteristic to the age of a structure first loaded. The comparative statistical analysis was carried out for the experimental data reported by the author and other researchers. The data set consisted of 23 experimental programs, 351 specimens and 7391 measurement points.

Shrinkage analysis has indicted that the *Bažant & Baweja* (*B3*) and the *Eurocode 2* methods gave the most accurate predictions for the time interval from 21 to 63 days. This time interval covers the test data employed for the deflection analysis. The *Eurocode 2* method, as the normative document accepted in the *European Union*, was chosen for further analysis.

The second part of the analysis was concerned with short-term deflections of reinforced concrete bending members. This investigation has employed data of seven experimental programs, one of which was reported by the author. The data set consisted of 57 specimens and 1468 measurement points. The comparative study was based on the predictions made by design codes (*Eurocode 2*, *ACI 318* and *SP 52-101*) and numerical techniques (*ATENA* and *Layer* section model).

Accuracy of the deflection/curvature predictions varied significantly with change of load intensity and reinforcement ratio, i.e. was increasing with growing of latter parameters. Strikingly different results were obtained for the members with minimal reinforcement ratios. Another point of sharp contrast was significantly larger data scatter at early cracking stages. The latter effect is particularly clear for the members with small amounts of reinforcement due to increased share of concrete in resisting tension forces acting in the section.

It should be pointed out that the *ACI 318* method significantly underestimated deflections/curvatures for members with relatively low reinforcement ratio ($p \leq 0{,}8\%$). For the members with moderate amounts of reinforcement ($p > 0{,}8\%$), only *ATENA* (taking into account shrinkage effect) demonstrated consistency, whereas all other methods underestimated deflections.

Reasonable results in terms of consistency and variation were demonstrated using the *Layer* section model. Future investigations are needed for proposing a more advanced *free-of-shrinkage* tension-stiffening relationship.

Three main conclusions can be made:

1. Consistency differences in predictions by different methods due to very high variation were not significant for the members with minimal reinforcement ratio ($p \leq 0{,}4\%$). Statistically significant results can be obtained, if the number of test members is increased. Therefore, experimental investigation of lightly reinforced members is of *priority*.
2. Predictions made by the *ACI 318* method for reinforcement ratio interval $0{,}4 < p \leq 0{,}8\%$ were significantly (5% significance level) different concerning other code techniques.
3. Difference in consistency of two deflection predictions by *ATENA* (when shrinkage was ignored and taken into account) was statistically significant. When shrinkage was not assessed, deflections were substantially underestimated. Therefore, shrinkage effect *should be taken into account* in the numerical analysis of reinforced concrete structures subjected to short-term load (what is not a common practice).

General Conclusions

Summary and Conclusions

Present study aims at contributing to a better understanding of the shrinkage influence on cracking resistance and deformation behaviour of reinforced concrete (RC) flexural members subjected to short-term loading. Based on the literature review, the following conclusions can be drawn:

1. Most known tension-stiffening relationships were derived from test data of reinforced concrete members exposed to shrinkage. Therefore, the tension-stiffening was coupled with shrinkage and accompanying creep effect.
2. While being confident about sufficient accuracy of deflection analysis of structures with moderate amounts of reinforcement, investigators and designers often raise concerns about the validity of the chosen tension-stiffening parameters for lightly reinforced members. Complexity of the issue is indicated by the wide-spread use of different code techniques (*Eurocode 2*, *ACI*, *Russian code*, etc) and disparity of their prediction results. For checking the accuracy of the predictive models, very few reports on tests of lightly reinforced flexural members are available.

An *innovative* numerical procedure has been proposed for deriving *free-of-shrinkage* tension-stiffening relationships using test data (moment-curvature relationships) of bending RC members. The procedure combines the *direct* and the *inverse* techniques. In the *direct* technique, moment-curvature diagrams are calculated using the assumed material stress-strain relationships. The *inverse* technique aims at determining tension-stiffening relationships for cracked tensile concrete from flexural tests of RC members. To eliminate shrinkage effect, a reverse shrinkage (expansion) strain is assumed in the *direct* technique.

New experimental data was obtained on crack resistance and deformation behaviour of lightly reinforced concrete beams subjected to short-term loading. Prior to the tests of the beams, measurements on concrete shrinkage and creep were performed. Based on the proposed procedure, *free-of-shrinkage* tension-stiffening relationships were derived for the beams. It was shown that:

3. For beams of same reinforcement ratio, tension-stiffening was more pronounced in those with a larger number of tensile reinforcing bars.

4. Shrinkage greatly affects tension-stiffening and might several times reduce the cracking resistance of the members. Although, in absolute terms, this was more clearly expressed in the members with higher reinforcement ratio, relative shrinkage influence on deflections was more profound for the members with small amounts of reinforcement.

A statistical procedure for assessing accuracy of deflection predictions of reinforced concrete members taking into account inconsistency of the test data has been developed. The proposed procedure based on grouping of statistical data allows obtaining results that are more reliable. The procedure introduces a relative error of predictions $\Delta = x_{\text{calc}} / x_{\text{obs}}$ (x_{calc} and x_{obs} are, respectively, the values calculated and observed experimentally) considered as a random variable. Statistics estimating the *central tendency* and *variability* serve to measure precision of the predictions. The central tendency was regarded as a consistency parameter of a calculation method. In the case of symmetrical probability distribution of error Δ, the central tendency can be estimated by the sample mean m_{Δ}, otherwise by the sample median $\xi_{\Delta,1/2}$. The postulate of minimum variance was used to evaluate accuracy of a model.

Using the proposed statistical procedure, a comparative analysis has been carried out to assess accuracy of predictions of free shrinkage strains occurring at relatively early age of concrete, characteristic to the age at first loading.

5. Shrinkage analysis has indicated that for the time interval from 21 to 63 days the *Eurocode 2* and the *Bažant & Baweja* (*B3*) methods gave the most accurate predictions ($\xi_{\Delta,1/2} = 0,98 \ldots 1,01$ and $0,93 \ldots 1,01$, respectively).

Similar statistical analysis has been performed for assessing accuracy of deflection/curvature predictions made by different calculation methods. It was shown that:

6. Accuracy of the predictions varied significantly within different ranges of load intensity and reinforcement ratio, i.e. was increasing with growing of latter parameters.
7. Strikingly different results were obtained for the members with minimal reinforcement ratios. Another point of sharp contrast was significantly larger data scatter at early cracking stages. Particularly inaccurate results were obtained when these two parameters (small reinforcement ratio and load just above the cracking point) were combined ($m_\Delta = 0,78\ldots1,83$ varied from 0,78 to 1,83).
8. The *ACI 318* method significantly underestimated deflections ($m_\Delta = 0,70\ldots0,90$) for the members with relatively low reinforcement ratio ($p \le 0,8\%$). The predictions for reinforcement ratio interval $0,4 < p \le 0,8\%$ were significantly (at 5% significance level) different in regard to other code techniques (compare $m_\Delta = 0,86\ldots0,91$ for *ACI* and $m_\Delta = 0,94\ldots1,45$ for other techniques).
9. Difference in consistency of two deflection predictions by finite element software *ATENA* (when shrinkage was ignored and taken into account) was statistically significant. When shrinkage was ignored, deflections were substantially underestimated ($m_\Delta = 0,64\ldots0,97$). Accuracy of the predictions has increased when shrinkage was assessed ($m_\Delta = 0,91\ldots1,16$). Therefore, shrinkage effect should be taken into account in the numerical analysis of reinforced concrete structures subjected to short-term load (what is not a common practice).
10. Reasonable results in terms of consistency and variation were demonstrated using the *Layer* section model with linear tension-stiffening relationship and taking into account shrinkage and accompanying creep effects. The extreme values of m_Δ ranged from 0,93 to 1,08 for all intervals of loading and reinforcement ratios.

Suggestions for Further Research

The serviceability techniques used in the design codes of different countries are based on different assumptions and approaches leading to different predictions. Future development of the serviceability models should be aimed at harmonising assumptions and approaches for crack width and deflection analysis of both ana-

lytical-empirical and numerical techniques. In the short-term prospective, regarding the author‘s investigations of serviceability problems, the following issues are to be dealt:

1. Developing alternative approaches in tension-stiffening (*steel-related*, *effective area*, *stress transfer*) may give new insights in the investigation of the phenomena.
2. Assessing influence of various geometrical parameters (cover, section height, reinforcement ratio, bar diameter and surface characteristics) on tension-stiffening for developing a more advanced *free-of-shrinkage* constitutive relationship.
3. Investigating the *effective area* of tension-stiffening concerning both crack width and deformation problems.
4. Investigating long-term tension-stiffening effect.
5. Investigating tension-stiffening in composite structures reinforced with non-metallic reinforcement.
6. Relating deformation and crack width analysis problems based on the unified approach.
7. Improving the developed *inverse* techniques regarding the aspects of convergence and versatility.
8. If not eliminated in the tests, shrinkage and associated creep recordings should be performed for subsequent numerical elimination of these effects.

References

ACI Committee 201. 2001. *Guide to Durable Concrete, ACI 201.2R-01*. Farmington Hills, Michigan: ACI. 41 p.

ACI Committee 209. 2008. *Guide for Modeling and Calculating Shrinkage and Creep in Hardened Concrete, ACI 209.2R-08*. Farmington Hills, Michigan: ACI. 48 p.

ACI Committee 318. 2008. *Building Code Requirements for Structural Concrete, ACI 318-08 and Commentary*. Farmington Hills, Michigan: ACI. 471 p.

Acker, P.; Ulm, F.-J. 2001. Creep and shrinkage of concrete: physical origins and practical measurements, *Nuclear Engineering and Design* 203(2–3): 143–158.

AIJ (Architectural Institute of Japan). 1991. *AIJ Standards for Structural Calculation of Steel Reinforced Concrete Structures* (English translation of 1987 edition). Tokyo: AIJ. 104 p.

Albenga, G. 1945. Synthetic look to the evolution of the reinforced concrete from the origin to the days ours (Sguardo sintetico all'evoluzione del cemento armato dall'origine ai giorni nostri), *Lezione del Corso la Tecnica del Cemento Armato*: 5–21 (in Italian).

Al-Manaseer, A.; Lakshmikantan, S. 1999. Comparison between current and future design code models for shrinkage and creep, *Revue Française de Génie Civil* 3(3–4): 39–59.

Al-Manaseer, A.; Lam, J.-P. 2005. Statistical evaluation of shrinkage and creep models, *ACI Materials Journal* 102(3): 170–176.

Altoubat, S. A.; Lange, D. A. 2001. The Pickett effect in early age concrete under restrained conditions, *Concrete Science and Engineering Journal* (*RILEM*) 3(11): 163–167.

Altoubat, S. A.; Lange, D. A. 2002. The Pickett effect at early age and experiment separating its mechanisms in tension, *Materials and Structures* (*RILEM*) 35(4): 211–218.

Alvaredo, A.; Wittmann, F. H. 1993. Shrinkage as influenced by strain softening and creep, in *Proc. of 5th International RILEM Symposium Creep and Shrinkage of Concrete*. New York: E & FN SPON, 103–113.

Argytis, J.; Kacianauskas, R. 1996. Semi-analytical finite elements in the higher-order theory of beams, *Computer Methods in Applied Mechanics and Engineering* 138(1–4): 19–72.

Artemjev, V. P. 1959. *Investigation of Strength, Stiffness and Crack Resistance of Reinforced and Pre-stressed Concrete Beams* (*Исследование прочности, трещиностойкости и жёсткости обычных и предварительно напряжённых железобетонных балок, армированных высокопрочными стержнями периодического профиля из стали 30ХТ2С упрочнённой вытяжкой*). PhD dissertation. Moscow Institute of Structural Engineering. 238 p. (in Russian).

Asanuma, K.; Takeshita, H.; Fujii, M. 1995. Effects and assessment of thickness of member for drying shrinkage, *Proceedings of Japan Concrete Institute* 17(1): 621–626 (in Japanese).

Ashour, S. A. 2000. Effect of compressive strength and tensile reinforcement ratio on flexural behaviour of high-strength concrete beams, *Engineering Structures* 22(5): 413–423.

Barenblatt, G. I. 1959. On equilibrium cracks formed in brittle fracture. General concepts and hypotheses. Axisymmetric cracks, *Journal of Applied Mathematics and Mechanics* 23(3): 622–636.

Barenblatt, G. I. 1962. Mathematical theory of equilibrium cracks in brittle fracture, *Advances in Applied Mechanics* 7: 55–129.

Barnard, P. R. 1964. Researches into the complete stress-strain curve for concrete, *Magazine of Concrete Research* 16(49): 203–210.

Barros, M.; Martins, R. A. F.; Ferreira, C. C. 2001. Tension stiffening model with increasing damage for reinforced concrete, *Engineering Computations* 18(5–6): 759–785.

Base, G. L.; Read, J. B.; Beeby, A. W.; Taylor, H. P. J. 1966. *An Investigation of the Crack Control Characteristics of Various Types of Bar in Reinforced Concrete Beams. Research Report* 18(1), Cement and Concrete Association, London. 44 p.

Bažant, Z. P. 1972. Prediction of concrete creep effects using age-adjusted effective modulus method, *ACI Journal* 69: 212–217.

Bažant, Z. P. 1976. Instability, ductility and size effect in strain softening concrete, *ASCE Journal of the Engineering Mechanics Division* 102(2): 331–344.

Bažant, Z. P.; Baweja, S. 1995a. Justification and refinements of model B3 for concrete creep and shrinkage. Statistics and sensitivity, *Materials and Structures* (*RILEM*) 28(7): 415–430.

Bažant, Z. P.; Baweja, S. 1995b. Justification and refinements of model B3 for concrete creep and shrinkage. Updating and theoretical basis, *Materials and Structures* (*RILEM*) 28(8): 488–495.

Bažant, Z. P.; Baweja, S. 2000. Creep and shrinkage prediction model for analysis and design of concrete structures: Model B3, in *Proc. of the Adam Neville Symposium: Creep and Shrinkage-Structural Design Effects, ACI Special Publications* 194: 1–83.

Bažant, Z. P.; Chern, J. C. 1985. Concrete creep at variable humidity: constitutive law and mechanisms, *Material and Structures* (*RILEM*) 18(1): 1–20.

Bažant, Z. P.; Hauggaaed, A. B.; Baweja, S.; Ulm, F. J. 1997. Microprestress-solidification theory for concrete creep. I: Aging and drying effects, *ASCE Journal of Engineering Mechanics* 123(11): 1188–1194.

Bažant, Z.P.; Oh, B. 1983. Crack band theory for fracture of concrete, *Materials and Structures* (*RILEM*) 16(93): 155–177.

Bažant, Z.P.; Planas, J. 1998. *Fracture and Size Effect in Concrete and Other Quasibrittle Structures*. Boca Raton: CRC Press. 640 p.

Bažant, Z. P.; Raftshol, W. J. 1982. Effect of cracking in drying and shrinkage specimens, *Cement and Concrete Research* 12(2): 209–226.

Bažant, Z. P.; Xi, Y. 1994. Drying creep of concrete: constitutive model and experiments separating its mechanisms, *Materials and Structures* (*RILEM*) 27(1): 3–14.

Beeby, A. W.; Scott, R. H. 2006. Mechanisms of long-term decay of tension stiffening, *Magazine of Concrete Research* 58(5): 255–266.

Belarbi, A.; Hsu, T. T. C. 1994. Constitutive laws of concrete in tension and reinforcing bars stiffened by concrete, *ACI Structural Journal* 91(4): 465–474.

Bentz, E. C. 2005. Explaining the riddle of tension stiffening models for shear panel experiments, *ASCE Journal of Structural Engineering* 131(9): 1422–1425

Bischoff, P. H. 1983. *Response of Prestressed Concrete Tension Members*. M. Eng. thesis. McGill University, Montreal. 122 p.

Bischoff, P. H. 2001. Effects of shrinkage on tension stiffening and cracking in reinforced concrete, *Canadian Journal of Civil Engineering* 28(3): 363–374.

Bischoff, P. H. 2008. Discussion of "Tension stiffening in lightly reinforced concrete slabs" by R. I. Gilbert, *ASCE Journal of Structural Engineering* 134(7): 1259–1260.

Bischoff, P. H.; Johnson, R. D. 2007. Effect of shrinkage on short-term deflection of reinforced concrete beams and slabs, in *Structural Implications of Shrinkage and Creep of Concrete*, *ACI SP* 246: 167–180.

Bischoff, P. H.; Mac Laggan, D. A. 2006. Bond and tension stiffening in concrete tension members with plain reinforcement, in *Proc. of 1st International Structural Specialty Conference of the Canadian Society for Civil Engineering, Calgary*, 2006, (CD) 10 p.

Bischoff, P. H.; Paixao, R. 2004. Tension stiffening and cracking of concrete reinforced with glass fiber reinforced polymer (GFRP) bars, *Canadian Journal of Civil Engineering* 31(4): 579–588.

Borosnyói, A.; Balázs, L. G. 2005. Models for flexural cracking in concrete: the state of the art, *Structural Concrete* 6(2): 53–62.

Borst de, R. 2002. Fracture in quasi-brittle materials: A review of continuum damage-based approaches, *Engineering Fracture Mechanics* 69(2): 95–112.

Bosco, C.; Carpinteri, A.; Debernardi, P. G. 1990a. Fracture of reinforced-concrete – scale effects and snap-back instability, *Engineering Fracture Mechanics* 35(4–5): 665–677.

Bosco, C.; Carpinteri, A.; Debernardi, P. G. 1990b. Minimum reinforcement in high-strength concrete, *ASCE Journal of Structural Engineering* 116(2): 427–437.

Bosnjak, D.; Kanstad, T. 1997. Analysis of hardening high performance concrete structures, in *Proc. of Second International DIANA Conference on Finite Elements in Engineering and Science – Computational Mechanics 97*, Amsterdam, 1997, 45–54.

Branch, J.; Hannant, D. J.; Mulheron, M. 2002. Factors affecting the plastic shrinkage cracking of high-strength concrete, *Magazine of Concrete Research* 54(5): 347–354.

Branson, D. E. 1963. *Instantaneous and Time-Dependent Deflections of Simple and Continuous Reinforced Concrete Beams. HPR Report* 7(1). Alabama Highway Department, Bureau of Public roads. 78 p.

Branson, D. E. 1977. *Deformation of Concrete Structures*. New York: McGaw-Hill. 546 p.

Broberg, K. B. 1999. *Cracks and Fracture*. San Diego: Academic Press. 752 p.

Brooks, J. J. 2001. The influence of pore stress on creep of hardened cement paste, in *Proc. of 6th International Conference Creep, Shrinkage and Durability Mechanics of Concrete and other Quasi-Brittle Materials* (*ConCreep 6*). Elsevier, 61–66.

Carpinteri, A. 1994. Scaling laws and renormalization groups for strength and toughness of disordered materials, *International Journal of Solids and Structures* 31(3): 291–330.

Carpinteri, A.; Ferro, G. 1994. Size effects on tensile fracture properties: a unified explanation based on disorder and fracture of concrete microstructure, *Materials and Structures* (*RILEM*) 27(10): 563–571.

CEB-FIP (Comité Euro International du Béton; Fédération International de la Précontraint). 1978. *CEB-FIP Model Code for Concrete Structures*. *CEB Bulletin d'Information* 124/125E. 348 p.

CEB-FIP (Comité Euro International du Béton; Fédération International de la Précontraint). 1990. *High Strength Concrete*. SR 90/1. 61 p.

CEB-FIP (Comité Euro International du Béton; Fédération International de la Précontraint). 1991. *CEB-FIB Model Code 1990: Design Code*. London: Thomas Telford. 437 p.

CEB-FIP (Comité Euro International du Béton; Fédération International de la Précontraint). 1997. *Serviceability Models. Behaviour and Modelling in Serviceability Limit States Including Repeated and Sustained Loads. Bulletin d'Information 235*. Lausanne: CEB. 280 p.

Cedolin, L.; Bažant, Z. P. 1980. Effect of finite element choice in blunt crack band analysis, *Computer Methods in Applied Mechanics and Engineering* 24(3): 305–316.

CEN (Comité Européen de Normalisation). 2004. *Eurocode 2: Design of Concrete Structures – Part 1: General Rules and Rules for Buildings, EN 1992-1-1:2004*. Brussels: CEN. 230 p.

Cervenka, V. 1985. Constitutive model for cracked reinforced concrete, *ACI Journal Proceedings* 82(6): 877–882.

Cervenka, V. 1995. Mesh sensitivity effects in smeared finite element analysis of concrete fracture, in *Proc. of The Second International Conference Fracture Mechanics of Concrete Structures* (*FraMCoS-2*). Freiburg: AEDIFICATIO Publishers: 1387–1396.

Cervenka, V. 2002. Computer simulation of failure of concrete structures for practice, in *Proc. First FIB* Congress, *Concrete Structures in 21 Century*, Osaka, Japan, 2002, 63.

Cervenka, J.; Cervenka, V.; Eligehausen, R. 1998. Fracture-plastic model for concrete. Application to analysis of powder actuated anchors, in *Proc. of the Third International Conference on Fracture Mechanics of Concrete Structures* (*FraMCoS 3*). Gifu, Japan, 1998, 2: 1107–1117.

Cervenka, V.; Cervenka, J.; Pukl, R. 2002. ATENA – A tool for engineering analysis of fracture in concrete, *Sādhanā* 27(4): 485–492.

Cervenka, J.; Chandra Kishen, J. M.; Saouma, A. E. 1998. Mixed mode fracture of cementitious biomaterial interfaces. Part II: Numerical simulation, *Engineering Fracture Mechanics* 60(1): 95–107.

Cervenka, V.; Pukl, R. 1994. SBETA analysis of size effect in concrete structures, in *Size effect in Concrete Structure*. London: E & F N Spon, 323–333.

Cervenka, V.; Pukl, R. 1995. Mesh sensitivity effects in smeared finite element analysis of concrete structures, in *Proc. of the Second International Conference on Fracture Mechanics of Concrete Structures* (*FraMCoS 2*). ETH Zurich, Switzerland, 1995, 1387-1396.

Cervenka, V.; Pukl, R.; Eligehausen, R. 1990. Computer simulation of anchoring technique in reinforced concrete beams, in *Proc. of the Second International Conference on Computer Aided Analysis and Design of Concrete Structures*. Swansea: Pineridge Press, 1–19.

Chew, V. 1976. Comparing treatment means: A compendium, *HortScience* 11(4): 348–357.

Choi, C.-K.; Cheung, S.-H. 1996. Tension stiffening model for planar reinforced concrete members, *Computers & Structures* 59(1): 179–190.

Ciampi, V.; Eligehausen, R.; Bertero, V. V.; Popov, E. P. 1981. Analytical model for deformed bar bond under generalised excitation, in *Proc. of the IABSE Colloquium on Advanced Mechanics of Reinforced Concrete*, Delft, the Netherlands, 1981, 53–67.

Clark, L. A.; Speirs, D. M. 1978. *Tension Stiffening in Reinforced Concrete Beams and Slabs under Short-Term Load. Technical Report* 42.521. Cement and Concrete Association. 19 p.

CNIIS (Central Institute of Research and Investigation in Civil Engineering). 1983. *Recommendations for Determination of Numerical Parameters of Creep and Shrinkage of Concrete for the Design of RC Structures in the Regions of Dry and Hot Climate* (*Рекомендации по определению числовых параметров деформации ползучести и усадки бетона при проектировании железобетонных конструкций для районов с сухим и жарким климатом*). Moscow: CNIIS. 40 p. (in Russian).

Cohen, I.; Kita, H.; Van Der Kloot, W. 1974. The intervals between miniature end-plate potentials in the frog are unlikely to be independently or exponentially distributed, *The Journal of Physiology* 236(2): 327–339.

Collins, M. P.; Mitchell, D. 1991. *Prestressed Concrete Structures*. Englewood Cliffs, New York: Prentice-Hall Inc. 766 p.

Considère, A. 1899a. Influence of metal reinforcement on the properties of the mortars and concrete (Influence des armature métalliques sur les propriétés des mortiers et de béton), *Le Génie Civil* V. XXXIV(14): 213–216 (in French).

Considère, A. 1899b. Influence of metal reinforcement on the properties of the mortars and concrete (Influence des armature métalliques sur les propriétés des mortiers et de béton), *Le Génie Civil* V. XXXIV(15): 229–233 (in French).

Cope, R. J.; Rao P. V.; Clark, L. A. 1979. Nonlinear design of concrete bridge slabs using FE procedures, in *Proc. of CSCE-ASCE-ACI-CEB International Symposium, University of Waterloo, Ontario*, 1979, 379–407.

Cornelissen, H. A.; Hordijk, D. A.; Reinhardt, H. W. 1986. Experimental determination of crack softening characteristics of normal and lightweight concrete, *Heron* 31(2): 45–46.

Crisfield, M. A. 1982. Local instabilities in the non-linear analysis of reinforced concrete beams and slabs, *ICE Proceedings* 73(1): 135–145.

Darwin, D.; Barham, S.; Kozul, R.; Luan, S. 2001. Fracture energy of high-strength concrete, *ACI Materials Journal* 98(5): 410–417.

David, H. A.; Nagaraja, H. N. 2003 *Order Statistics*. 3rd Edition. New Jersey: John Wiley & Sons. 488 p.

Debernardi, P. G.; Talano, M. 2001. Softening behaviour of concrete prisms under eccentric compressive forces, *Magazine of Concrete Research* 53(4): 239–249.

Debernardi, P. G.; Talano, M. 2006. Shear deformation in reinforced concrete beams with thin web, *Magazine of Concrete Research* 58(3): 157–171.

Dias, W. P. S. 2003. Influence of mix and environment on plastic shrinkage cracking, *Magazine of Concrete Research* 55(4): 385–394.

Dilger, W. H.; Koch, R.; Kowalczyk, R. 1984. Ductility of plain and confined concrete under different strain rates, *ACI Journal Proceedings* 81(1): 73–81.

Dugdale, D. S. 1960. Yielding of steel sheets containing slits, *Journal of the Mechanics and Physics of Solids* 8(2): 100–104.

Durbin, J. 1961. Some methods of constructing exact tests, *Biometrika* 48(1–2): 41–55.

Ebead, U. A.; Marzouk, H. 2005. Tension stiffening model for FRP-strengthened RC concrete two-way slabs, *Material and Structures* (*RILEM*) 38(276): 193–200.

Eckfeldt, L. 2005. *Possibilities and Limitations of the Computation of Crack Widths in Variable Structural Situations* (*Möglichkeiten und Grenzen der Berechnung von Rissbreiten in Veränderlichen Verbundsituationen*). PhD dissertation. Dresden Technical University. 440 p.

Edwards, A. D.; Yannopoulos, P. J. 1979. Local bond-stress to slip relationship for hot rolled deformed bars and mild steel plain bars, *ACI Journal Proceedings* 76(3): 405–420.

El-Badry, M. M.; Ghali, A. 2001. Analysis of time-dependent effects in concrete structures using conventional linear computer programs, *Canadian Journal of Civil Engineering* 28(2): 190–200.

Elices, M.; Guinea, G. V.; Gómez, J.; Planas. J. 2002. The cohesive zone model: advantages, limitations and challenges, *Engineering Fracture Mechanics* 69(2): 137–163.

Elices, M.; Planas. J. 1989. Material models, in *Fracture Mechanics of Concrete Structures*. London: Chapman & Hall, 16–62.

Evans, R. H.; Marathe, M. S. 1968. Microcracking and stress-strain curves for concrete in tension, *Material and Structures* (*RILEM*) 1(1): 61–64.

Fantilli, A. P.; Bićanić, N.; Mang, H.; Meschke, G. 1998a. Analysis of RC tensile members considering fracture mechanics and bond between steel and concrete, in *Computational Modelling of Concrete Structures*. Rotterdam: Balkema, 807–815.

Fantilli, A. P.; Ferretti, D.; Iori, I; Vallini, P. 1998b. Flexural deformability of reinforced concrete beams, *ASCE Journal of Structural Engineering* 124(9): 1041–1049.

Fantilli, A. P.; Ferretti, D.; Rosati, G. 2005. Effect of bar diameter on the behavior of lightly reinforced concrete beams, *ASCE Journal of Materials in Civil Engineering* 17(1): 10–18.

Feenstra, P. H.; Borst de, R. 1995. A constitutive model for reinforced concrete, *ASCE Journal of Engineering Mechanics* 121(5): 587–595.

FIB (Fédération Internationale du Béton). 1999. *Structural Concrete. Textbook on Behaviour, Design and Performance. Basis of Design*. Lausanne: Federal Institute of Technology Lausanne. 324 p.

Fields, K.; Bischoff, P. H. 2004. Tension stiffening and cracking of high-strength reinforced concrete tension members, *ACI Structural Journal* 101(4): 447–456.

Figarovskij, V. V. 1962. *Experimental Investigation of Stiffness and Cracking of Reinforced Concrete Flexural Members Subjected to Short-Term and Long-Term Loading* (*Экспериментальное исследование жёсткости и трещиностойкости изгибаемых железобетонных элементов при кратковременном и длительном действии нагрузки*). PhD dissertation. Moscow: NIIZhB. 210 p. (In Russian).

Fisher, R. A. 1925. *Statistical Methods for Research Workers*. Edinburgh, United Kingdom: Oliver & Boyd. 239 p.

Floegl, H.; Mang, H. A. 1982. Tension stiffening concept based on bond sleep, *ASCE Journal of Structural Engineering* 108(12): 2681–2701.

Foster, S. J.; Budiono, B.; Gilbert, R. I. 1996. Rotating crack FE model for reinforced concrete structures, *Computers & Structures* 58(1): 43–50.

Foster, S. J.; Marti, P. 2003. Cracked membrane model: Finite element implementation, *ASCE Journal of Structural Engineering* 129(9): 1155–1163.

Furushima, M.; Suzuki, K.; Ohno, Y.; Nakagawa, T. 1993. Resistance to drying shrinkage of concrete with high early strength cement and AE super-plasticizer, *Proceedings of Japan Concrete Institute* 15(1): 751–756 (in Japanese).

Gardner, N. J. 2004. Comparison of prediction provisions for drying shrinkage and creep of normal strength concretes, *Canadian Journal for Civil Engineering* 31(5): 767–775.

Gardner, N. J.; Lockman, M. J. 2001. Design provisions for drying shrinkage and creep of normal strength concrete, *ACI Materials Journal* 98(2): 159–167.

Ghali, A.; El-Badry, M. M. 1987. Cracking of composite prestressed concrete sections, *Canadian Journal of Civil Engineering* 14(3): 314–319.

Ghali, A.; Favre, R. 1986. *Concrete Structures: Stresses and Deformations*. London: Chapman and Hall. 352 p.

Gilbert, R. I. 1988. *Time Effects in Concrete Structures*. Amsterdam: Elsevier. 336 p.

Gilbert, R. I. 1999. Deflection calculation for RC structures – Why we sometimes get it wrong, *ACI Structural Journal* 96(6): 1027–1032.

Gilbert, R. I. 2001. Shrinkage, cracking and deflection – the serviceability of concrete structures, *Electronic Journal of Structural Engineering* 1: 15–37.

Gilbert, R. I. 2006. Tension stiffening in lightly reinforced concrete elements containing either steel or FRP reinforcement, in *Proc of 19th Australasian Conf. on the Mechanics of Structures and Materials*, Christchurch, New Zealand, 2006, 659–665.

Gilbert, R.I. 2007. Tension stiffening in lightly reinforced concrete slabs, *ASCE Journal of Structural Engineering* 133(6): 899–903.

Gilbert, R. I.; Warner, R. F. 1978. Tension stiffening in reinforced concrete slabs, *Journal of the Structural Division* 104(12): 1885–1900.

Giuriani, E.; Plizzari, G.; Schumm, C. 1991. Role of stirrups and residual tensile strength of cracker concrete on bond, *ASCE Journal of Structural Engineering* 124(9): 1032–1040.

Gohnert, M.; Xue, P. Y. 2000. A theoretical refinement of Branson's effective-moment-of-inertia equation, *Magazine of Concrete Research* 52(1): 39–42.

Gonnerman, H. F.; Shuman, E. C. 1928. Compression, flexure and tension tests of plain concrete, *Proceedings of American Society of Testing Materials* 28(2): 527–552.

Goto, Y. 1971. Cracks formed in concrete around deformed tension bars, *ACI Journal Proceedings* 68(4): 244–251.

Grassl, P.; Jirásek, M. 2005. Plastic model with non-local damage applied to concrete, *International Journal for Numerical and Analytical Methods in Geomechanics* 30(1): 71–90.

Griffin, M. L.; Kahn, F. K.; Lopez, M. 2004. Deck contraction induced deflection in a high performance concrete bridge, in *Proc. of the National Concrete Bridge Conference*, Atlanta. 30 p.

Guénot-Delahaie, I. 1997. *Contribution to Physical Analysis and Modelling of Concrete Basic Creep* (*Contribution à l'Analyse Physique et à la Modélisation du Fluage Propre du Béton*). *Research Report LPC, OA25*. Paris: LCPC. 180 p. (in French).

Guo Z.; Zhang, X. 1987. Investigation of complete stress-deformation curves for concrete in tension, *ACI Material Journal* 84(4): 278–285.

Gupta, A. K.; Maestrini, S. R. 1990. Tension-stiffness model for reinforced concrete bars, *ASCE Journal of Structural Engineering* 116(3): 769–790.

Gushcha, Yu. P. 1967. *Investigation of Elastic-Plastic Behaviour of Flexural Concrete Beams Reinforced with Deformed Bars* (*Исследование изгибаемых железобетонных элементов при работе стержневой арматуры в упруго-пластической стадии*). PhD dissertation. Concrete and Reinforced Concrete Research and Technological Institute (NIIZhB), Moscow. 210 p. (in Russian).

Gvozdev, A. A.; Dmitrijev, S. A.; Nemirovskij, J. M. 1962. On deflection calculation of reinforced concrete structures according to new design code SNiP II-V.I-62 (О расчете прогибов железобетонных конструкций по проекту новых норм СНиП II-В.I-62), *Beton i Zelezobeton* 6: 245–250 (in Russian).

Hand, F. R.; Pecknold, D. A.; Schnobrich, W. C. 1973. Nonlinear layered analysis of RC plates and shells, *ASCE Journal of the Structural Division* 99(7): 1491–1505.

Hashida, H.; Yamazaki, N. 2002. Deformation composed of autogenous shrinkage and thermal expansion due to hydration of high-strength concrete and stress in reinforced

structures, in *Proc. of the 3rd International Research Seminar Self-Desiccation and Its Importance in Concrete Technology*, Lund, 2002, 77–92.

Hillerborg, A. 1983. Examples of practical results achieved by means of the fictitious crack model, in *Preprints of Prager Symposium on Mechanics of Geomaterials: Rocks, Concretes, Solids*, 611–614.

Hillerborg, A. 1985a. The theoretical basis of a method to determine the fracture energy G_F of concrete, *Material and Structures* (*RILEM*) 18(4): 291–296.

Hillerborg, A. 1985b. Results of three comparative test series for determining the fracture energy G_F of concrete, *Material and Structures* (*RILEM*) 18(5): 407–413.

Hillerborg, A.; Modéer, M.; Petersson, P.-E. 1976. Analysis of crack formation and crack growth in concrete by means of fracture mechanics and finite elements, *Cement and Concrete Research* 6(6): 773–782.

Hofstetter, G.; Mang, H. A. 1995. *Computational Mechanics of Reinforced Concrete Structures*. Wiesbaden: Friedr. Vieweg & Son. 366 p.

Hognestad, H. E. 1951. Study of combined bending and axial load in reinforced concrete members, *University of Illinois Bulletin* 49(22). 128 p.

Hognestad, H. E.; Hanson, N. W.; Mc Henry, D. 1955. Concrete stress distribution in ultimate strength design, *ACI Journal Proceedings* 52(12): 455–480.

Hordijk, D. A. 1991. *Local Approach to Fatigue of Concrete*. PhD dissertation. Delft University of Technology, Delft, The Netherlands. 210 p.

Howells, R. W.; Lark, R. J.; Barr, B. I. G. 2005. A sensitivity study of parameters used in shrinkage and creep prediction models, *Magazine of Concrete Research* 57(10): 589–602.

Hughes, B. P.; Chapman, G. P. 1966. The deformations of concrete and microconcrete in compression and tension with particular reference to aggregate size, *Magazine of Concrete Research* 18(54): 19–24.

Husain, S. I.; Ferguson, P.M. 1968. *Flexural Crack Width at the Bars in Reinforced Concrete Beams. Research Report* 102-1F, Centre for Highway Research. 35 p.

Jiang, D. H.; Shah, S. P.; Andonian, A. T. 1984. Study of the transfer of tensile forces by bond, *ACI Structural Journal* 81(3): 251–259.

Joly de, G. 1898a. *Experimental Investigation on the Resistance and the Elasticity of Portland Cements* (*Expériences faites par le service des phares et balises sur la résistance et l'élasticité des ciments Portland*). 52 p. (in French).

Joly de, G. 1898b. Resistance of sealed Portland cement (Résistance des scellements exécutés au ciment Portland), *Annales des ponts et chaussés* 2: 221–242 (in French).

Kaklauskas, G. 2001. *Integral Flexural Constitutive Model for Deformational Analysis of Concrete Structures*. Vilnius: Technika. 140 p.

Kaklauskas, G. 2004. Flexural layered deformational model of reinforced concrete members, *Magazine of Concrete Research* 56(10): 575–584.

Kaklauskas, G.; Christiansen, M. B.; Bacinskas, D.; Gribniak, V. 2008. *Deformation Model of Reinforced Concrete Members Taking into Consideration Shrinkage and Creep Effects at the Pre-Loading Stage* (*Gelžbetoninių elementų deformacijų modelis, įvertinantis betono susitraukimą ir valkšnumą ikieksploatacinėje stadijoje*). *Final Report* No. T-1025/08. Vilnius Gediminas Technical University, Vilnius, Lithuania. 47 p. (in Lithuanian).

Kaklauskas, G.; Ghaboussi, J. 2001. Stress-strain relations for cracked tensile concrete from RC beam tests, *ASCE Journal of Structural Engineering* 127(1): 64–73.

Kankam, C. K. 1997. Relationship of bond stress, steel stress, and slip in reinforced concrete, *ASCE Journal of Structural Engineering* 123(1): 79–85.

Kaplan, M. F. 1961. Crack propagation and the fracture of concrete, *ACI Journal Proceedings* 58(11): 591–610.

Karihaloo, B. L. 1995. *Fracture Mechanics and Structural Concrete*. Essex: Longman Scientific & Technical. 330 p.

Kaufmann, W. 1998. *Strength and Deformations of Structural Concrete Subjected to In-Plane Shear and Normal Forces*. PhD dissertation. Institute of Structural Engineering, Swiss Federal Institute of Technology, Zurich. 155 p.

Kawahara, T.; Murano, G.; Sakakibara, I. 1964. *Research on Slag Cement Made by Wet Smashing Method. Report* No. 64042. Central Research Institute of Electric Power Industry. 77 p. (in Japanese).

Kawasumi, M.; Seki, S.; Kasahara, K.; Kuriyama, T. 1973. *Creep of Concrete at Elevated Temperatures. Report* No.72018. Central Research Institute of Electric Power Industry. 83 p. (in Japanese).

Kent, D. C.; Park, R. 1971. Flexural members with confined concrete, *ASCE Journal of the Structural Division* 97(7): 1969–1990.

Kesler, C. E.; Naus, D. J.; Lott, J. L. 1972. Fracture mechanics – its applicability to concrete, in *Proc. of the International Conference on the Mechanical Behavior of Materials,* Kyoto, 1971, IV: 113–124.

Kim, J.-K.; Lee, C.-S. 1998. Prediction of differential drying shrinkage in concrete, *Cement and Concrete Research* 28(7): 985–994.

Kolmar, W. 1986. *An Approach of the Force Transfer throughout Cracks by the Nonlinear Finite Element Analysis of the Reinforced Concrete Items*. PhD dissertation. Darmstadt: T. H. 94 p. (in German).

Kovler, K. 1995. Interdependence of creep and shrinkage for concrete under tension, *ACI Materials Journal* 7(2): 96–101.

Kudzys, A.; Kvedaras, A. K.; Kliukas, R. 2004. Methodological approaches on structural durability assessment, in *Proc. of the Seventh International Conference on Probabilistic Safety Assessment and Management,* Berlin, 2004, 4: 2167–2173.

Kwak, H.-G.; Filippou, F. 1995. A new reinforcing steel model with bond slip, *Structural Engineering & Mechanics* 3(4): 299–312.

Kwak, H.-G.; Song, J.-Y. 2002. Cracking analysis of RC members using polynomial strain distribution function, *Engineering Structures* 24(4): 455–468.

Lackner, R.; Mang, H. A. 2003. Scale transition in steel-concrete interaction. Part I: Model, *ASCE Journal of Engineering Mechanics* 129(4): 393–402.

Larson, M. G. 2008. Analysis of variance, *Circulation* 117(1): 115–121.

Lash, S. D. 1953. Ultimate strength and cracking resistance of lightly reinforced beams, *ACI Journal Proceedings* 49(2): 573–582.

Lee, H. K.; Lee, K. M.; Kim, B. G. 2003. Autogenous shrinkage of high-performance concrete containing fly ash, *Magazine of Concrete Research* 55(6): 507–515.

Lemnitzer, L.; Eckfeldt, L.; Lindorf, A.; Curbach, M. 2008. Biaxial tensile strength of concrete – answers from statistics, in *Proc. of the International fib Symposium Tailor Made Concrete Structures: New Solutions for Our Society*, Amsterdam, The Nederland, 2008. UK: CRC Press/Balkema, 1101–1102.

Leonhardt, F. 1977. Crack control in concrete structures, *IABSE Surveys* S-4/77: 1–26.

Leutbecher, T.; Fehling, E. 2009. Crack formation and tensile behaviour of concrete members reinforced with rebars and fibres exemplified by ultra-high-performance concrete Part 1: Crack mechanical relationships, *Beton und Stahlbetonbau* 104(6): 357–367 (in German).

L'Hermite, R. 1955. *Idées Actuelles sur la Technologie du Béton, Documentation Technique du BTP*. *Collection de l'ITBTP*. 242 p. (In French).

Li, Y.-J.; Zimmerman, Tt. 1998. Numerical evaluation of the rotating crack model, *Computers & Structures* 69(4): 487–497.

Liebenberg, A. C. 1962. A stress strain function for concrete subjected to short-term loading, *Magazine of Concrete Research* 14(41): 85–90.

Lin, C. S.; Scordelis, A. C. 1975. Nonlinear analysis of RC shells of general form, *Journal of Structural Engineering* 101(3): 523–538.

Liu, Y.; Ohno, Y.; Nakagawa, T. 2001. Calculation of shrinkage crack width estimation of concrete, in *Materials and Construction, Summaries of Technical Papers of Annual Meeting Architectural Institute of Japan*, 437–438 (in Japanese).

Liu, Y.; Teng, S.; Soh, C. K. 2008. Three-dimensional damage model for concrete. Part I: Theory, *ASCE Journal of Engineering Mechanics* 134(1): 72–81.

Maekawa, K.; Pimanmas, A.; Okamura, H. 2003. *Nonlinear Mechanics of Reinforced Concrete*. London: Taylor & Francis Group. 721 p.

Manfredi, G.; Pecce, M. 1998. A refined RC beam element including bond-slip relationship for the analysis of continuous beams, *Computers & Structures* 69(1): 53–62.

Mansur, M. A.; Chin, M. S.; Wee, T. H. 1997. Flexural behavior of high-strength concrete beams, *ACI Structural Journal* 94(6): 663–674.

Mardia, K. V.; Zemroch, P. J. 1978. *Tables of the F- and Related Distributions with Algorithms*. New York: Academic Press. 256 p.

Markeset, G. 1993. Size effect on stress-strain relationship of concrete in compression, in *Proc. of the Third International Symposium on Utilization of High Strength Concrete, Lillehammer*, 2:1146-1153.

Meyerson, R.; Weyers, R. E.; Via, C. E.; Mokarem, D. W., Lane, D. S. 2002. *Evaluation of Models for Predicting (Total) Creep of Prestressed Concrete Mixtures*. Final Contract Report VTRC 03-CR5. Virginia: TRC. 55 p.

Mier van, J. G. M. 1991. Mode I fracture of concrete: discontinuous crack growth and crack interface grain bridging, *Cement and Concrete Research* 21(1): 1–15.

Mier van, J. G. M.; Vervuut, A. 1995. Micronechanical analisis and experimental verification of boundary rotation effects in iniaxial tension tests on concrete, in *Fracture of Brittle Disordered Materials: Concrete, Rock and Ceramics*. London: E & FN Spon, 406–420.

Miller, R.; Mirmiran, A.; Ganesh, P.; Sappro, M. 2006. *Transverse Cracking of High Performance Concrete Bridge Decks After One Season or Six to Eight Months. Final Report* FHWA/OH-2006/6. Columbus: Ohio Department of Transportation. 108 p.

Milovanov, A. F.; Kambarov, H. U. 1994. *Design of Reinforced Concrete Structures Subjected to Thermal Loading* (*Расчёт железобетонных конструкций на воздействие температуры*). Tashkent: Ukituvchi. 360 p. (In Russian).

Mirza, S. M.; Houde, J. 1979. Study of bond stress-slip relationships in reinforced concrete, *ACI Journal Proceedings* 76(1): 19–46.

Mokarem, D. W. 2002. *Development of Concrete Shrinkage Performance Specifications*. PhD dissertation. Virginia Polytechnic Institute. 236 p.

Monti, G.; Spacone, E. 2000. Reinforced concrete fiber beam element with bond-slip, *ASCE Journal of Structural Engineering* 126(6): 654–661.

Mosegaard, K.; Tarantola, K. 1995. Monte Carlo sampling of solution to inverse problems, *Journal of Geophysical Research* 100(B7): 12431–12447.

Murao, M. 1997. A study on reducing shrinkage of highly-flowable concrete. Part 4: Properties of crack-resistant highly-flowable concrete, in *Materials and Construction, Summaries of Technical Papers of Annual Meeting Architectural Institute of Japan*, 241–242 (in Japanese).

Murashev, V. I. 1950. *Crack Resistance, Stiffness and Strength of Reinforced Concrete* (*Трещиноустойчивость, жёсткость и прочность железобетона*). Moscow: Mashinostroiizdat. 268 p. (in Russian)

Nakato, T.; Ishikura, T.; Sukekiyo, M.; Tateyashiki, H.; Shima, H. 2000. Development of production technique on high quality recyclable aggregates. Part 3: Basic properties of concrete with recycled aggregate produced by whole heating and grinding method, in *Materials and Construction, Summaries of Technical Papers of Annual Meeting Architectural Institute of Japan*, 1063–1064 (in Japanese).

Nejadi, S. 2005. *Time-Dependent Cracking and Crack Control in Reinforced Concrete Structures*. PhD dissertation. University of New South Wales. 390 p.

Nemirovskij, J. M.; Kochetkov, O. I. 1969. Effect of behaviour of tensile and compressive concrete on deformations of cracked reinforced concrete flexural members, in *Peculiarities of Deformations of Concrete and Reinforced Concrete and the Use of Computers for Assessing Their Influence on the Behaviour of Structures*. Moscow: Stroiizdat, 106–156 (in Russian).

Ngo, D.; Scordelis, A. C. 1967. Finite element analysis of reinforced concrete beams, *ACI Journal Proceedings* 64(3): 152–163.

NIIZhB (Concrete and Reinforced Concrete Research and Technology Institute). 2006. *Concrete and Reinforced Concrete Structures without Pre-Stressing, SP 52-101-2003*. Moscow: NIIZhB. 53 p. (in Russian).

Nilson, A. H. 1972. Internal measurement of bond slip, *ACI Journal Proceedings* 69(7): 439–441.

Ozaki, H.; Tuchida, S.; Kono, M. 2001. The durability examination of precast centrifugal compaction, in *Materials and Construction, Summaries of Technical Papers of Annual Meeting Architectural Institute of Japan*, 331–332 (in Japanese).

Ozbolt, J.; Reinhardt, H. W. 2002. Numerical study of mixed-mode fracture in concrete, *International Journal of Fracture* 118(2): 145–161.

Park, R.; Paulay, T. 1975. *Reinforced Concrete Structures*. London: John Wiley & Sons Ltd. 800 p.

Peiretti, H. C.; Caldentey, A. P.; Bernat, A. M. 1991. Time-dependent behavior of prestressed concrete structures – Theoretical model and experimental results, in *Proc. of the International Symposium on Modern Applications of Prestressed Concrete,* Beijing, 1991, 2: B148–B155.

Persson, B. 1998. Experimental studies on shrinkage of high-performance concrete, *Cement and Concrete Research* 28(7): 1023–1036.

Persson, B. 2001. *Validation of Fédération International du Béton, FIB, 2000 Shrinkage Model for Normal and High-Performance Concrete. Report* TVBM-7157. Lund: Lund Institute of Technology. 108 p.

Petersson, P. E. 1981. *Crack Growth and Development of Fracture Zone in Plain Concrete and Similar Materials. Report* TVBM-1006. Lund: Lund Institute of Technology. 174 p.

Philips, D. V.; Binsheng, Z. 1993. Direct tension tests on notched and unnotched plain concrete specimens, *Magazine of Concrete Research* 45(162): 25–35.

Pickett, G. 1942. The effect of change in moisture-content on the creep of concrete under a sustained load, *ACI Journal Proceedings* 38: 333–356.

Piyasena, R. 2002. *Crack Spacing, Crack Width and Tension Stiffening Effect in Reinforced Concrete Beams and One-Way Slabs*. PhD Dissertation. School of Engineering, Griffith University. 370 p.

Planas, J.; Elices, M. 1986. Towards a measure of G_F: An analysis of experimental results, in *Fracture Toughness and Fracture Energy of Concrete*. Amsterdam: Elsevier, 381–390.

Polak, M. A.; Blackwell, K. G. 1998. Modeling tension in reinforced concrete members subjected to bending and axial load, *ASCE Journal of Structural Engineering* 124(9): 1018–1024.

Pollard, J. H. 1979. *A Handbook of Numerical and Statistical Techniques*. Cambridge: CUP Archive. 368 p.

Popovics, S. 1970. A review of stress-strain relationships for concrete, *ACI Journal Proceedings* 67(3): 243–248.

Popovics, S. 1973. A numerical approach to the complete stress-strain curves for concrete, *Cement and Concrete Research* 3(5): 583–599.

Powers, T. C. 1965. Mechanisms of shrinkage and reversible creep of hardened cement paste, in *Proc. of the International Symposium: The Structure of Concrete and Its Behaviour under Load*. Cement and Concrete Association, London, September 1965, 319–344.

Powers, T. C. 1968. The thermodynamics of volume change and creep, *Materials and Structures* (*RILEM*) 1(6), 487–507.

Prakhya, G. K. V.; Morley, C. T. 1990. Tension-stiffening and moment-curvature relations of reinforced concrete elements, *ACI Structural Journal* 87(5): 597–605.

Rashid, Y. R. 1968. Ultimate strength analysis of prestressed concrete pressure vessels, *Nuclear Engineering and Design* 7(4): 334–344.

Raudys, S.; Young, D. M. 2004. Results in statistical discriminant analysis: a review of the former Soviet Union literature, *Journal of Multivariate Analysis* 89(1): 1–35.

Reinhardt, H. W.; Rinder, T. 2006. Tensile creep of high-strength concrete, *Journal of Advanced Concrete Technology* 4(2): 277–283.

Robert-Nicoud, Y.; Raphael, B.; Burdet, O.; Smith, I. F. C. 2005. Model identification of bridges using measurement data, *Computer-Aided Civil and Infrastructure Engineering* 20(2): 118–131.

Ros, M. 1950. *Material-technological foundation and problems in reinforced concrete* (*Die materialtechnischen Grundlagen und Probleme des Eisenbetons im Hinblick auf die zukünftige Gestaltung der Stahlbeton-Bauweise*). *EMPA-Bericht* 162. 305 p. (in German).

Rots, J. G. 1988. *Computational Modeling of Concrete Structures*. PhD dissertation. Delft University of Technology, Delft, The Netherlands. 127 p.

Roy, H. E. H.; Sozen, M. A. 1963. *A Model to Simulate the Response of Concrete to Multi-Axial Loading. Structural Research Series* 268, University of Illinois. 227 p.

Ruetz, W. 1966. *Creep of Cement in Concrete and the Influence on it by Simultaneous Shrinkage* (*Das Kriechen des Zementsteins im Beton und seine Beeinflussung durch gleichzeitiges Schwinden*). *Deutsche Ausschuss für Stahlbeton Heft* 183. Berlin: Wilhelm Ernst & Sohn. 51 p. (in German).

Ruetz, W. 1968. A hypothesis for the creep of hardened cement paste and the influence of simultaneous shrinkage, in *Proc. of International Conference on the Structure of Concrete*. London: Cement and Concrete Association, 365–387.

Ruiz, M. F.; Mattoni, A.; Gambarova, P. G. 2007. Analytical modeling of the pre- and postyield behavior of bond in reinforced concrete, *ASCE Journal of Structural Engineering* 133(10): 1364–1372.

Rüsch, H.; Hilsdorf, H. 1963. *Deformation Characteristics of Concrete under Centric Tension* (*Verformungseigenschaften von Beton unter zentrischen Zugspannungen*). *EMPA-Bericht* 44. 157 p. (in German)

Saenz, L. P. 1964. Discussion of "Equation for the stress strain curve of concrete" by P. Desayi and S. Krishnan, *ACI Journal Proceedings* 61(9): 1229–1235.

Sakata, K.; Ayano, T.; Imamoto, K.; Sato, Y. 2009. Database of creep and shrinkage based on Japanese researches, in *Proc. of 8th International Conference Creep, Shrinkage and Durability of Concrete and Concrete Structures (ConCreep 8), Ise-Shima, Japan,* 2008. Taylor & Francis, 2: 1253–1274.

Sakata, K.; Shimomura, T. 2004. Recent progress in research on and evaluation of concrete creep and shrinkage in Japan, *Journal of Advanced Concrete Technology* 2(2): 133–140.

Saliger, R. 1936. High-grade steel in reinforced concrete, in *Proc. of Second Congress of the International Association for Bridge and Structural Engineering* (*IABSE*), Berlin-Munich, 1936, 293–315.

Samiuddin, M.; Atiqullah, M. 1976. A test for equality of variance, *Biometrika* 63(1): 206–208.

Samiuddin, M.; Hanif, M.; Asad, H. 1978. Some comparisons of the Bartlett and cube root tests of homogeneity of variance, *Biometrika* 65(1): 218–221.

Sato, R.; Tanaka, S.; Hayakawa, T.; Tanimura, M. 1999. Experimental studies on reduction of autogenous shrinkage and its induced stress in high-strength concrete, in *Proc. of Second International Research Seminar Self-Desiccation and Its Importance in Concrete Technology*, *Lund University Report* TVBM-3085, 163–171.

Sato, R.; Maruyama, I.; Sogabe, T.; Sogo, M. 2007. Flexural behavior of reinforced recycled concrete beams, *Journal of Advanced Concrete Technology* 5(1): 43–61.

Sato, Y.; Tadokoro, T.; Ueda, T. 2004. Diagonal tensile failure mechanism of reinforced concrete beams, *Journal of Advanced Concrete Technology* 2(3): 327–341.

Scanlon, A.; Bischoff, P. H. 2008. Shrinkage restraint and loading history effects on deflections of flexural members, *ACI Structural Journal* 105(4): 498–506.

Scheffé, H. 1959. *The Analysis of Variance*. John Wiley. Wiley Classic. 477 p.

Schellenberg, K.; Vogel, T.; Fu, C. C.; Wang, S. 2005. Comparison of European and US practices concerning creep and shrinkage, in *Proc. of the fib Symposium Structural Concrete and Time*, La Plata, 2005, 445–452.

Scott, R. H.; Beeby, A. W. 2005. Long-term tension-stiffening effects in concrete, *ACI Structural Journal* 102(1): 31–39.

Shah, S. P.; Ahmad, S. H. 1985. Structural properties of high strength concrete and its implication for precast prestressed concrete, *PCI Journal* 30(4–6): 92–119.

Sigrist, V. 1995. *On the Deformation Capacity of Structural Concrete Girders* (*Zum Verformungsvermögen von Stahlbetonträgern*). *IBK Bericht* 210, 159 p. (in German).

Silliman, K. R.; Newtson, C. 2006. Effect of misting rate on concrete shrinkage, in *Proc. of HPC: Build Fast, Build to Last – 2006 Concrete Bridge Conference,* Reno, Nevada*,* 2005. PCA (CD). 19 p.

Siviero, E.; Simoncelli, B. 1997. Early experimental investigations to establish the tensile strength of concrete, *Concrete Tension and Size Effect – CEB Bulletin* 237: 17–36.

Sjoberg, B. D. 1999. *Crack Width in Reinforced Concrete*. MSc thesis. The University of Calgary. 199 p.

Smith, G.; Young, L. E. 1956. Ultimate flexural analysis based on stress-strain curves of cylinders, *ACI Journal Proceedings* 53(12): 597–609.

Somayaji, S.; Shah, S. P. 1981. Bond stress versus slip relationships and cracking response of tension members, *ACI Journal Proceedings* 78(3): 217–225.

Soong, T. T. 2004. *Fundamentals of Probability and Statistics for Engineers*. Chichester: John Wiley & Sons. 391 p.

Stephens, M. A. 1974. EDF statistics for goodness-to-fit and some comparisons, *Journal of the American Statistical Association* (*JASA*) 69(374): 730–737.

Stramandinoli, R. S. B.; Rovere, H. L. L. 2008. An efficient tension-stiffening model for nonlinear analysis of reinforced concrete members, *Engineering Structures* 30(7): 2069–2080.

Suidan, M.; Schnobrich, W. C. 1973. Finite element analysis of reinforced concrete, *ASCE Journal of the Structural Division* 99(10): 2109–2122.

Sule, M. S.; Breugel van K. 2004. Effect of reinforcement on early-age cracking in high strength concrete, *Heron* 49(3): 273–292.

Swaddiwudhipong, S.; Lu, H. R.; Wee, T. H. 2003. Tensile strain capacity of concrete under various states of stress, *Cement and Concrete Research* 33(12): 2077–2084.

Szulczynski, T.; Sozen, M. A. 1961. *Load-Deformation Characteristics of Reinforced Concrete Prisms with Rectilinear Transverse Reinforcement*. *Structural Research Series* 224, University of Illinois. 41 p.

Takafumi, T.; Akio, K.; Masafumi, K.; Junya, M. 2003. Study on drying shrinkage cracking tendency of recycled aggregate concrete. Part 2: Unixial restraint cracking test, in *Materials and Construction, Summaries of Technical Papers of Annual Meeting Architectural Institute of Japan*, 247–248 (in Japanese).

Takács, P. F. 2002. *Deformations in Concrete Cantilevel Bridges: Observations and Theoretical Modelling*. PhD dissertation. Trondheim: The Norwegian Univercity of Science and Technology. 205 p.

Takemura, K.; Yonekura, A.; Tanaka, T. 1987. Shrinkage of concrete with silica fume, *Proceedings of the Japan Concrete Institute* 9: 69–74 (in Japanese).

Tamtsia, B. T.; Beaudoin J. J. 2000. Basic creep of hardened cement paste: A reexamination of the role of water, *Cement and Concrete Research* 30(9): 1465–1475.

Tanimura, M.; Hyodo, H.; Nakamura, H.; Sato, R. 2002. Effectiveness of expansive additive on reduction of autogrnous shrinkage stress in high-strength concrete, in *Proc. of the Third International Research Seminar Self-Desiccation and Its Importance in Concrete Technology,* Lund, 2002, 205–216.

Tanimura, M.; Suzuki, M.; Maruyama, I.; Sato, R. 2005. Improvement of time-dependent flexural behavior in RC members by using low shrinkage-high strength concrete, in *Proc. of the Seventh International Symposium on the Utilization of High-Strength/High-Performance Concrete, ACI Special Publications* 228: 1373-1396.

Tanimura, M.; Sato, R.; Hiramatsu, Y. 2007. Serviceability performance evaluation of RC flexural members improved by using low-shrinkage high-strength concrete, *Journal of Advanced Concrete Technology* 5(2): 149–160.

Tarantola, A. 2005. *Inverse Problem Theory and Methods for Model Parameter Estimation*. Philadelphia: Society for Industrial and Applied Mathematics (SIAM). 357 p.

Thelandersson, S.; Mårtensson, A.; Dahlblom, O. 1988. Tension softening and cracking in drying concrete, *Materials and Structures* (*RILEM*) 21(126): 416–424.

Tomita, R. 1994. *Study on Mechanism and Effect of Organic Shrinkage Reducing Admixture*. PhD dissertation. Tokyo Institute of Technology. 157 p. (in Japanese).

Tomosawa, F.; Noguchi, T.; Park, Q. B.; Sano, H.; Yamazaki, N.; Hashida, H.; Kuroda, Y. 1997. Experimental determination and analysis of stress and strain distribution of reinforced high strength concrete column caused by self-desiccation and heat of hydration, in *Proc. of the First International Research Seminar Self-Desiccation and Its Importance in Concrete Technology*, *Lund University Report* TVBM-3075, 174–192.

Tongaroonsri, S.; Tangtermsirikul, S. 2009. Effect of mineral admixtures and curing periods on shrinkage and cracking age under restrained condition, *Construction and Building Materials* 23(2): 1050–1056.

Townsend, B. D. 2003. *Creep and Shrinkage of a High Strength Concrete Mixture*. MSc thesis. Virginia Polytechnic Institute. 130 p.

TRB (Transportation Research Board). 2006. *Control of Cracking in Concrete State of the Art. Transportation Research Circular* E-C107. TRB. 56 p.

Tremper, B. 1961. Factors influencing drying shrinkage of concrete, in *Proc. of Meeting of Structural Engineers Association of Northern California*, San Francisco, 1961. 5 p.

Tritsch, N.; Darwin, D.; Browning, J. 2005. *Evaluating Shrinkage and Cracking Behavior of Concrete Using Restrained Ring and Free Shrinkage Tests. SM Report* No. 77. Lawrence: The University of Kansas Center for Research, Inc. 197 p.

Ulickij, I. I.; Jhun-Yao, J.; Golyshev, A. B. 1960. *Design of Reinforced Concrete Structures Taking into Consideration Long-Term Effects* (*Расчёт железобетонных конструкций с учётом длительных процессов*). Kiev: Building and Architecture Ukrainian Republic Press. 496 p. (in Russian).

Ulm, F.-J.; Maou Le, F.; Boulay, C. 1999. Creep and shrinkage couplings: New review of some evidence, *Revue Française de Génie Civil* 3(3–4): 21–37.

Umezu, Y.; Shimizu, A.; Hamada, M.; Sinoda, T.; Fukushi, I. 2003. Experimental study on a test method for judging of recycled aggregate performance, Part 2: Experiment result, in *Materials and Construction, Summaries of Technical Papers of Annual Meeting Architectural Institute of Japan*, 235–234 (in Japanese).

Umezu, Y.; Shimizu, A.; Kuroha, K.; Takada, M. 2001. Experimental study on strength development of high fluidity fly ash concrete in structures, Part 4: Influence of different weather, in *Materials and Construction, Summaries of Technical Papers of Annual Meeting Architectural Institute of Japan*, 139–140 (in Japanese).

Vecchio, F. J.; Collins, M. P. 1986. The Modified Compression Field Theory for reinforced concrete elements subjected to shear, *ACI Structural Journal* 83 (6): 925–933.

Verzhbitsky, V. M. 2005. *Foundations of Numerical Methods* (*Основы численных методов*). Moscow: Vysshaya Shkola. 840 p. (in Russian).

Vítek, J. L.; Křístek, V.; Kohoutkova, A. 2004. Time development of deflections of large prestressed concrete bridges, in *Proc. of the fib Symposium Segmental Construction in Concrete*, New Delhi, 2004, 177–179.

Vollum, R. L.; Afshar, N.; Izzuddin, B. A. 2008. Modelling short-term tension stiffening in tension members, *Magazine of Concrete Research* 60(4): 291–300.

Walsh, P. F. 1972. Fracture of plain concrete, *The Indian Concrete Journal* 46(11): 469–470, 476.

Walsh, P. F. 1976. Crack initiation in plain concrete, *Magazine of Concrete Research* 28(94): 37–41.

Wang, P. T.; Shah, S. P.; Naaman, A. E. 1978. Stress-strain curves of normal and lightweight concrete in compression, *ACI Journal Proceedings* 75(11): 603–611.

Wang. E. Z.; Shrive, N. G. 1995. Brittle fracture in compression: mechanisms, models and criteria, *Engineering Fracture Mechanics* 52(6): 1107–1126.

Warner, R. F.; Rangan, B. V.; Hall, A. S.; Faulkes, K. A. 1998. *Concrete Structures*. South Melbourne: Addison Wesley Longman Ltd. 974 p.

Wee, T. H.; Lu, H. R.; Swaddiwudhipong, S. 2000. Tensile strain capacity of concrete under various states of stress, *Magazine of Concrete Research* 52(3): 185–193.

Weiss, W. J. 1999. *Prediction of Early-Age Shrinkage Cracking in Concrete*. PhD dissertation. Northwestern University, Evanston. 277 p.

Weiss, W. J.; Yang, W.; Shah, S. P. 1999. Factors influencing durability and early-age cracking in high strength concrete structures, *High Performance Concrete: Research to Practice*. *ACI Special Publication* 186: 387–409.

Wittmann, F. H. 1982. Creep and shrinkage mechanisms, in *Creep and Shrinkage of Concrete Structures*. New York: Wiley. 129–161

Wittmann, F. H. 1993. On the influence of stress on shrinkage of concrete, in *Proc. of Fifth International RILEM Symposium Creep and Shrinkage of Concrete*. New York: E & FN Spon, 151–157.

Wittmann, F. H. 2002. Crack formation and fracture energy of normal and high strength concrete, *Sādhanā* 27(4): 413–423.

Wittmann, F. H.; Roelfstra, P. E. 1980. Total deformation of loaded drying concrete, *Cement and Concrete Research* 10(5): 601–610.

Wu, H. Q.; Gilbert, R. I. 2008. *An Experimental Study of Tension Stiffening in Reinforced Concrete Members under Short-Term and Long-Term Loads. UNICIV Report* No. R-449. Sydney: The University of South Wales. 32 p.

Yamamoto, T.; Vecchio, F. J. 2001. Analysis of reinforced concrete shells for transverse shear and torsion, *ACI Structural Journal* 98(2): 191–200.

Young, L. E. 1960. Simplifying ultimate flexural theory by maximizing the moment of the stress block, *ACI Journal Proceedings* 57(11): 549–556.

Zheng, W.; Kwan, A. K. H.; Lee, P. K. K. 2001. Direct tension test of concrete, *ACI Material Journal* 98(1): 63–71.

List of Publications by the Author on the Topic of the Dissertation

Papers in the Reviewed Scientific Journals

Dulinskas, E.; Gribniak, V.; Kaklauskas, G. 2008. Influence of steam curing on high-cyclic behaviour of prestressed concrete bridge elements, *The Baltic Journal of Road and Bridge Engineering* 3(3): 115–120. ISSN 1822-427X (print), ISSN 1822-4288 (online).

Gribniak, V.; Bacinskas, D.; Kaklauskas, G. 2006. Numerical simulation strategy of bearing reinforced concrete tunnel members in fire, *The Baltic Journal of Road and Bridge Engineering* 1(1): 5–9. ISSN 1822-427X (print), ISSN 1822-4288 (online).

Gribniak, V.; Kaklauskas, G.; Bacinskas, D. 2008. Shrinkage in reinforced concrete structures: A computational aspect, *Journal of Civil Engineering and Management* 14(1): 49–60. ISSN 1392-3730 (print), ISSN 1822-3605 (online).

Gribniak, V.; Kaklauskas, G.; Bacinskas, D. 2007a. State-of-art review on shrinkage effect on cracking and deformations of concrete bridge elements, *The Baltic Journal of Road and Bridge Engineering* 2(4): 183–193. ISSN 1822-427X (print), ISSN 1822-4288 (online).

Kaklauskas, G.; Bacinskas, D.; Gribniak, V.; Geda, E. 2007a. Mechanical simulation of reinforced concrete slabs subjected to fire, *Technological and Economic Development of*

Economy 13(4): 295–302 (in Lithuanian). ISSN 1392-8619 (print), ISSN 1822-3613 (online).

Kaklauskas, G.; Gribniak, V. 2005a. Accuracy of methods of calculating the deformations of RC beams, *Деформация и разрушение материалов* 5: 41–47 (in Russian). ISSN 1814-4632.

Kaklauskas, G.; Gribniak, V.; Bacinskas, D. 2008a. Discussion of "Effect of shrinkage on short-term deflection of reinforced concrete beams and slabs" by P. H. Bischoff and R. D. Johnson, *ACI Structural Journal* 105(4): 516–518. ISSN 0889-3241.

Kaklauskas, G.; Gribniak, V.; Bacinskas, D. 2008b. Discussion of "Tension stiffening in lightly reinforced concrete slabs" by R. I. Gilbert, *ASCE Journal of Structural Engineering* 134(7): 1261–1262. ISSN 0733-9445.

Kaklauskas, G.; Gribniak, V.; Bacinskas, D.; Vainiūnas, P. 2009. Shrinkage influence on tension stiffening in concrete members, *Engineering Structures* 31(6): 1305–1312. ISSN 0141-0296.

Kaklauskas, G.; Gribniak, V.; Christiansen, M. B. 2006a. The influence of shrinkage on behaviour of cracked reinforced concrete member work, *Известия ВУЗ. Строительство* 5: 106–111 (in Russian). ISSN 0536-1052.

Salys, D.; Kaklauskas, G.; Gribniak, V. 2009. Modelling deformation behaviour of RC beams attributing tension-stiffening to tensile reinforcement, *Engineering Structures and Technologies*, in press (in Lithuanian). ISSN 2029-2317 (print), ISSN 2029-2325 (online).

Other Papers

Bacinskas, D.; Kaklauskas, G.; Gribniak, V. 2008. Layered section analysis of RC slabs subjected to fire, in *Proc. of the International fib Conference Fire Design of Concrete Structures*. Coimbra: University of Coimbra, 311–318. ISBN 978-972-96524-2-4.

Bacinskas; D.; Gribniak, V.; Kaklauskas, G. 2009. Statistical analysis of long-term deflections of RC beams, in *Proc. of the Eighth International Conference Creep, Shrinkage and Durability of Concrete and Concrete Structures* (*ConCreep 8*), Ise-Shima, Japan, 2008. London: CRC Press/Balkema, Taylor & Francis Group, 1: 565–570. ISBN 978-0-415-47586-0.

Bacinskas, D.; Kaklauskas, G.; Gribniak, V.; Geda, E. 2007. Computationally effective tool for mechanical simulation of reinforced concrete members subjected to fire, in *Proc. of the Ninth International Conference Modern Building Materials, Structures and Techniques*. Vilnius: Technika, 2: 461–467. ISBN 978-9955-28-201-3.

Dulinskas, E.; Gribniak, V.; Kaklauskas, G. 2007. Influence of curing conditions on the fatigue strength and cyclic creep of compressive concrete, in *Proc. of the Ninth International Conference Modern Building Materials, Structures and Techniques*. Vilnius: Technika, 2: 517–522. ISBN 978-9955-28-201-3.

Girdžius, R.; Gribniak, V. 2005. Effect of shrinkage on tension stiffening in RC tensile members (Betono traukimosi įtaka tempiamųjų gelžbetoninių elementų deformacijoms),

in *Proc. of the Eighth Lithuanian Conference of Young Scientists Science – Future of Lithuania*. Vilnius: Technika, 177–180 (in Lithuanian). ISBN 9986-05-893-7.

Gribniak, V.; Bacinskas, D.; Kaklauskas, G. 2007b. Non-linear modelling of reinforced concrete beams subjected to fire, in *Proc. of the International COST-C26 Workshop Urban Habitat Constructions under Catastrophic Events*. Prague: Czech Technical University, 53–58. ISBN 978-80-01-03583-2.

Gribniak, V.; Bacinskas, D.; Kaklauskas, G. 2005. Numerical modelling of reinforced concrete beams under couple thermal and mechanical loading (Численное моделирование железобетонных балок, подверженных термомеханическому воздействию), in *Proc. of the Sixth International Conference Computational Modelling 2005*. St. Petersburg: Polytechnic University, 262–269 (in Russian). ISBN 5-7422-0925-8.

Gribniak, V.; Christiansen, M. B.; Kaklauskas, G. 2004. Comparative statistical deflection analysis of RC beams by FE software ATENA, design code methods and the Flexural model, in *Proc. of the Eighth International Conference Modern Building Materials, Structures and Techniques*. Vilnius: Technika, 462–469. ISBN 9986-05-757-4.

Gribniak, V.; Girdžius, R. 2005. Mesh dependence on deformations of tensile reinforced concrete members (Baigtinių elementų dydžio ir formos įtaka tempiamųjų G/B elementų deformacijų skaičiavimo rezultatams), in *Proc. of the Eighth Lithuanian Conference of Young Scientists Science – Future of Lithuania*. Vilnius: Technika, 181–186 (in Lithuanian). ISBN 9986-05-893-7.

Gribniak, V.; Kaklauskas, G. 2004. Statistical deflection analysis of RC Beams by different calculation methods, in *Proc. of the Seventh Lithuanian Conference of Young Scientists Science – Future of Lithuania*. Vilnius: Technika, 94–99. ISBN 9986-05-775-2.

Gribniak, V.; Kaklauskas, G.; Bacinskas, D. 2007c. Experimental investigation of deformations of lightly reinforced concrete beams, in *Proc. of the Ninth International Conference Modern Building Materials, Structures and Techniques*. Vilnius: Technika, 2: 554–562. ISBN 978-9955-28-201-3.

Gribniak, V.; Kaklauskas, G.; Bacinskas, D. 2009. Experimental investigation of shrinkage influence on tension stiffening of RC beams, in *Proc. of the Eighth International Conference Creep, Shrinkage and Durability of Concrete and Concrete Structures* (*ConCreep 8*), Ise-Shima, Japan, 2008. London: CRC Press/Balkema, Taylor & Francis Group, 1: 571–577. ISBN 978-0-415-47586-0.

Gribniak, V.; Kaklauskas, G.; Sokolov, A.; Logunov, A. 2007d. Finite element size effect on post-cracking behaviour of reinforced concrete members, in *Proc. of the Ninth International Conference Modern Building Materials, Structures and Techniques*. Vilnius: Technika, 2: 563–570. ISBN 978-9955-28-201-3.

Gribniak, V.; Kondratenko, D. 2005. Finite element size dependence on the deformations calculation of RC beams (Baigtinių elementų dydžio įtaka G/B sijų deformacijų skaičiavimo rezultatams), in *Proc of the Eighth Lithuanian Conference of Young Scientists Science – Future of Lithuania*. Vilnius: Technika, 187–194 (in Lithuanian). ISBN 9986-05-893-7.

Kaklauskas, G.; Burtzev, B. I.; Gribniak, V. 2007b. Derivation of material diagrams from tests of reinforced concrete beams, in *Proc. of the Eleventh International Scientific and Practical Conference of Students, Post-Graduates and Young Scientists Modern Techniques and Technologies* (*MTT 2005*). Piscataway: IEEE, 122–125. ISBN 0-7803-8877-1.

Kaklauskas, G.; Cervenka, V.; Cervenka, J.; Vainiunas, P.; Gribniak, V. 2004. Deflection calculation of RC beams: finite element software versus analytical and design code methods, in *Proc. of the Tenth International Conference on Computing in Civil and Building Engineering* (*ICCCBE-X*). Weimar: VDG, 8 p. (CD). ISBN 3-86068-213-X.

Kaklauskas, G.; Gribniak, V. 2005b. Effects of shrinkage on tension stiffening in RC members, in *Proc. of the fib Symposium Structural Concrete and Time*. La Plata: Grafikar Sociedad, 1: 453–460. ISBN 987-21660-1-3.

Kaklauskas, G.; Gribniak, V.; Bacinskas, D. 2006b. Effect of shrinkage on deformation of cracked reinforced concrete members (Betono susitraukimo įtaka supleišėjusių gelžbetoninių elementų deformacijoms), in *Proc. of the Lithuanian Conference Building Constructions: Design of Civil Engineering Constructions using Eurocode*. Vilnius: Technika, 113–121 (in Lithuanian). ISBN 9986-05-984-4.

Kaklauskas, G.; Gribniak, V.; Bacinskas, D. 2008c. Free of shrinkage tension stiffening relationships derived from RC beam tests, in *Proc. of the Sixth International Conference Analytical Models and New Concepts in Concrete and Masonry Structures* (*AMCM'2008*), Lodz, Poland, 2008, 8 p. (CD). ISBN 978-83-7283-263-4.

Kondratenko, D.; Gribniak, V. 2004. RC beam deflection calculation software based on layer model (Gelžbetoninių sijų įlinkių skaičiavimo programa, taikant sluoksnių modelį), in *Proc. of the Seventh Lithuanian Conference of Young Scientists Science – Future of Lithuania*. Vilnius: Technika, 118–122 (in Lithuanian). ISBN 9986-05-775-2.

Lopes, N.; Vila Real, P.; Uppfeldt, B.; Veljkovic, M.; Simões da Silva, L.; Franssen, J. M.; Bouchaïr, A.; Muzeau, J.-P.; Vassart, O.; Bacinskas, D.; Kaklauskas, G.; Gribniak, V.; Cvetkova, M.; Lazarov, L.; Nigro, E.; Cefarelli, G. 2008. Structural member behaviour and analysis in case of fire, in *Proc. of the International Symposium Urban Habitat Constructions under Catastrophic Events*, Valetta, Malta, 2008, 45–50. ISBN 978-999-09-44-40-2.

Mikūta, A.; Gribniak, V. 2006. Analysis of vehicle accidental impacts on bridge decks in Vilnius (Transporto priemonių atsitiktinių atsitrenkimų į viadukų perdangos konstrukciją Vilniaus mieste analizė), in *Proc. of the Ninth Lithuanian Conference of Young Scientists Science – Future of Lithuania*. Vilnius: Technika, 227–233 (in Lithuanian). ISBN 9955-28-047-6.

Pintea, D.; Zaharia, R.; Kaliske, M.; Kaklauskas, G.; Bacinskas, D.; Gribniak, V.; Török, A.; Hajpál, M. 2008. Mechanical properties of materials, in *Proc. of the International Symposium Urban Habitat Constructions under Catastrophic Events*, Valetta, Malta, 2008, 28–33. ISBN 978-999-09-44-40-2.

Annexes[1]

Annex A. Shrinkage and creep prediction techniques

Annex B. Computer code for derivation of *free-of-shrinkage* tension-stiffening relationships using *MATLAB*

Annex C. Measurements of curvature and deflection of the beam specimens

[1]The annexes are supplied in the enclosed compact disc

Viktor GRIBNIAK

SHRINKAGE INFLUENCE ON TENSION-STIFFENING OF CONCRETE STRUCTURES

Doctoral Dissertation

Technological Sciences,
Civil Engineering (02T)

Viktor GRIBNIAK

SUSITRAUKIMO ĮTAKA GELŽBETONINIŲ ELEMENTŲ TEMPIAMOSIOS ZONOS ELGSENAI

Daktaro disertacija

Technologijos mokslai,
statybos inžinerija (02T)

2009 07 27. 15,75 sp. l. Tiražas 20 egz.
Vilniaus Gedimino technikos universiteto
leidykla „Technika“,
Saulėtekio al. 11, 10223 Vilnius,
http://leidykla.vgtu.lt
Spausdino UAB „Biznio mašinų kompanija“,
J. Jasinskio g. 16A, 01112 Vilnius

Annex A. Shrinkage and Creep Prediction Techniques

A.1. *Eurocode 2*

Main equations presented here were published in the final draft of the *MC 90* (CEB-FIP 1991) and modified in the *fib Bulletin* (FIB 1999). The model is valid for normal density concrete exposed to a mean relative humidity in the range of 40 to 100% (CEN 2004).

A.1.1. Shrinkage

The shrinkage model represents a major change in respect to *MC 90*. The total shrinkage is subdivided into the autogenous shrinkage component $\varepsilon_{ca}(t)$ and the drying shrinkage component $\varepsilon_{cd}(t)$. With this approach, it was possible to formulate a model that is valid for both normal strength concrete and high performance concrete having compressive cylinder strength up to 90 MPa. The total shrinkage strain at time t is calculated as

$$\varepsilon_{cs} = \varepsilon_{ca}(t) + \varepsilon_{cd}(t) \tag{A.1}$$

with

$$\begin{aligned} \varepsilon_{ca}(t) &= \varepsilon_{ca}(\infty)\beta_{as}(t) = \left[-2,5\cdot 10^{-6}\left(f_{ck}-10\right)\right]\cdot\left[1-e^{-0,2\sqrt{t}}\right]; \\ \varepsilon_{cd}(t) &= \varepsilon_{cd,0}k_h\beta_{ds}(t,t_s) = \varepsilon_{cd,0}k_h(t-t_s)\left[t-t_s+0,04\sqrt{h_0^3}\right]^{-1}. \end{aligned} \tag{A.2}$$

Here $f_{ck} = f_{cm} - 8$ is the characteristic compressive cylinder strength of concrete [MPa]; t is the age of the concrete [days]; t_s is the age of the concrete at the beginning of drying shrinkage (normally, the end of curing) [days]; k_h is a coefficient depending on the notional size h_0 in mm according to Table A.1; $\varepsilon_{cd,0}$ is the basic drying shrinkage strain calculated from

$$\begin{aligned} \varepsilon_{cd,0} &= -0,85\cdot 10^{-6}\left[\left(220+110\alpha_{ds1}\right)\cdot\exp\left(-0,1\alpha_{ds2}f_{cm}\right)\right]\beta_{RH}; \\ \beta_{RH} &= 1,55\left[1-\left(RH/100\right)^3\right]. \end{aligned} \tag{A.3}$$

Here α_{ds1} and α_{ds2} are the coefficients which depend on the cement type. Coefficient α_{ds1} is assumed equal to 3 for slowly hardening cement (Class S), 4 for normal and rapidly hardening cement (Class N) and 6 for rapidly hardening high strength cement (Class R). Coefficient α_{ds2} is assumed equal to 0,13 for cement Class S, 0,12 for cement Class N and 0,11 for cement Class R. Alternatively, the value of the basic drying shrinkage strain $\varepsilon_{cd,0}$ may be taken from Table A.2.

Table A.1. Correction factor k_h

h_0, mm	100	200	300	≥ 500
k_h	1,00	0,85	0,75	0,70

Table A.2. Basic drying shrinkage strain of concrete $\varepsilon_{cd,0} \times 10^{-4}$

$f_{ck}/f_{ck,cube}$, MPa	*RH*, %					
	20	40	60	80	90	100
20/25	–6,2	–5,8	–4,9	–3,0	–1,7	0,0
40/50	–4,8	–4,6	–3,8	–2,4	–1,3	0,0
60/75	–3,8	–3,6	–3,0	–1,9	–1,0	0,0
80/95	–3,0	–2,8	–2,4	–1,5	–0,8	0,0
90/105	–2,7	–2,5	–2,1	–1,3	–0,7	0,0

A.1.2. Creep

The updated creep model was in fact first published in *Eurocode 2* in 2001. It is closely related to the model in the *MC 90*, but three strength dependent coefficients were introduced into the original model. The extended model is valid for both normal strength concrete and high performance concrete up to cylinder strength of 120 MPa. Three coefficients were introduced into the *MC 90* model:

$$\alpha_1 = \left(\frac{35}{f_{cm}}\right)^{0,7}; \quad \alpha_2 = \left(\frac{35}{f_{cm}}\right)^{0,2}; \quad \alpha_3 = \left(\frac{35}{f_{cm}}\right)^{0,5}. \tag{A.4}$$

The relationship between the total stress-dependent strain and the stress described with the compliance function:

$$J(t,t_0) = \frac{1}{E_c(t_0)} + \frac{\varphi(t,t_0)}{E_c}, \tag{A.5}$$

where t_0 is the age of concrete at loading [days]; $E_c = 1,05 \cdot E_{cm}$ is the tangent modulus at the age of 28 days [MPa]; $E_c(t_0)$ is the tangent modulus at the age of loading t_0 [MPa] $\varphi(t,t_0)$; is the creep coefficient estimated from

$$\varphi(t,t_0) = \varphi_0 \beta_c(t,t_0). \tag{A.6}$$

Here $\beta_c(t,t_0)$ is the coefficient describing the development of creep with time; φ_0 is the notional creep coefficient derived from

$$\varphi_0 = \varphi_{RH} \beta(f_{cm}) \beta(t_0). \tag{A.7}$$

Here φ_{RH}, $\beta(f_{cm})$ and $\beta(t_0)$ are the factors to allow for the effect of relative humidity, concrete strength and concrete age at loading on the notional creep coefficient, respectively. Above factors can be found using following equations:

$$\varphi_{RH} = \begin{cases} 1 + \dfrac{10 - RH/10}{\sqrt[3]{h_0}}; & \text{for } f_{cm} \le 35 \text{ MPa} \\ \left[1 + \dfrac{10 - RH/10}{\sqrt[3]{h_0}}\alpha_1\right]\alpha_2; & \text{for } f_{cm} > 35 \text{ MPa} \end{cases} \tag{A.8}$$

$$h_0 = 2A_c/u; \quad \beta(f_{cm}) = 16{,}8/\sqrt{f_{cm}}; \quad \beta(t_0) = \left[0{,}1 + t_0^{0{,}20}\right]^{-1}.$$

Here RH is the relative humidity of the ambient environment [%]; f_{cm} is the mean compressive cylinder strength of concrete in MPa at the age of 28 days; A_c is the cross-sectional area [mm^2]; u is the perimeter of the member in contact with the atmosphere [mm].

Coefficient $\beta_c(t, t_0)$ in Equation (A.6) may be estimated using the following expression:

$$\beta_c(t, t_0) = \left(\frac{t - t_0}{\beta_H + t - t_0}\right)^{0{,}3}, \tag{A.9}$$

where t is the age of concrete in days at the moment considered; t_0 is the age of concrete at loading in days; β_H is a coefficient depending on the relative humidity (RH in %) and the notional member size (h_0 in mm). It may be estimated from

$$\beta_H = \begin{cases} 1{,}5\left[1 + \left(\dfrac{1{,}2RH}{100}\right)^{18}\right]h_0 + 250 \le 1500; & f_{cm} \le 35 \text{ MPa}, \\ 1{,}5\left[1 + \left(\dfrac{1{,}2RH}{100}\right)^{18}\right]h_0 + 250\alpha_3 \le 1500\alpha_3; & f_{cm} > 35 \text{ MPa}. \end{cases} \tag{A.10}$$

When the compressive stress of concrete at an age t_0 exceeds the value $0{,}45 f_{ck}(t_0)$ then creep non-linearity should be considered. In such cases, the non-linear notional creep coefficient should be obtained as follows:

$$\varphi_{nl}(\infty, t_0) = \varphi(\infty, t_0)\exp\left[1{,}5\left(k_\sigma - 0{,}45\right)\right]. \tag{A.11}$$

Here $\varphi(\infty, t_0)$ is the final creep coefficient; $k_\sigma = \sigma_c / f_{ck}(t_0)$ is the stress-strength ratio, where σ_c is the compressive stress and $f_{ck}(t_0)$ is the characteristic concrete compressive strength at the time of loading.

A.2. *ACI 209*

ACI Committee 209 (2008) reported the equations presented here.

A.2.1. Shrinkage

The shrinkage strain at time t measured from the start of drying is calculated by following equation:

$$\varepsilon_{cs}(t) = \varepsilon_u \frac{t}{k+t}, \quad k = \begin{cases} 35; & \text{for moist cured,} \\ 55; & \text{for steam cured.} \end{cases} \tag{A.12}$$

Here ε_u is the ultimate shrinkage strain at time infinity. The shape and size effect can be considered on the shrinkage development by replacing in above equation coefficient k :

$$k = 26,0 \exp\left(1,42 \times 10^{-2} \frac{A_c}{u}\right). \tag{A.13}$$

Here A_c is the cross-sectional area [mm^2]; u is the perimeter of the member in contact with the atmosphere [mm]. Ultimate shrinkage strain represents the product of the applicable correction factors $\gamma_{cs,i}$:

$$\varepsilon_u = -7,8 \times 10^{-4} \prod_{i=1}^{7} \gamma_{cs,i} \ . \tag{A.14}$$

Coefficient $\gamma_{cs,1}$ includes the effect of initial moist curing period, t_c [days]:

$$\gamma_{cs,1} = \begin{cases} 1,202 - 0,2337 \log_{10}(t_c); & \text{for moist cured,} \\ 1; & \text{for steam cured.} \end{cases} \tag{A.15}$$

Coefficient $\gamma_{cs,2}$ includes the effect of variations in the ambient relative humidity, RH [%]:

$$\gamma_{cs,2} = \begin{cases} 1,40 - 0,0102RH; & \text{for } 10 \le RH \le 80\%, \\ 3,00 - 0,030RH; & \text{for } 80 < RH \le 100\%. \end{cases} \tag{A.16}$$

Coefficient $\gamma_{cs,3}$ accounts the size and shape of the member. Two alternative methods as in creep analysis are given for the estimation of $\gamma_{cs,3}$. Herein presented technique is based on the average thickness d (see Table A.3). For average thickness of member, less than 152 mm factor $\gamma_{cs,3}$ given in Table A.3 can be used. For average thickness of members greater than 152 mm and up to 381 mm, $\gamma_{cs,3}$ is calculated using following equation

$$\gamma_{cs,3} = \begin{cases} 1,23 - 0,0015d; & \text{for } t \le 1 \text{ year}, \\ 1,17 - 0,00114d; & \text{for } t > 1 \text{ year}. \end{cases} \tag{A.17}$$

Here t is the time measured from the start of drying.

Coefficients $\gamma_{cs,4} \ldots \gamma_{cs,7}$ depend on the composition of the concrete:

$$\begin{gathered} \gamma_{cs,4} = 0,89 + 1,61 \times 10^{-3} s; \quad \text{for } s > 130 \text{ mm}; \\ \gamma_{cs,5} = \begin{cases} 0,30 + 14 \times 10^{-3} \psi; & \text{for } \psi \le 50\%; \\ 0,90 + 2 \times 10^{-3} \psi; & \text{for } \psi > 50\%; \end{cases} \\ \gamma_{cs,6} = 0,65 + 8 \times 10^{-3} \alpha \ge 1; \quad \text{for } \alpha > 8\%; \\ \gamma_{cs,7} = 0,75 + 6,1 \times 10^{-4} c, \end{gathered} \tag{A.18}$$

where s is the slump of the fresh concrete [mm]; ψ is the ratio of the fine aggregate to total aggregate by weight [%]; α is the air content [%] and c is cement content in concrete [kg/m^3]. These coefficients in undefined intervals are assumed equal to 1,0.

A.2.2. Creep

The compliance function $J(t, t_0)$ that represents the total stress-dependent strain by unit stress is given by

$$J(t, t_0) = \frac{1 + \varphi(t, t_0)}{E_{cm}(t_0)}. \tag{A.19}$$

Here $E_{cm}(t_0)$ is the secant modulus of elasticity at the time of loading [MPa]; $\varphi(t, t_0)$ is the creep coefficient (defined as the ratio of creep strain to initial strain). Secant modulus of elasticity of concrete can be obtained from Table 1.1.

The creep model proposed by *ACI* has two components that determine the asymptotic value and the time development of creep. The predicted parameter is not creep strain, but creep coefficient $\varphi(t, t_0)$. The model uses a hyperbolic function to represent the creep-time relationship:

$$\varphi(t, t_0) = \varphi_u \frac{(t - t_0)^{0,6}}{10 + (t - t_0)^{0,6}} = \varphi_u \frac{\Delta t^{0,6}}{10 + \Delta t^{0,6}}. \tag{A.20a}$$

Here t is the age of concrete (days); t_0 is the time of load applying (days); φ_u is the ultimate creep coefficient. Above equation may be rearranged to assess shape and size effects as following

$$\varphi(t,t_0)=\varphi_u\frac{\Delta t}{k+\Delta t};\quad k=26,0\exp\left(1,42\times10^{-2}\frac{A_c}{u}\right). \tag{A.20b}$$

Here k is the coefficient calculated by Equation (A.13). Ultimate creep coefficient is expressed as product of the applicable correction factors $\gamma_{c,i}$:

$$\varphi_u=2,35\prod_{i=1}^{6}\gamma_{c,i}\ . \tag{A.21}$$

Coefficient $\gamma_{c,1}$ accounts the age of concrete at the time of first loading, t_0:

$$\gamma_{c,1}=\begin{cases}1,25\cdot t_0^{-0,118}, & t_0>7\text{ days}; \quad \text{for moist curing},\\ 1,13\cdot t_0^{-0,094}, & t_0>1-3\text{ days}; \quad \text{for steam curing}.\end{cases} \tag{A.22}$$

Coefficient $\gamma_{c,2}$ includes the effect of variations in the ambient relative humidity, RH [%]:

$$\gamma_{c,2}=1,27-6,7\times10^{-3}RH,\quad RH>40\%\ . \tag{A.23}$$

Coefficient $\gamma_{c,3}$ accounts the size and shape of the member. Two alternative methods are given for the estimation of $\gamma_{c,3}$. Here presented technique is based on the average thickness $d=2h_0$ [see Equation (A.8)] and recommended for average thicknesses up to 381 mm. For average thickness d less than 152 mm, $\gamma_{c,3}$ is obtained from Table A.3. For average thickness of members greater than 152 mm and up to 381 mm, $\gamma_{c,3}$ is calculated using following equation

$$\gamma_{c,3}=\begin{cases}1,14-9,2\times10^{-4}d; & \text{for } \Delta t\le1\text{ year},\\ 1,10-6,7\times10^{-4}d; & \text{for } \Delta t>1\text{ year}.\end{cases} \tag{A.24}$$

Coefficients $\gamma_{c,4}\ldots\gamma_{c,6}$ depend on the composition of the concrete

$$\begin{gathered}\gamma_{c,4}=0,82+2,64\times10^{-3}s;\quad \text{for } s>130\text{ mm};\\ \gamma_{c,5}=0,88+2,4\times10^{-3}\psi;\quad \text{for } \psi<40\%\text{ or }\psi>60\%;\\ \gamma_{c,6}=0,46+0,09\alpha\ge1;\quad \text{for } \alpha>8\%.\end{gathered} \tag{A.25}$$

Table A.3. Correction factors to account size and shape of the member for creep $\gamma_{c,3}$ and shrinkage $\gamma_{cs,3}$

***d*, mm**	**51**	**76**	**102**	**127**	**152**
$\gamma_{c,3}$	1,30	1,17	1,11	1,04	1,00
$\gamma_{cs,3}$	1,35	1,25	1,17	1,08	1,00

In Equation (A. 25), s, ψ and α are the parameters similar to those from Equation (A.18), the coefficients in undefined intervals are assumed equal to 1,0.

A.3. *Central Institute of Research and Investigation in Civil Engineering* (*CNIIS*)

Central Institute of Research and Investigation in Civil Engineering (CNIIS 1983) has proposed a method for calculation of creep and shrinkage deformations. The equations are presented here published in *Milovanov & Kambarov* (1994).

A.3.1. Shrinkage

The shrinkage strain at time t measured from the start of drying is calculated by following equation:

$$\varepsilon_{cs}(t) = \varepsilon_{cs,u}\Delta t / (a_{cs} + \Delta t). \quad \text{(A.26)}$$

Here a_{cs} is the rate of shrinking obtained from Table A.4; $\varepsilon_{cs,u}$ is the ultimate shrinkage at time infinity and represents the product of correction factors:

$$\varepsilon_{cs,u} = \varepsilon_{cs}\varphi_h\varphi_w = -0{,}125\cdot 10^{-6}\varphi_h\varphi_w\sqrt{W^3}. \quad \text{(A.27)}$$

Here ε_{cs} is the shrinkage strain of concrete; W is the water content [kg/m^3]; φ_h accounts for average thickness of the member and the environment conditions (see Table A.4), and φ_w takes into account the effect of variations in the ambient relative humidity RH presented in Table A.5.

Table A.4. Rate of shrinking a_{cs} / factor φ_h / rate of creep a_n

Environment conditions[1]	**Parameters**	**Average thickness h_0, cm**						
		≤ 3,5	**5,0**	**10,0**	**20,0**	**30,0**	**40,0**	**≥ 50,0**
Warm	a_{cs}	15	20	40	80	120	160	200
	φ_h	1,80	1,50	1,05	0,85	0,75	0,75	0,75
	a_n	25	35	50	90	120	160	200
Cold	a_{cs}	40	60	120	240	360	480	600
	φ_h	0,90	0,80	0,70	0,65	0,60	0,60	0,60
	a_n	40	60	90	150	210	270	330

[1]Averaged values (between warm and cold) should be used for members cured under normal conditions

If composition of concrete is not known, the shrinkage strain in above equation defined from Table A.6. Ultimate shrinkage strain of the element non-protected from direct solar radiation can be also obtained from Table A.7. Shrinkage strains given in Table A.7 should be multiplied by 0,85 for elements produced from weak concrete ($B < 25$ MPa) or protected from solar radiation.

Table A.5. Correction factor φ_w

***RH*, %**	**≤20**	**40**	**50**	**70**	**80**	**90**
φ_w	1,5	1,3	1,2	1,0	0,9	0,8

Table A.6. Shrinkage strain of concrete $\varepsilon_{cs} \times 10^{-4}$

Slump, cm	**Normative strength (Class) of concrete *B*, MPa**	
	12,5–15	**25–65**
0–1	–2,30	–2,70
2–3	–2,90	–3,30
5–7	–3,50	–4,00
9–12	–3,80	–4,30

Table A.7. Ultimate shrinkage strain of concrete $\varepsilon_{cs,u} \times 10^{-4}$

***RH*, %**	**Average thickness h_0, cm**						
	3,5	**5,0**	**10,0**	**20,0**	**30,0**	**50,0**	**≥ 100,0**
0	–8,00	–7,20	–6,30	–5,85	–5,70	–5,60	–5,50
20	–7,10	–6,30	–5,40	–4,90	–4,75	–4,60	–4,45
40	–6,15	–5,40	–4,50	–4,00	–3,80	–3,65	–3,40
60	–5,30	–4,50	–3,60	–3,10	–2,90	–2,70	–2,40
75	–4,60	–3,80	–2,90	–2,40	–2,20	–2,00	–1,60
90	–3,90	–3,10	–2,20	–1,70	–1,60	–1,55	–1,50

A.3.2. Plastic Shrinkage

Plastic shrinkage strains, given Table A.8, may be taken into consideration for cast-in-situ constructions produced in warm environment. Plastic shrinkage strain depends on relative humidity solar exposure conditions and average thickness of the element h_0 [see Equation (A.8)].

Table A.8. Plastic shrinkage strain $\varepsilon_{cp} \times 10^{-4}$

Relative humidity *RH*	**Element exposed to direct solar radiation**		**Element protected from direct solar radiation**	
	$h_0 \le 10$	$h_0 > 10$	$h_0 \le 10$	$h_0 > 10$
$RH \le 20\%$	–3,50	–2,50	–2,00	–1,50
$20\% < RH < 60\%$	–2,50	–1,50	–1,50	–0,50
$RH \ge 60\%$	–1,50	–	–	–

A.3.3. Creep

Creep factor $\varphi(t, t_0)$ is given by

$$\varphi(t, t_0) = C(t, t_0) \cdot E_c(t_0). \tag{A.28}$$

The creep parameter at time $\Delta t = t - t_0$ is calculated by following equation:

$$C(t, t_0) = C_u \frac{\Delta t}{a_n + \Delta t}. \tag{A.29}$$

Here a_n is the rate of creep obtained from Table A.4; C_u is the ultimate creep parameter at time infinity [MPa^{-1}] and representing the product of the correction factors:

$$C_u = C\varphi_t\varphi_h\varphi_w = 12,5 \cdot 10^{-6}\varphi_t\varphi_h\varphi_w \frac{W}{B}. \tag{A.30}$$

Here C is the normative specific linear creep parameter [MPa^{-1}]; W is the water content [kg/m^3]; B is the class of concrete, $B \approx 0,778 \cdot f_{cube,m} \approx 0,973 \cdot f_{cm}$ [MPa]; φ_t, φ_h, φ_w are the correction factors given in Tables A.9, A.4 and A.5, respectively. Factors φ_h and φ_w are the same as in Equation (A.27); factor φ_t depends on relative compressive strength of concrete f_c/f_{cm} and the age at loading t [days]. The normative specific linear creep parameter can also be obtained from Table A.10.

Table A.9. Correction factor φ_t

f_c/f_{cm}	**0,6**	**0,7**	**0,8**	**0,9**	**1,0**	**> 1,0**				
***t*, days**	**< 28**				**28**	**45**	**60**	**90**	**180**	**≥ 360**
φ_t	1,50	1,40	1,25	1,15	1,00	0,90	0,85	0,75	0,65	0,60

Table A.10. Normative specific linear creep parameter $C \times 10^{-6}$, [MPa^{-1}]

Slump, cm	Normative strength (Class) of concrete *B*, MPa							
	12,5	**15**	**25**	**30**	**40**	**45**	**55**	**65**
0–1	140	108	77	62	52	45	40	36
2–3	162	124	89	72	60	53	47	42
5–7	182	140	101	81	68	59	52	46
9–12	192	148	107	85	72	62	55	50

A.4. *Bažant & Baweja B3* Model

The *Bažant & Baweja* (1995a, 1995b) *B3* model is the latest variant in a number of shrinkage and creep prediction methods developed by *Bažant* and his co-workers. According to *Bažant & Baweja* (2000), the *B3* model is simpler and is better theoretically justified than the previous models.

A.4.1. Shrinkage

The mean shrinkage strain $\varepsilon_{cs}(t, t_s)$ at age of concrete t [days], measured from the start of drying at t_s [days], is calculated by following equation:

$$\varepsilon_{cs}(t, t_s) = \varepsilon_u k_{RH} \tanh\left(\sqrt{(t - t_s)/\tau_{cs}}\right). \tag{A.31}$$

Here k_{RH} is the humidity dependence factor; τ_{cs} is the shrinkage half-time; $\varepsilon_{cs,u}$ is the ultimate shrinkage strain:

$$\varepsilon_u = -\alpha_1\alpha_2 \frac{607\left[4 + 0{,}85(t_s + \tau_{cs})\right]}{520(t_s + \tau_{cs})}\left(\frac{0{,}019W^{2,1}}{f_{cm}^{0,28}} + 270\right)\times 10^{-6}. \tag{A.32}$$

Here W is the water content [kg/m^3]. Coefficient α_1 is assumed equal to 0,85 for slowly hardening cement (Class S / Type II), 1,00 for normal and rapidly hardening cement (Class N / Type I) and 1,10 for rapidly hardening high strength cement (Class R / Type III). Coefficient α_2 is assumed equal to 0,75 for steam cured concrete, 1,00 for concrete cured in water or at 100% relative humidity and 1,20 for concrete sealed during curing or normal curing in air with initial protection against drying.

The humidity dependence factor k_{RH} is defined as following

$$k_{RH} = \begin{cases} 1 - (RH/100)^3; & \text{for } RH \le 98\%, \\ 12{,}74 - 0{,}1296RH; & \text{for } 98 < RH < 100\%, \\ -0{,}2; & \text{for } RH = 100\%. \end{cases} \tag{A.33}$$

The shrinkage half-time τ_{cs} is calculated by following equation:

$$\tau_{cs} = 0,085\left(k_s h_0\right)^2 t_s^{-0,08} f_{cm}^{-0,25}. \tag{A.34}$$

Here h_0 is the average thickness [see Equation (A.8)]; k_s is the cross-section shape-correction factor that equal to 1,00 for infinite slab, 1,15 for infinite cylinder, 1,25 for infinite square prism, 1,30 for sphere and 1,55 for cube.

A.4.2. Creep

An important feature of the *B3* creep model is that the compliance function is decomposed into the instantaneous response, the compliance function for basic creep and the additional compliance function for drying creep. The creep compliance is written as

$$J\left(t,t_0\right) = \frac{1}{E_0} + C_0\left(t,t_0\right) + C_d\left(t,t_0,t_s\right), \tag{A.35}$$

where E_0 is the so-called asymptotic modulus (see Table 1.1) where $f_{cm} = f_c' + 8,3$ [MPa]; $C_0\left(t,t_0\right)$ and $C_d\left(t,t_0,t_s\right)$ are the compliance function for basic and drying creep, respectively; t, t_s and t_0 are the age of concrete, the age drying began or end of moist curing, and age of loading [days].

According to this model, the basic creep is composed of three terms: an aging viscoelastic term, a non-aging viscoelastic term, and an aging flow term

$$C_0\left(t,t_0\right) = q_1 Q\left(t,t_0\right) + q_2 \ln\left[1+\left(t-t_0\right)^{0,1}\right] + q_3 \ln\left(\frac{t}{t_0}\right);$$

$$Q\left(t,t_0\right) = \frac{Q_f\left(t_0\right)}{\left\{1+\left[\frac{Q_f\left(t_0\right)}{Z\left(t,t_0\right)}\right]^{r\left(t_0\right)}\right\}^{\frac{1}{r\left(t_0\right)}}}, \tag{A.36}$$

where

$$q_1 = 1,854\times10^{-4} f_{cm}^{-0,9}\sqrt{C}; \qquad Q_f\left(t_0\right) = \frac{1}{0,086\left(t_0\right)^{2/9} + 1,21\left(t_0\right)^{4/9}};$$

$$q_2 = 0,29 q_1 \left(W/C\right)^4; \qquad Z\left(t,t_0\right) = t_0^{-0,5}\ln\left[1+\left(t-t_0\right)^{0,1}\right]; \tag{A.37}$$

$$q_3 = 0,203\times10^{-4}\left(A/C\right)^{-0,7}; \qquad r\left(t_0\right) = 1,7\left(t_0\right)^{0,12} + 8.$$

Here C is the cement content [kg/m^3]; W/C and A/C are the water-cement and the aggregate-cement ratios (by weight), respectively.

The compliance function for drying creep is defined by following equation:

$$C_{\mathrm{d}}\left(t,t_0,t_{\mathrm{s}}\right)=q_4\sqrt{e^{-8H(t)}-e^{8H(t_0)}};\quad q_4=0,757\cdot f_{\mathrm{cm}}^{-1}\left(\varepsilon_{\mathrm{u}}\times 10^6\right)^{-0,6}. \quad \text{(A.38)}$$

Here ε_{u} is the ultimate shrinkage strain as given below in Equation (A.32); $H\left(t\right)$ and $H\left(t_0\right)$ are spatial averages of pore relative humidity:

$$H\left(X\right)=1-\left(1-RH/100\right)\tanh\left[\sqrt{\left(X-t_{\mathrm{s}}\right)/\tau_{\mathrm{cs}}}\right],\quad X=t \text{ or } t_0. \quad \text{(A.39)}$$

Here τ_{cs} is the shrinkage half-time as given below in Equation (A.34).

A.5. *Gardner & Lockman GL 2000* Model

The model presented herein corresponds to the last version of the model (Gardner 2004), including minor modifications of the original model (Gardner & Lockman 2001). It presents a design procedure for calculating the creep and shrinkage of normal strength concretes, defined as concretes with mean compressive strengths less than 82 MPa.

A.5.1. Shrinkage

The shrinkage strain $\varepsilon_{\mathrm{cs}}\left(t,t_{\mathrm{s}}\right)$ at age of concrete t [days], measured from the start of drying at t_{s} [days], is calculated using following relationship:

$$\varepsilon_{\mathrm{cs}}\left(t,t_{\mathrm{s}}\right)=\varepsilon_{\mathrm{u}}\beta\left(RH\right)\beta\left(t-t_{\mathrm{s}}\right),$$
$$\beta\left(RH\right)=1-1,18\left(\frac{RH}{100}\right)^4;\quad \beta\left(t-t_{\mathrm{s}}\right)=\sqrt{\frac{t-t_{\mathrm{s}}}{t-t_{\mathrm{s}}+0,03h_0^2}}. \quad \text{(A.40)}$$

Here $\beta\left(\mathrm{RH}\right)$ is the humidity dependence factor; $\beta\left(t-t_{\mathrm{s}}\right)$ is the correction term for the effect of time of drying; $\varepsilon_{\mathrm{cs,u}}$ is the ultimate shrinkage strain:

$$\varepsilon_{\mathrm{u}}=-9\times 10^{-4}k\sqrt{30/f_{\mathrm{cm}}}. \quad \text{(A.41)}$$

Here f_{cm} is the concrete mean compressive strength at 28 days [MPa]; k is the shrinkage constant that depends on the cement type. It assumed equal to 1,0 for normal and rapidly hardening cement (Class N / Type I), 0,75 for slowly hardening cement (Class S / Type II), and 1,15 for rapidly hardening high strength cement (Class R / Type III).

A.5.2. Creep

The compliance is composed of the elastic and the creep strains. The elastic strain is the reciprocal of the modulus of elasticity at the age of loading $E_{\mathrm{cm}}\left(t_0\right)$. Creep strain represents the 28-day creep coefficient $\varphi_{28}\left(t,t_0\right)$ divided by the modulus of elasticity at 28 days E_{cm}:

$$J\left(t,t_0\right)=\frac{1}{E_{\mathrm{cm}}\left(t_0\right)}+\frac{\varphi_{28}\left(t,t_0\right)}{E_{\mathrm{cm}}}. \tag{A.42}$$

The modules of elasticity in above relationship derived using Equation (1.1) and Table 1.1. The 28-day creep coefficient $\varphi_{28}\left(t,t_0\right)$ is calculated as follows

$$\varphi_{28}\left(t,t_0\right)=\Phi\left(t_{\mathrm{s}}\right)k_{\varphi},$$
$$k_{\varphi}=\frac{2\Delta t^{0,3}}{\Delta t^{0,3}+14}+\sqrt{\frac{7\Delta t}{t_0\left(\Delta t+7\right)}}+\frac{2,5\left[1-1,086\left(\frac{RH}{100}\right)^2\right]}{\sqrt{1+0,03\frac{h_0^2}{\Delta t}}}. \tag{A.43}$$

Here h_0 is the average thickness see [Equation (A.8)]; $\Delta t=t-t_0$ is the age of loading [days]; $\Phi\left(t_{\mathrm{s}}\right)$ is the correction term for the effect of drying before loading:

$$\Phi\left(t_{\mathrm{s}}\right)=\begin{cases}1; & \text{for } t_0=t_{\mathrm{s}},\\ \sqrt{1-\sqrt{\dfrac{\Delta t}{\Delta t+0,03h_0^2}}}; & \text{for } t_0>t_{\mathrm{s}}.\end{cases} \tag{A.44}$$

Annex B. Computer Code for Derivation of *Free-of-Shrinkage* Tension-Stiffening Relationships using *MATLAB*

B.1. *MATLAB* Function for the *Direct* Analysis

This Section presents the implementation of the *direct* deformation analysis using *MATLAB* software. Three extra *Excel*-files named '*Crossection*', '*MomentCurvature*', and '*SigmaEpsilon*' should be saved in the working directory. Structure of these files is shown if Fig. B.1.

'*Crossection*'

	A	B
1	Height, m	‹value›
2	Width, m	‹value›
3	d, m	‹value›
4	a_{s2}, m	‹value›
5	A_{s1}, m^2	‹value›
6	A_{s2}, m^2	‹value›
7	E_{s1}, MPa	‹value›
8	f_{s1}, MPa	‹value›
9	E_{s2}, MPa	‹value›
10	f_{s2}, MPa	‹value›
11	E_{cm}, MPa	‹value›
12	f_{cm}, MPa	‹value›
13	Shrinkage strain	‹value›
14	Creep coefficient	‹value›

'*MomentCurvature*'

	A	B
1	0	0
2	‹Moment$_1$, MNm›	‹Curvature$_1$, m^{-1}›
3	‹Moment$_2$, MNm›	‹Curvature$_2$, m^{-1}›
4	‹Moment$_3$, MNm›	‹Curvature$_3$, m^{-1}›
...	...	...
n	‹Moment$_{max}$, MNm›	‹Curvature$_{max}$, m^{-1}›

'*SigmaEpsilon*'

	A	B
1	0	0
2	‹Stress$_1$, MPa›	‹Strain$_1$, m/m›
3	‹Stress$_2$, MPa›	‹Strain$_2$, m/m›
4	‹Stress$_3$, MPa›	‹Strain$_3$, m/m›
...	...	...
n	‹Stress$_n$, MPa›	‹Strain$_{max}$, m/m›

Fig. B.1. Structure of *Excel*-files required for performing the *direct* and *inverse* procedures

The listing presented below should be saved in the working directory as m-file named '*Direct*':

```
function MC = Direct(name1, name2, name3, No, Colour)
Crossection = xlsread(name1);
MomentCurvature = xlsread(name2);
SigmaEpsilon = xlsread(name3);
DataLength = size(MomentCurvature);
```

```
M = MomentCurvature(:, 1);
Curvature = zeros(1, DataLength(1));
[Numbers, Geometry] = layers(name1, No);
A = Geometry(1, :);
y = Geometry(2, :);
AY = Geometry(3, :);
AI = Geometry(4, :);
EcUpper = 1.05 * Crossection(11);
EpsilonShrinkage = zeros(size(Numbers(1)));
Layer = zeros(size(Numbers(1)));
Fi = zeros(size(Numbers(1)));
Ec = zeros(size(Numbers(1)));
fs = zeros(size(Numbers(1)));
sigma = zeros(size(Numbers(1)));
error = zeros(size(Numbers(1)));
for N = 1:1:Numbers(1)
    if N == Numbers(2)
        Ec(N) = Crossection(9);
        fs(N) = Crossection(10);
    elseif N == Numbers(3)
        Ec(N) = Crossection(7);
        fs(N) = Crossection(8);
    else
        Ec(N) = EcUpper;
        fs(N) = Crossection(12);
        EpsilonShrinkage(N) = - Crossection(13);
        Layer(N) = 1;
        Fi(N) = Crossection(14);
    end
end
Geometry = cat(1, Geometry, fs, Ec);
AE = A * Ec';
AEcon = A .* Layer * Ec';
SE = AY * Ec';
SEcon = AY .* Layer * Ec';
Yc = SE / AE;
Yccon = SEcon / AEcon;
IE = (AI + A .* (y - Yc) .^ 2) * Ec';
Shr = Creep(Geometry, EpsilonShrinkage, Fi, Layer, No);
NShr = Shr .* A * Ec';
MShr = NShr * (Yccon - Yc);
Ind = DataLength(1);
for i = 1:1:DataLength(1)
    Parametr = true;
    ER = 1;
    Sk = 0;
    while ER > 1e-7 && Sk < 500
        EcCalc = Ec;
        Sk = Sk + 1;
        eps = (M(i) + MShr) / IE * (y - Yc) + NShr / AE - Shr;
        for N = 1:1:Numbers(1)
```

```
            if N == Numbers(2) || N == Numbers(3)
                sigma(N) = Steel(eps(N), fs(N), Ec(N));
            elseif eps(N) < 0
                sigma(N) = Compressive(eps(N), fs(N), EcUpper);
            elseif eps(N) > 0
                if eps(N) > max(SigmaEpsilon(:,2))
                    Parametr = false;
                    Ind = i - 1;
                    break
                end
                sigma(N) = Tensile(eps(N), SigmaEpsilon);
            else
                sigma(N) = 0;
            end
            if eps(N) ~= 0
                Ec(N) = sigma(N) / eps(N);
            end
            if EcCalc(N) == 0
                error(N) = Ec(N);
            else
                error(N) = (EcCalc(N) - Ec(N)) / abs(EcCalc(N));
            end
        end
        if Parametr == false
            break
        end
        ER = max(abs(max(error)), abs(min(error)));
        AE = A * Ec';
        AEcon = A .* Layer * Ec';
        SE = AY * Ec';
        SEcon = AY .* Layer * Ec';
        Yc = SE / AE;
        if AEcon == 0
            Yccon = Yc;
        else
            Yccon = SEcon / AEcon;
        end
        IE = (AI + A .* (y - Yc) .^ 2) * Ec';
        NShr = Shr .* A * Ec';
        MShr = NShr * (Yccon - Yc);
        if i == 1
            MShr0 = MShr;
            IE0 = IE;
        end
        Curvature(i) = (M(i) + MShr) / IE - MShr0 / IE0;
    end
    if Parametr == false
        disp('GetCurvature stoped')
        break
    else
        disp([i, M(i) / M(DataLength(1)) * 100])
```

```
    end
end
MomentC = zeros(1, Ind);
CurvatureC = zeros(1, Ind);
for i = 1:1:Ind
    MomentC(i) = M(i);
    CurvatureC(i) = Curvature(i);
end
MC = cat(2, MomentC', CurvatureC');
if i > 1
    plot(MomentCurvature(:, 2), M, 'k.'); grid on; hold on
    plot(CurvatureC, MomentC, Colour); grid on; hold on
end

function [Numbers, Geometry] = layers(name, LayersN)
Crossection = xlsread(name);
b = Crossection(2);
nR = zeros(1, 3);
hR = zeros(1, 3);
yR = zeros(1, 3);
AR = zeros(1, 3);
lR = zeros(1, 3);
if Crossection(6) == 0 && Crossection(5) == 0
    Num = 1;
elseif Crossection(6) == 0 || Crossection(5) == 0
    Num = 2;
    if Crossection(6) < Crossection(5)
        nR(1) = round(0.85 * LayersN);
        hR(1) = Crossection(5) / b;
        yR(1) = Crossection(3);
        AR(1) = Crossection(5);
        lR(1) = 1;
    else
        nR(1) = round(0.15 * LayersN);
        hR(1) = Crossection(6) / b;
        yR(1) = Crossection(4);
        AR(1) = Crossection(6);
        lR(1) = 1;
    end
else
    Num = 3;
    nR(2) = round (0.15 * LayersN);
    hR(2) = Crossection(6) / b;
    yR(2) = Crossection(4);
    AR(2) = Crossection(6);
    lR(2) = 1;
    nR(1) = round (0.85 * LayersN);
    hR(1) = Crossection(5) / b;
    yR(1) = Crossection(3);
    AR(1) = Crossection(5);
    lR(1) = 1;
```

```
end
N = LayersN;
Lay = Crossection(1);
LayNo = LayersN;
h = zeros(1, N);
A = zeros(1, N);
y = zeros(1, N);
y2 = zeros(1, N);
AY = zeros(1, N);
AI = zeros(1, N);
for i = 1:1:Num
    while N > nR(i)
        h(N) = (Lay - yR(i) - hR(i) / 2) / (LayNo - nR(i));
        A(N) = h(N) * b;
        if N == LayersN
            y(N) = Crossection(1) - h(N) / 2;
        else
            y(N) = y(N + 1) - (h(N + 1) + h(N)) / 2;
        end
        N = N - 1;
    end
    if N > 1
        h(N) = hR(i);
        A(N) = AR(i);
        y(N) = yR(i);
        N = N - 1;
    end
    Lay = yR(i) - hR(i) / 2;
    LayNo = nR(i) - lR(i);
end
for G = 1:1:LayersN
    if G == 1
        y2(G) = h(G) / 2;
    elseif G == nR(2)
        y2(G) = Crossection(4);
    elseif G == nR(1)
        y2(G) = Crossection(3);
    else
        y2(G) = y2(G - 1) + h(G - 1) / 2 + h(G) / 2;
    end
    y(G) = (y(G) + y2(G)) / 2;
    AY(G) = y(G) * A(G);
    AI(G) = b * h(G) ^ 3 / 12;
end
Numbers = [LayersN nR(2) nR(1)];
Geometry = cat(1, A, y, AY, AI);

function Shrinkage = Creep(Geometry, eps, Fi, Layer, No)
A = Geometry(1, :);
y = Geometry(2, :);
AY = Geometry(3, :);
```

```
AI = Geometry(4, :);
Ec = Geometry(6, :);
AE = zeros(2, 1);
Yc = zeros(2, 1);
Yccon = zeros(2, 1);
IE = zeros(2, 1);
sigma = zeros(2, 1);
R = zeros(3, No);
E = ones(size(Fi));
for i = 1:1:2
    if i == 1
        F = zeros(size(Fi));
    else
        F = Fi;
    end
    AE(i) = A * (Ec ./ (E + F))';
    AEcon = A .* Layer * (Ec ./ (E + F))';
    SE = AY * (Ec ./ (E + F))';
    SEcon = AY .* Layer * (Ec ./ (E + F))';
    Yc(i) = SE / AE(i);
    Yccon(i) = SEcon / AEcon;
    IE(i) = (AI + A .* (y - Yc(i)) .^ 2) * (Ec ./ (E + F))';
    N = eps .* A * (Ec ./ (E + F))';
    M = N * (Yccon(i) - Yc(i));
    sigma1=(M/IE(i)*(y(1)-Yc(i))+N/AE(i)-eps(1))*(Ec(1)/(1+F(1)));
    sigmaN=(M/IE(i)*(y(No)-Yc(i))+N/AE(i)-eps(No))*(Ec(No)/(1+F(No)));
    if abs(sigma1) > abs(sigmaN)
        sigma(i) = sigma1;
        L = 1;
    else
        sigma(i) = sigmaN;
        L = No;
    end
    R(i, :) = eps ./ (E + F);
end
E1 = sigma(1) - sigma(2);
E2=(R(2, :).*A*Ec'*(Yccon(1)-Yc(1))'/IE(1)*(y(L)-
Yc(1))+R(2,:).*A*Ec'/AE(1)-R(2, L))*Ec(L)-sigma(2);
while abs(E1) > 1e-10 * abs(sigma(2)) && E1 ~= E2
    R(3, :) = R(1, :) - E1 * (R(1, :) - R(2, :)) / (E1 - E2);
    R(2, :) = R(1, :);
    R(1, :) = R(3, :);
    E2 = E1;
    E1=(R(1,:).*A*Ec'*(Yccon(1)-Yc(1))'/IE(1)*(y(L)-
Yc(1))+R(1,:).*A *Ec'/AE(1)-R(1,L))*Ec(L)-sigma(2);
end
Shrinkage = R(1, :);

function sigma = Steel(eps, fs, Es)
sigma = eps * Es;
if abs (eps) > abs (fs / Es)
```

```
    sigma = fs * sign (eps);
end

function sigma = Compressive(eps, fcm, Ec)
fck = fcm - 8;
if fck < 50
    eps_cu1 = -3.5e-3;
else
    eps_cu1 = -2.8e-3 - 27e-3 * ((98 - fcm) / 100) ^ 4;
end
if abs(eps) > abs(eps_cu1)
    sigma = 0;
else
    eps_c1 = -0.7e-3 * fcm ^ 0.31;
    eta = eps / eps_c1;
    k = Ec * abs(eps_c1) / fcm;
    sigma=sign(eps)*fcm*(k*eta-eta^2)/(1+(k-2)*eta);
end

function sigma = Tensile(eps, SE)
n = size(SE);
i = 1;
while eps > SE(i, 2)
    i = i + 1;
    if i > n(1)
        i = n(1);
        break
    end
end
sigma=(SE(i,1)*(eps-SE(i-1,2))+SE(i-1,1)*(SE(i,2)-eps))/(SE(i,2)-SE(i-1,2));
```

To start the *direct* analysis using *MATLAB*, the following text should be written in the command line:

```
MomentCurvature = Direct('Crossection', 'MomentCurvature',
'SigmaEpsilon', 100, 'g-');
```

Here 100 defines the number of layers in the *Layer* section model (recommended to be not less than 50); 'g-' is the parameter that defines colour and type of the resulting moment-curvature diagram (results in creating a green solid line).

B.2. *MATLAB* Function for the *Inverse* Analysis

This Section presents the implementation of the *inverse* analysis using *MATLAB* software. Two additional Excel-files named '*Crossection*' and '*MomentCurvature*' should be saved in the working directory. These files are similar to those shown in Fig. B.1 with the exception that last two positions in file '*Crossection*' are not necessary. The listing presented below should be saved in the working directory as m-file named '*Inverse*':

```
function [SEAver, SE] = Inverse(nm1, nm2, N1, N2, Dt, St)
rand('state',sum(100*clock));
P = round(70 + 50 * rand(1, N2));
for N = 1:1:N2
    SEn = GetDiagram(nm1, nm2, N1, P(N), N, Dt, St);
    if N == 1
        SE = SEn;
    else
        SE = sortrows(cat(1, SE, SEn), 2);
    end
end
plot(SE(:, 2), SE(:, 1), 'k.'); grid on; hold on
try
    SEAver = Hardy(SE, N2);
    plot (SEAver(:, 2), SEAver(:, 1), 'r-'); grid on; hold on
catch
    SEAver = 0;
end

function SEn = GetDiagram(nm1, nm2, N1, APts, N2, Dt, P)
Crossection = xlsread(nm1);
MC0 = xlsread(nm2);
DataLength = size(MC0);
rand('state',sum(100 * clock));
RRR = ceil(P * rand);
set(1, :) = MC0(1, :);
x = 1;
for u = RRR + 1:P:(DataLength(1) - 1)
    x = x + 1;
    set(x, :) = MC0(u, :);
end
set(x + 1, :) = MC0(DataLength(1), :);
clear global MC0;
MC0 = set;
DataLength = size(MC0);
[Nrs, Ge] = layers(nm1, N1);
EcU = 1.05 * Crossection(11);
Ec = ones(1, Nrs(1)) * EcU;
fs = ones(1, Nrs(1)) * Crossection(12);
if Nrs(2) ~= 0
    Ec(Nrs(2)) = Crossection(9);
    fs(Nrs(2)) = Crossection(10);
end
if Nrs(3) ~= 0
    Ec(Nrs(3)) = Crossection(7);
    fs(Nrs(3)) = Crossection(8);
end
Yc = (Ge(3, :) * Ec') / (Ge(1, :) * Ec');
EIel = (Ge(4, :) + Ge(1, :) .* (Ge(2, :) - Yc) .^ 2) * Ec';
g = 1;
f = 1;
CurvatureCorrect(1) = MC0(1, 2);
```

```
MC(1, 1) = MC0(1, 1);
MC(2, 1) = CurvatureCorrect(1);
MC(3, 1) = 0;
SEn(2, 1) = MC(2, 1) * (Ge(2, Nrs(1)) - Yc);
SEn(1, 1) = SEn(2, 1) * EcU;
a1 = MC0(DataLength(1), 1);
a = MC0(DataLength(1), 2);
CurvatureCorrect = zeros(1, DataLength(1));
Ge = cat(1, Ge, fs, Ec);
for i = 2:1:DataLength
    if MC0(i, 2) <= MC0(i, 1) / EIel
        CurvatureCorrect(i) = MC0(i, 1) / EIel;
    else
        CurvatureCorrect(i) = MC0(i, 2);
    end
    c1 = MC0(i, 1);
    c = CurvatureCorrect(i);
    b1 = MC0(i - 1, 1);
    b = CurvatureCorrect(i - 1);
    exPts1 = round(APts * (c - b) / a);
    exPts2 = round(0.5 * APts * (c1 - b1) / a1);
    exPts = max([1 exPts1 exPts2]);
    for m = 1:1:exPts
        g = g + 1;
        f = f + 1;
        MC(1,g)=MC0(i-1,1)+(MC0(i,1)-MC0(i-1,1))*m/exPts;
        MC(2, g) = b + (c - b)* m / exPts;
        MC(3, g) = 0;
        try
            [MC(:,g),Prm,SENew,Ge]=A2(Nrs,Ge,Dt,MC(:,g),EcU,SEn);
            if Prm(1) == true && Prm(3) == true
                SEn = SENew;
                disp([N2, f, MC(2, g) / a * 100])
            else
                g = g - 1;
            end
        catch
            g = g - 1;
        end
    end
end
SEn = SEn';

function [Nrs, Ge] = layers(name, LayersN)
Crossection = xlsread(name);
b = Crossection(2);
nR = zeros(1, 3);
hR = zeros(1, 3);
yR = zeros(1, 3);
AR = zeros(1, 3);
lR = zeros(1, 3);
if Crossection(6) == 0 && Crossection(5) == 0
```

```
    Num = 1;
elseif Crossection(6) == 0 || Crossection(5) == 0
    Num = 2;
    if Crossection(6) < Crossection(5)
        nR(1) = round(0.85 * LayersN);
        hR(1) = Crossection(5) / b;
        yR(1) = Crossection(3);
        AR(1) = Crossection(5);
        lR(1) = 1;
    else
        nR(1) = round(0.15 * LayersN);
        hR(1) = Crossection(6) / b;
        yR(1) = Crossection(4);
        AR(1) = Crossection(6);
        lR(1) = 1;
    end
else
    Num = 3;
    nR(2) = round (0.15 * LayersN);
    hR(2) = Crossection(6) / b;
    yR(2) = Crossection(4);
    AR(2) = Crossection(6);
    lR(2) = 1;
    nR(1) = round (0.85 * LayersN);
    hR(1) = Crossection(5) / b;
    yR(1) = Crossection(3);
    AR(1) = Crossection(5);
    lR(1) = 1;
end
N = LayersN;
Lay = Crossection(1);
LayNo = LayersN;
h = zeros(1, N);
A = zeros(1, N);
y = zeros(1, N);
y2 = zeros(1, N);
AY = zeros(1, N);
AI = zeros(1, N);
for i = 1:1:Num
    while N > nR(i)
        h(N) = (Lay - yR(i) - hR(i) / 2) / (LayNo - nR(i));
        A(N) = h(N) * b;
        if N == LayersN
            y(N) = Crossection(1) - h(N) / 2;
        else
            y(N) = y(N + 1) - (h(N + 1) + h(N)) / 2;
        end
        N = N - 1;
    end
    if N > 1
        h(N) = hR(i);
        A(N) = AR(i);
```

```
        y(N) = yR(i);
        N = N - 1;
    end
    Lay = yR(i) - hR(i) / 2;
    LayNo = nR(i) - lR(i);
end
for G = 1:1:LayersN
    if G == 1
        y2(G) = h(G) / 2;
    elseif G == nR(2)
        y2(G) = Crossection(4);
    elseif G == nR(1)
        y2(G) = Crossection(3);
    else
        y2(G) = y2(G - 1) + h(G - 1) / 2 + h(G) / 2;
    end
    y(G) = (y(G) + y2(G)) / 2;
    AY(G) = y(G) * A(G);
    AI(G) = b * h(G) ^ 3 / 12;
end
Nrs = [LayersN nR(2) nR(1)];
Ge = cat(1, A, y, AY, AI);

function [MC, Prm, SEn, Ge] = A2(Nrs, Ge, Dt, MC, EcU, SEn)
Prm = [true false false];
root = 0;
Count = 0;
while isequal(Prm, [1 0 0]) && Count < 30
    Count = Count + 1;
    [Der, RE, Prm] = Derive(Nrs, Ge, Dt, MC, EcU, SEn, root);
    if Prm(3) == true
        if abs(RE(2)) < abs(RE(4))
            root = RE(1);
        else
            root = RE(3);
        end
        [MC(3),Prm(1),SEn,Ge(6,:)]=A1(Nrs,Ge,MC(1),EcU,SEn,root);
    end
    if isequal(Prm, [1 0 0])
        if Der == 0
            [MC(3),Prm(1),SEn,Ge(6,:)]=A1(Nrs,Ge,MC(1),EcU,SEn, root);
            Prm(3) = true;
        else
            if abs(RE(2)) < abs(RE(4))
                root = RE(1) - RE(2) / Der;
                root1 = RE(1);
                EE1 = RE(2);
            else
                root = RE(3) - RE(4) / Der;
                root1 = RE(3);
                EE1 = RE(4);
            end
```

```
        end
        if isequal(Prm, [1 0 0])
            try
                [MC(3),Prm(1),SENew,EcNew]=A1(Nrs,Ge,MC(1),EcU, SEn,root);
                [Prm(3), error] = RootF(MC, Dt);
                if Prm(3) == true
                    Ge(6, :) = EcNew;
                    SEn = SENew;
                elseif error * EE1 < 0
                    RE = [root1 EE1 root error];
                    Prm(2) = true;
                end
            catch
                root = (root + root1) / 2;
            end
        end
    end
end
if Prm(1) == true && Prm(3) == false
    if Prm(2) == false
        Prm(1) = false;
    else
        st = 0;
        Steps=ceil(log2((max(RE(1),RE(3))-min(RE(1),RE(3)))/Dt));
        while abs(error) > Dt && st < Steps
            root = (RE(1) + RE(3)) / 2;
            try
                [MC(3),Prm(1),SENew,EcNew]=A1(Nrs,Ge,MC(1),EcU, SEn,root);
                [Prm(3), error] = RootF(MC, Dt);
                st = st + 1;
                if Prm(3) == true
                    Ge(6, :) = EcNew;
                    SEn = SENew;
                elseif RE(2) * error > 0
                    RE(1) = root;
                    RE(2) = error;
                else
                    RE(3) = root;
                    RE(4) = error;
                end
            catch
                if abs(RE(2)) <= abs(RE(4))
                    root = RE(1);
                else
                    root = RE(3);
                end
                [MC(3),Prm(1),SENew,EcNew]=A1(Nrs,Ge,MC(1),EcU, SEn,root);
                Prm(3) = RootF(MC, Dt);
                break
            end
        end
        if Prm(1) == true && Prm(3) == false
```

```
            Prm(1) = false;
        end
    end
    Ge(6, :) = EcNew;
    SEn = SENew;
end

function [Der, RE, Prm] = Derive(Nrs, Ge, Dt, MC, EcU, SEn, root)
Prm = [true false false];
Step = 0.1;
D0 = zeros(1, 5);
D = zeros(1, 5);
RE = zeros(1, 4);
for ind = 1:1:5
    if isequal(Prm, [1 0 0])
        D0(ind) = root + Step * (ind - 3);
        try
            [MC(3),Prm(1)]=A1(Nrs,Ge,MC(1),EcU,SEn,D0(ind));
            [Prm(3), D(ind)] = RootF(MC, Dt);
            if Prm(3) == true
                RE = [D0(ind) D(ind) D0(ind) D(ind)];
            elseif ind > 1
                if D(ind) * D(ind - 1) < 0
                    Prm(2) = true;
                    RE = [D0(ind - 1) D(ind - 1) D0(ind) D(ind)];
                end
            end
        catch
            Prm(1) = false;
        end
    end
end
if isequal(Prm, [1 0 0])
    Der = (- D(5) + 8 * D(4) - 8 * D(2) + D(1)) / (12 * Step);
    RE = [D0(1) D(1) D0(5) D(5)];
else
    Der = 0;
end

function [CNew, Prm, SEn, Ec1]=A1(Nrs, Ge, MOM, EcU, SEn, EcLower)
g = size(SEn);
Precision = 1e-3;
Count = 0;
A = Ge(1, :);
y = Ge(2, :);
AY = Ge(3, :);
AI = Ge(4, :);
fs = Ge(5, :);
Ec = Ge(6, :);
Ec(Nrs(1)) = EcLower;
if A * Ec' == 0
    Yc = 0;
```

```
else
    Yc = (AY * Ec') / (A * Ec');
end
EI = (AI + A .* (y - Yc) .^ 2) * Ec';
error = 1;
Ec1 = Ec;
eps = zeros(1, Nrs(1));
sigma = zeros(1, Nrs(1));
Err = zeros(1, Nrs(1));
while abs(error) > Precision && Count < 1000
    Count = Count + 1;
    SEn(2, g(2) + 1) = MOM / EI * (y(Nrs(1)) - Yc);
    SEn(1, g(2) + 1) = SEn(2, g(2) + 1) * EcLower;
    for N = 1:1:Nrs(1)
        eps(N) = MOM / EI * (y(N) - Yc);
        if N == Nrs(2) || N == Nrs(3)
            sigma(N) = Steel(eps(N), fs(N), Ec(N));
        elseif N == Nrs(1)
            sigma(N) = SEn(1, g(2) + 1);
        elseif y(N) <= Yc
            sigma(N) = Compressive(eps(N), fs(N), EcU);
        elseif y(N) > Yc
            sigma(N) = Tensile(eps(N), SEn');
        else
            sigma(N) = 0;
        end
        if N == Nrs(1)
            Ec1(N) = EcLower;
        elseif eps(N) == 0
            Ec1(N) = Ec(N);
        else
            Ec1(N) = sigma(N) / eps(N);
        end
        if Ec1(N) == 0
            Err(N) = Ec(N);
        else
            Err(N) = (Ec1(N) - Ec(N)) / abs(Ec1(N));
        end
    end
    error = max(abs(max(Err)), abs(min(Err)));
    Ec = Ec1;
    if A * Ec1' == 0
        Yc = 0;
    else
        Yc = (AY * Ec1') / (A * Ec1');
    end
    EI = (AI + A .* (y - Yc) .^ 2) * Ec1';
end
if abs(error) > Precision
    Prm = false;
else
    Prm = true;
```

```
end
CNew = MOM / EI;

function sigma = Compressive(eps, fcm, Ec)
fck = fcm - 8;
if fck < 50
    eps_cu1 = -3.5e-3;
else
    eps_cu1 = -2.8e-3 - 27e-3 * ((98 - fcm) / 100) ^ 4;
end
if abs(eps) > abs(eps_cu1)
    sigma = 0;
else
    eps_c1 = -0.7e-3 * fcm ^ 0.31;
    eta = eps / eps_c1;
    k = Ec * abs(eps_c1) / fcm;
    sigma=sign(eps)*fcm*(k*eta-eta^2)/(1+(k-2)*eta);
end

function sigma = Steel(eps, fs, Es)
sigma = eps * Es;
if abs (eps) > abs (fs / Es)
    sigma = fs * sign (eps);
end

function sigma = Tensile(eps, SE)
n = size(SE);
i = 1;
while eps > SE(i, 2)
    i = i + 1;
    if i > n(1)
        i = n(1);
        break
    end
end
sigma=(SE(i,1)*(eps-SE(i-1,2))+SE(i-1,1)*(SE(i,2)-eps))/(SE(i,2)-SE(i-1,2));

function [R, Error] = RootF(MC, Dt)
if MC(2) == 0
    Error = MC(3);
else
    Error = (MC(2) - MC(3)) / abs(MC(2));
end
if abs(Error) > Dt
    R = false;
else
    R = true;
end

function SEAver = Hardy(SE, N2)
ind = 1;
N2 = N2 * 5;
```

```
if rem(N2, 2) == 0
    Pts = N2 + 1;
else
    Pts = N2;
end
Length = size(SE);
NPts = 3 * Pts;
SEAver = zeros(Length(1) - NPts + 1, 2);
for X = 1:1:(Length(1) - NPts)
    ind = ind + 1;
    sum = zeros(3, 2);
    for XX = 1:1:Pts
        sum=sum+cat(1,SE(X+XX,:),SE(X+XX+Pts,:),SE(X+XX+2*Pts,:));
    end
    SEAver(ind,:)=(sum(2,:)-(sum(3,:)-2*sum(2,:)+sum(1,:))*(Pts^2-1)/(24*Pts^2))/Pts;
end
```

To start *inverse* procedure using *MATLAB*, the following text should be written in the command line:

```
SigmaEpsilonAverage = Inverse('Crossection', 'MomentCurvature',
100, 5, 0.00001, 1);
```

Here 100 indicates the number of layers in the *Layer* section model (recommended to be not less than 50); 5 defines the number of *Monte-Carlo* generations (should be taken as odd number, see Section 2.5.3); 0,00001 is the tolerance; 1 is the number of generated sets. It is assumed from the condition: $n \approx N_{\text{tot}}/N_{\text{set}}$ were N_{tot} is the total number of test points, N_{set} is the number of test points in each set recommended to by taken between 20 and 30.

Annex C. Measurements of Curvature and Deflection of the Beam Specimens

As mentioned, the beams were tested under a four-point loading. The loading scheme and the gauge positioning are shown in Fig. 3.9. The testing equipment acting on the beam weighed 232 kg. The latter summed up with the beam's own weight has in the mid-span induced a 3,5 kNm bending moment.

Section C.1 presents concrete surface strains measured at test. The strains were measured throughout the length of the pure bending zone on a 200 mm gauge length, using 0,001 mm mechanical gauges. As shown in Fig. 3.9 (view 'A'), four continuous gauge lines were located at different depths. The two extreme gauge lines were placed along the top and the bottom reinforcement. Measured strains were averaged along each gauge line.

Section C.2 presents deflections of the beams measured at test. To measure deflections, linear variable differential transducers (*L* 1-*L* 8, see Fig. 3.9) were placed beneath the soffit of each of the beam at the load position. Deflections were recorded automatically.

C.1. Curvatures of the Beams

S-1	1st layer's displacement, mm					2nd layer's displacement, mm					3rd layer's displacement, mm					4th layer's displacement, mm					Results	
D_p, mm	201,0	199,7	200,5	201,0	200,0	200,0	200,2	200,5	200,0	200,5	200,5	200,2	200,0	201,0	200,0	200,0	201,0	200,2	200,5	200,0	M_i,	κ,
N, kN	**D 1-1**	**D 1-2**	**D 1-3**	**D 1-4**	**D 1-5**	**D 2-1**	**D 2-2**	**D 2-3**	**D 2-4**	**D 2-5**	**D 3-1**	**D 3-2**	**D 3-3**	**D 3-4**	**D 3-5**	**D 4-1**	**D 4-2**	**D 4-3**	**D 4-4**	**D 4-5**	kNm	km^{-1}
0,13	0,130	0,250	0,150	0,201	0,200	0,570	0,550	0,600	0,600	0,570	0,900	0,930	1,000	1,030	1,070	1,000	1,050	1,100	1,070	1,000	3,390	0,129
5,1	0,132	0,252	0,152	0,201	0,201	0,571	0,551	0,601	0,601	0,570	0,899	0,929	0,999	1,029	1,069	0,998	1,050	1,099	1,070	0,998	5,873	0,175
7,2	0,133	0,253	0,154	0,203	0,202	0,572	0,552	0,602	0,602	0,569	0,899	0,928	0,999	1,028	1,068	0,997	1,047	1,097	1,068	0,997	6,926	0,239
9,3	0,134	0,254	0,155	0,204	0,204	0,572	0,552	0,602	0,603	0,569	0,898	0,926	0,998	1,027	1,067	0,995	1,045	1,096	1,067	0,996	7,955	0,290
11,3	0,136	0,255	0,156	0,206	0,206	0,573	0,553	0,603	0,604	0,568	0,898	0,923	0,997	1,026	1,067	0,995	1,040	1,095	1,066	0,995	8,969	0,333
13,3	0,137	0,257	0,158	0,207	0,207	0,573	0,553	0,604	0,604	0,568	0,897	0,921	0,996	1,023	1,067	0,994	1,036	1,094	1,062	0,994	9,971	0,425
15,3	0,138	0,259	0,159	0,208	0,209	0,574	0,554	0,604	0,605	0,567	0,896	0,920	0,995	1,022	1,066	0,992	1,034	1,090	1,059	0,993	10,97	0,502
17,3	0,140	0,260	0,161	0,210	0,211	0,575	0,554	0,605	0,605	0,574	0,895	0,918	0,993	1,021	1,065	0,990	1,032	1,087	1,057	0,992	11,95	0,572
19,2	0,141	0,260	0,162	0,211	0,213	0,575	0,555	0,605	0,606	0,575	0,894	0,915	0,991	1,019	1,064	0,988	1,029	1,083	1,054	0,991	12,94	0,641
21,2	0,143	0,262	0,164	0,213	0,215	0,576	0,555	0,606	0,606	0,575	0,892	0,913	0,989	1,019	1,057	0,985	1,025	1,080	1,054	0,988	13,91	0,730
23,1	0,145	0,264	0,166	0,214	0,217	0,577	0,556	0,607	0,607	0,575	0,890	0,910	0,987	1,017	1,053	0,983	1,022	1,077	1,051	0,973	14,89	0,869
25,1	0,147	0,266	0,168	0,215	0,218	0,577	0,556	0,607	0,607	0,576	0,888	0,907	0,984	1,014	1,050	0,980	1,016	1,073	1,047	0,966	15,86	0,996
27,0	0,148	0,268	0,171	0,218	0,223	0,577	0,556	0,608	0,608	0,577	0,885	0,901	0,981	1,010	1,044	0,977	1,011	1,067	1,041	0,959	16,83	1,155
28,9	0,150	0,270	0,175	0,221	0,226	0,578	0,555	0,609	0,608	0,578	0,883	0,892	0,976	0,998	1,037	0,973	1,000	1,059	1,028	0,948	17,79	1,391
30,9	0,152	0,274	0,181	0,223	0,229	0,578	0,555	0,610	0,608	0,578	0,879	0,879	0,969	0,984	1,029	0,968	0,988	1,046	1,011	0,934	18,75	1,694
32,8	0,154	0,278	0,185	0,226	0,234	0,577	0,554	0,608	0,606	0,576	0,875	0,869	0,952	0,975	1,014	0,963	0,969	1,024	0,995	0,917	19,71	2,078
34,7	0,158	0,280	0,189	0,231	0,237	0,577	0,552	0,606	0,606	0,574	0,873	0,859	0,938	0,961	0,999	0,960	0,953	1,007	0,979	0,892	20,67	2,452
36,6	0,161	0,285	0,192	0,235	0,241	0,572	0,550	0,604	0,606	0,571	0,840	0,851	0,925	0,949	0,982	0,915	0,940	0,989	0,962	0,867	21,63	2,992
38,5	0,166	0,288	0,195	0,238	0,246	0,568	0,548	0,602	0,605	0,568	0,821	0,840	0,913	0,931	0,961	0,885	0,924	0,961	0,937	0,851	22,59	3,520
40,4	0,169	0,290	0,199	0,241	0,249	0,564	0,546	0,600	0,602	0,565	0,803	0,826	0,898	0,906	0,948	0,862	0,913	0,932	0,916	0,837	23,54	3,956
42,3	0,171	0,292	0,202	0,243	0,252	0,560	0,543	0,599	0,598	0,562	0,789	0,813	0,883	0,880	0,944	0,848	0,884	0,905	0,891	0,829	24,49	4,411
44,2	0,174	0,294	0,205	0,245	0,254	0,557	0,540	0,597	0,596	0,560	0,777	0,800	0,862	0,867	0,935	0,838	0,862	0,875	0,873	0,817	25,44	4,819
46,1	0,176	0,295	0,208	0,247	0,257	0,556	0,538	0,595	0,593	0,558	0,768	0,790	0,841	0,860	0,927	0,829	0,847	0,848	0,861	0,809	26,39	5,140
48,0	0,177	0,296	0,210	0,249	0,260	0,553	0,535	0,592	0,590	0,555	0,754	0,775	0,813	0,847	0,919	0,816	0,824	0,813	0,840	0,794	27,34	5,594
49,9	0,179	0,298	0,212	0,251	0,262	0,551	0,532	0,591	0,588	0,553	0,745	0,766	0,797	0,834	0,913	0,808	0,806	0,797	0,827	0,783	28,29	5,891
51,8	0,181	0,300	0,215	0,254	0,264	0,548	0,530	0,590	0,586	0,551	0,732	0,753	0,778	0,822	0,906	0,795	0,785	0,771	0,809	0,769	29,24	6,300
53,7	0,183	0,301	0,217	0,256	0,267	0,545	0,528	0,588	0,584	0,549	0,721	0,741	0,758	0,808	0,899	0,783	0,764	0,744	0,792	0,756	30,18	6,693
55,6	0,184	0,303	0,219	0,258	0,269	0,542	0,526	0,585	0,582	0,547	0,710	0,733	0,739	0,797	0,892	0,773	0,748	0,716	0,776	0,755	31,13	7,006
57,5	0,186	0,305	0,222	0,260	0,271	0,541	0,524	0,582	0,581	0,546	0,700	0,725	0,722	0,784	0,887	0,761	0,735	0,692	0,762	0,749	32,07	7,319
59,4	0,189	0,307	0,224	0,262	0,273	0,539	0,523	0,578	0,580	0,545	0,689	0,717	0,699	0,772	0,879	0,750	0,719	0,662	0,744	0,740	33,02	7,691
63,2	0,191	0,309	0,227	0,264	0,276	0,537	0,522	0,575	0,579	0,544	0,680	0,709	0,684	0,761	0,872	0,739	0,705	0,640	0,730	0,734	34,90	8,001
66,9	0,194	0,313	0,231	0,268	0,280	0,533	0,519	0,569	0,577	0,542	0,660	0,691	0,652	0,740	0,859	0,718	0,678	0,597	0,702	0,719	36,79	8,598
70,7	0,197	0,315	0,234	0,269	0,283	0,528	0,516	0,561	0,575	0,540	0,643	0,674	0,623	0,722	0,847	0,700	0,648	0,557	0,680	0,702	38,67	9,145
74,4	0,201	0,321	0,240	0,276	0,289	0,523	0,514	0,556	0,572	0,538	0,624	0,647	0,591	0,696	0,829	0,678	0,614	0,505	0,646	0,682	40,55	9,892
78,2	0,207	0,326	0,245	0,280	0,295	0,520	0,511	0,550	0,569	0,536	0,603	0,619	0,559	0,678	0,812	0,655	0,572	0,465	0,617	0,660	42,42	10,61
81,9	0,211	0,332	0,252	0,287	0,303	0,516	0,509	0,546	0,567	0,534	0,586	0,590	0,534	0,652	0,793	0,632	0,538	0,422	0,586	0,640	44,30	11,32
85,7	0,214	0,335	0,256	0,291	0,306	0,511	0,505	0,541	0,564	0,531	0,569	0,566	0,505	0,631	0,776	0,611	0,506	0,385	0,559	0,620	46,17	11,92
89,4	0,218	0,339	0,260	0,294	0,311	0,507	0,504	0,535	0,562	0,528	0,556	0,540	0,479	0,613	0,760	0,593	0,477	0,348	0,535	0,600	48,04	12,50
93,2	0,222	0,342	0,265	0,297	0,317	0,503	0,500	0,490	0,559	0,524	0,543	0,509	0,412	0,590	0,738	0,575	0,442	0,320	0,505	0,573	49,91	13,12

Fig. C.1. Surface deformations of beam *S-1* measured at the test

S-1R	1st layer's displacement, mm					2nd layer's displacement, mm					3rd layer's displacement, mm					4th layer's displacement, mm					Results	
l_{D2}, mm	200,5	200,7	200,2	199,5	200,2	200,5	200,0	199,7	200,5	200,5	200,2	201,0	200,0	200,5	200,7	200,5	200,5	200,0	200,2	200,2	*M*,	κ,
N, kN	*D* 1-1	*D* 1-2	*D* 1-3	*D* 1-4	*D* 1-5	*D* 2-1	*D* 2-2	*D* 2-3	*D* 2-4	*D* 2-5	*D* 3-1	*D* 3-2	*D* 3-3	*D* 3-4	*D* 3-5	*D* 4-1	*D* 4-2	*D* 4-3	*D* 4-4	*D* 4-5	kNm	km^{-1}
0,13	0,050	0,050	0,020	0,050	0,200	0,400	0,360	0,519	0,400	0,400	1,090	1,000	0,900	1,000	1,000	1,050	1,000	1,050	1,010	0,780	3,434	0,122
2,9	0,051	0,051	0,020	0,051	0,201	0,400	0,361	0,520	0,401	0,401	1,089	1,000	0,900	1,000	1,000	1,050	0,999	1,050	1,009	0,780	4,818	0,145
5,1	0,052	0,053	0,021	0,053	0,202	0,400	0,362	0,521	0,402	0,401	1,089	1,000	0,900	1,000	1,000	1,049	0,998	1,049	1,008	0,779	5,917	0,195
7,2	0,053	0,053	0,022	0,054	0,204	0,401	0,362	0,521	0,402	0,401	1,087	0,999	0,899	0,999	0,999	1,048	0,997	1,048	1,007	0,779	6,971	0,230
9,3	0,054	0,054	0,023	0,056	0,205	0,401	0,363	0,522	0,403	0,402	1,087	0,999	0,899	0,999	0,999	1,048	0,996	1,047	1,006	0,778	8,000	0,271
11,3	0,055	0,056	0,024	0,057	0,206	0,402	0,364	0,523	0,404	0,402	1,085	0,998	0,898	0,998	0,998	1,046	0,995	1,046	1,005	0,778	9,013	0,313
13,3	0,056	0,057	0,025	0,058	0,208	0,402	0,364	0,523	0,405	0,403	1,084	0,997	0,897	0,998	0,997	1,044	0,994	1,045	1,004	0,777	10,02	0,361
15,3	0,057	0,058	0,027	0,060	0,210	0,403	0,365	0,524	0,406	0,403	1,084	0,997	0,897	0,997	0,997	1,043	0,993	1,044	1,003	0,777	11,01	0,410
17,3	0,059	0,060	0,028	0,061	0,211	0,404	0,366	0,525	0,406	0,405	1,082	0,996	0,896	0,997	0,996	1,042	0,991	1,043	1,002	0,776	12,00	0,460
19,2	0,060	0,061	0,030	0,062	0,212	0,404	0,366	0,526	0,407	0,406	1,082	0,996	0,896	0,996	0,995	1,039	0,990	1,042	1,001	0,776	12,98	0,509
21,2	0,061	0,063	0,031	0,064	0,213	0,405	0,367	0,527	0,408	0,406	1,078	0,995	0,895	0,995	0,994	1,035	0,989	1,041	1,000	0,774	13,96	0,572
23,1	0,063	0,064	0,033	0,066	0,215	0,405	0,368	0,527	0,408	0,406	1,071	0,994	0,894	0,994	0,991	1,030	0,988	1,040	0,999	0,771	14,93	0,650
25,1	0,064	0,066	0,034	0,068	0,218	0,405	0,368	0,528	0,409	0,407	1,068	0,992	0,894	0,994	0,989	1,027	0,985	1,040	0,998	0,769	15,90	0,722
27,0	0,066	0,068	0,036	0,069	0,219	0,406	0,369	0,529	0,410	0,408	1,065	0,989	0,894	0,993	0,986	1,023	0,982	1,040	0,997	0,768	16,87	0,786
28,9	0,068	0,070	0,038	0,071	0,221	0,406	0,370	0,530	0,411	0,409	1,060	0,986	0,893	0,991	0,984	1,021	0,978	1,039	0,994	0,766	17,84	0,871
30,9	0,069	0,072	0,040	0,074	0,223	0,407	0,371	0,530	0,411	0,409	1,054	0,984	0,893	0,989	0,980	1,018	0,973	1,039	0,990	0,763	18,80	0,970
32,8	0,070	0,075	0,042	0,078	0,227	0,407	0,371	0,531	0,413	0,410	1,045	0,980	0,893	0,987	0,973	1,015	0,967	1,039	0,986	0,761	19,76	1,080
34,7	0,072	0,078	0,046	0,090	0,230	0,408	0,372	0,532	0,415	0,410	1,039	0,976	0,893	0,953	0,969	1,013	0,963	1,037	0,934	0,760	20,72	1,417
36,6	0,074	0,081	0,049	0,095	0,234	0,408	0,373	0,532	0,415	0,410	1,039	0,970	0,889	0,939	0,961	1,007	0,953	1,029	0,916	0,756	21,67	1,670
38,5	0,077	0,083	0,053	0,100	0,240	0,408	0,373	0,531	0,413	0,410	1,025	0,964	0,875	0,926	0,948	1,000	0,946	1,003	0,897	0,751	22,63	1,999
40,4	0,080	0,087	0,060	0,104	0,244	0,407	0,370	0,531	0,411	0,405	0,989	0,948	0,851	0,912	0,925	0,955	0,924	0,980	0,877	0,726	23,58	2,618
42,3	0,090	0,090	0,063	0,108	0,247	0,402	0,366	0,529	0,409	0,402	0,963	0,931	0,838	0,900	0,908	0,922	0,893	0,960	0,860	0,692	24,54	3,261
44,2	0,093	0,099	0,067	0,110	0,250	0,395	0,365	0,525	0,405	0,400	0,941	0,888	0,824	0,879	0,895	0,890	0,855	0,939	0,830	0,671	25,49	3,909
46,1	0,094	0,101	0,069	0,112	0,254	0,391	0,355	0,522	0,403	0,396	0,916	0,843	0,811	0,862	0,880	0,878	0,793	0,924	0,809	0,668	26,44	4,391
48,0	0,096	0,103	0,072	0,115	0,255	0,390	0,350	0,519	0,401	0,392	0,885	0,822	0,801	0,851	0,862	0,860	0,762	0,909	0,792	0,658	27,39	4,787
49,9	0,098	0,105	0,074	0,116	0,259	0,388	0,345	0,517	0,399	0,389	0,857	0,796	0,791	0,837	0,840	0,844	0,740	0,895	0,775	0,649	28,34	5,121
51,8	0,100	0,106	0,076	0,119	0,261	0,386	0,341	0,515	0,397	0,386	0,840	0,790	0,782	0,827	0,829	0,826	0,721	0,881	0,761	0,638	29,28	5,470
53,7	0,102	0,108	0,077	0,121	0,263	0,382	0,336	0,512	0,395	0,382	0,831	0,774	0,768	0,812	0,820	0,802	0,702	0,858	0,747	0,622	30,23	5,897
55,6	0,103	0,110	0,078	0,123	0,265	0,378	0,334	0,510	0,392	0,381	0,821	0,764	0,760	0,805	0,814	0,781	0,690	0,846	0,733	0,608	31,17	6,230
57,5	0,104	0,111	0,080	0,124	0,268	0,374	0,331	0,510	0,389	0,379	0,810	0,752	0,754	0,790	0,807	0,765	0,675	0,836	0,715	0,595	32,12	6,553
59,4	0,105	0,113	0,082	0,128	0,269	0,371	0,327	0,510	0,387	0,378	0,796	0,738	0,746	0,776	0,799	0,746	0,656	0,823	0,698	0,581	33,06	6,923
63,2	0,108	0,116	0,086	0,131	0,274	0,368	0,321	0,509	0,384	0,373	0,782	0,718	0,731	0,760	0,791	0,723	0,623	0,799	0,675	0,564	34,95	7,487
66,9	0,111	0,119	0,089	0,135	0,278	0,364	0,314	0,507	0,379	0,370	0,763	0,693	0,711	0,740	0,779	0,690	0,602	0,763	0,649	0,543	36,83	8,109
70,7	0,115	0,121	0,092	0,141	0,282	0,361	0,307	0,505	0,376	0,370	0,741	0,670	0,693	0,722	0,767	0,657	0,575	0,739	0,627	0,522	38,71	8,695
74,4	0,119	0,125	0,095	0,144	0,286	0,358	0,300	0,503	0,373	0,369	0,721	0,649	0,673	0,702	0,751	0,618	0,546	0,712	0,605	0,494	40,59	9,352
78,2	0,123	0,130	0,099	0,148	0,290	0,355	0,296	0,502	0,371	0,368	0,700	0,628	0,658	0,690	0,738	0,581	0,520	0,687	0,585	0,471	42,47	9,967
81,9	0,128	0,134	0,103	0,152	0,305	0,349	0,289	0,500	0,369	0,365	0,686	0,603	0,637	0,673	0,720	0,539	0,487	0,656	0,561	0,441	44,34	10,75
85,7	0,131	0,137	0,108	0,157	0,307	0,340	0,281	0,498	0,364	0,361	0,650	0,572	0,616	0,651	0,703	0,490	0,450	0,623	0,534	0,405	46,21	11,56
89,4	0,135	0,143	0,112	0,161	0,302	0,330	0,272	0,496	0,360	0,358	0,620	–	0,596	0,633	0,681	0,439	–	0,590	0,510	0,371	48,08	12,00
93,2	0,139	0,132	0,118	0,173	–	0,319	–	0,461	0,354	–	–	–	0,570	0,605	–	–	–	–	0,482	–	49,95	12,78

Fig. C.2. Surface deformations of beam *S-1R* measured at the test

S-2	1st layer's displacement, mm					2nd layer's displacement, mm					3rd layer's displacement, mm					4th layer's displacement, mm					Results	
D_p, mm	200,2	199,8	199,8	200,8	200,0	199,5	201,8	199,8	200,0	200,0	200,5	200,0	201,8	199,8	200,0	200,2	200,5	199,8	201,0	200,8	M_z,	κ,
N, kN	*D* 1-1	*D* 1-2	*D* 1-3	*D* 1-4	*D* 1-5	*D* 2-1	*D* 2-2	*D* 2-3	*D* 2-4	*D* 2-5	*D* 3-1	*D* 3-2	*D* 3-3	*D* 3-4	*D* 3-5	*D* 4-1	*D* 4-2	*D* 4-3	*D* 4-4	*D* 4-5	kNm	km^{-1}
0,13	0,120	0,200	0,230	0,150	0,200	0,680	0,650	0,600	0,650	0,600	1,050	0,980	0,860	1,100	1,070	1,020	1,060	1,100	0,999	1,050	3,400	0,129
2,9	0,120	0,200	0,230	0,151	0,201	0,681	0,651	0,600	0,651	0,600	1,050	0,980	0,860	1,099	1,069	1,019	1,059	1,099	0,998	1,049	4,784	0,155
5,1	0,122	0,202	0,232	0,153	0,203	0,681	0,651	0,600	0,652	0,601	1,049	0,978	0,860	1,099	1,069	1,018	1,058	1,097	0,998	1,048	5,884	0,216
7,2	0,123	0,203	0,233	0,154	0,204	0,682	0,652	0,600	0,652	0,602	1,049	0,978	0,861	1,099	1,069	1,017	1,058	1,096	0,997	1,047	6,937	0,254
9,3	0,124	0,204	0,234	0,155	0,205	0,682	0,653	0,600	0,653	0,602	1,049	0,978	0,859	1,099	1,068	1,016	1,057	1,095	0,996	1,045	7,966	0,297
11,3	0,125	0,205	0,236	0,157	0,207	0,683	0,654	0,601	0,654	0,602	1,049	0,978	0,858	1,098	1,068	1,015	1,056	1,094	0,996	1,045	8,979	0,340
13,3	0,127	0,207	0,237	0,159	0,208	0,683	0,654	0,601	0,655	0,603	1,048	0,977	0,857	1,098	1,068	1,014	1,055	1,092	0,995	1,044	9,982	0,397
15,3	0,128	0,208	0,239	0,160	0,209	0,684	0,655	0,601	0,656	0,603	1,048	0,977	0,856	1,097	1,067	1,013	1,055	1,090	0,993	1,043	10,98	0,444
17,3	0,130	0,209	0,240	0,162	0,211	0,685	0,656	0,602	0,656	0,604	1,047	0,977	0,855	1,097	1,067	1,012	1,054	1,088	0,992	1,042	11,96	0,500
19,2	0,131	0,210	0,242	0,164	0,212	0,685	0,657	0,602	0,657	0,605	1,047	0,976	0,853	1,096	1,066	1,010	1,054	1,085	0,990	1,041	12,95	0,559
21,2	0,133	0,212	0,244	0,165	0,214	0,686	0,657	0,603	0,658	0,606	1,046	0,976	0,851	1,096	1,066	1,007	1,053	1,082	0,989	1,040	13,92	0,631
23,1	0,135	0,214	0,245	0,167	0,215	0,686	0,658	0,604	0,659	0,607	1,045	0,976	0,850	1,094	1,065	1,002	1,053	1,078	0,986	1,038	14,90	0,719
25,1	0,137	0,216	0,247	0,169	0,217	0,687	0,659	0,605	0,660	0,608	1,042	0,976	0,846	1,093	1,064	0,994	1,054	1,073	0,984	1,036	15,87	0,821
27,0	0,139	0,218	0,250	0,169	0,219	0,687	0,659	0,605	0,660	0,608	1,041	0,975	0,842	1,091	1,063	0,984	1,059	1,065	0,988	1,028	16,84	0,927
28,9	0,142	0,220	0,252	0,173	0,221	0,688	0,659	0,605	0,661	0,609	1,034	0,975	0,837	1,090	1,062	0,975	1,062	1,056	0,988	1,023	17,80	1,057
30,9	0,144	0,222	0,254	0,176	0,223	0,688	0,659	0,605	0,662	0,610	1,027	0,975	0,828	1,088	1,057	0,964	1,064	1,046	0,987	1,017	18,76	1,198
32,8	0,147	0,225	0,258	0,181	0,226	0,688	0,659	0,605	0,663	0,611	1,016	0,976	0,819	1,080	1,052	0,945	1,066	1,033	0,975	1,005	19,72	1,483
34,7	0,150	0,227	0,261	0,185	0,230	0,688	0,659	0,604	0,662	0,611	1,000	0,977	0,807	1,065	1,032	0,912	1,072	1,015	0,955	0,995	20,68	1,832
36,6	0,154	0,233	0,264	0,189	0,235	0,685	0,659	0,602	0,661	0,609	0,979	0,978	0,797	1,054	1,009	0,880	1,072	1,000	0,940	0,943	21,64	2,376
38,5	0,158	0,237	0,268	0,192	0,239	0,682	0,658	0,599	0,659	0,608	0,961	0,967	0,789	1,037	1,000	0,860	1,054	0,989	0,938	0,922	22,60	2,730
40,4	0,161	0,240	0,271	0,197	0,244	0,679	0,655	0,598	0,652	0,607	0,949	0,948	0,781	0,990	1,003	0,840	1,026	0,976	0,934	0,885	23,55	3,202
42,3	0,164	0,243	0,275	0,201	0,249	0,675	0,653	0,596	0,645	0,603	0,932	0,936	0,771	0,925	0,995	0,820	1,012	0,957	0,937	0,807	24,50	3,767
44,2	0,168	0,245	0,278	0,204	0,252	0,672	0,652	0,596	0,643	0,603	0,913	0,926	0,759	0,919	0,987	0,792	1,004	0,937	0,929	0,786	25,45	4,162
46,1	0,171	0,247	0,280	0,206	0,255	0,666	0,650	0,591	0,639	0,601	0,895	0,918	0,735	0,910	0,978	0,769	0,994	0,907	0,928	0,761	26,40	4,562
48,0	0,173	0,249	0,282	0,209	0,257	0,663	0,649	0,589	0,636	0,601	0,882	0,911	0,721	0,897	0,971	0,751	0,988	0,888	0,927	0,743	27,35	4,844
49,9	0,176	0,252	0,286	0,211	0,260	0,659	0,648	0,586	0,632	0,601	0,866	0,905	0,707	0,887	0,960	0,732	0,978	0,868	0,921	0,716	28,30	5,229
51,8	0,179	0,254	0,288	0,214	0,263	0,657	0,647	0,584	0,630	0,601	0,857	0,900	0,702	0,874	0,953	0,719	0,972	0,853	0,917	0,699	29,25	5,498
53,7	0,181	0,257	0,291	0,216	0,266	0,655	0,645	0,581	0,625	0,600	0,844	0,892	0,684	0,866	0,942	0,702	0,961	0,834	0,909	0,675	30,20	5,861
55,6	0,183	0,259	0,293	0,219	0,268	0,653	0,645	0,580	0,623	0,600	0,834	0,887	0,675	0,856	0,935	0,690	0,954	0,821	0,903	0,659	31,14	6,115
57,5	0,185	0,261	0,296	0,221	0,271	0,650	0,643	0,577	0,620	0,598	0,822	0,880	0,671	0,849	0,922	0,675	0,944	0,804	0,894	0,637	32,09	6,459
59,4	0,187	0,263	0,298	0,223	0,274	0,649	0,642	0,576	0,618	0,598	0,813	0,874	0,651	0,834	0,915	0,661	0,938	0,790	0,888	0,622	33,03	6,706
63,2	0,192	0,267	0,303	0,227	0,279	0,645	0,640	0,573	0,614	0,595	0,793	0,864	0,631	0,817	0,902	0,634	0,924	0,759	0,875	0,589	34,91	7,266
66,9	0,197	0,271	0,308	0,231	0,284	0,641	0,637	0,568	0,610	0,593	0,773	0,852	0,608	0,800	0,889	0,608	0,908	0,727	0,860	0,563	36,80	7,812
70,7	0,201	0,276	0,313	0,236	0,289	0,637	0,634	0,562	0,607	0,591	0,753	0,841	0,582	0,788	0,878	0,582	0,894	0,698	0,844	0,535	38,68	8,356
74,4	0,207	0,280	0,318	0,241	0,294	0,634	0,633	0,559	0,605	0,590	0,733	0,833	0,561	0,775	0,867	0,563	0,880	0,672	0,829	0,511	40,56	8,840
78,2	0,211	0,285	0,323	0,246	0,299	0,632	0,632	0,557	0,604	0,590	0,719	0,826	0,545	0,757	0,859	0,538	0,871	0,643	0,818	0,494	42,43	9,294
81,9	0,218	0,290	0,330	0,251	0,304	0,628	0,631	0,552	0,600	0,589	0,694	0,816	0,517	0,734	0,846	0,508	0,856	0,603	0,798	0,460	44,31	9,957
85,7	0,222	0,295	0,336	0,257	0,310	0,624	0,629	0,543	0,597	0,588	0,671	0,806	0,479	0,705	0,833	0,477	0,843	0,551	0,780	0,434	46,18	10,61
89,4	0,228	0,300	0,345	0,264	0,316	0,619	0,628	0,508	0,591	0,587	0,645	0,796	0,452	0,247	0,819	0,440	0,856	0,468	0,749	0,406	48,05	11,25

Fig. C.3. Surface deformations of beam *S-2* measured at the test

S-2R	1st layer's displacement, mm					2nd layer's displacement, mm					3rd layer's displacement, mm					4th layer's displacement, mm					Results	
l_{D_i}, mm	201,0	199,7	200,5	201,0	200,0	200,0	200,2	200,5	200,0	200,5	200,5	200,2	200,0	201,0	200,0	200,0	201,0	200,2	200,5	200,0	*M*,	κ,
N, kN	***D* 1-1**	***D* 1-2**	***D* 1-3**	***D* 1-4**	***D* 1-5**	***D* 2-1**	***D* 2-2**	***D* 2-3**	***D* 2-4**	***D* 2-5**	***D* 3-1**	***D* 3-2**	***D* 3-3**	***D* 3-4**	***D* 3-5**	***D* 4-1**	***D* 4-2**	***D* 4-3**	***D* 4-4**	***D* 4-5**	kNm	km^{-1}
0,13	0,050	0,050	0,080	0,070	0,040	0,300	0,401	0,520	0,420	0,538	1,000	1,010	1,080	1,100	1,050	1,020	1,052	0,999	1,081	1,080	3,456	0,123
2,9	0,050	0,051	0,082	0,070	0,040	0,300	0,401	0,521	0,421	0,538	1,000	1,010	1,080	1,100	1,050	1,020	1,051	0,999	1,081	1,079	4,840	0,143
5,1	0,051	0,052	0,083	0,071	0,042	0,301	0,401	0,521	0,421	0,539	1,000	1,010	1,080	1,099	1,050	1,019	1,051	0,997	1,081	1,078	5,940	0,184
7,2	0,052	0,053	0,085	0,073	0,044	0,301	0,402	0,522	0,422	0,540	1,000	1,009	1,080	1,099	1,050	1,019	1,051	0,996	1,081	1,077	6,993	0,223
9,3	0,053	0,055	0,086	0,074	0,045	0,302	0,402	0,523	0,422	0,540	1,000	1,009	1,080	1,099	1,050	1,018	1,050	0,996	1,081	1,076	8,022	0,261
11,3	0,053	0,056	0,087	0,076	0,046	0,303	0,403	0,523	0,423	0,541	1,000	1,009	1,079	1,099	1,051	1,018	1,050	0,994	1,080	1,075	9,035	0,296
13,3	0,054	0,057	0,089	0,078	0,051	0,303	0,404	0,524	0,424	0,541	0,999	1,008	1,078	1,098	1,052	1,017	1,050	0,992	1,079	1,073	10,04	0,365
15,3	0,054	0,058	0,090	0,079	0,051	0,304	0,405	0,524	0,424	0,542	0,999	1,008	1,077	1,097	1,052	1,016	1,050	0,990	1,077	1,071	11,03	0,405
17,3	0,055	0,060	0,092	0,080	0,051	0,304	0,405	0,525	0,425	0,543	0,999	1,008	1,076	1,096	1,053	1,014	1,050	0,987	1,075	1,070	12,02	0,462
19,2	0,056	0,061	0,093	0,081	0,051	0,305	0,406	0,526	0,425	0,543	0,998	1,007	1,075	1,095	1,054	1,012	1,050	0,986	1,072	1,068	13,00	0,510
21,2	0,057	0,063	0,095	0,081	0,053	0,306	0,406	0,526	0,426	0,544	0,997	1,007	1,074	1,094	1,055	1,011	1,050	0,985	1,069	1,065	13,98	0,570
23,1	0,058	0,064	0,097	0,084	0,055	0,306	0,407	0,527	0,427	0,545	0,996	1,006	1,073	1,093	1,056	1,009	1,048	0,983	1,067	1,063	14,95	0,647
25,1	0,059	0,065	0,098	0,086	0,056	0,307	0,408	0,527	0,428	0,545	0,996	1,005	1,072	1,091	1,058	1,007	1,047	0,981	1,066	1,060	15,92	0,708
27,0	0,060	0,068	0,102	0,087	0,058	0,307	0,409	0,528	0,428	0,545	0,995	1,005	1,071	1,090	1,040	1,004	1,047	0,979	1,064	1,054	16,89	0,796
28,9	0,061	0,069	0,104	0,089	0,060	0,308	0,409	0,529	0,429	0,546	0,993	1,005	1,069	1,090	1,037	1,002	1,046	0,977	1,063	1,050	17,86	0,865
30,9	0,062	0,071	0,106	0,091	0,061	0,308	0,409	0,530	0,430	0,546	0,992	1,002	1,069	1,089	1,035	1,001	1,040	0,975	1,061	1,042	18,82	0,975
32,8	0,063	0,073	0,108	0,093	0,066	0,308	0,409	0,530	0,430	0,547	0,991	0,999	1,068	1,085	1,026	1,001	1,033	0,974	1,055	1,025	19,78	1,146
34,7	0,064	0,076	0,111	0,096	0,071	0,308	0,409	0,531	0,430	0,547	0,989	0,990	1,068	1,080	1,010	0,997	1,022	0,973	1,045	0,995	20,74	1,428
36,6	0,066	0,080	0,120	0,100	0,075	0,308	0,408	0,532	0,430	0,547	0,987	0,986	1,060	1,067	0,998	0,993	1,016	0,962	1,025	0,990	21,70	1,698
38,5	0,070	0,085	0,128	0,103	0,079	0,300	0,406	0,528	0,427	0,545	0,951	0,986	1,028	1,048	0,986	0,983	1,012	0,923	0,995	0,974	22,65	2,171
40,4	0,073	0,089	0,130	0,108	0,083	0,297	0,404	0,523	0,425	0,541	0,939	0,981	1,019	1,040	0,977	0,929	1,000	0,898	0,961	0,948	23,61	2,877
42,3	0,074	0,093	0,134	0,116	0,091	0,290	0,404	0,521	0,411	0,535	0,922	0,959	1,010	0,990	0,938	0,904	0,956	0,880	0,911	0,910	24,56	3,661
44,2	0,075	0,096	0,138	0,120	0,096	0,287	0,389	0,519	0,408	0,530	0,910	0,927	1,000	0,960	0,914	0,889	0,918	0,862	0,891	0,889	25,51	4,160
46,1	0,077	0,098	0,141	0,123	0,101	0,284	0,383	0,517	0,402	0,527	0,902	0,906	0,990	0,946	0,892	0,874	0,897	0,845	0,874	0,855	26,46	4,633
48,0	0,078	0,100	0,143	0,125	0,104	0,282	0,381	0,514	0,400	0,524	0,896	0,899	0,982	0,935	0,880	0,864	0,886	0,834	0,864	0,837	27,41	4,911
49,9	0,080	0,103	0,146	0,128	0,108	0,281	0,379	0,513	0,395	0,518	0,886	0,888	0,971	0,925	0,855	0,850	0,869	0,817	0,850	0,796	28,36	5,382
51,8	0,081	0,105	0,148	0,131	0,112	0,279	0,376	0,511	0,391	0,514	0,880	0,879	0,962	0,917	0,839	0,837	0,856	0,803	0,841	0,780	29,31	5,690
53,7	0,082	0,107	0,150	0,132	0,115	0,276	0,374	0,510	0,393	0,510	0,871	0,869	0,953	0,908	0,821	0,821	0,843	0,783	0,829	0,756	30,25	6,061
55,6	0,083	0,109	0,153	0,135	0,119	0,274	0,372	0,508	0,385	0,508	0,865	0,859	0,945	0,900	0,810	0,808	0,830	0,776	0,819	0,740	31,20	6,352
57,5	0,085	0,111	0,155	0,137	0,122	0,272	0,370	0,507	0,379	0,505	0,856	0,850	0,936	0,890	0,797	0,794	0,817	0,762	0,806	0,718	32,14	6,700
59,4	0,086	0,112	0,157	0,139	0,123	0,271	0,367	0,505	0,376	0,499	0,850	0,842	0,927	0,883	0,784	0,783	0,806	0,751	0,794	0,699	33,09	6,986
63,2	0,089	0,116	0,161	0,143	0,130	0,268	0,364	0,502	0,372	0,498	0,837	0,828	0,914	0,869	0,760	0,762	0,786	0,730	0,773	0,689	34,97	7,435
66,9	0,091	0,121	0,166	0,148	0,136	0,264	0,360	0,499	0,376	0,486	0,822	0,811	0,896	0,850	0,730	0,737	0,763	0,706	0,749	0,628	36,85	8,153
70,7	0,093	0,124	0,170	0,151	0,141	0,261	0,357	0,495	0,376	0,478	0,810	0,798	0,882	0,835	0,705	0,714	0,745	0,685	0,727	0,598	38,73	8,673
74,4	0,096	0,128	0,173	0,155	0,146	0,257	0,355	0,493	0,375	0,471	0,796	0,784	0,868	0,820	0,684	0,692	0,726	0,666	0,705	0,569	40,61	9,189
78,2	0,100	0,132	0,179	0,160	0,152	0,255	0,351	0,491	0,372	0,466	0,783	0,773	0,854	0,807	0,665	0,672	0,708	0,648	0,683	0,541	42,49	9,714
81,9	0,103	0,136	0,183	0,164	0,158	0,248	0,346	0,484	0,365	0,454	0,760	0,751	0,829	0,779	0,622	0,634	0,681	0,611	0,644	0,465	44,36	10,66
85,7	0,106	0,140	0,187	0,168	0,163	0,244	0,342	0,477	0,359	0,444	0,741	0,735	0,802	0,749	0,588	0,604	0,659	0,574	0,609	0,400	46,23	11,50

Fig. C.4. Surface deformations of beam *S-2R* measured at the test

S-3	1st layer's displacement, mm					2nd layer's displacement, mm					3rd layer's displacement, mm					4th layer's displacement, mm					Results	
D_p, mm	–	200,0	200,0	200,5	200,0	–	199,5	200,5	200,5	200,2	–	199,5	200,5	201,0	200,0	200,0	200,0	201,0	200,0	201,5	200,5	M_z,	κ,
N, kN	*D* 1-1	*D* 1-2	*D* 1-3	*D* 1-4	*D* 1-5	*D* 2-1	*D* 2-2	*D* 2-3	*D* 2-4	*D* 2-5	*D* 3-1	*D* 3-2	*D* 3-3	*D* 3-4	*D* 3-5	*D* 4-1	*D* 4-2	*D* 4-3	*D* 4-4	*D* 4-5	kNm	km^{-1}
0,13	–	0,080	0,080	0,153	0,101	–	0,280	0,250	0,150	0,550	–	–	0,948	0,999	0,899	0,999	0,979	0,998	–	1,029	3,362	0,136
2,9	–	0,080	0,082	0,152	0,101	–	0,281	0,251	0,151	0,550	–	–	0,948	0,999	0,898	0,999	0,978	0,996	–	1,028	4,745	0,160
5,1	–	0,082	0,084	0,153	0,103	–	0,281	0,252	0,151	0,551	–	–	0,946	0,998	0,898	0,998	0,976	0,994	–	1,027	5,845	0,225
7,2	–	0,083	0,085	0,154	0,104	–	0,282	0,252	0,152	0,552	–	–	0,944	0,998	0,898	0,997	0,975	0,991	–	1,026	6,898	0,274
9,3	–	0,085	0,087	0,155	0,105	–	0,282	0,253	0,153	0,552	–	–	0,943	0,997	0,897	0,995	0,974	0,989	–	1,024	7,927	0,339
11,3	–	0,086	0,089	0,156	0,107	–	0,283	0,254	0,154	0,553	–	–	0,941	0,996	0,896	0,994	0,972	0,986	–	1,023	8,941	0,402
13,3	–	0,088	0,091	0,158	0,109	–	0,284	0,254	0,154	0,553	–	0,900	0,939	0,994	0,895	0,992	0,971	0,982	–	1,021	9,944	0,487
15,3	–	0,090	0,094	0,160	0,111	–	0,285	0,255	0,156	0,555	–	0,899	0,935	0,993	0,893	0,991	0,968	0,979	–	1,019	10,94	0,573
17,3	–	0,092	0,096	0,161	0,113	–	0,285	0,256	0,157	0,556	–	0,898	0,934	0,991	0,892	0,988	0,966	0,975	–	1,016	11,93	0,669
19,2	–	0,095	0,099	0,163	0,116	–	0,286	0,258	0,158	0,557	–	0,897	0,931	0,989	0,890	0,984	0,964	0,969	0,950	1,013	12,91	0,798
21,2	–	0,097	0,103	0,166	0,119	–	0,287	0,259	0,159	0,558	–	0,897	0,925	0,986	0,887	0,977	0,959	0,961	0,946	1,007	13,89	0,979
23,1	–	0,102	0,109	0,170	0,123	–	0,288	0,260	0,161	0,560	–	0,896	0,913	0,979	0,880	0,973	0,954	0,943	0,938	0,994	14,86	1,262
25,1	–	0,105	0,114	0,174	0,126	–	0,289	0,260	0,162	0,561	–	0,893	0,907	0,962	0,871	0,961	0,943	0,930	0,927	0,978	15,83	1,583
27,0	–	0,110	0,119	0,183	0,137	–	0,287	0,258	0,164	0,557	–	0,865	0,896	0,935	0,830	0,958	0,912	0,930	0,881	0,910	16,80	2,299
28,9	–	0,115	0,122	0,188	0,140	–	0,285	0,254	0,164	0,555	–	0,845	0,875	0,919	0,813	0,956	0,875	0,911	0,852	0,875	17,76	2,856
30,9	–	0,118	0,127	0,192	0,143	–	0,282	0,250	0,160	0,550	–	0,829	0,855	0,904	0,792	0,942	0,846	0,893	0,821	0,848	18,73	3,403
32,8	–	0,121	0,131	0,195	0,145	–	0,280	0,248	0,157	0,546	–	0,810	0,838	0,869	0,776	0,911	0,825	0,881	0,781	0,829	19,69	3,935
34,7	–	0,124	0,134	0,200	0,152	–	0,276	0,246	0,152	0,541	–	0,796	0,826	0,810	0,772	0,889	0,810	0,866	0,705	0,855	20,65	4,411
36,6	–	0,126	0,137	0,203	0,156	–	0,271	0,244	0,149	0,539	–	0,769	0,812	0,786	0,761	0,848	0,794	0,852	0,670	0,863	21,60	4,846
38,5	–	0,129	0,140	0,206	0,159	–	0,269	0,242	0,144	0,537	–	0,750	0,796	0,764	0,748	0,812	0,781	0,840	0,644	0,856	22,56	5,267
40,4	–	0,131	0,143	0,209	0,162	–	0,268	0,239	0,136	0,536	–	0,738	0,783	0,735	0,738	0,791	0,766	0,828	0,610	0,852	23,51	5,655
42,3	–	0,135	0,146	0,212	0,166	–	0,266	0,236	0,132	0,534	–	0,718	0,764	0,709	0,724	0,759	0,745	0,821	0,585	0,847	24,46	6,063
44,2	–	0,137	0,149	0,214	0,168	–	0,265	0,234	0,129	0,533	–	0,706	0,751	0,689	0,716	0,740	0,730	0,816	0,567	0,842	25,42	6,341
46,1	–	0,141	0,152	0,216	0,171	–	0,265	0,232	0,125	0,530	–	0,692	0,737	0,665	0,706	0,718	0,715	0,810	0,543	0,838	26,37	6,668
48,0	–	0,143	0,155	0,218	0,174	–	0,264	0,230	0,122	0,528	–	0,679	0,725	0,639	0,695	0,698	0,700	0,801	0,518	0,833	27,32	6,997
49,9	–	0,146	0,157	0,219	0,177	–	0,264	0,228	0,118	0,525	–	0,665	0,711	0,616	0,682	0,673	0,682	0,796	0,495	0,828	28,26	7,328
51,8	–	0,148	0,160	0,222	0,179	–	0,264	0,226	0,116	0,523	–	0,654	0,701	0,594	0,675	0,656	0,669	0,791	0,476	0,821	29,21	7,608
53,7	–	0,152	0,164	0,224	0,182	–	0,264	0,224	0,113	0,521	–	0,639	0,686	0,573	0,670	0,631	0,634	0,785	0,455	0,811	30,16	7,970
55,6	–	0,154	0,167	0,226	0,184	–	0,263	0,224	0,110	0,519	–	0,628	0,674	0,554	0,664	0,616	0,639	0,780	0,439	0,800	31,10	8,251
57,5	–	0,158	0,170	0,229	0,187	–	0,263	0,221	0,107	0,518	–	0,612	0,658	0,532	0,656	0,594	0,620	0,775	0,418	0,787	32,05	8,621
59,4	–	0,161	0,172	0,231	0,190	–	0,263	0,220	0,105	0,517	–	0,602	0,648	0,520	0,651	0,580	0,610	0,770	0,404	0,778	32,99	8,872
61,3	–	0,164	0,175	0,233	0,192	–	0,262	0,218	0,102	0,516	–	0,590	0,635	0,489	0,643	0,563	0,595	0,766	0,384	0,768	33,93	9,164
63,2	–	0,168	0,178	0,235	0,195	–	0,262	0,216	0,099	0,514	–	0,578	0,621	0,476	0,633	0,544	0,579	0,759	0,361	0,758	34,88	9,517
65,0	–	0,172	0,181	0,237	0,197	–	0,261	0,214	0,096	0,512	–	0,566	0,607	0,460	0,624	0,524	0,559	0,758	0,341	0,747	35,82	9,851
66,9	–	0,175	0,185	0,240	0,200	–	0,260	0,212	0,094	0,510	–	0,556	0,593	0,437	0,615	0,510	0,546	0,749	0,321	0,738	36,76	10,16
68,8	–	0,177	0,188	0,243	0,204	–	0,260	0,211	0,092	0,509	–	0,546	0,578	0,420	0,607	0,496	0,530	0,743	0,308	0,730	37,70	10,43
70,7	–	0,181	0,190	0,245	0,207	–	0,260	0,210	0,090	0,508	–	0,538	0,568	0,410	0,599	0,482	0,517	0,738	0,294	0,720	38,64	10,71
72,6	–	0,183	0,193	0,247	0,209	–	0,259	0,208	0,088	0,506	–	0,532	0,558	0,393	0,593	0,472	0,507	0,731	0,277	0,713	39,58	10,95
74,4	–	0,185	0,194	0,248	0,212	–	0,259	0,207	0,088	0,504	–	0,526	0,548	0,382	0,583	0,458	0,494	0,727	0,267	0,706	40,52	11,17
76,3	–	0,189	0,198	0,251	0,214	–	0,259	0,207	0,088	0,504	–	0,521	0,537	0,372	0,577	0,450	0,485	0,719	0,256	0,701	41,46	11,39
78,2	–	0,190	0,199	0,252	0,215	–	0,259	0,206	0,088	0,503	–	0,517	0,531	0,370	0,573	0,445	0,480	0,717	0,256	0,698	42,39	11,46
81,9	–	0,196	0,206	0,256	0,222	–	0,258	0,203	0,086	0,500	–	0,505	0,501	0,341	0,557	0,421	0,459	0,685	0,226	0,680	44,27	12,07
85,7	–	0,226	0,224	0,261	0,234	–	0,252	–	0,074	0,489	–	0,484	–	0,294	0,510	0,392	0,438	–	0,183	0,640	46,14	14,02

Fig. C.5. Surface deformations of beam *S-3* measured at the test

S-3R	1st layer's displacement, mm					2nd layer's displacement, mm					3rd layer's displacement, mm					4th layer's displacement, mm					Results	
l_D, mm	200,2	200,0	201,0	200,2	200,0	200,7	200,0	200,0	200,2	200,0	200,0	200,2	200,0	200,2	200,2	–	–	–	–	–	*M*,	κ,
N, kN	*D* 1-1	*D* 1-2	*D* 1-3	*D* 1-4	*D* 1-5	*D* 2-1	*D* 2-2	*D* 2-3	*D* 2-4	*D* 2-5	*D* 3-1	*D* 3-2	*D* 3-3	*D* 3-4	*D* 3-5	*D* 4-1	*D* 4-2	*D* 4-3	*D* 4-4	*D* 4-5	kNm	km^{-1}
0,75	0,079	0,147	0,066	0,212	0,222	0,269	0,181	0,245	0,254	0,298	0,946	0,850	0,969	0,914	0,976	–	–	–	–	–	3,748	0,127
21,2	0,095	0,160	0,087	0,222	0,232	0,276	0,186	0,245	0,258	0,302	0,939	0,840	0,924	0,904	0,970	–	–	–	–	–	13,96	0,904
40,4	0,123	0,186	0,120	0,251	0,259	0,262	0,168	0,188	0,210	0,231	0,923	0,678	0,770	0,804	0,680	–	–	–	–	–	23,59	5,623
42,3	0,124	0,187	0,115	0,247	0,255	0,248	0,161	0,180	0,211	0,229	0,922	0,640	0,632	0,796	0,664	–	–	–	–	–	24,54	6,482
44,2	0,126	0,188	0,117	0,249	0,256	0,248	0,161	0,179	0,210	0,227	0,922	0,636	0,624	0,790	0,671	–	–	–	–	–	25,49	6,599
46,1	0,128	0,190	0,120	0,250	0,259	0,248	0,160	0,176	0,209	0,225	0,920	0,629	0,614	0,784	0,645	–	–	–	–	–	26,44	6,916
48,0	0,130	0,192	0,121	0,253	0,260	0,248	0,160	0,175	0,208	0,224	0,920	0,623	0,601	0,776	0,639	–	–	–	–	–	27,39	7,129
49,9	0,132	0,193	0,122	0,254	0,261	0,247	0,159	0,173	0,207	0,222	0,919	0,616	0,591	0,775	0,631	–	–	–	–	–	28,34	7,308
51,8	0,133	0,194	0,124	0,256	0,262	0,247	0,159	0,171	0,206	0,220	0,918	0,611	0,582	0,766	0,621	–	–	–	–	–	29,29	7,518
53,7	0,134	0,195	0,124	0,256	0,264	0,246	0,158	0,169	0,205	0,219	0,917	0,605	0,574	0,760	0,618	–	–	–	–	–	30,23	7,666
55,6	0,137	0,196	0,127	0,257	0,265	0,245	0,157	0,167	0,204	0,216	0,916	0,601	0,554	0,755	0,604	–	–	–	–	–	31,18	7,942
57,5	0,137	0,198	0,128	0,260	0,266	0,245	0,157	0,166	0,203	0,216	0,915	0,591	0,551	0,747	0,600	–	–	–	–	–	32,12	8,108
59,4	0,139	0,199	0,130	0,262	0,269	0,244	0,156	0,164	0,202	0,214	0,914	0,584	0,539	0,739	0,589	–	–	–	–	–	33,07	8,367
61,3	0,141	0,201	0,131	0,264	0,270	0,243	0,155	0,161	0,200	0,212	0,912	0,575	0,525	0,730	0,580	–	–	–	–	–	34,01	8,634
63,2	0,142	0,203	0,134	0,265	0,271	0,241	0,155	0,157	0,199	0,208	0,911	0,566	0,510	0,722	0,565	–	–	–	–	–	34,95	8,928
65,0	0,143	0,205	0,135	0,266	0,274	0,240	0,154	0,154	0,198	0,206	0,909	0,557	0,495	0,714	0,558	–	–	–	–	–	35,89	9,183
66,9	0,145	0,206	0,137	0,268	0,275	0,239	0,153	0,151	0,196	0,205	0,908	0,549	0,483	0,706	0,546	–	–	–	–	–	36,83	9,439
68,8	0,146	0,209	0,138	0,270	0,276	0,237	0,152	0,149	0,194	0,202	0,905	0,540	0,467	0,696	0,536	–	–	–	–	–	37,77	9,730
70,7	0,148	0,210	0,140	0,271	0,278	0,235	0,152	0,146	0,194	0,200	0,904	0,532	0,453	0,690	0,527	–	–	–	–	–	38,71	9,970
72,6	0,150	0,212	0,141	0,273	0,280	0,233	0,151	0,143	0,191	0,197	0,901	0,525	0,438	0,680	0,516	–	–	–	–	–	39,65	10,27
74,4	0,151	0,214	0,143	0,275	0,281	0,229	0,151	0,138	0,189	0,194	0,898	0,516	0,419	0,670	0,500	–	–	–	–	–	40,59	10,61
76,3	0,153	0,215	0,144	0,277	0,284	0,228	0,150	0,137	0,188	0,194	0,896	0,512	0,408	0,662	0,490	–	–	–	–	–	41,53	10,83
78,2	0,154	0,215	0,145	0,277	0,284	0,227	0,150	0,135	0,187	0,191	0,894	0,509	0,401	0,659	0,485	–	–	–	–	–	42,47	10,95
80,1	0,155	0,217	0,147	0,279	0,284	0,225	0,149	0,132	0,185	0,189	0,891	0,499	0,387	0,650	0,474	–	–	–	–	–	43,41	11,23
81,9	0,157	0,219	0,149	0,281	0,287	0,225	0,149	0,130	0,184	0,186	0,889	0,495	0,375	0,640	0,462	–	–	–	–	–	44,34	11,50
83,8	0,161	0,223	0,152	0,283	0,290	0,222	0,149	0,125	0,182	0,183	0,884	0,488	0,349	0,629	0,446	–	–	–	–	–	45,28	11,93
85,7	0,163	0,228	0,157	0,286	0,294	0,217	0,149	0,113	0,179	0,175	0,877	0,479	0,302	0,616	0,415	–	–	–	–	–	46,21	12,60

Fig. C.6. Surface deformations of beam *S-3R* measured at the test

S-4	1st layer's displacement, mm					2nd layer's displacement, mm					3rd layer's displacement, mm					4th layer's displacement, mm					Results	
l_D, mm	199,0	200,5	200,0	200,7	200,0	200,0	199,5	200,5	200,2	200,0	200,0	200,7	200,5	200,0	200,0	201,0	199,3	199,7	200,0	200,0	M_z,	κ,
N, kN	*D* 1-1	*D* 1-2	*D* 1-3	*D* 1-4	*D* 1-5	*D* 2-1	*D* 2-2	*D* 2-3	*D* 2-4	*D* 2-5	*D* 3-1	*D* 3-2	*D* 3-3	*D* 3-4	*D* 3-5	*D* 4-1	*D* 4-2	*D* 4-3	*D* 4-4	*D* 4-5	kNm	km^{-1}
0,13	0,150	0,130	0,100	0,200	0,150	0,271	0,170	0,301	0,270	0,250	1,080	0,631	0,649	0,630	0,730	0,804	0,770	0,850	0,751	0,800	3,390	0,126
2,9	0,152	0,131	0,101	0,200	0,151	0,271	0,171	0,302	0,271	0,250	1,080	0,630	0,648	0,630	0,730	0,802	0,769	0,848	0,750	0,799	4,773	0,175
5,1	0,153	0,133	0,103	0,204	0,153	0,273	0,172	0,302	0,271	0,251	1,079	0,630	0,648	0,629	0,730	0,802	0,768	0,847	0,749	0,799	5,873	0,231
7,2	0,155	0,134	0,104	0,205	0,154	0,273	0,172	0,303	0,273	0,252	1,078	0,630	0,647	0,629	0,729	0,801	0,767	0,846	0,748	0,798	6,926	0,274
9,3	0,156	0,135	0,105	0,206	0,155	0,274	0,172	0,304	0,273	0,253	1,076	0,629	0,646	0,628	0,728	0,800	0,766	0,844	0,746	0,797	7,955	0,320
11,3	0,157	0,135	0,107	0,208	0,157	0,275	0,174	0,305	0,275	0,254	1,075	0,628	0,645	0,628	0,728	0,798	0,764	0,842	0,745	0,797	8,969	0,374
13,3	0,159	0,137	0,109	0,210	0,159	0,276	0,175	0,305	0,275	0,255	1,075	0,627	0,644	0,627	0,727	0,797	0,763	0,840	0,743	0,796	9,971	0,443
15,3	0,161	0,139	0,111	0,212	0,161	0,277	0,176	0,306	0,277	0,256	1,075	0,626	0,642	0,626	0,726	0,795	0,762	0,835	0,742	0,795	10,97	0,522
17,3	0,163	0,140	0,114	0,214	0,163	0,278	0,176	0,307	0,278	0,257	1,073	0,625	0,640	0,624	0,725	0,792	0,760	0,829	0,741	0,794	11,95	0,613
19,2	0,166	0,142	0,117	0,215	0,165	0,279	0,177	0,307	0,279	0,258	1,072	0,623	0,635	0,624	0,723	0,789	0,759	0,819	0,741	0,793	12,94	0,716
21,2	0,168	0,144	0,120	0,219	0,167	0,280	0,178	0,308	0,280	0,259	1,070	0,622	0,626	0,624	0,722	0,782	0,757	0,804	0,741	0,790	13,91	0,877
23,1	0,172	0,146	0,123	0,221	0,170	0,281	0,179	0,308	0,280	0,259	1,051	0,620	0,614	0,619	0,719	0,771	0,755	0,789	0,748	0,783	14,89	1,030
25,1	0,175	0,149	0,127	0,225	0,173	0,282	0,180	0,308	0,280	0,259	1,035	0,619	0,600	0,624	0,710	0,761	0,751	0,760	0,752	0,776	15,86	1,278
27,0	0,180	0,151	0,131	0,233	0,181	0,283	0,181	0,306	0,280	0,258	0,972	0,617	0,584	0,637	0,664	0,745	0,749	0,738	0,759	0,766	16,83	1,507
28,9	0,184	0,153	0,138	0,237	0,185	0,282	0,182	0,305	0,280	0,256	0,850	0,613	0,560	0,639	0,645	0,714	0,747	0,690	0,764	0,743	17,79	1,918
30,9	0,189	0,156	0,142	0,240	0,188	0,279	0,183	0,304	0,280	0,256	0,820	0,600	0,548	0,641	0,631	0,681	0,747	0,664	0,767	0,720	18,75	2,294
32,8	0,194	0,162	0,145	0,242	0,190	0,275	0,183	0,302	0,276	0,254	0,789	0,564	0,544	0,643	0,615	0,656	0,708	0,652	0,771	0,700	19,71	2,721
34,7	0,198	0,168	0,150	0,247	0,195	0,274	0,183	0,302	0,275	0,254	0,768	0,532	0,534	0,644	0,600	0,634	0,684	0,630	0,773	0,685	20,67	3,130
36,6	0,201	0,171	0,154	0,249	0,196	0,272	0,181	0,302	0,273	0,249	0,738	0,517	0,520	0,645	0,587	0,618	0,657	0,611	0,776	0,674	21,63	3,449
38,5	0,209	0,179	0,159	0,252	0,201	0,266	0,166	0,303	0,271	0,242	0,690	0,405	0,509	0,646	0,564	0,610	0,510	0,585	0,779	0,664	22,59	4,281
40,4	0,211	0,181	0,160	0,254	0,204	0,263	0,164	0,304	0,270	0,238	0,647	0,388	0,499	0,647	0,546	0,601	0,499	0,566	0,779	0,655	23,54	4,481
42,3	0,214	0,183	0,163	0,258	0,207	0,260	0,162	0,304	0,268	0,232	0,611	0,369	0,485	0,650	0,525	0,585	0,474	0,539	0,780	0,643	24,49	4,838
44,2	0,217	0,186	0,165	0,258	0,207	0,256	0,160	0,304	0,266	0,229	0,575	0,358	0,474	0,652	0,508	0,572	0,457	0,520	0,781	0,632	25,44	5,087
46,1	0,221	0,189	0,168	0,261	0,211	0,253	0,157	0,305	0,264	0,224	0,542	0,336	0,461	0,654	0,488	0,559	0,434	0,496	0,776	0,619	26,39	5,449
48,0	0,224	0,191	0,171	0,263	0,214	0,252	0,155	0,305	0,262	0,221	0,515	0,313	0,450	0,650	0,470	0,555	0,412	0,480	0,773	0,603	27,34	5,720
49,9	0,227	0,193	0,172	0,265	0,214	0,248	0,152	0,305	0,261	0,218	0,488	0,302	0,440	–	0,458	0,579	0,389	0,474	–	0,586	28,29	6,964
51,8	0,230	0,197	0,176	0,268	0,217	0,245	0,149	0,305	0,260	0,215	0,460	0,276	0,425	–	0,439	0,579	0,359	0,455	–	0,570	29,24	7,324
53,7	0,233	0,198	0,178	0,271	0,218	0,243	0,145	0,305	0,258	0,211	0,432	0,260	0,414	–	0,426	0,580	0,337	0,445	–	0,556	30,19	7,563
55,6	0,235	0,200	0,180	0,273	0,220	0,241	0,143	0,305	0,256	0,208	0,408	0,243	0,402	–	0,412	0,579	0,314	0,436	–	0,543	31,13	7,806
57,5	0,237	0,202	0,182	0,275	0,222	0,239	0,139	0,305	0,254	0,205	0,380	0,224	0,389	–	0,398	0,577	0,288	0,427	–	0,528	32,07	8,077
59,4	0,238	0,204	0,184	0,279	0,224	0,238	0,136	0,306	0,252	0,202	0,371	0,200	0,383	–	0,385	0,580	0,275	0,418	–	0,523	33,02	8,218
61,3	0,242	0,207	0,186	0,280	0,225	0,235	0,133	0,306	0,251	0,200	0,340	0,191	0,368	–	0,375	0,577	0,243	0,419	–	0,505	33,96	8,499
63,2	0,244	0,208	0,189	0,284	0,228	0,233	0,129	0,307	0,250	0,198	0,313	0,173	0,355	–	0,362	0,577	0,214	0,418	–	0,493	34,90	8,730
65,0	0,246	0,210	0,191	0,287	0,230	0,232	0,125	0,307	0,248	0,195	0,300	0,158	0,348	–	0,350	0,575	0,199	0,418	–	0,482	35,85	8,897
68,8	0,250	0,212	0,192	0,291	0,232	0,230	0,120	0,307	0,247	0,192	0,268	0,143	0,330	–	0,330	0,574	0,153	0,425	–	0,468	37,73	9,184
72,6	0,255	0,216	0,198	0,296	0,237	0,226	0,116	0,307	0,244	0,190	0,240	0,100	0,309	–	0,285	–	0,122	0,436	–	0,446	39,61	10,73
76,3	0,260	0,221	0,201	0,303	0,241	0,222	0,111	0,308	0,242	0,187	0,093	0,081	0,290	–	0,251	–	0,095	0,441	–	0,422	41,48	11,00
80,1	0,264	0,225	0,206	0,309	0,245	0,216	0,105	0,302	0,237	0,185	0,045	0,041	0,265	–	0,219	–	0,043	0,425	–	0,389	43,36	11,72

Fig. C.7. Surface deformations of beam *S-4* measured at the test

S-4R	1st layer's displacement, mm				2nd layer's displacement, mm				3rd layer's displacement, mm				4th layer's displacement, mm				Results	
l_D, mm	199,5	201,0	200,2	200,0	200,5	200,2	200,0	200,1	200,7	200,0	201,5	200,2	200,0	200,0	201,0	200,0	201,0	200,0	200,0	200,0	*M*,	κ,
N, kN	*D* 1-1	*D* 1-2	*D* 1-3	*D* 1-4	*D* 1-5	*D* 2-1	*D* 2-2	*D* 2-3	*D* 2-4	*D* 2-5	*D* 3-1	*D* 3-2	*D* 3-3	*D* 3-4	*D* 3-5	*D* 4-1	*D* 4-2	*D* 4-3	*D* 4-4	*D* 4-5	kNm	km^{-1}
0,13	0,249	0,071	0,147	0,126	0,195	0,446	0,391	0,428	0,402	0,444	0,972	0,797	0,750	0,817	0,898	1,000	0,950	1,021	1,004	0,648	3,484	0,119
2,9	0,250	0,071	0,148	0,127	0,197	0,446	0,392	0,429	0,403	0,444	0,971	0,797	0,749	0,817	0,898	1,000	0,949	1,020	1,004	0,649	4,867	0,142
5,1	0,252	0,072	0,150	0,128	0,198	0,446	0,392	0,429	0,404	0,444	0,971	0,797	0,749	0,816	0,898	1,000	0,949	1,019	1,003	0,649	5,967	0,179
7,2	0,253	0,072	0,151	0,129	0,199	0,446	0,392	0,430	0,404	0,444	0,970	0,797	0,748	0,815	0,896	0,997	0,948	1,018	1,001	0,649	7,020	0,223
9,3	0,255	0,073	0,152	0,131	0,201	0,446	0,393	0,431	0,405	0,444	0,969	0,796	0,747	0,815	0,895	0,996	0,947	1,016	1,000	0,648	8,049	0,280
11,3	0,256	0,074	0,153	0,133	0,203	0,447	0,392	0,431	0,406	0,444	0,967	0,796	0,746	0,814	0,895	0,994	0,946	1,014	0,999	0,647	9,063	0,337
13,3	0,258	0,075	0,154	0,135	0,203	0,447	0,392	0,431	0,407	0,444	0,966	0,796	0,745	0,813	0,894	0,992	0,945	1,011	0,998	0,646	10,07	0,395
15,3	0,259	0,076	0,155	0,136	0,204	0,448	0,392	0,432	0,408	0,444	0,965	0,795	0,744	0,813	0,893	0,991	0,944	1,010	0,996	0,645	11,06	0,438
17,3	0,260	0,077	0,156	0,138	0,206	0,449	0,392	0,433	0,409	0,444	0,963	0,795	0,743	0,812	0,892	0,989	0,944	1,007	0,995	0,644	12,05	0,494
19,2	0,262	0,078	0,157	0,140	0,207	0,450	0,392	0,433	0,409	0,445	0,962	0,795	0,741	0,811	0,891	0,987	0,943	1,003	0,995	0,643	13,03	0,554
21,2	0,263	0,079	0,159	0,142	0,209	0,450	0,392	0,433	0,410	0,445	0,960	0,794	0,737	0,810	0,889	0,985	0,943	0,995	0,991	0,642	14,01	0,647
23,1	0,265	0,080	0,160	0,145	0,211	0,451	0,392	0,434	0,411	0,446	0,958	0,794	0,732	0,809	0,887	0,977	0,943	0,988	0,988	0,640	14,98	0,764
25,1	0,267	0,082	0,161	0,148	0,213	0,452	0,392	0,434	0,411	0,446	0,955	0,794	0,728	0,808	0,885	0,970	0,943	0,982	0,986	0,637	15,95	0,878
27,0	0,269	0,084	0,164	0,152	0,215	0,452	0,392	0,434	0,412	0,446	0,948	0,798	0,718	0,807	0,880	0,962	0,943	0,955	0,983	0,634	16,92	1,099
28,9	0,272	0,087	0,170	0,155	0,217	0,453	0,392	0,423	0,412	0,447	0,942	0,800	0,655	0,804	0,877	0,957	0,950	0,872	0,973	0,631	17,88	1,539
30,9	0,276	0,098	0,174	0,158	0,227	0,453	0,392	0,408	0,412	0,428	0,903	0,805	0,610	0,801	0,790	–	0,952	0,790	0,873	0,600	18,85	2,763
32,8	0,290	0,099	0,174	0,171	0,227	0,451	0,392	0,399	0,390	0,419	0,866	0,801	0,579	0,790	0,762	–	0,915	–	0,825	0,505	19,81	3,217
34,7	0,294	0,100	0,174	0,172	0,228	0,447	0,392	0,394	0,384	0,415	0,749	0,777	0,563	0,665	0,746	–	0,885	–	0,793	0,490	20,77	3,635
38,5	0,298	0,101	0,174	0,174	0,232	0,419	0,392	0,386	0,374	0,403	0,709	0,745	0,534	0,633	0,711	–	0,853	–	0,743	0,431	22,68	4,633
40,4	0,299	0,103	0,174	0,175	0,234	0,413	0,392	0,379	0,369	0,397	0,678	0,724	0,514	0,611	0,696	–	0,832	–	0,719	0,408	23,63	5,099
42,3	0,302	0,104	0,177	0,177	0,236	0,411	0,392	0,375	0,366	0,392	0,656	0,713	0,495	0,598	0,680	–	0,818	–	0,702	0,393	24,59	5,438
44,2	0,303	0,105	0,178	0,178	0,237	0,405	0,387	0,373	0,363	0,386	0,638	0,700	0,480	0,583	0,661	–	0,807	–	0,680	0,376	25,54	5,785
46,1	0,305	0,106	0,178	0,181	0,238	0,400	0,384	0,370	0,359	0,382	0,620	0,688	0,464	0,572	0,648	–	0,794	–	0,665	0,361	26,49	6,095
48,0	0,307	0,107	0,179	0,183	0,239	0,397	0,381	0,365	0,357	0,376	0,607	0,675	0,450	0,556	0,632	–	0,784	–	0,644	0,350	27,44	6,397
49,9	0,308	0,108	0,179	0,185	0,240	0,393	0,376	0,359	0,352	0,369	0,597	0,657	0,429	0,536	0,616	–	0,768	–	0,618	0,335	28,39	6,794
53,7	0,311	0,110	0,180	0,189	0,243	0,384	0,369	0,352	0,344	0,358	0,577	0,630	0,396	0,503	0,592	–	0,746	–	0,573	0,311	30,28	7,450
57,5	0,314	0,112	0,182	0,192	0,244	0,377	0,362	0,343	0,335	0,348	0,540	0,600	0,367	0,467	0,573	–	0,726	–	0,545	0,287	32,17	7,951
61,3	0,316	0,114	0,183	0,194	0,246	0,368	0,355	0,335	0,327	0,340	0,510	0,580	0,338	0,432	0,562	–	0,702	–	0,518	0,266	34,06	8,459
65,0	0,318	0,117	0,184	0,196	0,246	0,361	0,350	0,327	0,319	0,329	0,482	0,563	0,308	0,407	0,551	–	0,685	–	0,502	0,244	35,94	8,847
68,8	0,321	0,119	0,185	0,198	0,249	0,353	0,360	0,318	0,310	0,321	0,458	0,540	0,280	0,367	0,534	–	0,667	–	0,463	0,226	37,82	9,370
72,6	0,323	0,121	0,187	0,201	0,250	0,345	0,340	0,313	0,303	0,313	0,434	0,522	0,253	0,341	0,523	–	0,649	–	0,441	0,209	39,70	9,790
76,3	0,326	0,123	0,190	0,203	0,253	0,338	0,335	0,302	0,290	0,304	0,408	0,499	0,223	0,295	0,501	–	0,632	–	0,388	0,186	41,58	10,46

Fig. C.8. Surface deformations of beam *S-4R* measured at the test

C.2. Deflections of the Beams

S-1	Deflection, mm								*M*,	κ,	*S-1*	Deflection, mm								*M*,	κ,
N, kN	*L1*	*L2*	*L3*	*L4*	*L5*	*L6*	*L7*	*L8*	kNm	km^{-1}	N, kN	*L1*	*L2*	*L3*	*L4*	*L5*	*L6*	*L7*	*L8*	kNm	km^{-1}
0,13	0	0	0	0	0	0	0	0	3,390	0,129	49,0	–	4,367	4,397	5,042	5,055	4,330	4,359	0,760	27,82	5,611
4,0	–	0,030	0,120	0,020	0,135	0,010	0,129	-0,020	5,332	0,173	49,9	–	4,445	4,477	5,135	5,144	4,395	4,435	0,769	28,29	5,742
5,1	–	0,038	0,153	0,037	0,174	0,050	0,160	-0,020	5,873	0,171	50,9	–	4,704	4,715	5,432	5,429	4,652	4,708	1,144	28,77	6,015
6,2	–	0,056	0,180	0,046	0,207	0,074	0,175	-0,020	6,404	0,173	51,8	–	4,785	4,797	5,517	5,522	4,740	4,794	1,155	29,24	6,053
8,2	–	0,110	0,184	0,128	0,217	0,112	0,185	-0,011	7,443	0,331	52,8	–	5,029	5,042	5,797	5,791	4,974	5,028	1,230	29,71	6,337
9,3	–	0,130	0,205	0,140	0,252	0,130	0,216	0,000	7,955	0,335	53,7	–	5,149	5,184	5,955	5,936	5,101	5,168	1,246	30,18	6,489
10,3	–	0,143	0,219	0,158	0,286	0,152	0,240	0,001	8,464	0,400	54,7	–	5,411	5,409	6,233	6,235	5,505	5,444	1,306	30,66	6,460
11,3	–	0,167	0,277	0,200	0,320	0,196	0,283	0,019	8,969	0,362	55,6	–	5,485	5,498	6,343	6,350	5,610	5,522	1,338	31,13	6,671
12,3	–	0,215	0,300	0,242	0,367	0,228	0,325	0,022	9,471	0,429	56,6	–	5,688	5,686	6,554	6,545	5,787	5,705	1,340	31,60	6,791
13,3	–	0,246	0,335	0,269	0,388	0,258	0,348	0,035	9,971	0,384	57,5	–	5,770	5,800	6,672	6,664	5,873	5,805	1,354	32,07	6,977
14,3	–	0,278	0,380	0,310	0,435	0,288	0,391	0,044	10,47	0,433	58,4	–	6,046	6,045	6,983	6,975	6,206	6,068	1,426	32,55	7,228
15,3	–	0,306	0,403	0,338	0,476	0,314	0,421	0,050	10,97	0,500	59,4	–	6,146	6,141	7,085	7,070	6,283	6,159	1,443	33,02	7,289
16,3	–	0,345	0,450	0,405	0,514	0,366	0,458	0,064	11,46	0,564	60,3	–	6,329	6,291	7,296	7,280	6,475	6,343	1,335	33,49	7,560
17,3	–	0,377	0,460	0,420	0,545	0,390	0,478	0,070	11,95	0,580	61,3	–	6,425	6,405	7,399	7,394	6,563	6,448	1,340	33,96	7,618
18,2	–	0,418	0,502	0,481	0,580	0,426	0,517	0,073	12,45	0,646	62,2	–	6,658	6,630	7,651	7,643	6,814	6,651	1,368	34,43	7,798
19,2	–	0,452	0,534	0,514	0,620	0,466	0,556	0,080	12,94	0,648	63,2	–	6,743	6,702	7,757	7,726	6,896	6,732	1,399	34,90	7,918
20,2	–	0,501	0,575	0,570	0,680	0,508	0,597	0,088	13,43	0,768	64,1	–	6,848	6,813	7,879	7,870	6,996	6,835	1,410	35,38	8,142
21,2	–	0,510	0,606	0,609	0,705	0,554	0,625	0,098	13,91	0,797	65,0	–	7,013	6,964	8,035	8,031	7,134	6,983	1,439	35,85	8,209
22,2	–	0,572	0,652	0,676	0,765	0,593	0,662	0,112	14,40	0,940	66,0	1,636	7,223	7,189	8,302	8,281	7,347	7,189	1,470	36,32	8,564
23,1	–	0,608	0,694	0,717	0,816	0,640	0,713	0,120	14,89	0,955	66,9	1,655	7,329	7,284	8,411	8,395	7,459	7,288	1,511	36,79	8,635
24,1	–	0,682	0,713	0,795	0,888	0,706	0,776	0,130	15,37	1,106	67,9	1,686	7,435	7,392	8,551	8,522	7,564	7,398	1,539	37,26	8,842
25,1	–	0,730	0,780	0,843	0,935	0,755	0,835	0,130	15,86	1,042	68,8	1,723	7,598	7,550	8,735	8,687	7,728	7,550	1,550	37,73	8,967
26,0	–	0,777	0,821	0,903	0,985	0,805	0,881	0,140	16,34	1,113	69,7	1,796	7,852	7,793	8,961	8,961	8,061	7,810	1,607	38,20	9,007
27,0	–	0,815	0,868	0,948	1,029	0,836	0,921	0,145	16,83	1,158	70,7	1,810	7,973	7,906	9,142	9,085	8,163	7,914	1,636	38,67	9,124
28,0	–	0,918	0,965	1,070	1,157	0,948	1,027	0,160	17,31	1,322	71,6	1,833	8,092	8,037	9,274	9,220	8,278	8,036	1,664	39,14	9,217
28,9	–	0,968	1,037	1,150	1,242	1,011	1,079	0,175	17,79	1,506	72,6	1,870	8,234	8,188	9,457	9,383	8,437	8,195	1,695	39,61	9,380
29,9	–	1,094	1,158	1,298	1,368	1,143	1,213	0,203	18,27	1,580	73,5	1,959	8,525	8,470	9,778	9,692	8,778	8,457	1,750	40,08	9,547
30,9	–	1,131	1,216	1,353	1,447	1,187	1,260	0,214	18,75	1,740	74,4	2,000	8,655	8,612	9,927	9,819	8,906	8,595	1,760	40,55	9,578
31,8	–	1,371	1,442	1,625	1,710	1,418	1,483	0,253	19,23	2,040	75,4	1,995	8,828	8,765	10,11	10,02	9,082	8,746	1,783	41,01	9,809
32,8	–	1,435	1,485	1,683	1,766	1,479	1,533	0,268	19,71	2,060	76,3	2,016	9,002	8,918	10,30	10,19	9,253	8,900	1,824	41,48	9,966
33,7	–	1,649	1,711	1,946	2,017	1,700	1,757	0,310	20,19	2,349	77,3	2,120	9,261	9,180	10,61	10,48	9,571	9,190	1,883	41,95	10,10
34,7	–	1,756	1,809	2,058	2,139	1,805	1,863	0,320	20,67	2,451	78,2	2,145	9,358	9,279	10,71	10,59	9,660	9,268	1,896	42,42	10,17
35,7	–	1,950	2,025	2,307	2,387	2,007	2,070	0,351	21,15	2,804	79,1	2,164	9,449	9,377	10,82	10,70	9,765	9,363	1,918	42,89	10,33
36,6	–	2,090	2,175	2,457	2,527	2,132	2,198	0,380	21,63	2,877	80,1	2,180	9,574	9,504	10,97	10,84	9,903	9,490	1,933	43,36	10,41
37,6	–	2,333	2,390	2,725	2,790	2,359	2,420	0,420	22,11	3,188	81,0	2,266	9,804	9,709	11,23	11,07	10,12	9,706	1,980	43,83	10,65
38,5	–	2,468	2,535	2,876	2,945	2,489	2,545	0,445	22,59	3,342	81,9	2,270	9,905	9,830	11,35	11,21	10,22	9,814	2,012	44,30	10,83
39,5	–	2,743	2,807	3,185	3,243	2,756	2,799	0,485	23,06	3,628	82,9	2,310	10,04	9,963	11,51	11,35	10,36	9,937	2,040	44,76	10,99
40,4	–	2,816	2,885	3,278	3,323	2,831	2,875	0,496	23,54	3,718	83,8	2,326	10,19	10,12	11,69	11,51	10,52	10,09	2,051	45,23	11,07
41,4	–	3,118	3,160	3,610	3,657	3,126	3,160	0,560	24,02	4,069	84,8	2,426	10,58	10,53	12,12	11,98	10,94	10,47	2,119	45,70	11,51
42,3	–	3,179	3,215	3,689	3,722	3,180	3,223	0,566	24,49	4,178	85,7	2,444	10,58	10,49	12,08	11,91	10,94	10,43	2,130	46,17	11,20
43,3	–	3,440	3,480	3,975	4,011	3,425	3,465	0,605	24,97	4,455	86,6	2,450	10,63	10,57	12,19	12,03	11,00	10,53	2,140	46,64	11,54
44,2	–	3,535	3,580	4,106	4,129	3,526	3,569	0,630	25,44	4,651	87,6	2,457	10,75	10,71	12,34	12,17	11,12	10,66	2,180	47,10	11,68
45,2	–	3,715	3,749	4,290	4,319	3,687	3,727	0,651	25,92	4,809	88,5	2,490	10,96	10,92	12,59	12,42	11,35	10,88	2,215	47,57	11,94
46,1	–	3,813	3,839	4,393	4,409	3,778	3,809	0,676	26,39	4,858	89,4	2,510	11,09	11,05	12,75	12,56	11,47	11,01	2,239	48,04	12,10
47,1	–	4,096	4,146	4,747	4,759	4,062	4,106	0,729	26,87	5,333	90,4	2,530	11,26	11,22	12,94	12,75	11,65	11,17	2,265	48,51	12,32
48,0	–	4,190	4,210	4,836	4,850	4,150	4,186	0,740	27,34	5,402	91,3	2,581	11,47	11,43	13,20	13,01	11,86	11,38	2,306	48,97	12,68

Fig. C.9. Deflections of beam *S-1* measured at the test

S-1R	Deflection, mm								M,	κ,	S-1R	Deflection, mm								M,	κ,
N, kN	L1	L2	L3	L4	L5	L6	L7	L8	kNm	km-1	N, kN	L1	L2	L3	L4	L5	L6	L7	L8	kNm	km-1
0,13	0	0	0	0	0	0	0	0	3,434	0,122	48,0	0,620	3,662	3,545	4,173	4,108	3,420	3,546	0,601	27,39	4,899
1,7	0,008	0,073	0,035	0,035	0,060	0,036	0,030	-0,016	4,226	0,157	49,0	0,644	3,875	3,755	4,411	4,358	3,630	3,762	0,653	27,86	5,155
2,9	0,020	0,120	0,040	0,100	0,053	0,080	0,020	-0,020	4,818	0,213	49,9	0,650	3,996	3,882	4,565	4,480	3,756	3,883	0,669	28,34	5,266
4,0	0,030	0,147	0,061	0,130	0,081	0,096	0,022	-0,030	5,376	0,313	50,9	0,650	4,201	4,070	4,797	4,722	3,970	4,109	0,681	28,81	5,499
5,1	0,040	0,168	0,077	0,150	0,104	0,110	0,049	-0,030	5,917	0,328	51,8	0,650	4,339	4,199	4,935	4,844	4,085	4,226	0,733	29,28	5,535
6,2	0,040	0,177	0,113	0,159	0,151	0,122	0,105	-0,012	6,448	0,328	52,8	0,663	4,609	4,483	5,270	5,175	4,395	4,550	0,778	29,76	5,830
7,2	0,040	0,189	0,135	0,165	0,168	0,138	0,127	-0,010	6,971	0,279	53,7	0,674	4,716	4,577	5,365	5,295	4,495	4,640	0,798	30,23	5,904
8,2	0,040	0,206	0,156	0,202	0,193	0,161	0,158	-0,010	7,487	0,337	54,7	0,717	4,880	4,750	5,577	5,497	4,665	4,821	0,835	30,70	6,188
9,3	0,050	0,236	0,170	0,232	0,215	0,196	0,160	-0,010	8,000	0,386	55,6	0,723	4,968	4,827	5,677	5,585	4,740	4,898	0,851	31,17	6,302
10,3	0,060	0,264	0,197	0,264	0,239	0,223	0,188	-0,010	8,508	0,390	56,6	0,740	5,188	5,055	5,919	5,813	4,958	5,116	0,890	31,65	6,413
11,3	0,060	0,290	0,230	0,290	0,289	0,235	0,235	0,000	9,013	0,457	57,5	0,730	5,290	5,154	6,049	5,940	5,053	5,217	0,900	32,12	6,651
12,3	0,070	0,315	0,247	0,314	0,310	0,255	0,265	0,012	9,516	0,453	58,4	0,726	5,415	5,265	6,180	6,075	5,195	5,354	0,925	32,59	6,686
13,3	0,076	0,338	0,273	0,338	0,320	0,277	0,277	0,020	10,02	0,424	59,4	0,730	5,497	5,355	6,305	6,165	5,295	5,468	0,947	33,06	6,773
14,3	0,085	0,351	0,311	0,355	0,351	0,310	0,290	0,020	10,51	0,421	60,3	1,042	5,842	5,683	6,665	6,544	5,634	5,797	1,029	33,53	7,048
15,3	0,096	0,375	0,330	0,388	0,378	0,337	0,317	0,020	11,01	0,468	61,3	1,063	5,915	5,755	6,763	6,639	5,711	5,884	1,030	34,01	7,202
16,3	0,100	0,421	0,350	0,420	0,409	0,355	0,340	0,030	11,50	0,506	62,2	1,080	6,030	5,886	6,895	6,764	5,830	6,008	1,040	34,48	7,246
17,3	0,110	0,450	0,370	0,450	0,420	0,370	0,363	0,030	12,00	0,497	63,2	1,094	6,176	6,029	7,061	6,916	5,977	6,144	1,059	34,95	7,379
18,2	0,119	0,475	0,405	0,485	0,455	0,414	0,395	0,030	12,49	0,504	64,1	1,155	6,458	6,322	7,397	7,259	6,252	6,453	1,130	35,42	7,779
19,2	0,114	0,507	0,427	0,514	0,493	0,439	0,410	0,032	12,98	0,581	65,0	1,160	6,540	6,408	7,490	7,344	6,345	6,524	1,148	35,89	7,824
20,2	0,117	0,516	0,455	0,555	0,518	0,459	0,435	0,048	13,47	0,681	66,0	1,190	6,667	6,535	7,638	7,497	6,464	6,657	1,173	36,36	8,019
21,2	0,120	0,548	0,500	0,578	0,548	0,460	0,457	0,050	13,96	0,697	66,9	1,200	6,787	6,651	7,761	7,625	6,578	6,775	1,191	36,83	8,084
22,2	0,120	0,594	0,514	0,610	0,579	0,514	0,498	0,050	14,45	0,641	67,9	1,240	7,041	6,917	8,048	7,904	6,828	7,033	1,248	37,30	8,291
23,1	0,130	0,616	0,542	0,655	0,612	0,540	0,525	0,060	14,93	0,742	68,8	1,246	7,135	7,013	8,143	8,005	6,916	7,124	1,260	37,77	8,340
24,1	0,130	0,653	0,573	0,697	0,644	0,559	0,564	0,070	15,42	0,790	69,7	1,266	7,245	7,111	8,265	8,125	7,025	7,232	1,265	38,24	8,457
25,1	0,133	0,698	0,615	0,730	0,692	0,620	0,590	0,080	15,90	0,764	70,7	1,295	7,370	7,266	8,443	8,305	7,176	7,383	1,300	38,71	8,724
26,0	0,140	0,725	0,641	0,765	0,741	0,650	0,640	0,089	16,39	0,837	71,6	1,336	7,705	7,546	8,695	8,635	7,565	7,712	1,371	39,18	8,380
27,0	0,140	0,747	0,684	0,820	0,766	0,680	0,680	0,090	16,87	0,886	72,6	1,349	7,772	7,627	8,786	8,716	7,633	7,796	1,388	39,65	8,477
28,0	0,157	0,793	0,722	0,868	0,820	0,720	0,697	0,092	17,35	1,011	73,5	1,373	7,864	7,721	8,889	8,824	7,721	7,875	1,400	40,12	8,611
28,9	0,160	0,834	0,749	0,890	0,840	0,746	0,728	0,100	17,84	0,928	74,4	1,430	7,963	7,833	9,012	8,936	7,825	7,992	1,416	40,59	8,690
29,9	0,160	0,882	0,802	0,952	0,915	0,785	0,790	0,111	18,32	1,070	75,4	1,435	8,121	7,961	9,178	9,100	7,965	8,134	1,445	41,06	8,875
30,9	0,170	0,923	0,835	0,998	0,945	0,831	0,823	0,120	18,80	1,075	76,3	1,440	8,187	8,033	9,256	9,170	8,030	8,214	1,451	41,53	8,900
31,8	0,175	0,984	0,924	1,072	1,009	0,881	0,887	0,130	19,28	1,095	77,3	1,469	8,281	8,119	9,349	9,283	8,115	8,300	1,470	42,00	9,020
32,8	0,173	1,021	0,947	1,117	1,050	0,924	0,913	0,139	19,76	1,182	78,2	1,515	8,471	8,310	9,592	9,503	8,316	8,504	1,525	42,47	9,299
33,7	0,175	1,077	1,014	1,175	1,139	0,990	0,991	0,160	20,24	1,237	79,1	1,595	8,892	8,690	10,02	9,925	8,692	8,885	1,602	42,93	9,568
34,7	0,207	1,112	1,066	1,233	1,193	1,036	1,048	0,160	20,72	1,299	80,1	1,620	9,011	8,807	10,14	10,07	8,805	8,995	1,634	43,40	9,702
35,7	0,253	1,360	1,267	1,519	1,475	1,284	1,312	0,211	21,20	1,651	81,0	1,635	9,100	8,902	10,23	10,15	8,886	9,079	1,662	43,87	9,722
36,6	0,260	1,413	1,325	1,573	1,528	1,316	1,346	0,220	21,67	1,726	81,9	1,680	9,281	9,073	10,42	10,35	9,047	9,243	1,699	44,34	9,900
37,6	0,270	1,541	1,443	1,736	1,688	1,460	1,493	0,243	22,15	1,948	82,9	1,713	9,521	9,306	10,67	10,60	9,255	9,468	1,740	44,81	10,08
38,5	0,278	1,616	1,518	1,831	1,767	1,537	1,572	0,260	22,63	2,028	83,8	1,735	9,641	9,439	10,81	10,74	9,376	9,605	1,775	45,28	10,18
39,5	0,315	1,943	1,803	2,208	2,139	1,825	1,890	0,320	23,11	2,591	84,8	1,760	9,761	9,570	10,95	10,90	9,505	9,756	1,810	45,74	10,33
40,4	0,340	2,085	1,950	2,366	2,296	1,961	2,021	0,335	23,58	2,739	85,7	1,783	9,919	9,710	11,10	11,06	9,653	9,896	1,827	46,21	10,41
41,4	0,425	2,460	2,345	2,783	2,737	2,317	2,388	0,379	24,06	3,181	86,6	1,850	10,35	10,13	11,53	11,48	10,05	10,30	1,919	46,68	10,53
42,3	0,434	2,518	2,413	2,865	2,814	2,377	2,450	0,395	24,54	3,319	87,6	1,872	10,46	10,24	11,67	11,62	10,16	10,42	1,944	47,15	10,73
43,3	0,460	2,781	2,684	3,171	3,112	2,619	2,715	0,468	25,01	3,657	88,5	1,889	10,55	10,33	11,76	11,71	10,23	10,51	1,960	47,61	10,80
44,2	0,496	2,924	2,809	3,315	3,256	2,733	2,813	0,486	25,49	3,850	89,4	1,917	10,69	10,45	11,92	11,87	10,36	10,64	1,980	48,08	10,98
45,2	0,530	3,195	3,087	3,615	3,567	2,981	3,059	0,517	25,96	4,204	90,4	1,966	10,92	10,69	12,16	12,13	10,58	10,86	2,025	48,55	11,21
46,1	0,560	3,319	3,216	3,771	3,709	3,095	3,186	0,540	26,44	4,408	91,3	1,982	11,02	10,79	12,29	12,26	10,67	10,97	2,050	49,02	11,36
47,1	0,614	3,579	3,476	4,091	4,019	3,354	3,472	0,591	26,91	4,801	-	-	-	-	-	-	-	-	-	-	-

Fig. C.10. Deflections of beam *S-1R* measured at the test

S-2	Deflection, mm								*M*,	κ,	*S-2*	Deflection, mm								*M*,	κ,
N, kN	*L1*	*L2*	*L3*	*L4*	*L5*	*L6*	*L7*	*L8*	kNm	km^{-1}	N, kN	*L1*	*L2*	*L3*	*L4*	*L5*	*L6*	*L7*	*L8*	kNm	km^{-1}
0,13	0	0	0	0	0	0	0	0	3,400	0,129	49,0	0,747	4,215	4,200	4,736	4,688	4,151	4,072	0,732	27,83	4,553
2,9	0,000	0,064	0,100	0,060	0,130	0,080	0,090	0,020	4,784	0,222	49,9	0,760	4,303	4,275	4,795	4,754	4,218	4,129	0,753	28,30	4,476
4,0	0,004	0,093	0,110	0,098	0,130	0,092	0,113	0,021	5,342	0,227	50,9	0,760	4,464	4,453	4,989	4,944	4,385	4,282	0,780	28,78	4,694
5,1	0,010	0,112	0,129	0,122	0,130	0,108	0,135	0,030	5,884	0,169	51,8	0,760	4,545	4,512	5,075	5,040	4,464	4,369	0,783	29,25	4,807
6,2	–	0,138	0,166	0,146	0,147	0,136	0,148	0,040	6,414	0,125	52,8	0,855	4,830	4,805	5,389	5,373	4,740	4,645	0,835	29,72	5,136
7,2	–	0,166	0,189	0,189	0,172	0,161	0,155	0,040	6,937	0,231	53,7	0,869	4,926	4,890	5,480	5,488	4,844	4,727	0,866	30,20	5,227
8,2	–	0,178	0,207	0,217	0,205	0,190	0,203	0,040	7,454	0,260	54,7	0,870	5,096	5,041	5,658	5,649	4,978	4,887	0,895	30,67	5,353
9,3	–	0,207	0,234	0,248	0,230	0,222	0,224	0,040	7,966	0,269	55,6	0,880	5,196	5,127	5,754	5,761	5,068	4,970	0,910	31,14	5,463
10,3	0,040	0,251	0,263	0,268	0,244	0,240	0,246	0,053	8,474	0,176	56,6	0,920	5,494	5,448	6,095	5,976	5,377	5,261	0,960	31,61	5,256
11,3	0,035	0,273	0,278	0,291	0,266	0,266	0,265	0,060	8,979	0,193	57,5	0,940	5,565	5,521	6,171	6,067	5,456	5,338	0,983	32,09	5,320
12,3	0,045	0,308	0,317	0,317	0,333	0,319	0,299	0,068	9,482	0,242	58,4	0,971	5,706	5,678	6,349	6,245	5,597	5,505	0,990	32,56	5,534
13,3	0,053	0,325	0,341	0,348	0,348	0,346	0,321	0,070	9,982	0,249	59,4	1,073	5,810	5,769	6,452	6,356	5,691	5,597	1,006	33,03	5,627
14,3	0,060	0,354	0,375	0,397	0,377	0,363	0,350	0,075	10,48	0,345	60,3	1,074	6,075	6,032	6,765	6,660	5,931	5,904	1,075	33,50	5,945
15,3	0,060	0,383	0,397	0,420	0,420	0,384	0,380	0,090	10,98	0,402	61,3	1,086	6,136	6,108	6,853	6,739	6,017	5,976	1,095	33,97	6,020
16,3	0,069	0,414	0,421	0,455	0,444	0,405	0,412	0,090	11,47	0,418	62,2	1,099	6,225	6,187	6,956	6,846	6,075	6,050	1,102	34,44	6,265
17,3	0,070	0,445	0,450	0,505	0,480	0,455	0,447	0,097	11,96	0,474	63,2	1,142	6,330	6,305	7,071	6,951	6,173	6,147	1,117	34,91	6,307
18,2	0,080	0,481	0,489	0,535	0,522	0,491	0,470	0,100	12,46	0,496	64,1	1,187	6,713	6,676	7,525	7,394	6,565	6,591	1,170	35,39	6,711
19,2	0,083	0,518	0,509	0,565	0,548	0,515	0,488	0,107	12,95	0,520	65,0	1,200	6,777	6,747	7,587	7,470	6,641	6,648	1,184	35,86	6,731
20,2	0,097	0,545	0,536	0,609	0,583	0,564	0,518	0,118	13,44	0,571	66,0	1,215	6,866	6,838	7,682	7,564	6,733	6,740	1,206	36,33	6,756
21,2	0,100	0,575	0,580	0,651	0,610	0,589	0,549	0,125	13,92	0,587	66,9	1,220	6,977	6,938	7,805	7,680	6,829	6,825	1,230	36,80	6,931
22,2	0,109	0,617	0,628	0,685	0,675	0,621	0,595	0,131	14,41	0,645	67,9	1,260	7,242	7,203	8,101	7,978	7,127	7,120	1,270	37,27	7,062
23,1	0,110	0,670	0,655	0,745	0,718	0,658	0,638	0,147	14,90	0,736	68,8	1,260	7,329	7,314	8,219	8,083	7,212	7,190	1,290	37,74	7,247
24,1	0,140	0,721	0,690	0,786	0,752	0,729	0,665	0,160	15,38	0,671	69,7	1,294	7,418	7,406	8,325	8,201	7,311	7,295	1,301	38,21	7,374
25,1	0,155	0,755	0,738	0,833	0,798	0,748	0,694	0,160	15,87	0,783	70,7	1,300	7,557	7,555	8,480	8,347	7,438	7,427	1,320	38,68	7,482
26,0	0,144	0,794	0,780	0,894	0,857	0,800	0,749	0,170	16,35	0,887	71,6	1,409	7,912	7,907	8,871	8,757	7,796	7,814	1,393	39,15	7,783
27,0	0,155	0,824	0,811	0,931	0,875	0,821	0,786	0,173	16,84	0,871	72,6	1,420	7,995	7,995	8,965	8,857	7,870	7,886	1,411	39,62	7,927
28,0	0,185	0,903	0,885	1,022	0,981	0,909	0,845	0,190	17,32	1,054	73,5	1,420	8,103	8,080	9,065	8,963	7,955	7,975	1,430	40,09	8,016
28,9	0,195	0,937	0,922	1,078	1,016	0,940	0,878	0,195	17,80	1,153	74,4	1,431	8,149	8,154	9,139	9,018	8,018	8,037	1,440	40,56	8,042
29,9	0,194	1,036	1,015	1,137	1,098	1,007	0,933	0,212	18,28	1,087	75,4	1,470	8,325	8,291	9,303	9,185	8,158	8,185	1,465	41,02	8,163
30,9	0,200	1,095	1,055	1,206	1,145	1,045	0,987	0,220	18,76	1,169	76,3	1,474	8,393	8,375	9,395	9,282	8,238	8,260	1,475	41,49	8,305
31,8	0,214	1,225	1,160	1,322	1,330	1,172	1,103	0,240	19,24	1,418	77,3	1,476	8,436	8,420	9,436	9,323	8,275	8,295	1,481	41,96	8,311
32,8	0,220	1,285	1,247	1,425	1,366	1,247	1,193	0,250	19,72	1,353	78,2	1,480	8,527	8,505	9,530	9,412	8,348	8,375	1,494	42,43	8,387
33,7	0,274	1,430	1,395	1,585	1,525	1,402	1,315	0,278	20,20	1,485	79,1	1,580	8,969	8,914	10,02	9,886	8,765	8,801	1,590	42,90	8,869
34,7	0,285	1,515	1,465	1,679	1,624	1,478	1,381	0,290	20,68	1,660	80,1	1,580	9,050	9,007	10,11	9,999	8,855	8,893	1,592	43,37	8,958
35,7	0,332	1,836	1,795	2,046	1,992	1,829	1,747	0,343	21,16	1,865	81,0	1,580	9,140	9,090	10,21	10,10	8,945	8,982	1,605	43,84	9,060
36,6	0,340	1,880	1,838	2,115	2,056	1,876	1,794	0,350	21,64	2,036	81,9	1,623	9,255	9,220	10,35	10,25	9,072	9,095	1,617	44,31	9,249
37,6	0,360	2,071	2,066	2,332	2,275	2,051	1,961	0,400	22,12	2,256	82,9	1,687	9,482	9,437	10,62	10,50	9,315	9,327	1,667	44,77	9,480
38,5	0,360	2,157	2,131	2,426	2,352	2,122	2,035	0,400	22,60	2,353	83,8	1,703	9,573	9,543	10,72	10,61	9,405	9,420	1,685	45,24	9,540
39,5	0,451	2,385	2,357	2,675	2,598	2,334	2,248	0,436	23,07	2,576	84,8	1,725	9,687	9,660	10,85	10,74	9,513	9,529	1,704	45,71	9,711
40,4	0,480	2,479	2,434	2,758	2,692	2,405	2,328	0,460	23,55	2,638	85,7	1,747	9,860	9,840	11,05	10,95	9,670	9,684	1,717	46,18	10,05
41,4	0,525	2,843	2,816	3,206	3,107	2,815	2,736	0,515	24,03	2,962	86,6	1,779	10,31	10,28	11,57	11,48	10,15	10,16	1,814	46,65	10,53
42,3	0,540	2,908	2,890	3,276	3,179	2,888	2,802	0,520	24,50	2,974	87,6	1,790	10,39	10,36	11,65	11,58	10,22	10,24	1,825	47,11	10,62
43,3	0,580	3,137	3,100	3,506	3,435	3,099	2,987	0,560	24,98	3,245	88,5	1,790	10,51	10,48	11,80	11,72	10,33	10,36	1,848	47,58	10,84
44,2	0,589	3,204	3,193	3,605	3,505	3,162	3,056	0,570	25,45	3,336	89,4	1,808	10,73	10,70	12,06	12,00	10,54	10,57	1,880	48,05	11,28
45,2	0,600	3,515	3,505	3,952	3,870	3,455	3,386	0,623	25,93	3,693	90,4	1,830	11,36	11,33	12,85	12,91	11,18	11,21	1,969	48,52	13,00
46,1	0,610	3,574	3,548	4,043	3,959	3,513	3,450	0,637	26,40	3,967	–	–	–	–	–	–	–	–	–	–	–
47,1	0,645	3,768	3,730	4,247	4,163	3,700	3,631	0,675	26,88	4,111	–	–	–	–	–	–	–	–	–	–	–
48,0	0,662	3,885	3,839	4,355	4,298	3,799	3,739	0,700	27,35	4,218	–	–	–	–	–	–	–	–	–	–	–

Fig. C.11. Deflections of beam *S-2* measured at the test

S-2R	Deflection, mm								*M*,	κ,	*S-2R*	Deflection, mm								*M*,	κ,
N. kN	*L1*	*L2*	*L3*	*L4*	*L5*	*L6*	*L7*	*L8*	kNm	km^{-1}	N. kN	*L1*	*L2*	*L3*	*L4*	*L5*	*L6*	*L7*	*L8*	kNm	km^{-1}
0,13	0	0	0	0	0	0	0	–	3,456	0,123	47,1	0,663	3,754	3,727	4,315	4,213	3,580	3,696	–	26,94	4,721
2,9	0,006	0,030	0,020	0,040	0,030	0,030	0,020	–	4,840	0,203	48,0	0,679	3,832	3,815	4,417	4,319	3,667	3,779	–	27,41	4,881
4,0	0,007	0,053	0,055	0,074	0,086	0,055	0,065	–	5,398	0,310	49,0	0,754	4,180	4,169	4,797	4,697	4,001	4,120	–	27,88	5,161
5,1	0,010	0,068	0,083	0,103	0,097	0,064	0,076	–	5,940	0,341	49,9	0,776	4,275	4,261	4,893	4,803	4,086	4,195	–	28,36	5,270
6,2	0,019	0,090	0,092	0,114	0,119	0,075	0,101	–	6,470	0,337	50,9	0,797	4,496	4,484	5,135	5,030	4,302	4,418	–	28,83	5,381
7,2	0,020	0,120	0,107	0,148	0,145	0,094	0,123	–	6,993	0,406	51,8	0,805	4,586	4,573	5,238	5,126	4,396	4,511	–	29,31	5,448
8,2	0,020	0,132	0,127	0,158	0,166	0,119	0,151	–	7,510	0,363	52,8	0,840	4,873	4,839	5,577	5,466	4,675	4,809	–	29,78	5,905
9,3	0,028	0,170	0,186	0,184	0,194	0,160	0,182	–	8,022	0,236	53,7	0,860	4,972	4,932	5,671	5,550	4,783	4,895	–	30,25	5,845
10,3	0,040	0,182	0,190	0,203	0,215	0,170	0,195	–	8,530	0,321	54,7	0,892	5,147	5,123	5,895	5,778	4,992	5,108	–	30,72	6,074
11,3	0,040	0,207	0,201	0,232	0,237	0,205	0,206	–	9,035	0,359	55,6	0,920	5,235	5,207	6,016	5,878	5,055	5,190	–	31,20	6,326
12,3	0,050	0,249	0,238	0,267	0,271	0,225	0,243	–	9,538	0,365	56,6	0,948	5,530	5,505	6,324	6,212	5,366	5,509	–	31,67	6,443
13,3	0,055	0,260	0,275	0,297	0,306	0,240	0,272	–	10,04	0,445	57,5	0,969	5,605	5,587	6,435	6,292	5,444	5,565	–	32,14	6,628
14,3	0,060	0,266	0,275	0,314	0,314	0,255	0,278	–	10,54	0,485	58,4	1,005	5,779	5,759	6,636	6,505	5,628	5,775	–	32,61	6,803
15,3	0,060	0,315	0,301	0,345	0,356	0,303	0,331	–	11,03	0,428	59,4	1,030	5,874	5,842	6,755	6,616	5,718	5,871	–	33,09	6,997
16,3	0,063	0,336	0,337	0,381	0,391	0,323	0,351	–	11,53	0,516	60,3	1,080	6,190	6,161	7,106	6,981	6,086	6,236	–	33,56	7,125
17,3	0,070	0,355	0,365	0,414	0,418	0,340	0,365	–	12,02	0,599	61,3	1,090	6,278	6,245	7,225	7,068	6,161	6,328	–	34,03	7,272
18,2	0,080	0,422	0,406	0,449	0,462	0,378	0,416	–	12,51	0,521	62,2	1,103	6,355	6,332	7,304	7,160	6,241	6,415	–	34,50	7,290
19,2	0,084	0,437	0,436	0,493	0,482	0,390	0,445	–	13,00	0,605	63,2	1,130	6,464	6,442	7,435	7,281	6,360	6,530	–	34,97	7,394
20,2	0,090	0,445	0,475	0,520	0,514	0,417	0,470	–	13,49	0,645	64,1	1,204	6,855	6,824	7,865	7,719	6,743	6,925	–	35,44	7,768
21,2	0,093	0,478	0,498	0,535	0,535	0,460	0,491	–	13,98	0,545	65,0	1,218	6,917	6,895	7,944	7,818	6,819	7,005	–	35,91	7,897
22,2	0,102	0,506	0,497	0,561	0,571	0,490	0,510	–	14,47	0,643	66,0	1,227	7,002	6,980	8,035	7,900	6,899	7,085	–	36,38	7,930
23,1	0,115	0,544	0,523	0,601	0,611	0,500	0,535	–	14,95	0,768	66,9	1,239	7,111	7,087	8,165	8,015	7,007	7,200	–	36,85	8,028
24,1	0,116	0,550	0,530	0,610	0,602	0,500	0,522	–	15,44	0,766	67,9	1,288	7,345	7,328	8,404	8,255	7,211	7,392	–	37,32	8,206
25,1	0,120	0,601	0,598	0,677	0,674	0,577	0,590	–	15,92	0,794	68,8	1,302	7,438	7,424	8,490	8,362	7,294	7,473	–	37,79	8,274
26,0	0,125	0,624	0,641	0,726	0,715	0,621	0,632	–	16,41	0,856	69,7	1,317	7,544	7,531	8,620	8,480	7,409	7,589	–	38,26	8,377
27,0	0,130	0,641	0,666	0,749	0,743	0,635	0,654	–	16,89	0,897	70,7	1,330	7,677	7,659	8,774	8,634	7,527	7,716	–	38,73	8,577
28,0	0,130	0,682	0,689	0,793	0,791	0,653	0,697	–	17,38	1,016	71,6	1,392	7,955	7,939	9,084	8,944	7,860	8,000	–	39,20	8,723
28,9	0,140	0,729	0,737	0,827	0,826	0,691	0,751	–	17,86	0,921	72,6	1,404	8,041	8,030	9,179	9,035	7,936	8,083	–	39,67	8,797
29,9	0,144	0,795	0,795	0,908	0,889	0,775	0,814	–	18,34	0,956	73,5	1,410	8,114	8,103	9,265	9,125	8,008	8,167	–	40,14	8,899
30,9	0,150	0,834	0,834	0,925	0,927	0,795	0,842	–	18,82	0,921	74,4	1,410	8,219	8,194	9,387	9,252	8,113	8,253	–	40,61	9,123
31,8	0,150	0,850	0,850	0,945	0,951	0,820	0,860	–	19,30	0,945	75,4	1,470	8,427	8,410	9,633	9,488	8,326	8,499	–	41,08	9,281
32,8	0,164	0,915	0,924	1,045	1,040	0,890	0,943	–	19,78	1,123	76,3	1,471	8,487	8,454	9,695	9,556	8,383	8,543	–	41,55	9,397
33,7	0,190	1,090	1,066	1,206	1,202	1,048	1,081	–	20,26	1,185	77,3	1,490	8,565	8,526	9,785	9,644	8,447	8,624	–	42,02	9,512
34,7	0,200	1,123	1,118	1,268	1,280	1,104	1,149	–	20,74	1,328	78,2	1,508	8,679	8,655	9,922	9,774	8,574	8,736	–	42,49	9,617
35,7	0,200	1,298	1,278	1,471	1,466	1,278	1,316	–	21,22	1,530	79,1	1,596	9,158	9,128	10,46	10,30	9,065	9,246	–	42,96	9,986
36,6	0,202	1,331	1,315	1,514	1,499	1,318	1,350	–	21,70	1,546	80,1	1,622	9,269	9,245	10,60	10,44	9,195	9,359	–	43,42	10,17
37,6	0,300	1,682	1,655	1,911	1,878	1,618	1,667	–	22,17	2,034	81,0	1,638	9,384	9,371	10,75	10,60	9,316	9,496	–	43,89	10,36
38,5	0,307	1,747	1,710	1,980	1,946	1,649	1,718	–	22,65	2,179	81,9	1,654	9,534	9,518	10,93	10,77	9,475	9,649	–	44,36	10,60
39,5	0,371	2,091	2,074	2,385	2,323	1,953	2,015	–	23,13	2,686	82,9	1,734	9,872	9,835	11,30	11,13	9,819	9,964	–	44,83	10,87
40,4	0,386	2,154	2,143	2,469	2,402	2,014	2,082	–	23,61	2,823	83,8	1,750	9,970	9,944	11,42	11,27	9,931	10,09	–	45,30	11,01
41,4	0,455	2,604	2,582	3,015	2,945	2,490	2,572	–	24,08	3,468	84,8	1,769	10,11	10,07	11,59	11,43	10,08	10,23	–	45,77	11,22
42,3	0,474	2,682	2,671	3,101	3,037	2,578	2,660	–	24,56	3,494	85,7	1,805	10,27	10,25	11,80	11,64	10,26	10,41	–	46,23	11,48
43,3	0,542	3,094	3,079	3,556	3,491	2,964	3,051	–	25,04	3,937	86,6	1,920	10,76	10,76	12,31	12,18	10,71	10,87	–	46,70	11,91
44,2	0,560	3,184	3,176	3,678	3,605	3,046	3,146	–	25,51	4,148	87,6	1,928	10,83	10,85	12,42	12,29	10,81	10,97	–	47,17	12,04
45,2	0,616	3,512	3,461	4,037	3,928	3,344	3,457	–	25,99	4,437	88,5	2,056	11,59	11,62	13,51	13,37	11,98	12,18	–	47,64	12,92
46,1	0,630	3,605	3,556	4,154	4,048	3,435	3,541	–	26,46	4,656	–	–	–	–	–	–	–	–	–	–	–

Fig. C.12. Deflections of beam *S-2R* measured at the test

S-3	Deflection, mm								*M*,	κ,	*S-3*	Deflection, mm								*M*,	κ,
N, kN	*L 1*	*L 2*	*L 3*	*L 4*	*L 5*	*L 6*	*L 7*	*L 8*	kNm	km^{-1}	N, kN	*L 1*	*L 2*	*L 3*	*L 4*	*L 5*	*L 6*	*L 7*	*L 8*	kNm	km^{-1}
0,13	–	0	0	0	0	0	0	0	3,362	0,136	35,7	–	3,078	3,173	3,835	3,825	3,090	3,216	0,609	21,12	5,220
2,9	–	0,039	0,063	0,093	0,086	0,058	0,070	0,017	4,745	0,392	36,6	–	3,271	3,374	4,059	4,051	3,289	3,409	0,655	21,60	5,445
4,0	–	0,108	0,115	0,133	0,132	0,104	0,116	0,020	5,304	0,309	37,6	–	3,598	3,723	4,449	4,439	3,630	3,755	0,715	22,08	5,776
5,1	–	0,120	0,136	0,166	0,163	0,130	0,148	0,020	5,845	0,383	38,5	–	3,714	3,843	4,586	4,570	3,735	3,865	0,737	22,56	5,929
6,2	–	0,148	0,155	0,199	0,185	0,154	0,190	0,024	6,376	0,376	39,5	–	3,863	3,997	4,775	4,773	3,894	4,034	0,778	23,04	6,140
7,2	–	0,195	0,170	0,257	0,210	0,191	0,196	0,024	6,898	0,502	40,4	–	3,975	4,105	4,915	4,907	4,022	4,144	0,798	23,51	6,278
8,2	–	0,206	0,179	0,278	0,224	0,211	0,209	0,025	7,415	0,532	41,4	–	4,265	4,407	5,260	5,260	4,313	4,456	0,864	23,99	6,565
9,3	–	0,254	0,219	0,309	0,250	0,248	0,238	0,030	7,927	0,454	42,3	–	4,376	4,515	5,385	5,394	4,423	4,575	0,878	24,46	6,645
10,3	–	0,300	0,257	0,355	0,300	0,285	0,259	0,039	8,436	0,554	43,3	–	4,530	4,666	5,569	5,573	4,567	4,725	0,913	24,94	6,900
11,3	–	0,330	0,280	0,400	0,317	0,309	0,289	0,040	8,941	0,589	44,2	–	4,642	4,805	5,734	5,736	4,717	4,863	0,940	25,42	7,114
12,3	–	0,357	0,310	0,423	0,383	0,349	0,314	0,048	9,443	0,698	45,2	–	4,854	5,042	6,026	6,009	4,965	5,125	0,988	25,89	7,274
13,3	–	0,370	0,345	0,448	0,417	0,376	0,359	0,056	9,944	0,698	46,1	–	4,949	5,133	6,145	6,131	5,065	5,225	1,018	26,37	7,438
14,3	–	0,415	0,384	0,493	0,450	0,400	0,416	0,079	10,44	0,676	47,1	–	5,146	5,332	6,362	6,345	5,257	5,425	1,065	26,84	7,569
15,3	–	0,438	0,413	0,515	0,488	0,435	0,434	0,089	10,94	0,709	48,0	–	5,244	5,437	6,489	6,478	5,361	5,533	1,088	27,32	7,743
16,3	–	0,469	0,465	0,583	0,543	0,472	0,464	0,100	11,43	0,900	49,0	–	5,544	5,728	6,847	6,812	5,685	5,876	1,143	27,79	7,761
17,3	–	0,511	0,508	0,605	0,581	0,500	0,516	0,110	11,93	0,807	49,9	–	5,676	5,877	7,014	6,984	5,826	6,013	1,178	28,26	8,023
18,2	–	0,533	0,526	0,639	0,625	0,531	0,545	0,115	12,42	0,923	50,9	–	5,795	5,977	7,159	7,135	5,956	6,147	1,201	28,74	8,132
19,2	–	0,587	0,587	0,707	0,696	0,590	0,617	0,120	12,91	0,987	51,8	–	5,943	6,129	7,328	7,295	6,100	6,295	1,227	29,21	8,263
20,2	–	0,673	0,683	0,795	0,798	0,660	0,689	0,140	13,40	1,102	52,8	–	6,236	6,429	7,693	7,657	6,418	6,616	1,308	29,68	8,605
21,2	–	0,705	0,727	0,870	0,865	0,709	0,730	0,145	13,89	1,336	53,7	–	6,322	6,510	7,792	7,743	6,505	6,703	1,326	30,16	8,652
22,2	–	0,766	0,785	0,934	0,943	0,762	0,807	0,160	14,37	1,400	54,7	–	6,455	6,635	7,948	7,890	6,649	6,851	1,339	30,63	8,681
23,1	–	0,850	0,865	1,033	1,063	0,842	0,888	0,170	14,86	1,629	55,6	–	6,628	6,810	8,155	8,095	6,815	7,020	1,366	31,10	8,980
24,1	–	0,978	0,987	1,179	1,209	0,971	1,018	0,200	15,35	1,780	56,6	–	6,864	7,057	8,436	8,396	7,045	7,248	1,420	31,57	9,481
25,1	–	1,036	1,065	1,245	1,291	1,026	1,078	0,217	15,83	1,871	57,5	–	7,016	7,208	8,604	8,561	7,197	7,407	1,447	32,05	9,536
26,0	–	1,145	1,169	1,395	1,425	1,140	1,210	0,246	16,31	2,087	58,4	–	7,088	7,273	8,684	8,638	7,272	7,474	1,469	32,52	9,452
27,0	–	1,370	1,395	1,686	1,692	1,390	1,450	0,295	16,80	2,438	59,4	–	7,238	7,429	8,856	8,836	7,423	7,635	1,507	32,99	9,751
28,0	–	1,590	1,636	1,986	1,981	1,627	1,705	0,335	17,28	2,887	60,3	–	7,490	7,672	9,092	9,092	7,616	7,819	1,550	33,46	10,32
28,9	–	1,716	1,769	2,154	2,142	1,758	1,834	0,373	17,76	3,163	61,3	–	7,652	7,835	9,294	9,266	7,779	7,998	1,582	33,93	10,28
29,9	–	1,940	1,999	2,404	2,412	1,956	2,049	0,398	18,24	3,509	62,2	–	7,848	8,039	9,525	9,492	7,978	8,188	1,608	34,41	10,57
30,9	–	2,072	2,141	2,581	2,594	2,103	2,206	0,420	18,73	3,791	63,2	–	7,955	8,145	9,648	9,615	8,089	8,304	1,625	34,88	10,63
31,8	–	2,368	2,444	2,926	2,945	2,360	2,459	0,472	19,21	4,012	64,1	–	8,286	8,471	9,993	9,969	8,386	8,600	1,705	35,35	11,09
32,8	–	2,485	2,571	3,079	3,087	2,484	2,596	0,504	19,69	4,132	65,0	–	8,419	8,605	10,15	10,12	8,505	8,738	1,727	35,82	11,22
33,7	–	2,716	2,795	3,384	3,380	2,716	2,831	0,535	20,17	4,685	66,0	–	8,527	8,721	10,27	10,25	8,631	8,839	1,743	36,29	11,45
34,7	–	2,838	2,920	3,535	3,537	2,848	2,972	0,564	20,65	4,860	–	–	–	–	–	–	–	–	–	–	–

Fig. C.13. Deflections of beam *S-3* measured at the test

S-3R	Deflection, mm								*M*,	κ,	*S-3R*	Deflection, mm								*M*,	κ,
N, kN	*L* 1	*L* 2	*L* 3	*L* 4	*L* 5	*L* 6	*L* 7	*L* 8	kNm	km^{-1}	N, kN	*L* 1	*L* 2	*L* 3	*L* 4	*L* 5	*L* 6	*L* 7	*L* 8	kNm	km^{-1}
0,13	–	0	0	0	0	0	0	0	3,437	0,127	68,8	–	8,115	8,427	9,358	9,396	8,422	7,942	1,590	37,77	9,334
11,3	–	0,245	0,263	0,289	0,307	0,249	0,168	0,051	9,016	0,662	69,7	–	8,224	8,546	9,475	9,532	8,552	8,075	1,610	38,24	9,362
21,2	–	0,538	0,572	0,630	0,666	0,549	0,407	0,125	13,96	1,180	70,7	–	8,315	8,624	9,572	9,615	8,623	8,146	1,621	38,71	9,462
30,9	–	1,652	1,732	2,048	2,107	1,859	1,655	0,379	18,80	2,954	71,6	–	8,698	9,009	9,931	9,981	8,927	8,445	1,687	39,18	9,616
40,4	–	3,263	3,445	3,844	3,865	3,392	3,059	0,645	23,59	4,643	72,6	–	8,803	9,129	10,04	10,10	9,015	8,529	1,715	39,65	9,725
41,4	–	5,332	5,538	6,125	6,147	5,492	5,094	1,049	24,06	6,307	73,5	–	9,124	9,464	10,37	10,44	9,277	8,823	1,770	40,12	9,967
42,3	–	5,389	5,596	6,195	6,227	5,562	5,155	1,057	24,54	6,414	74,4	–	9,214	9,550	10,46	10,54	9,357	8,908	1,787	40,59	10,07
43,3	–	5,476	5,687	6,312	6,338	5,640	5,245	1,067	25,02	6,629	75,4	–	9,312	9,665	10,58	10,65	9,474	9,005	1,824	41,06	10,13
44,2	–	5,530	5,753	6,361	6,409	5,688	5,305	1,070	25,49	6,656	76,3	–	9,375	9,725	10,64	10,73	9,538	9,091	1,836	41,53	10,16
45,2	–	5,620	5,852	6,483	6,503	5,787	5,385	1,078	25,97	6,782	77,3	–	9,476	9,846	10,78	10,86	9,655	9,193	1,850	42,00	10,35
46,1	–	5,687	5,923	6,565	6,577	5,863	5,450	1,090	26,44	6,849	78,2	–	9,497	9,849	10,79	10,86	9,670	9,196	1,853	42,47	10,32
47,1	–	5,763	6,014	6,663	6,675	5,950	5,528	1,114	26,92	6,971	79,1	–	9,694	10,04	11,00	11,08	9,860	9,388	1,892	42,94	10,52
48,0	–	5,842	6,108	6,752	6,777	6,021	5,603	1,127	27,39	7,096	80,1	–	9,769	10,11	11,09	11,17	9,943	9,455	1,905	43,41	10,57
49,0	–	5,925	6,196	6,853	6,870	6,097	5,693	1,158	27,86	7,196	81,0	–	9,891	10,23	11,23	11,30	10,06	9,575	1,930	43,87	10,69
49,9	–	5,966	6,241	6,917	6,940	6,154	5,744	1,175	28,34	7,347	81,9	–	9,974	10,31	11,32	11,39	10,15	9,655	1,937	44,34	10,82
50,9	–	6,109	6,377	7,054	7,075	6,285	5,861	1,197	28,81	7,380	82,9	–	10,21	10,55	11,58	11,67	10,38	9,877	1,975	44,81	11,06
51,8	–	6,162	6,433	7,103	7,139	6,332	5,931	1,210	29,29	7,380	83,8	–	10,34	10,66	11,70	11,81	10,50	9,984	1,995	45,28	11,20
52,8	–	6,215	6,509	7,183	7,196	6,394	5,975	1,217	29,76	7,456	84,8	–	10,77	11,11	12,19	12,31	10,94	10,42	2,074	45,75	11,67
53,7	–	6,280	6,574	7,255	7,318	6,475	6,101	1,230	30,23	7,562	85,7	–	10,89	11,26	12,36	12,48	11,07	10,55	2,106	46,21	11,92
54,7	–	6,185	6,476	7,180	7,196	6,409	5,974	1,218	30,70	7,543	–	–	–	–	–	–	–	–	–	–	–
55,6	–	6,490	6,761	7,496	7,540	6,706	6,264	1,275	31,18	7,831	–	–	–	–	–	–	–	–	–	–	–
56,6	–	6,548	6,838	7,566	7,597	6,746	6,313	1,286	31,65	7,891	–	–	–	–	–	–	–	–	–	–	–
57,5	–	6,628	6,925	7,650	7,676	6,828	6,380	1,308	32,12	7,909	–	–	–	–	–	–	–	–	–	–	–
58,4	–	6,760	7,045	7,789	7,829	6,948	6,507	1,315	32,59	8,078	–	–	–	–	–	–	–	–	–	–	–
59,4	–	6,842	7,130	7,882	7,918	7,033	6,591	1,330	33,07	8,136	–	–	–	–	–	–	–	–	–	–	–
60,3	–	6,945	7,247	8,034	8,042	7,152	6,706	1,343	33,54	8,329	–	–	–	–	–	–	–	–	–	–	–
61,3	–	7,028	7,340	8,115	8,137	7,238	6,790	1,356	34,01	8,342	–	–	–	–	–	–	–	–	–	–	–
62,2	–	7,206	7,513	8,336	8,353	7,454	6,995	1,412	34,48	8,549	–	–	–	–	–	–	–	–	–	–	–
63,2	–	7,318	7,625	8,452	8,480	7,572	7,118	1,437	34,95	8,589	–	–	–	–	–	–	–	–	–	–	–
64,1	–	7,505	7,812	8,686	8,709	7,785	7,329	1,478	35,42	8,849	–	–	–	–	–	–	–	–	–	–	–
65,0	–	7,600	7,906	8,783	8,806	7,890	7,418	1,494	35,89	8,854	–	–	–	–	–	–	–	–	–	–	–
66,0	–	7,730	8,028	8,914	8,972	8,035	7,580	1,512	36,36	8,922	–	–	–	–	–	–	–	–	–	–	–
66,9	–	7,824	8,116	9,013	9,045	8,117	7,637	1,521	36,83	8,971	–	–	–	–	–	–	–	–	–	–	–
67,9	–	8,018	8,337	9,254	9,286	8,319	7,842	1,582	37,30	9,254	–	–	–	–	–	–	–	–	–	–	–

Fig. C.14. Deflections of beam *S-3R* measured at the test

S-4	Deflection, mm								*M*,	κ,	*S-4*	Deflection, mm								*M*,	κ,
N, kN	*L 1*	*L 2*	*L 3*	*L 4*	*L 5*	*L 6*	*L 7*	*L 8*	kNm	km^{-1}	N, kN	*L 1*	*L 2*	*L 3*	*L 4*	*L 5*	*L 6*	*L 7*	*L 8*	kNm	km^{-1}
0,13	0	0	0	0	0	0	0	–	3,390	0,126	68,8	1,560	8,826	8,604	9,846	9,835	8,620	8,750	–	37,73	9,254
2,9	0,015	0,105	0,080	0,095	0,100	0,090	0,076	–	4,773	0,206	72,6	1,689	9,435	9,185	10,51	10,49	9,221	9,347	–	39,61	9,743
5,1	0,030	0,130	0,126	0,150	0,141	0,120	0,120	–	5,873	0,297	76,3	1,820	10,06	9,796	11,24	11,21	9,859	10,01	–	41,48	10,48
7,2	0,040	0,196	0,169	0,195	0,184	0,172	0,168	–	6,926	0,232	80,1	1,905	10,73	10,51	12,08	12,05	10,57	10,79	–	43,36	11,44
9,3	0,056	0,247	0,226	0,250	0,250	0,223	0,228	–	7,955	0,277	–	–	–	–	–	–	–	–	–	–	–
11,3	0,070	0,289	0,299	0,323	0,301	0,276	0,277	–	8,969	0,337	–	–	–	–	–	–	–	–	–	–	–
13,3	0,087	0,365	0,340	0,390	0,387	0,350	0,357	–	9,971	0,410	–	–	–	–	–	–	–	–	–	–	–
15,3	0,090	0,433	0,399	0,459	0,458	0,400	0,406	–	10,97	0,519	–	–	–	–	–	–	–	–	–	–	–
17,3	0,110	0,499	0,490	0,555	0,555	0,470	0,497	–	11,95	0,657	–	–	–	–	–	–	–	–	–	–	–
19,2	0,136	0,566	0,568	0,628	0,645	0,538	0,555	–	12,94	0,763	–	–	–	–	–	–	–	–	–	–	–
21,2	0,160	0,670	0,663	0,764	0,748	0,643	0,663	–	13,91	0,897	–	–	–	–	–	–	–	–	–	–	–
23,1	0,190	0,837	0,815	0,946	0,940	0,786	0,829	–	14,89	1,137	–	–	–	–	–	–	–	–	–	–	–
25,1	0,230	1,002	0,976	1,145	1,140	0,972	1,011	–	15,86	1,346	–	–	–	–	–	–	–	–	–	–	–
27,0	0,270	1,275	1,241	1,497	1,468	1,283	1,336	–	16,83	1,717	–	–	–	–	–	–	–	–	–	–	–
28,9	0,298	1,513	1,483	1,780	1,745	1,525	1,576	–	17,79	2,030	–	–	–	–	–	–	–	–	–	–	–
30,9	0,369	1,826	1,775	2,129	2,110	1,805	1,862	–	18,75	2,548	–	–	–	–	–	–	–	–	–	–	–
32,8	0,439	2,266	2,185	2,604	2,586	2,268	2,282	–	19,71	2,885	–	–	–	–	–	–	–	–	–	–	–
34,7	0,465	2,528	2,442	2,928	2,894	2,549	2,565	–	20,67	3,245	–	–	–	–	–	–	–	–	–	–	–
36,6	0,510	2,830	2,732	3,258	3,251	2,853	2,866	–	21,63	3,601	–	–	–	–	–	–	–	–	–	–	–
38,5	0,603	3,415	3,311	3,922	3,895	3,385	3,412	–	22,59	4,348	–	–	–	–	–	–	–	–	–	–	–
40,4	0,654	3,783	3,680	4,320	4,298	3,770	3,817	–	23,54	4,499	–	–	–	–	–	–	–	–	–	–	–
42,3	0,720	4,127	3,976	4,688	4,685	4,092	4,129	–	24,49	4,972	–	–	–	–	–	–	–	–	–	–	–
44,2	0,810	4,625	4,471	5,171	5,179	4,532	4,548	–	25,44	5,174	–	–	–	–	–	–	–	–	–	–	–
46,1	0,864	4,989	4,810	5,594	5,579	4,869	4,920	–	26,39	5,641	–	–	–	–	–	–	–	–	–	–	–
48,0	0,921	5,257	5,082	5,886	5,872	5,147	5,196	–	27,34	5,794	–	–	–	–	–	–	–	–	–	–	–
49,9	1,004	5,715	5,522	6,391	6,360	5,561	5,626	–	28,29	6,283	–	–	–	–	–	–	–	–	–	–	–
51,8	1,045	6,025	5,841	6,725	6,705	5,855	5,927	–	29,24	6,545	–	–	–	–	–	–	–	–	–	–	–
53,7	1,150	6,420	6,214	7,182	7,162	6,264	6,325	–	30,19	7,057	–	–	–	–	–	–	–	–	–	–	–
55,6	1,190	6,750	6,557	7,550	7,520	6,570	6,650	–	31,13	7,352	–	–	–	–	–	–	–	–	–	–	–
57,5	1,270	7,086	6,876	7,918	7,894	6,896	7,000	–	32,07	7,656	–	–	–	–	–	–	–	–	–	–	–
59,4	1,310	7,298	7,091	8,145	8,134	7,112	7,203	–	33,02	7,835	–	–	–	–	–	–	–	–	–	–	–
61,3	1,369	7,712	7,497	8,602	8,585	7,506	7,623	–	33,96	8,195	–	–	–	–	–	–	–	–	–	–	–
63,2	1,427	8,105	7,905	9,051	9,030	7,890	8,027	–	34,90	8,594	–	–	–	–	–	–	–	–	–	–	–
65,0	1,485	8,351	8,141	9,312	9,301	8,142	8,282	–	35,85	8,746	–	–	–	–	–	–	–	–	–	–	–

Fig. C.15. Deflections of beam *S-4* measured at the test

S-4R	Deflection, mm								*M*,	κ,	*S-4R*	Deflection, mm								*M*,	κ,
N, kN	*L 1*	*L 2*	*L 3*	*L 4*	*L 5*	*L 6*	*L 7*	*L 8*	kNm	km^{-1}	N, kN	*L 1*	*L 2*	*L 3*	*L 4*	*L 5*	*L 6*	*L 7*	*L 8*	kNm	km^{-1}
0,13	0	0	0	0	0	0	0	–	3,484	0,119	38,5	0,715	3,705	3,505	4,167	4,023	3,440	3,496	–	22,68	4,588
2,9	0,020	0,070	0,050	0,045	0,030	0,064	0,050	–	4,867	-0,050	39,5	0,760	4,051	3,831	4,572	4,414	3,830	3,896	–	23,16	4,844
4,0	0,040	0,089	0,063	0,075	0,059	0,080	0,050	–	5,426	0,093	40,4	0,770	4,135	3,928	4,667	4,527	3,910	3,997	–	23,63	4,955
5,1	0,060	0,120	0,098	0,105	0,085	0,133	0,070	–	5,967	0,033	41,4	0,822	4,365	4,138	4,929	4,770	4,144	4,238	–	24,11	5,144
6,2	0,063	0,152	0,127	0,130	0,118	0,148	0,103	–	6,498	0,052	42,3	0,830	4,491	4,242	5,055	4,911	4,266	4,347	–	24,59	5,292
7,2	0,063	0,170	0,150	0,150	0,135	0,160	0,140	–	7,020	0,017	43,3	0,887	4,717	4,484	5,346	5,173	4,507	4,583	–	25,06	5,613
8,2	0,057	0,200	0,166	0,192	0,163	0,174	0,156	–	7,537	0,144	44,2	0,904	4,797	4,548	5,413	5,256	4,560	4,672	–	25,54	5,641
9,3	0,060	0,221	0,194	0,220	0,196	0,190	0,179	–	8,049	0,217	45,2	0,920	5,080	4,837	5,696	5,536	4,819	4,914	–	26,01	5,750
10,3	0,070	0,241	0,227	0,244	0,226	0,227	0,209	–	8,558	0,190	46,1	0,938	5,214	4,972	5,833	5,686	4,919	5,039	–	26,49	5,908
11,3	0,080	0,261	0,240	0,270	0,250	0,250	0,220	–	9,063	0,257	47,1	1,020	5,564	5,302	6,170	6,014	5,190	5,305	–	26,96	6,133
12,3	0,097	0,296	0,259	0,303	0,256	0,271	0,241	–	9,565	0,221	48,0	1,020	5,669	5,408	6,296	6,140	5,308	5,418	–	27,44	6,257
13,3	0,108	0,335	0,275	0,337	0,278	0,305	0,270	–	10,07	0,213	49,0	1,071	5,970	5,719	6,617	6,460	5,602	5,738	–	27,91	6,370
14,3	0,129	0,378	0,315	0,375	0,337	0,340	0,294	–	10,56	0,317	49,9	1,086	6,101	5,841	6,769	6,603	5,717	5,845	–	28,39	6,597
15,3	0,130	0,404	0,345	0,413	0,347	0,361	0,300	–	11,06	0,341	50,9	1,134	6,310	6,055	6,999	6,843	5,923	6,080	–	28,86	6,750
16,3	0,121	0,451	0,380	0,444	0,359	0,400	0,319	–	11,55	0,230	51,8	1,145	6,452	6,194	7,170	7,000	6,079	6,216	–	29,33	6,917
17,3	0,128	0,473	0,397	0,471	0,407	0,423	0,345	–	12,05	0,355	52,8	1,172	6,586	6,337	7,313	7,149	6,194	6,351	–	29,81	7,030
18,2	0,145	0,513	0,412	0,518	0,420	0,465	0,376	–	12,54	0,341	53,7	1,215	6,765	6,499	7,511	7,343	6,374	6,526	–	30,28	7,206
19,2	0,159	0,538	0,436	0,556	0,455	0,495	0,397	–	13,03	0,430	54,7	1,290	7,067	6,791	7,895	7,698	6,754	6,947	–	30,75	7,372
20,2	0,172	0,571	0,464	0,604	0,489	0,521	0,435	–	13,52	0,508	55,6	1,307	7,178	6,902	8,031	7,840	6,865	7,076	–	31,22	7,559
21,2	0,200	0,637	0,527	0,640	0,546	0,556	0,465	–	14,01	0,492	56,6	1,325	7,297	7,017	8,155	7,963	6,974	7,186	–	31,70	7,642
22,2	0,210	0,683	0,564	0,685	0,575	0,597	0,525	–	14,49	0,421	57,5	1,360	7,492	7,204	8,382	8,166	7,165	7,376	–	32,17	7,839
23,1	0,220	0,719	0,612	0,735	0,625	0,630	0,550	–	14,98	0,541	58,4	1,420	7,774	7,523	8,728	8,505	7,490	7,716	–	32,64	8,048
24,1	0,252	0,749	0,635	0,774	0,665	0,670	0,579	–	15,47	0,608	59,4	1,428	7,854	7,595	8,825	8,592	7,565	7,795	–	33,11	8,170
25,1	0,260	0,805	0,674	0,833	0,720	0,725	0,617	–	15,95	0,688	60,3	1,442	7,959	7,701	8,956	8,726	7,674	7,909	–	33,58	8,364
26,0	0,260	0,859	0,735	0,874	0,769	0,775	0,674	–	16,44	0,604	61,3	1,470	8,165	7,894	9,181	8,937	7,869	8,112	–	34,06	8,513
27,0	0,268	0,915	0,785	0,940	0,833	0,812	0,725	–	16,92	0,737	63,2	1,540	8,522	8,245	9,567	9,315	8,217	8,442	–	35,00	8,799
28,0	0,266	1,083	0,943	1,168	1,060	0,975	0,891	–	17,40	1,248	65,0	1,571	8,783	8,491	9,843	9,587	8,448	8,694	–	35,94	9,008
28,9	0,279	1,187	1,043	1,283	1,188	1,074	0,975	–	17,88	1,444	66,9	1,617	9,054	8,750	10,15	9,874	8,696	8,957	–	36,88	9,288
29,9	0,321	1,292	1,153	1,431	1,333	1,180	1,109	–	18,37	1,706	68,8	1,673	9,355	9,069	10,49	10,22	9,006	9,255	–	37,82	9,591
30,9	0,373	1,548	1,386	1,729	1,627	1,456	1,409	–	18,85	1,944	70,7	1,773	9,790	9,490	10,95	10,69	9,431	9,680	–	38,76	9,901
31,8	0,465	2,123	1,937	2,366	2,254	1,935	1,932	–	19,33	2,744	72,6	1,801	10,04	9,750	11,23	10,96	9,660	9,940	–	39,70	10,09
32,8	0,540	2,676	2,469	3,000	2,886	2,485	2,496	–	19,81	3,412	74,4	1,811	10,04	9,742	11,24	10,96	9,660	9,932	–	40,64	10,14
33,7	0,580	2,920	2,730	3,312	3,175	2,714	2,734	–	20,29	3,873	76,3	1,906	10,55	10,25	11,79	11,52	10,15	10,43	–	41,58	10,57
34,7	0,600	3,048	2,855	3,440	3,310	2,826	2,850	–	20,77	3,961	78,2	2,010	11,36	11,02	12,76	12,44	11,00	11,28	–	42,52	11,61
37,6	0,675	3,526	3,328	3,971	3,810	3,264	3,325	–	22,20	4,355	–	–	–	–	–	–	–	–	–	–	–

Fig. C.16. Deflections of beam *S-4R* measured at the test